Active Vibration Control of Flexible Structures by Optimally Placed Sensors and Actuators

By

Daraji A. H.

2013

Submitted to the School of Mechanical & Systems Engineering in Fulfilment of the Requirements for the Degree of Doctor of Philosophy

Newcastle University

United Kingdom

This thesis is dedicated to my parents and
family and all students and researchers

ABSTRACT

The active vibration reduction of plane and stiffened plates was investigated using a genetic algorithm based on finite element modelling to optimise the location of sensors and actuators. The main aspects of this work were:

- Development of a finite element model for a plate stiffened by beams with discrete sensors and actuators bonded to its surface.
- Development of a finite element program for steel plates with various symmetrical and asymmetrical stiffening and edge conditions.
- Development of a genetic algorithm program based on the finite element modelling for the optimisation of the location and number of sensor/actuator pairs and feedback gain.
- Determination of optimum locations and feedback gain for collocated piezoelectric sensors and actuators on steel plates with various symmetrical and asymmetrical stiffening and edge conditions.
- Development of fitness and objective functions to locate sensors and actuators.
- Development of fitness and objective functions to determine the optimal number of sensors and actuators.
- Development of a reduced search space technique for symmetrical problems.
- Optimisation of vibration reduction control scheme parameters using the genetic algorithm.
- Optimisation of the number and location of sensor/actuator pairs and feedback gain to reduce material costs and structural weight and to achieve effective vibration reduction.

The modelling was validated by comparison with conventional finite element analysis using ANSYS, and by experiment.

The modelling was developed using a quadrilateral isoparametric finite element, based on first order shear deformation theory and Hamilton's principle, which may be arbitrarily stiffened by beams on its edges. The model can be applied to flat plates with or without stiffening, with discrete piezoelectric sensors and actuators bonded to its surfaces. The finite element modelling was tested for flat and stiffened plates with different boundary conditions and geometries, and the results of the first six natural frequencies were validated with the ANSYS package and experimentally.

A genetic algorithm placement strategy is proposed to find the global optimal distribution of two, four, six and ten sensor/actuator pairs and feedback gain based on the minimisation of optimal linear quadratic index as an objective function, and applied to a cantilever plate to attenuate the first six modes of vibration. The configuration of this global optimum was found to be symmetrically distributed about the dynamic axes of symmetry and gave higher vibration attenuation than previously published results with an asymmetrical distribution which was claimed to be optimal.

Another genetic algorithm placement strategy is proposed to optimise sensor/actuator locations using new fitness and objective functions based on H_∞. This is applied to the same cantilever plate, and was also found to give a symmetrical optimal sensor/actuator configuration. As before, it was found that the optimal transducer locations are distributed with the same axes of symmetry and in agreement with the ANSYS results.

A program to simulate the active vibration reduction of stiffened plates with piezoelectric sensors and actuators was written in the ANSYS Parametric Design Language (APDL). This makes use of the finite element capability of ANSYS and incorporates an estimator based on optimal linear quadratic and proportional differential control schemes to investigate the open and closed loop time responses.

The complexity of the genetic algorithm problem is represented by the number of finite elements, sensor/actuator pairs and modes required to be suppressed giving a very large search space. In this study, this problem was reduced by the development of a new half and quarter chromosomes technique exploiting the symmetries of the structure. This greatly reduces the number of generations, and hence the computing time, required for the genetic algorithm to converge on the global optimal solution. This could be significant when the technique is applied to large and complex structures.

Finally, new fitness and objective functions were proposed to optimise the number of sensor/actuator pairs required for effective active vibration reduction in order to reduce the added cost and weight. The number, location and feedback gain were optimised for the same cantilever plate and it was found that two sensor/actuator pairs in optimal locations could be made to give almost as much vibration reduction as ten pairs.

ACKNOWLEDGEMENTS

I would like to sincerely acknowledge the support, encouragement and mentorship given by my supervisor Dr. Jack Hale. I have not only learnt from him the technical aspects related to my work but also how to manage my research plan. I would also like to sincerely thank all the technical and administrative staff of the School of Mechanical and Systems Engineering and Faculty of Science, Agriculture and Engineering (SAgE) for their support during my studies. Last but least, I also thank my colleagues, PhD students at Newcastle University.

I would especially like to thank the Ministry of higher education and scientific research of Iraq, and in particular the cultural attaché of the Iraqi Embassy in London for the financial and material support given to me and my family throughout my studies.

Finally, I would like to express my deep appreciation to my mother and father. Also, I convey my sincere gratitude to my wife and children for their endurance, understanding, moral encouragement and support during my study.

Table of contents

List of Figures

List of Tables

Nomenclature

Chapter two

A	State matrix
B	Actuator input matrix
C	Output sensor matrix
M_c	Controllability
M_o	Observability
n	Matrix rank
W_c	Grammian controllability
W_o	Grammian observability

Chapter three

A	State matrix
B	Actuator input matrix
B_b	Element differential matrix relating bending strain to nodal displacement
B_m	Element differential matrix relating membrane strain to nodal displacement
B_{sh}	Element differential matrix relating shear strain to nodal displacement
B_ϕ^s	Element matrix relating electric field to element sensor voltage
B_ϕ^a	Element matrix relating electric field to element actuator voltage
C	Output sensor matrix
C^E	Piezoelectric elasticity constants matrix under constant electric field
D_b	Plate bending elasticity matrix
D_{sh}	Plate shear elasticity matrix
D_z	Piezoelectric electric charge density displacement
δ	Nodal displacements vector in physical coordinates
E	Modules of elasticity
EE	electrical energy
E_s , E_a	Electrical field across sensor and actuator
e	Piezoelectric coupling constants matrix
F_u	External mechanical force
F_ϕ	External charging force
G	Modules of rigidity
h_a, h_p, h_s	Actuator, plate and sensor thickness
J	Linear quadratic index
$\|J\|$	Jacobin determinant
K	feedback gain matrix

K_{pz}^{a}	Piezoelectric actuator stiffness matrix
K_{pz}^{s}	Piezoelectric sensor stiffness matrix
K_{uu}	Total element structural stiffness matrix including beam, sensor and actuator
$K_{u\emptyset}^{a}$	Piezoelectric actuator coupling matrix
$K_{\emptyset\emptyset}^{a}$	Piezoelectric actuator capacitance
$K_{u\emptyset}^{s}$	Piezoelectric sensor coupling matrix
$K_{\emptyset\emptyset}^{s}$	Piezoelectric sensor capacitance
KE	Kinetic energy
KE_a	Kinetic energy for piezoelectric actuator
KE_s	Kinetic energy for piezoelectric sensor
KE_p	Kinetic energy for plate
KE_{bsi}	Kinetic energy for beam stiffener $i = 1 \dots 4$
M_a , M_a	Piezoelectric actuator and sensor mass matrix
M_{bsi}	Beam stiffener mass matrix $i = 1 \dots 4$
M_p	Plate mass matrix
M_{uu}	Total element structural mass matrix including beam, sensor and actuator
$N_i(s,r)$	Plate element nodal shape function $i = 1 \dots 4$
$N_i(s)$	Beam element nodal shape function $i = 1{,}2$
n_m	Number of modes
ng	Number of Gaussian integration points
nbs	Number of beam stiffeners
PB	Offset distance between plate and beam stiffener
P	Riccati equation solution matrix
Q, R	Optimal linear quadratic control weighted matrices
r_a	Number of piezoelectric actuators
SE	Strain energy
SE_a	Strain energy in actuator
SE_{bsi}	Strain energy in beam stiffener $i = 1 \dots 4$
SE_p	Strain energy in plate
SE_s	Strain energy in sensor
s, r	Natural coordinates various -1,1
T_{bx} , T_{by}	Beam stiffener transformation matrix in x and y direction
u, v, w	Element displacement as a function of x, y, z ,t
VW	Virtual work
w_i, w_i	Weighted Gaussian integration points
$X, \dot{X}$	state vector

x, y, z	Element coordinate (m)
x_i, y_i, z_i	Element nodal coordinate $i = 1 \ldots 4$
δ	Element nodal degree of freedom
$\mathcal{L}$	Lagrange
ε	Element strain
γ	element shear strain
σ	element stress
α	shear correction factor
ϕ_a , ϕ_s	Piezoelectric element actuator and sensor voltage
μ_{33}^{ε}	Element piezoelectric permittivity
$\eta, \dot{\eta}, \ddot{\eta}$	Principal modal coordinate
φ	Truncated mode shape matrix
ξ	Damping ratio
ω	Natural frequency
$[\Omega] = \omega^2 I$	Natural frequency matrix

Chapter six

A	State matrix
B	Actuator input matrix
C	Output sensor matrix
$G(s), G(\omega)$	Transfer function
$GO_{i,j}$	Open loop transfer function at sensor number i and mode number j
H_∞	H infinity norm
$J(x, y)$	Fitness function
$J_o(x, y)$	Optimal fitness function (objective function)
n_{sa}	Number of sensor/actuator pairs
n_m	Number of modes
$X, \dot{X}$	State vectors
ϕ_a, ϕ_s	Actuator and sensor voltage

Chapter nine

A	State matrix
Ac	Closed loop state matrix
B	Actuator input matrix
C	Output sensor matrix

$GC_{j,i}$	Closed loop transfer function at sensor/actuator j and mode number i
$GO(\omega)$	Open loop transfer function at natural frequency ω
MGC	Average closed loop transfer function for all sensor/actuator pairs and modes to be suppressed and for various values of weighted matrices of LQR
MGR	Average closed loop vibration reduction for all sensor/actuator pairs and modes to be suppresses and for various values of weighted matrices of LQR
MGO	Average open loop transfer function for all sensors and modes
n_{sa}	Number of sensor/actuator pairs
n_m	Number of modes
Q, R	Optimal linear quadratic weighted matrices
$J(n_{sa}+1)$	Fitness function
$J_{opt}(n_{sa})$	Objective function
ϕ_a, ϕ_s	Actuator and sensor voltage

Chapter 1. Introduction

1.1. Background and Motivation of the Research

Demand for the development of mechanical structures with high strength to weight ratios has increased recently among industrial companies wishing to build lightweight aerospace structures, tall buildings and long bridges. The objectives of the construction of mechanical structures with high specific strengths are to optimise loading capacity, energy consumption and material costs. However, these structures are associated with complicated vibration problems. Traditionally, vibration has been reduced passively by adding mass, damping and stiffness in suitable locations on a structure. However, this method leads to increased weight, low response and sensing to low vibration energy. The alternative is active vibration reduction, in which vibration is measured using sensors and opposed by forces generated by actuators, with a control system linking the two. Piezoelectric sensors and actuators have been investigated in terms of their size, number and location on structures to optimise vibration attenuation. Arbitrarily placing discrete sensors and actuators on a structure leads to weak vibration suppression, whereas more suitable placement can give very effective results. Placement for the suppression of a single vibration mode is quite straightforward, but the effective suppression of a number of modes simultaneously is more challenging.

The purpose of this study is to optimise vibration reduction of flat plates and plates stiffened by beams with various geometries and end fixations. This is achieved by the optimisation of feedback gain and the placement and number of sensor/actuator pairs. Genetic algorithms are used as the optimisation tool, using conventional and newly developed objective functions to characterise optimum vibration reduction of multiple vibration modes, and a new technique is developed to exploit symmetries to greatly improve computational efficiency.

1.2. Research Gaps

Firstly, the active vibration reduction of flexible structures fully or partially covered by single sensor/actuator pair has been investigated thoroughly. This method is little effective for certain vibration modes and does not work for others, because the strain and hence the electric charge induced in the sensor surface is distributed between negative and positive values and this charge is spatially integrated over the area of the sensor. This distribution varies from one mode to another, reducing sensor and actuator

performance. Some studies have solved this problem by discretising sensor and actuator into multi-segments. Moreover, the effects of discretised sensors and actuators have been optimised by the placement of these segments in efficient locations using optimisation algorithms.

A limited number of studies have investigated active vibration reduction in plates stiffened by beams with the sensor/actuator pair either fully covering or randomly located on the structure, as explained in section 2.10. This method gives only low vibration suppression and does not work in all the low modes. It also requires high external energy, with considerable added weight and material costs. The present research investigates vibration attenuation of symmetrical and asymmetric stiffened plates using discrete sensor/actuator pairs optimally placed using genetic algorithms.

Secondly, previous studies have found what are claimed to be optimal locations for sensor/actuator pairs for the active vibration reduction of plates and shells with various degrees of dynamic symmetry. In this work techniques are developed to find better locations, believed to be globally optimal. This technique is then developed further to exploit any symmetry to reduce the optimisation search space and so reduce the computational effort required to find these optimum locations.

Thirdly, most studies in the area of the active vibration reduction of plates and shells by optimally placed sensors and actuators have selected the number of sensors and actuators arbitrarily and optimised just their location. However, this causes weak vibration suppression or high added weight, costs and energy requirement. This study investigates the optimum number of sensor/actuator pairs as well as their location and feedback gain using a new objective function based on a closed loop optimal linear quadratic control scheme.

1.3. Objectives of the Research

1. To develop a finite element model of a flat plate with or without beam stiffeners, with and without piezoelectric elements bonded to its surfaces as sensors and actuators.
2. To build this model into a genetic algorithm program suitable for optimising aspects of the model such as sensor/actuator locations and active vibration reduction and system control parameters.

3. To determine the optimum locations of various numbers of sensor/actuator pairs for active vibration reduction on plates with or without stiffeners, over several vibration modes.
4. To determine the optimum number of sensor/actuator pairs, optimally located, for the same plates.
5. To investigate the feasibility of reducing the genetic algorithm search space for these optimisations by exploiting the symmetry of the plate.
6. To validate the finite element model and the results of the active vibration reduction system optimisation experimentally and using the ANSYS finite element package.

1.4. Overview of the Thesis

The thesis consists of eleven chapters. The first chapter gives an introduction to the work, its background and motivation, the research gaps and the objectives of this study. Chapter two provides a literature review on sources of vibration, solutions, genetic algorithms, objective functions, finite element analysis and the active vibration control of flat plates and plates stiffened by beams.

Chapter three develops a finite element model for plate stiffened by beams with discrete sensors and actuators bonded to its surface. In this model, the plate and piezoelectric layers are represented by quadrilateral isoparametric four nodes element with five degrees of freedom per node, and the piezoelectric element has an additional element electric voltage degree of freedom. The plate element is stiffened by an isoparametric two nodes beam element with three degrees of freedom per node fixed on the edge of the plate element. The modelling is based on Hamilton's principle and first order shear deformation theory and the model is used to optimise the location, number and size of sensors and actuators. Chapter four tests various flat and stiffened plates with several different geometries and boundary conditions using a finite element program based on the model derived in chapter three and validated by the ANSYS finite element package and experimentally. In this chapter, the optimal number of finite elements required to give accurate natural frequencies and mode shapes was determined by convergence study in order to minimise the search space in the optimisation algorithms.

Chapter five focuses on the active vibration reduction of the cantilever plate by optimally placed sensors and actuators. In this chapter, an effective placement strategy is developed for optimal placement of two, four, six and ten sensor/actuator pairs,

respectively, suppressing the first six modes of vibration using minimisation of the linear quadratic index as an objective function. The modelling is validated in the ANSYS finite element package using optimal linear quadratic control and proportional differential control schemes.

Chapter six develops new fitness and objective functions in order to optimise the location of sensors based on modified H_∞ control. The same cantilever plate used in chapter five was tested in order to verify the findings dealing with the global optimal configuration. The developed objective function greatly reduced the search space compared with previously published studies and gave the same level of vibration suppression compared to that reported in chapter five.

Chapter seven describes two new research topics: the vibration reduction of stiffened plates by optimally placed sensors and actuators and the effect of the dynamic axes of symmetry on the global optimal configuration of sensors and actuators. Various symmetrical and asymmetrical plates in geometries and edge fixations were studied to generalise the findings in the previous chapters.

Chapter eight develops a new half- and quarter-length chromosome technique in the genetic algorithm to optimise the location of sensors and actuators in symmetrical structures. The use of this technique gives the same global optimal distribution of sensor/actuator pairs obtained by using the full-length chromosome, but with greatly reduced search space and computational effort.

Chapter nine develops new fitness and objective functions used to optimise the number, location and feedback gain of sensor/actuator pairs using closed loop optimal linear quadratic control. The aim of this chapter is to find the minimum number of sensor/actuator pairs in the optimal location to achieve the same level of vibration reduction as when more pairs are used. The results were validated against those achieved using the proportional differential control scheme.

In chapter ten, the forgoing work is tested experimentally using a cantilever plate bonded with single sensor/actuator pair in the optimal location. The controller hardware required was designed and built in this part of the research, including the charge to voltage converter, DAC and voltage manipulator electronic boards and these electronic boards used with a microcontroller.

Chapter eleven gives the conclusions of this study, suggests future work and describes publications from this research.

Chapter 2. Literature Review

This chapter reviews the literature relevant to the active vibration suppression of a flexible structure with optimally located sensors and actuators and optimal control schemes obtained using genetic algorithms. This chapter presents previous studies relating to vibration reduction of plates and shells, piezoelectric vibration sensors and actuators, genetic algorithm optimisation, finite element structural analysis and application to stiffened plates and shells in order to clarify the research gaps that require further investigation.

2.1. Sources of Vibration and the Importance of their Investigation

Vibration is known for its ability to cause disruption, discomfort, damage and destruction, and these potential effects have encouraged industrial companies to spend many millions of dollars in developing equipment and materials in order to suppress it. Levels of vibration vary from those involving destruction caused by earthquakes at the top end of scale to the annoyance caused by the vibration of washing machines at the lowest end of the scale [1].

Most mechanical vibration is induced as a result of either rotation of unbalanced mass or the friction of moving parts which may occur due to poor manufacturing and faulty design. Vibration leads to the progressive wear of machine components such as bearings and gears and also causes fasteners such as nuts to become loosened in mechanical joints as well as creating excessive noise. Vibration causes the cyclic variation of induced stress in machine components and mechanical structures and leads to failure due to material fatigue. The bad effects of vibration have a direct bearing on human beings because they may be considered to be integral parts of many engineering systems. Vibration can be transmitted to human beings and may cause discomfort and reduction in efficiency and focus. Vibration can also cause damage or malfunction in electronic equipment or panels of instruments located in modern vehicles and processing plants.

The resonance phenomenon is another significant source of vibration and cause of the failure of mechanical structures. This happens when a natural frequency of a mechanical structure coincides with an external excitation frequency, which causes an extreme deflection at all points of a structure at the same time and may lead to structural failure. Therefore, the investigation of vibration is accepted as a significant topic in standard design procedures for the construction of structures and the manufacturing of systems.

The structural failure caused by resonance and excessive vibration has been investigated extensively in order to prevent types of failure such as bridge collapse, as shown in Figure 2.1. The effects of vibration on structures and humans encourages engineers to conduct further investigation in order to reduce it through the proper design of engineering systems and structures [2].

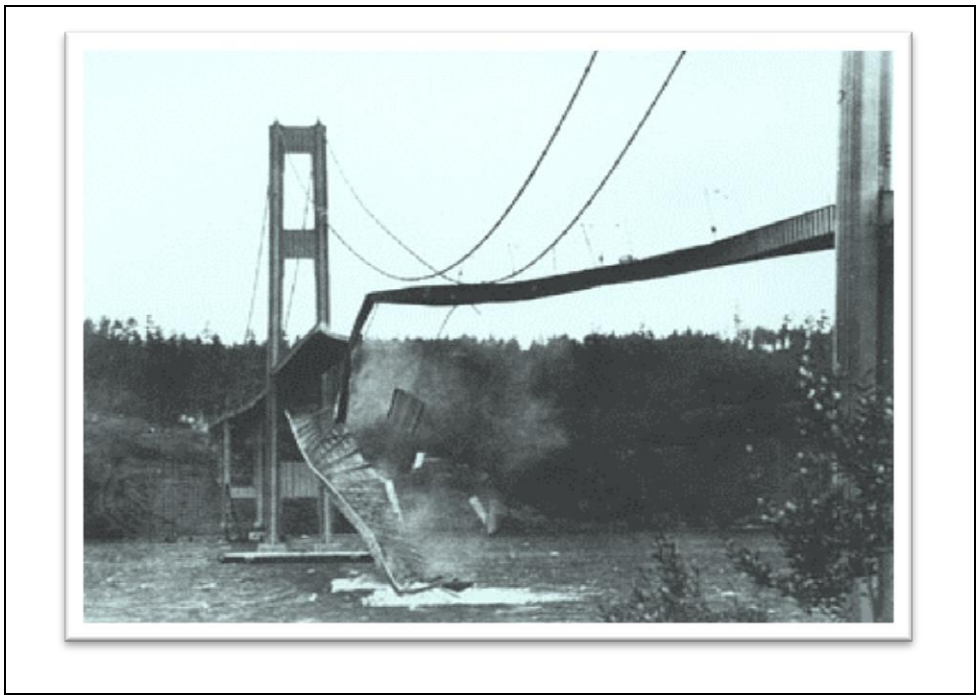

Figure 2.1 Tacoma Narrows bridge during wind-induced vibration. The bridge opened on 1.July.1940 and collapsed on 7Nov1940. (Farquhar son photo, Historical photography collection. University of Washington libraries) [2]

2.2. Vibration Problems

Systems of mechanical vibration can be classified in terms of the energy stored in the vibrating system, which may be conservative or non-conservative. In a conservative system the amount of energy remains constant during motion, or in other case the energy is dissipated by damping or the system may involve friction or a non-conservative force. Dynamic systems can be also classified as linear or non-linear based on the behaviour of their basic elements in terms of mass or inertia, spring and damper. If the variables associated with these elements remain constant over time and behave linearly, then the motion of such a system can be described by using linear ordinary differential equations with constant coefficients, whereas otherwise alternative methods should be used to describe the motion of a system with time-variant coefficients or which is nonlinear. Conservative or perfectly linear vibrating systems are unlikely to exist in real-world applications, just on paper for simplification purposes after reasonable assumptions are proposed [3].

In this study, the system is considered to be non-conservative because it includes structural damping and non-conservative forces, and linear since it is assumed that the variables associated with basic elements of the vibrating system are behave linearly for small displacements, and remain constant over time. These assumptions are made in order to simplify the problem, but in reality there is no linear dynamic system especially during resonance phenomenon or transient closed loop control.

2.3. Methods of Vibration Reduction

Mechanical vibration can be reduced using passive, semi-active and active vibration reduction methods based on the type of problem involved. Stiffening, damping and isolation are considered as the main methods used to suppress vibration passively. The mechanical structure can be stiffened and changed inherently by adding beam stiffeners or increasing layers in the structure of the same material or a different material as in composites. This stiffening shifts the structural resonance frequency beyond the band of excitation frequency in order to reduce the effects of resonance. This method works effectively if the band of external excitation frequency is known.

A damper can be added to a structure in order to reduce structural resonance peaks by dissipating the vibration energy through the damper. Damping can be achieved passively with fluid dampers, eddy currents, elastomer elements or by diverting dynamic energy from the main structure to the dynamic vibration absorber. Vibration

energy can also be converted to electrical energy using transducer and dissipated into electrical network or stored as harvested energy [4].

A number of studies presented by Manjunatah et al showed that smart materials, such as piezoelectric, magneto-rheological fluids and shape memory alloys, mounted with a mechanical structure can produce a second response which interacts with the first mechanical structure's response in order to improve the overall response [5].

Recently, semi-active (also called semi-passive) devices have been developed which consist of passive devices with controllable properties. Notable examples include magneto-rheological (MR) fluids and piezoelectric transducers with switched electric networks. A large change in the viscosity effect (rheological) was first observed in electro-rheological fluids when subjected to electric fields by Winslow in 1947. An electro-rheological fluid (ER) is insulating oil containing micro-sized particles. The MR fluid was discovered by Rabinowin (1951), who observed the same rheological effects by the application of a magnetic field to a fluid containing magnetized particles. The particles make columnar chain-like structures parallel to the magnetic field in fluids, as shown in Figure 2.2. These structures limit the flow of the fluid and require a minimum shear stress for the flow to be initiated. This phenomenon consumes very little power, is reversible and leads to a rapid response within milliseconds [6].

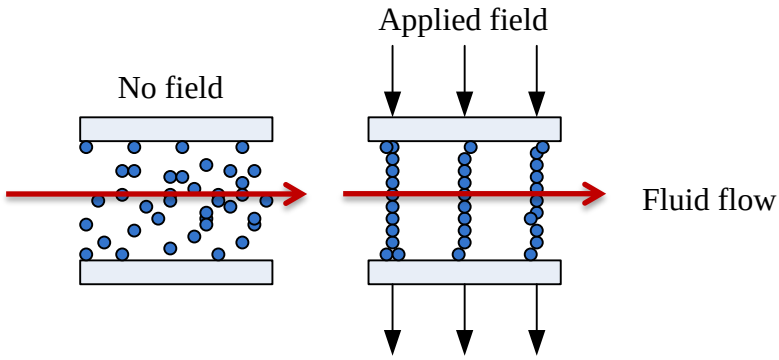

Figure 2.2 Chain-like structure create under an applied field [6]

The application of magnetorheological fluid is already part of the design of many structures such as automotive vehicles, tall buildings, robotic manipulator arms and spacecraft. Magnetorheological dampers are highly nonlinear devices and their force-velocity relationship can be difficult to define. MR damper has two recognised modes; the off and active states. MR dampers give a good solution to dissipate energy in mechanical systems and structures. They are available in three types, and the mono tube is the most common type which is compact in size and easy to mount in any

direction. It is mounted between the mass of the oscillator and the base. Figure 2.3 shows a mono tube MR damper and its characteristic curve of damping force against speed for several values of magnetic field. More information about MR dampers can be found in the reference book [7].

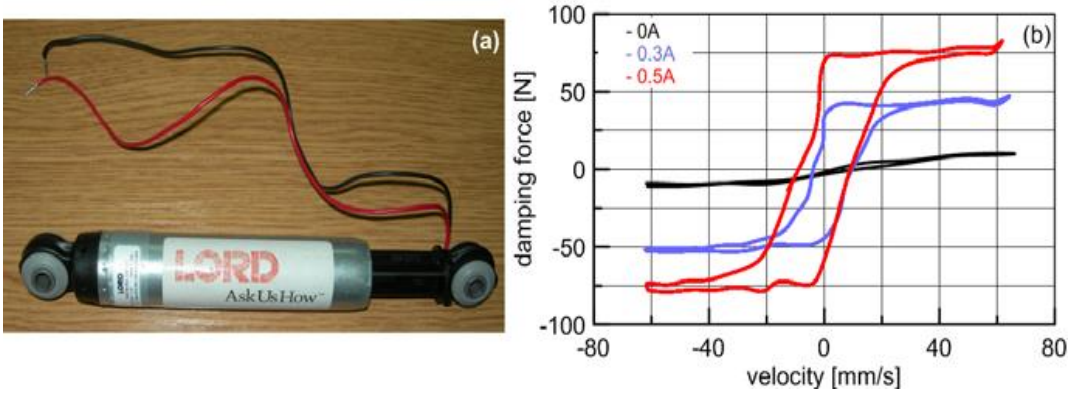

Figure 2.3 Magnetorheological composite damper RD 1097-01**a**, and its characteristic damping force versus piston velocity **b** [7]

Żak et al reported that the further investigation of composite materials is required to extend their field of application in industry by development of their dynamic behaviour using new smart materials such as shape memory alloys (SMAs) laminated with traditional composite material. These materials have the ability to inherently change their properties such as modulus and damping capacity, and the ability to produce large internal forces[8]. Cartmell et al reported that SMAs exhibit special two unique effects known as shape memory and superelasticity. These effects are valuable and interesting mechanical properties. The shape memory effect is the recovery of its original cold-work shape during heating and can produce large internal recovery stresses, while superelasticity happens in conditions of elevated temperature and is related to large nonlinear-loading and unloading retention strains [9]. Many studies have investigated the dynamic performance of multilayer composite beams and plates laminated with SMAs with various geometries and boundary conditions, considering the effects of the location, orientation, volume fraction and length to weight ratios of SMA wires[8-14]. More details about SMAs can be found in the reference book [9].

Banks et al reported that SMAs exhibit slow responses time compared to other smart materials such as piezoceramic [15]. Preumont reported that SMAs are used as an actuator only for low frequencies and low precision applications because of their difficulties with cooling [6]. Roh and Kim said that the SMAs could have many

adaptive abilities, but their applications was limited in composite material as fibre reinforcement or actuator because of their low response [16]. Mani et al found that SMAs are suitable for actuation at low frequencies and piezoelectric at a wide range of frequencies [17].

Piezoelectric materials have received more attention than other smart materials in the active vibration control of flexible structures because of their superior properties. It is considered to be lighter and smarter and to give higher vibration attenuation and faster response than passive and semi-active vibration suppression, but it requires external energy, smart sensors, actuators and a microcontroller. It is achieved by taking a signal from the sensor and feeding it to an actuator after it is modified by a controller. Figure 2.4 shows a basic active vibration control system for a cantilever beam with a single piezoelectric sensor/actuator pair bonded to its surface. The control system works to suppress vibration actively through the following process. The piezoelectric sensor detects any vibration and generates an electric charge on its electrode. This is converted to a voltage signal which is sent to the microcontroller, before which this voltage is manipulated according to the microcontroller input port requirements. The microcontroller modifies the input signal according to the control scheme software built into it, and produces a digital output signal which is passed through a DAC and then to the high voltage driving unit in order to drive the piezoelectric actuator. If the locations of the sensor/actuator and the control scheme in the microcontroller are well designed, this effectively reduces the vibration in the structure.

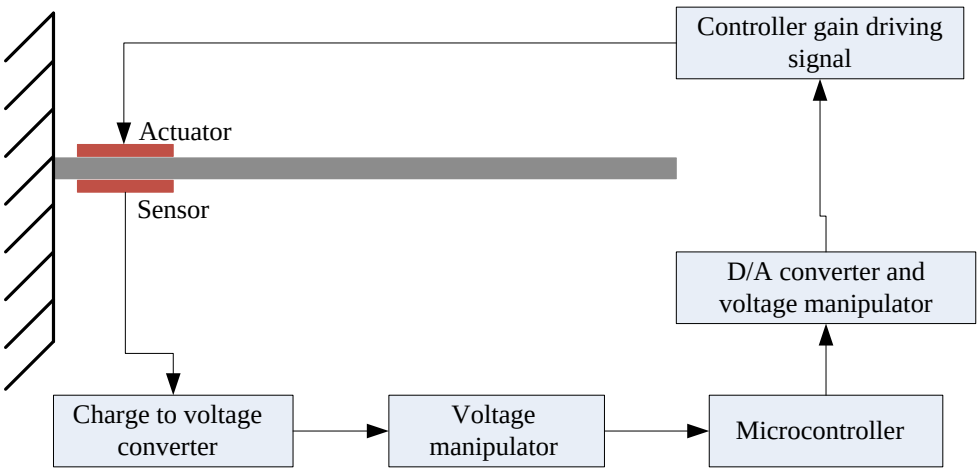

Figure 2.4 Active vibration control system for a cantilever beam bonded with single piezoelectric sensor/actuator pair

The general concept of active vibration reduction is just an extension of this simple case. There can be multiple sensors and actuators, and many possible control schemes, all of which need optimisation if effective active vibration control is to be achieved at low cost and with a small external power requirement. This topic becomes more complicated for large structures and for the control of multiple vibration modes. Piezoelectric working mechanism is explained in the next section.

2.4. Piezoelectric Sensor and Actuator

In 1880, Pierre and Jacques Curie experimentally discovered a relation between the macroscopic piezoelectric phenomenon and crystallographic structure. In 1964, Cady reported that the coupling generated between mechanical, electrical and thermal states for a dielectric crystal solid state, when subjected to mechanical force, is called piezoelectricity. Piezoelectric materials generate an electric charge when subjected to mechanical strain and vice versa. This property makes piezoelectric materials suitable for sensor and actuator functions [18].

Piezoelectric materials and applications have been gradually developed ever since their first discovery, and have become a popular and essential part of many control system applications. Piezoceramic lead-zirconate-titanate (PZT) and polymer polyvinylidene fluoride (PVDF) are well known smart materials used in sensors and actuators and are available with a wide range of properties and geometries [19]. Piezoceramics are used extensively as sensors and actuators for a wide range of frequencies including ultrasonic applications and with nanometre movement precision [6].

The working mechanism of thin plate piezoceramic materials is demonstrated in Figure 2.5 and Figure 2.6. As shown in Figure 2.5, if the direction of polarization of the piezoceramic sheet is parallel to the thickness direction, and when an electric field is applied in the direction of polarization, then the piezoceramic expands in the thickness direction and contracts in the transverse directions at the same time; and vice versa when the field is reversed.

The motion in the thickness direction of such piezoceramic plates is very small, perhaps tens of nanometers; while the motion in the transverse direction is generally larger, and measured in micrometers. If this piezoceramic sheet is bonded to a mechanical structure, then the induced motion in the piezoceramic is enough to stretch or bend this structure. This feature is usually employed in the control of mechanical structures.

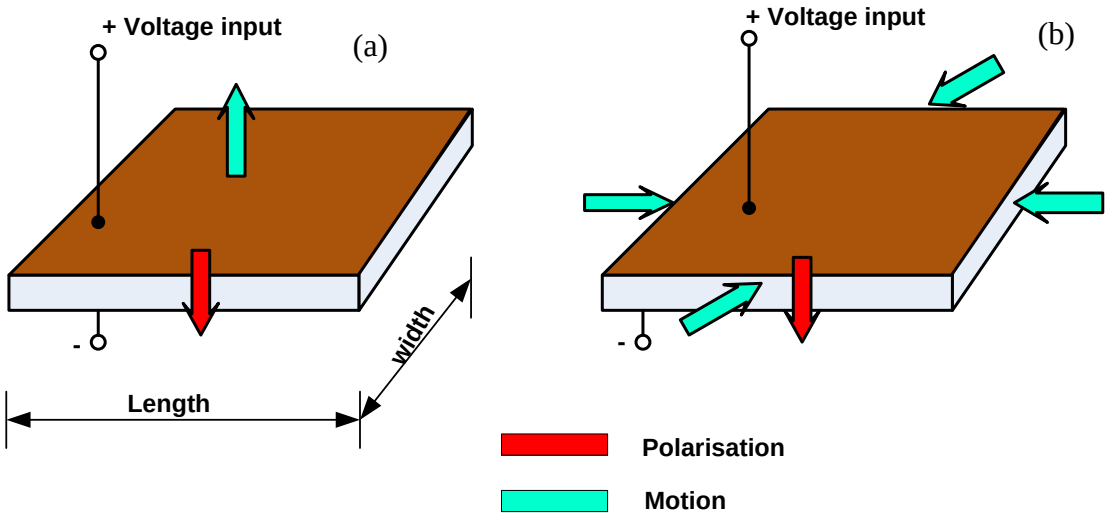

Figure 2.5 (a), single layer longitudinal motor getting thicker (b), single layer transverse motor with sides contracting [20]

A voltage is generated on the electrodes of a piezoceramic electrode when subjected to a mechanical stress in the direction parallel to the polarization, as shown in Figure 2.6(a), and in the directions perpendicular to the polarization, as shown in Figure 2.6(b). Consequently, a piece of piezoceramic bonded to a mechanical structure generates an electrical voltage when the structure stretches or bends, and this makes it useful as a sensor [20]. The piezoelectric constitutive equation is explained in section 3.3.

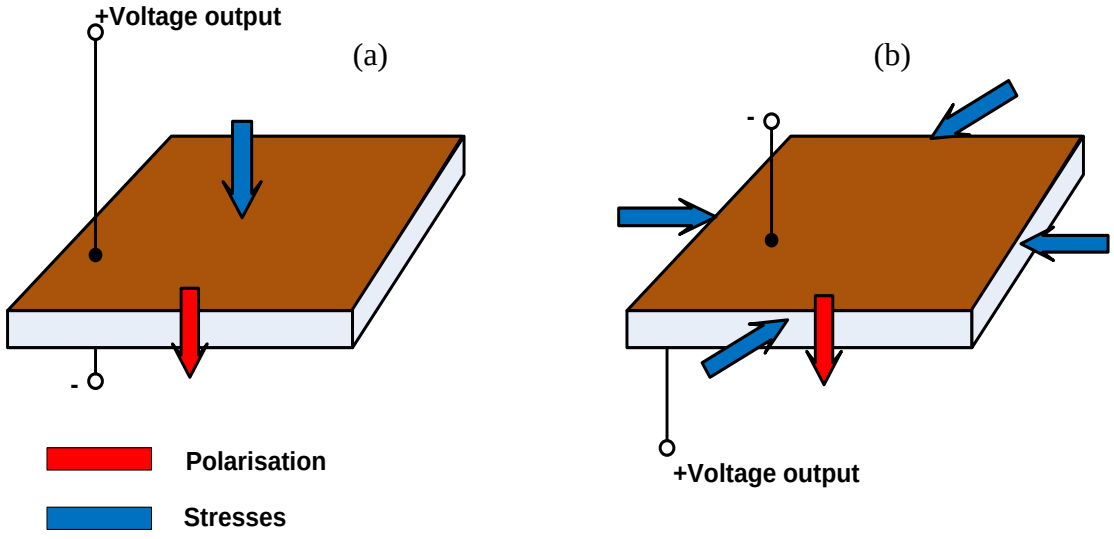

Figure 2.6 (**a**) Longitudinal generator being compressed from the top and bottom, and (**b**) transverse generator being compressed from the sides [20]

2.5. Placement of Sensors and Actuators

Recently, complex engineering problems have been investigated using a number of modern techniques in order to find optimal solutions. These methods are significantly more powerful and effective than traditional or simple classical optimisation methods. The principle mechanisms of modern methods are taken from the behaviour and principles of life and nature, such as biological, molecular, insect swarm and neurobiological systems. These modern optimization methods include genetic algorithms, simulated annealing, particle swarms, ant colonies, fuzzy and neural-network based methods [21].

The genetic algorithm is a powerful optimisation method based on the principle of "natural evolution" or the "survival of the fittest". Many studies [22-47] have used it to optimise the location of discrete sensors and actuators on different types of flexible structure.

2.6. Genetic Algorithms

Holland built the first model of genetic algorithms to describe and solve optimisation problems based on the "survival of the fittest". He started to build his model in 1960 at the University of Michigan and published his first work (Adaptation in Natural and Artificial System) in 1975. Genetic algorithms have gradually developed and become an established method to search and solve complex optimisation problems [48]. The genetic algorithm is a random optimisation method guided by fitness and objective functions and based on the principles of genetics, evolution and natural selection. Optimisation problems consist of a massive number of possible solutions, called the search space, and each possible solution in the search space can be marked by a fitness value depending on a problem defined by an objective function. The optimal solution is that with the minimum or maximum value of the objective function based on the optimisation problem design.

2.6.1. Genes, chromosomes, the search space and coding

The genetic algorithm is based on a "breeding population" of individuals, each defined by a chromosome which is made up of a sequence of genes. The gene is the basic unit of a search space and is defined by a string of binary or integer numbers. The fittest individuals within the breeding population "breed" to form a new generation of individuals, each defined by a chromosome composed of a combination of its parents'

genes. In active vibration control, each gene represents the location of a single sensor or actuator on a mechanical structure. Thus the search space is the collection of all the possible combinations of sensor/actuator placements on the structure.

Figure 2.7 shows a demonstration of a simple search space and the chromosome coding used in sensor and actuator placement on a mechanical structure. Suppose a structure discretises to a number of locations 1-12 and it is required to find optimal locations for four actuators. The search space then contains 495 possible solutions (the combination of 4 from 12), one of which is the global optimal solution. The chromosome codes as an integer or a binary number as shown in Figure 2.7. Integer coding is much simpler and lower computational effort and computer memory storage are required than with binary coding. In the chromosomes shown in Figure 2.7, the integer numbers 5, 1, 4, and 9 are equal to the binary numbers 0101, 0001, 0100 and 1001 respectively. It is clear from this demonstration that a small structure discretised to 12 elements requires a string of binary numbers of four bits to represent each gene in the chromosome. This requires more computational effort to convert binary to digital alternatively and becomes too complicated for a large mechanical structure discretised to hundreds or thousands of elements which also requires high computer memory capacity.

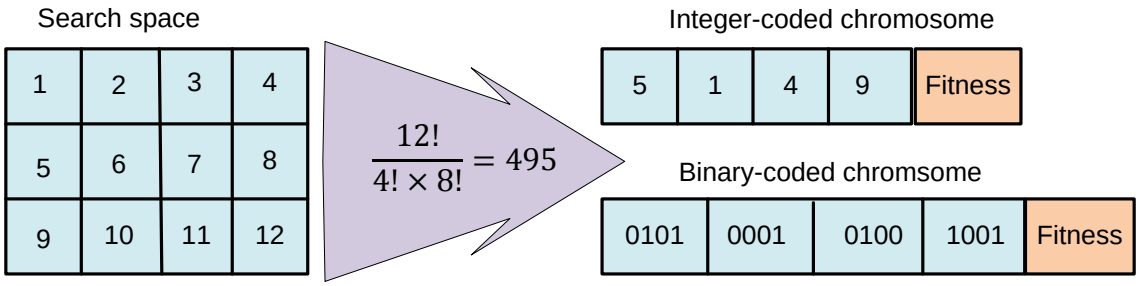

Figure 2.7 Demonstration of a search space and chromosome coding

Many studies have used binary numbers for chromosome coding in order to locate sensors and actuators on different types of structure [25, 26, 28, 30, 35, 38, 49, 50]. However, Roy and Chakraborty have used integer-coded chromosomes for the optimisation of actuators location and found this efficient in reducing computational time because the binary-coded chromosome leads to an increase in string length, and most of the crossovers and mutations gave designs with the wrong number of actuators.

Increased computation effort is necessary to resolve these anomalies, especially for large structures where many sensors or actuators need to be optimised [40].

2.6.2. Crossover and mutation

Crossover and mutation represent the main genetic algorithm operators used to explore the search space in order to determine the local or global optimal solution. The crossover operator explores the search space to get a sub-optimal solution if the primary population has poor gene variety, and mutation helps to explore the optimal solution. The crossover operator works by interchanging a percentage of genetic material between parents in order to produce offspring after applying mutation. The mutation operator works by randomly replacing an individual gene after the crossover operation with another gene from the search space. This has the effect of preventing the search becoming "stuck" in a local optimum and increases the possibility of obtaining the global optimal solution. Figure 2.8 shows the process of single point crossover and mutation for two chromosomes, usually called parents, which produce offspring.

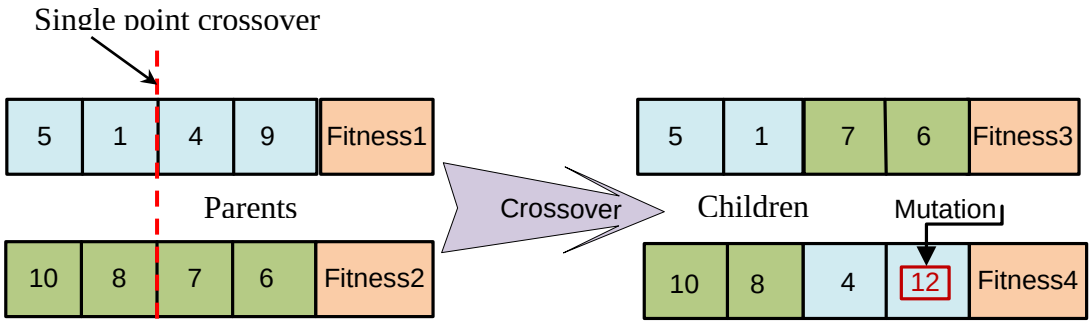

Figure 2.8 Crossover and mutation process

Many crossover techniques are available and may be chosen by the system designer. These include single, two and multiple point crossover, three-parent crossover, uniform crossover and shuffle crossover. These and other types are explained in standard reference works [48].

2.6.3. Fitness measure and selection

The fitness measure applies to each individual and is considered as guidance for the genetic algorithm to the optimal solution. The fitness measure is calculated from the values held in each individual gene according to the fitness equation. The value of fitness demonstrates the quality of the individual and this value is either maximised or minimised to reach the optimal solution.

The selection process is carried out for each generation according to the theory of natural selection or survival of the fittest. According to this theory, the fit individuals procreate and carry their genes into the next generation, while those that are less fit do not breed and so their genes tend to die out.

The selection process is defined by picking sets of two (or occasionally more) parents from the population based on their high fitness. The speed of convergence is strongly influenced by the selection process, with fast convergence being desirable in terms of computational efficiency but tending to miss the global optimum by premature convergence onto a local optimum.

Some of the common selection operators used in genetic algorithms are the roulette wheel, random, rank, tournament, and truncation selection. The roulette wheel proposed by Holland assigns a probability of selection to each individual based on its fitness. The roulette wheel is divided into a number of sectors or slots equal to the number of individuals. The width of the slot is calculated based on the individual fitness value. For example, the roulette wheel shown in Figure 2.8 is designed for four individuals with the random fitness values shown in Table 2.1. The width of a roulette wheel slot equals the fitness value of the individual divided by the total fitness values of all individuals. Roulette wheel selection does not guarantee the fittest individuals will breed, but they are more likely to be selected than those of lower fitness levels.

Table 2.1Information for a generation composed from four individuals

No	Chromosome code	Fitness	slot width
1	5 1 3 9	1	100×1/21=4.7%
2	2 6 8 6	7	100×7/21=33.3%
3	9 1 7 6	10	100×10/21=47.6%
4	10 3 4 2	3	100×2/21=14.2%
Total		21	100%

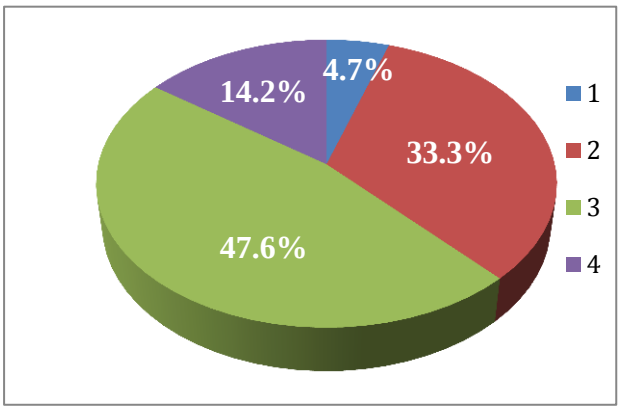

Figure 2.9 Roulette wheel for a single generation with four individual

The roulette wheel is simple to implement but is noisy and has problems when fitness values differ significantly [48]. The truncation selection method is considered to be a deterministic method and is carried out by sorting all individuals according to their fitness and choosing those with the best fitness as parents [51]. The random and ranking selection methods are described in detail elsewhere [48], as is tournament selection method in the reference book [51]. In this study, the truncation selection method was used because it is deterministic, is simpler in computation, and showed faster convergence to the optimal solution than other methods.

Figure 2.10 shows a flowchart of a genetic algorithm for an optimisation problem. Usually, the process starts by the selection of an initial random population. The individual string length is formulated and coded based on problem requirements. Then fitness measures for each individual are calculated and the individuals are selected for the next regeneration process. The regeneration stage starts with crossover and mutation and then fitness measurement in order to select the individuals for the next generation. The regeneration process is then repeated to start again from crossover to the pre-set total number of generations.

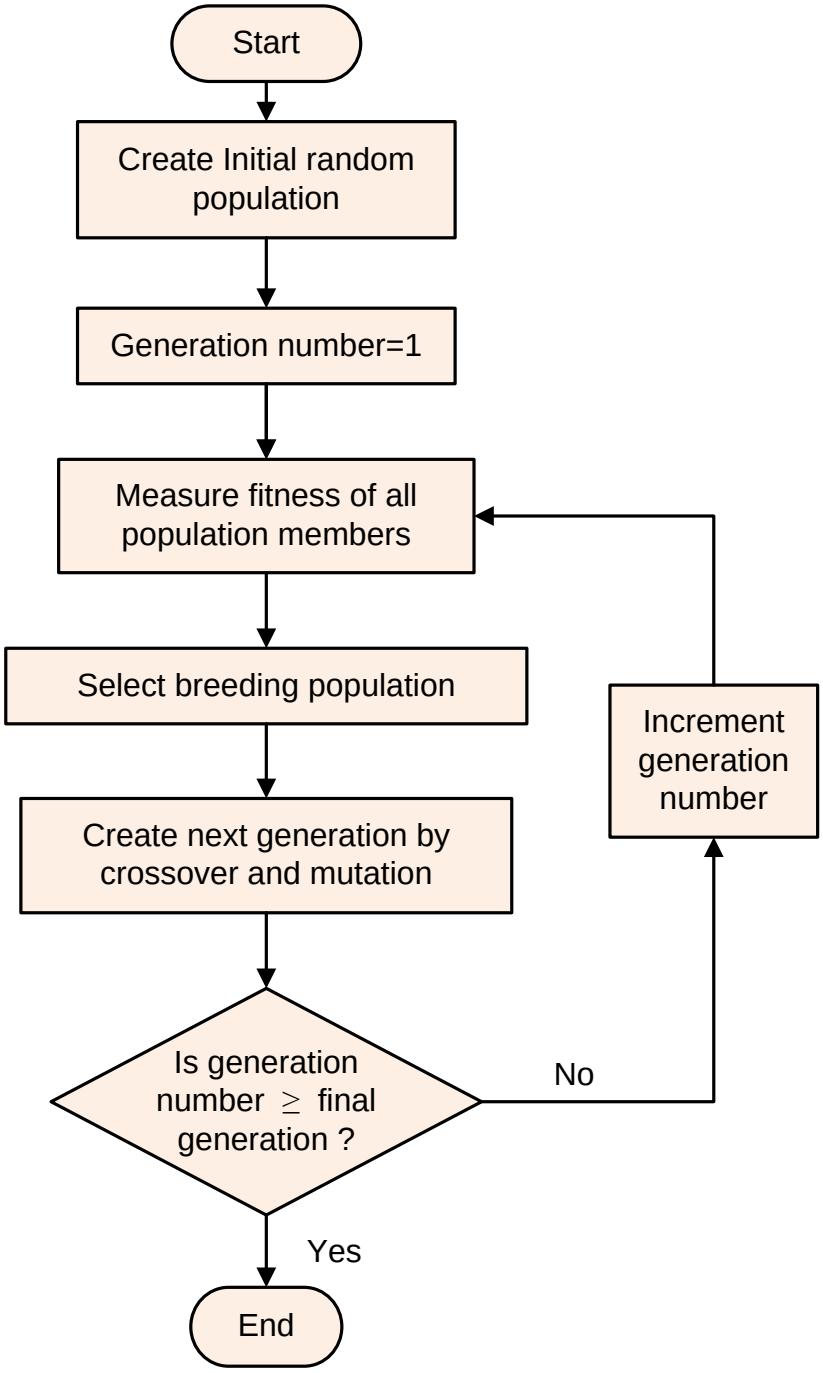

Figure 2.10 Block diagram for a general genetic optimisation problem

2.7. Fitness and Objective Functions

Fitness and objective functions are used by genetic algorithms to locate sensors and actuators in the optimal positions on structures. Previous studies have used various fitness and objective functions in order to increase the effectiveness of sensors and actuators, or to reduce the numbers of generations required, or to optimise specific variables in dynamic structures.

2.7.1. Observability and controllability

A system is said to be controllable if the configuration of located actuators has the capability to excite all modes of a structure. A system is said to be observable if the configuration of located sensors has the ability to measure the motions of all the modes. This information is essential and useful in locating sensors and actuators, but too limited. The controllability and observability criteria as represented in equations 2.1 and 2.2 give binary answers of either yes or no. The structure is observable and controllable if the rank of the matrices M_c and M_o is equal to the number of states *n.*, the matrices *A*, *B* and *C* refer to the matrices for state, actuators and sensors respectively. These criteria have two disadvantages concerning the output answer results of yes/no and the fact that the computational effort required for large system may give an overflow [52].

$$M_c = [B \quad AB \quad A^2B \quad \cdots \quad A^{n-1}B] \tag{2.1}$$

$$M_o = [C \quad AC \quad A^2C \quad \cdots \quad A^{n-1}C]^T \tag{2.2}$$

Alternative criteria to determine system properties are grammian controllability W_c and observability W_o. Measures of these criteria give more quantitative answers than yes/no. The Grammian solutions W_c and W_o of equations 2.3 and 2.4 give degrees of controllability and observability for each mode. These criteria are represented by the following equations [52].

$$AW_c + W_c\mathrm{A}^T + \mathrm{BB}^T = 0 \tag{2.3}$$

$$AW_o + W_o\mathrm{A}^T + \mathrm{CC}^T = 0 \tag{2.4}$$

The optimisation of sensor and actuator location has been investigated for different types of structures based on the maximisation of observability and controllability [25, 26, 35, 43, 53-56].

A methodology based on the minimisation of the optimal linear quadratic control index as an objective function was proposed by Devasia et al. This objective function was applied to a simply-supported beam in order to optimise the size and location of an actuator using a simple search method, and the result was compared with another objective function based on the maximisation of grammian controllability. The authors found that this objective function is more suitable than grammian controllability for the placement and sizing of actuators. They reported that this objective function achieves stability of closed-loop control system and allows a designer to choose various values of weighted matrices of optimal linear quadratic index in order to optimise actuator location and vibration reduction [53]. The objective function based on maximisation of controllability gives the optimal location of actuators, but minimisation of the optimal linear quadratic index achieves the optimal actuator locations, stability of closed loop control system and minimises the feedback gain, as explained in the next chapter.

2.7.2. Minimisation of optimal linear quadratic control index

Kondoh et al proposed an objective function based on the minimisation of the linear quadratic index to optimise sensor and actuator location and feedback gain for a cantilever beam. The results were compared with those using the maximisation of energy dissipation as an objective function. The authors reported that the optimal linear quadratic control has a clear physical meaning and the flexibility to allow the implementation of varying weighted matrices [57].

This objective function achieves the optimal location of actuators and minimum control feedback gain, as explained in the next chapter in sections 3.5 and 3.7. The linear quadratic index has been applied to various types of mechanical structures as an objective function to optimise actuator location and feedback gain [38, 39, 58-61].

2.7.3. H_∞ and H_2 norms

H_∞ and H_2 norm functions are a measure of open and closed loop system frequency response to an external disturbance. These measures have been used as objective functions to optimise the location of sensors and actuators on flexible structures. A limited number of studies [49, 62-64] have investigated the optimal locations of sensor and actuator under closed loop control using optimisation algorithms to find the optimal combinations of sensors and actuators needed to suppress a number of modes collectively. Open loop H_∞ and H_2 control implemented by Gawronski was based on an exhaustive search method for a small search space and a sub-search space for a large-scale structure to find the optimal locations of individual sensors or actuators to suppress individual modes and then grading them [65].

In chapter six of this study, an optimal placement strategy using a genetic algorithm and open loop modified H_∞ control is proposed and implemented to find the optimal combinations of six and ten sensors to suppress the first six modes of vibration collectively for a cantilever plate.

2.8. Finite Element Analysis

The finite element method (FEM) is a powerful numerical method used to solve both simple and complex engineering problems. The modelling of any physical engineering problem using the FEM produces a system of many hundreds or thousands of algebraic equations which require a high-speed processor and large computer memory capacity. The application of the FEM to solve complex engineering problems has increased as a result of developments in computer design. The engineering problems to which FEM has been applied include simple and multi-physical problems coupling two or more of structural, hydraulic, thermal, electrical and magnetic field problems.

2.9. Optimal Configurations of Sensors and Actuators for Plates and Shells

A few studies have concentrated on the active vibration control in plates and shells with optimally placed sensors and actuators using optimisation techniques and control schemes. These are summarised in Table 2.2, which shows that most previous studies have focused on the optimal distributions of sensors and actuators on plates and shells which are symmetrical in both geometry and boundary conditions. It is important to recognize from this table that there is no consensus on the global optimum distribution, and it can be seen that different optimum configurations have been obtained which used

arbitrary numbers of sensors and actuators for either the same cantilever plate [26, 30, 35, 38, 54, 66], or simply supported plate [25], or spherical and cylindrical shells [40, 67]. These distributions might be considered as good local solutions, but it is not clear which, if any, are global optimum solutions. The table also shows two different studies which investigated the same cantilever plate and found different and opposite optimal solutions, one at the root [30] and the other at the free end [54] of the cantilever plate. Different optimal actuator configurations can be seen for the same simply supported plate [25]. The most recent study has reported that the "existing optimisation schemes for optimal actuator placement may be inaccurate or computationally impractical" [66]. This may be as a result of the search space involving massive numbers of candidate solutions where the programme of the genetic optimisation problem gives a different optimal solution at each run. Therefore, a more efficient genetic algorithm placement strategy is required and the search space of the optimisation problem needs to be reduced. A smart structure might contain hundreds or thousands of local optimum solutions but only one unique global optimum solution. Liu has reported that the global optimum solution is often difficult to find for a large-scale structure with many thousands of degrees of freedom [49]. Genetic algorithms can find optimum solutions and excellent results may be achieved if applied properly, but are not guaranteed to find the global optimum solution [48]. From this it can be concluded that the research topics described below require investigation:

1. Vibration reduction in flexible plates and shells by optimally placed sensors and actuators.
2. The identification of global optimal configurations of sensors and actuators.
3. The effect of the dynamic axes of symmetry of plates and shells on the global optimal distribution of sensors and actuators.
4. Reduction of the search space in the optimisation problem has also never been investigated.
5. Furthermore, investigation of the optimal number, placement and feedback gain of sensor/actuator pairs for flexible structures

Table 2.2 Main previous studies focusing on the optimal configurations of sensors and actuators for plates and shells

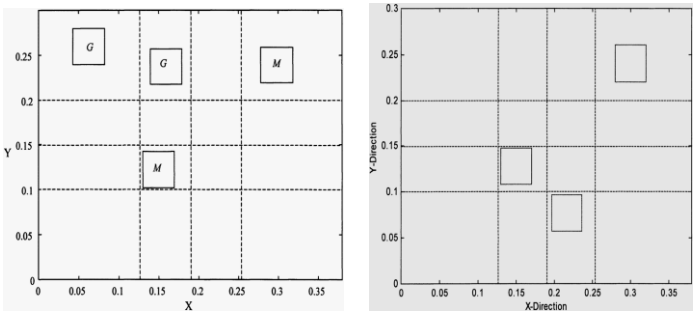

[25]

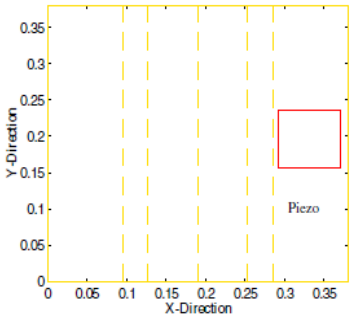

[30]

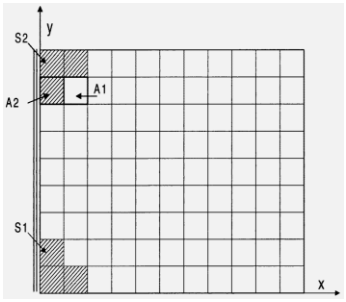

[26]

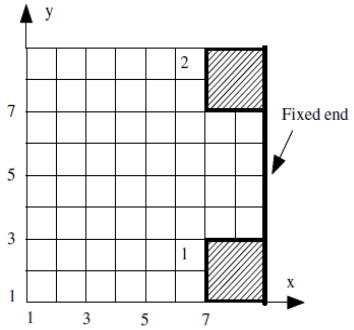

[54]

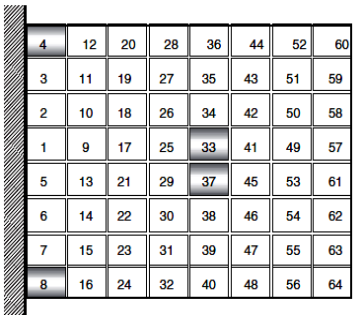

[35]

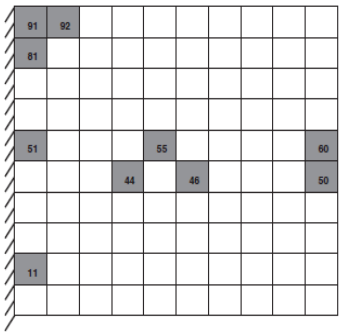

[38]

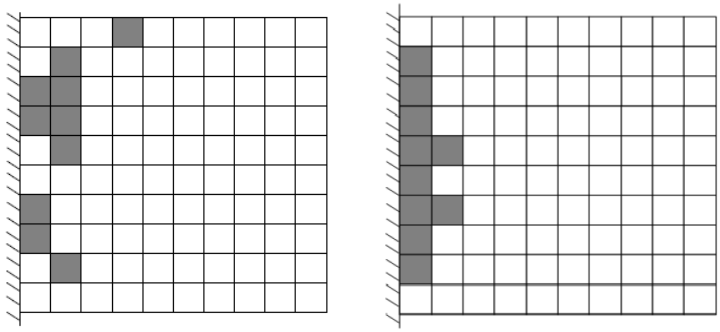

[66]

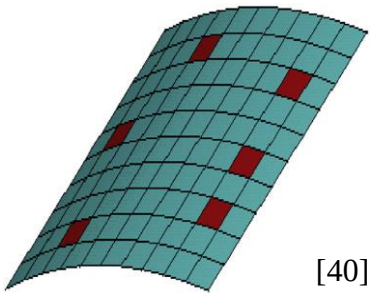

[40]

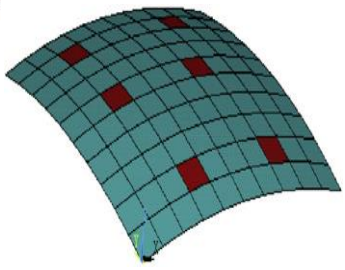

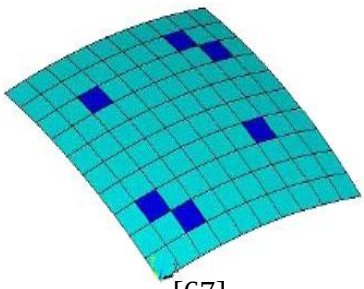

[67]

2.10. Active Vibration Control of Stiffened Plates and Shells

Plates and shells stiffened by beams have been used intensively in the manufacturing of mechanical structures with high specific strength. Recently, these structures have been investigated extensively using powerful numerical methods such as the finite element in order to improve their static and dynamic characteristics. Sadek and Tawfik reported that the finite element method has given more accurate and reasonable results than all other numerical methods for the modelling of stiffened plates. The modelling of the plate and stiffener separately while retaining compatibility between them achieves high model accuracy [68]. The analytical solution for stiffened plates with geometrical non-linearity subjected to transverse loading is very difficult to find, and the finite element method is adaptable and accurate enough to solve such complex problems, but it requires considerable computational effort and large computer memory [69]. Lots of studies have investigated plates and shells stiffened by beams to improve specific strength and dynamic characteristics. However, only a limited number of studies have been published on research into the active vibration control of plates and shells stiffened by beams.

Birman and Adali studied an orthotropic plate stiffened by piezoelectric actuators placed opposite to the plate surface and symmetrically distributed with respect to the plate's middle plane, as shown in Figure 2.11. The stiffener-actuator was activated by applying a voltage. They reported that increasing actuator voltage and the width of stiffener-actuators led to reduced vibration suppression time [70].

Beams, plates and cylinders stiffened by piezoelectric beams were studied theoretically and experimentally by Young and Hansen. Their beam stiffener had a flange and actuators were placed between the stiffener flange and the plate, and a row of error sensors was located near the stiffener as shown in Figure 2.12. The authors found that one row of piezoelectric stiffeners and one row of error sensors was quite enough to suppress vibration in the beams and plates, but a cylinder required three or four rows to suppress vibration. However, they reported that the locations of piezoelectric stiffeners and error sensors are inconvenient for many modes of vibration [71]. These sensors and actuators required be located efficiently on the stiffened plate in order to account for the effects of all the modes to be attenuated, using optimisation methods based on appropriate fitness and objective functions in order to achieve efficient vibration suppression.

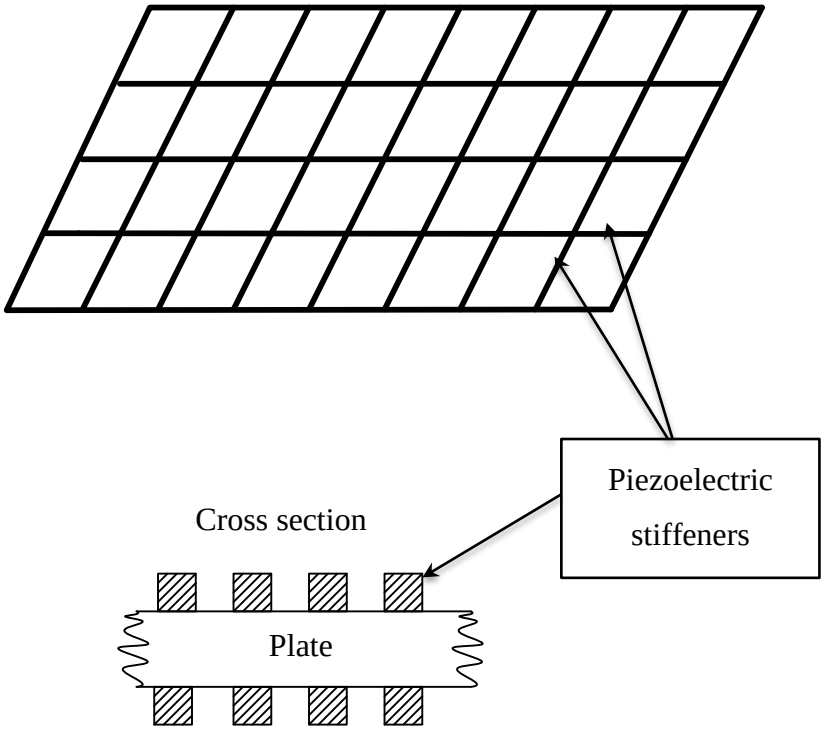

Figure 2.11The geometry of the stiffened plate[70]

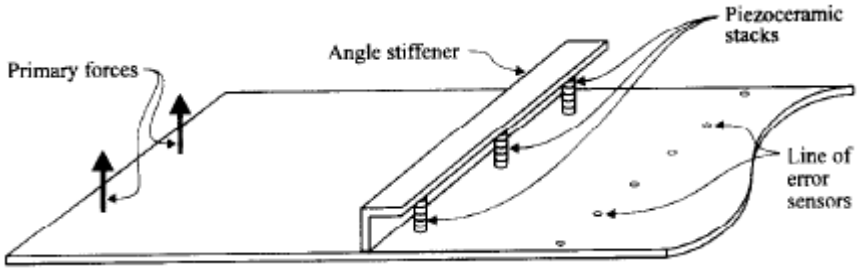

Figure 2.12 Application of piezoelectric stack actuator vibration control to a plate [71]

Mukherjee et al investigated the active vibration control of piezolaminated stiffened plates, but neglected the coupling between the direct and converse piezoelectric effects. The beam stiffener could take any direction on the plate and did not need to pass through nodal elements. Displacement and negative velocity feedback control were used to suppress vibration and they identified the problem that this tended to excite higher order modes [72].

The most recent study in this area was conducted in 2010 by Balamurugan and Narayanan, who considered active vibration control for a composite shell and plate stiffened by beams with distributed piezoelectric sensor/actuator pair bonded to its surfaces. The stiffener was positioned anywhere within the shell element along lines of natural coordinates. A number of examples was studied of cantilever stiffened plates and cylindrical shells bonded to partial and full coverage piezoelectric sensor and actuator to attenuate the first eight modes of vibration using optimal linear quadratic control, as shown in Figure 2.13. They reported that these structures with full coverage sensor and actuator did not detect vibration and actuate the structure effectively for all the modes. This was because of the elimination of sensor voltage for some modes in full coverage [73].

Balamurugan and Narayanan assumed that the value of the open loop damping ratio of the plates and shells would be 0.1% for all of the first eight modes during the investigation. They found that the closed loop damping ratio increased to 6.5% at the second and third modes, while for the other modes it increased by between 0.1% to 2% using linear quadratic optimal control. This improvement in the closed loop damping ratio could be considered insufficient considering the high value of the linear quadratic control weighted matrix required ($Q = 10^{10}$) and this improvement in damping ratio was found only for the best configuration of partial coverage by sensor and actuator in the example shown in Figure 2.13 (c). Moreover, the structures with arbitrary coverage of sensor and actuator layers of 0.25mm in thickness increased the material cost and structural weight. However, these drawbacks in terms of material costs, structural weight and control system performance could be solved by locating discrete sensors and actuators in efficient locations.

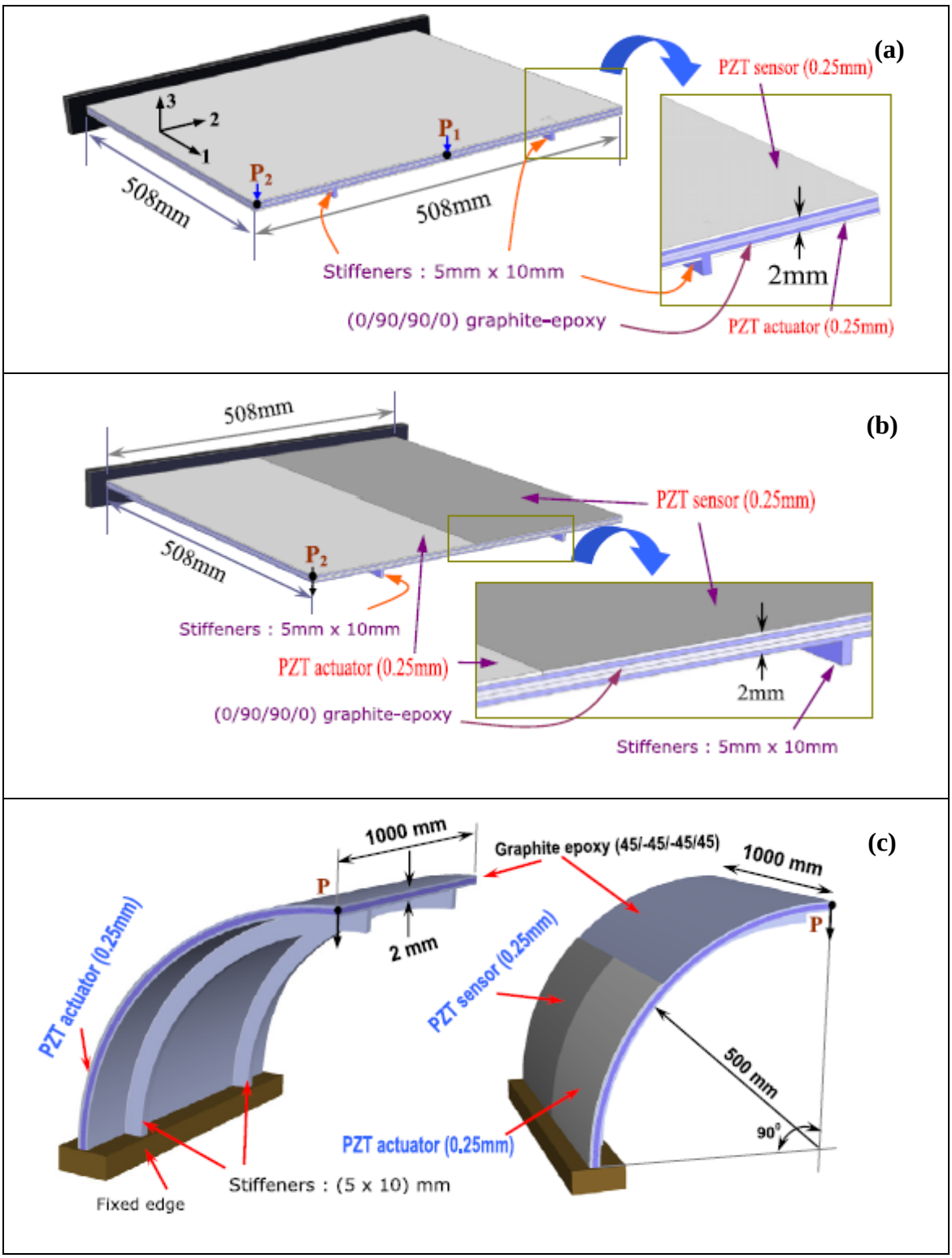

Figure 2.13 Cantilever stiffened composite plate and cylindrical shell, full and partially covered with piezoelectric sensors and actuators [73]

Limited studies [70-73] have focused on plates and shells stiffened by beams and bonded to piezoelectric sensor/actuator pair distributed over the whole surface area of the structure or randomly located at discrete points on the surface. However, many studies have drawn attention to the importance of discrete sensors and actuators and

their location in achieving high sensing and actuating effects with low feedback voltage, high response and stability.

Meirovitch [74] stated that misallocated sensors and actuators cause problems such as lack of observability, controllability and spillover, and also that Tzou and Fu [75] showed that the structure fully covered with single sensor and actuator cannot control some vibrational modes because of the lack of observability and controllability[26]. Junkins and Kim said that the optimisation of the number and locations of sensors and actuators is a significant area of research in suppressing mechanical vibration in flexible structures. whereas randomly choosing their number and location may degrade system performance and limit the range of practical applications[76]. Lim investigated vibration reduction in a clamped square plate, and found that discrete piezoelectric sensor/actuator pairs in specified locations achieved higher control effects, required less power and were lighter in weight than fully distributed piezoelectric layers [77].

Shen and Homaifar reported that active damping control and lightweight structures are achieved by the use of discrete point piezoelectric sensors and actuators [78, 79]. Balamurugan and Narayanan found that a full coverage piezoelectric sensor or actuator layer bonded on the surface of various types of composite structures, including flat and stiffened plates and shells, gave low sensing and control effects for all modes of vibration [73, 80]. Kumar and Narayanan stated that the placement of sensors and actuators has an important effect on the performance of the control system and if misplaced , this led to problems such as lack of observability and controllability [38].

Kumar et al showed that controllability depends on the area covered by the piezoelectric sensor/actuator. Moreover, increasing the area beyond a certain limit does not improve controllability, so that the use of piezoelectric patches near the free end of a cantilever cylindrical shell has little effect [50]. Moheimani found that the increased length of the piezoelectric layer bonded on a beam leads to zero controllability for some modes[81]. Kapuria and Yasin reported that the closed loop response exhibits faster attenuation when multi-segment electrodes are used rather than a single-segment electrode for the same gain and for all control laws [82, 83].

From this discussion, it is clear that the literature indicates two significant points: firstly, the importance of using discrete sensors and actuators located efficiently on a structure in order to optimise active vibration control; and secondly, the fact that the active vibration control of stiffened plates by optimally placed discrete sensors and actuators has never been investigated.

2.11. Control Scheme

A high performance control system can be achieved by designing a control scheme after the determination of the optimal locations of sensors and actuators. This is realised by determination of optimum values of feedback gain to attenuate vibration and to bring the closed loop poles of the control system to the stable region.

Classical direct proportional feedback, negative-gain velocity feedback and optimal linear quadratic control schemes have been implemented in several studies [38, 39, 84, 85] to attenuate vibration in flexible structures and it has been reported that optimal linear quadratic control gives higher effective and lower actuator peak voltage than the classical approach. Active vibration control was investigated by Kapuria and Yasin for a cantilever fibre reinforced plate fully covered with multi-segment piezoelectric sensors/actuator pairs. It was found that this multiple piezoelectric segmentation gives faster vibration suppression for the same gain in classical direct feedback control and for the same output weighted parameters of the optimal linear quadratic control [83].

Vibration suppression of a composite cantilever beam with a single sensor/actuator pair bonded near the beam root was investigated theoretically and experimentally by Zabihollah et al using an optimal linear quadratic control scheme. They said that this is most efficient control scheme to find the optimal feedback control gain matrix [86].

Active vibration suppression in a fully clamped composite plate with five randomly located piezoelectric pairs using an optimal linear quadratic control scheme was investigated by Uyanik. He reported that the active damping may become unstable as a result of large values in the control gain matrix and that it is necessary to explore the optimum feedback gain matrix in order to suppress vibration effectively with stable active damping [87]. In an optimal linear quadratic control scheme, the optimum feedback control matrix is related to the optimal location of actuators and is not so easy to determine using an optimisation method such as genetic algorithms.

Han and Lee experimentally investigated active vibration control of a cantilever plate by optimally placed sensors and actuators using classical proportional feedback control and this significantly suppressed vibration at the first five modes [26] .

The literature identifies three important points about active vibration control of flexible structures: firstly, the importance of using discrete rather than distributed sensor/actuator; then the need to find optimal locations for the sensor/actuators on a structure rather than locating them randomly; and finally the type of control scheme has a significant effect on the effectiveness of the sensor/actuators for vibration suppression.

In this study, an optimal linear quadratic control scheme was implemented to optimise the discrete piezoelectric actuators and controller feedback gain matrix in order to suppress vibration effectively, as explained in chapter three.

The placement and feedback gain was determined based on the reduced modal system using modal instead of physical coordinates. The modelling of a smart structure using the finite element method produces many hundreds or thousands of coupled equations and requires a large computational effort to study the response of the first modes. A powerful alternative method is to convert the dynamic system of equations from coupled physical coordinates to uncoupled modal coordinates. This reduced modal method is used in most of this work to find optimal locations for sensors and actuators and vibration suppression in a range of continuous flexible structures.

2.12. Conclusions

This chapter identifies the sources of mechanical vibration in engineering systems and describes solutions to reduce their effects an mechanical structures and human beings. This study deals with the reduction of structural vibration caused by resonance, by construction of intelligent mechanical structures which work by detecting disturbance signals and suppressing vibration actively. This involves many topics, including, smart materials, types of structures and the methods used to find solutions. From the literature review it is clear that many relevant topics have not yet been properly investigated. These research topics are summarised as follows:

1. The determination and identification of the global optimal distribution of sensors and actuators on flexible structures.
2. Investigation of the effects of the dynamic axes of symmetry of structures on the global optimal distributions of sensors and actuators.
3. Investigation of active vibration reduction in stiffened plates, with and without symmetry, by the optimal placement of sensors and actuators.
4. Investigation the effect of the dynamic axes of symmetry of plates and shells on the global optimal distribution of sensors and actuators.
5. Investigation of reducing the search space in the optimisation problem for active vibration control in flexible structures.
6. Investigation of the optimal number, placement and feedback gain of sensor/actuator pairs for flexible structures.

Chapter 3. Modelling

The optimisation of vibration reduction is an important research aim, and it can be achieved by optimally locating discrete sensors and actuators on a flexible structure. However, finding optimal locations for such sensors and actuators requires perfect modelling in order to implement optimisation methods such as genetic algorithms. It is clear from the literature that flexible structures such as beams, plates and shells have been investigated thoroughly, whereas plates stiffened by beams bonded with discrete sensors and actuators have never been optimised.

In this chapter, a new type of dynamic modelling is developed for stiffened plates with discrete piezoelectric sensor/actuator pairs. An isotropic plate element stiffened by a number of beam elements on its edges and having a discrete piezoelectric sensor and actuator pair bonded to its surface is modelled using the finite element method and Hamilton's principle, taking into account the effects of piezoelectric mass, stiffness and electromechanical coupling. The modelling is based on first order shear deformation theory taking into account bending, membrane and shear deformation effects. This model could be implemented for flat plates with or without stiffening by beams bonded to its surface, with discrete sensors and actuators in different configurations. In chapter four, the derived model is tested for flat and stiffened plates and the results are compared with those of both the ANSYS finite element package and experimental tests. Moreover, the foundations are also laid for the optimisation of sensors, actuators and vibration reduction in chapters five to ten.

3.1. Introduction

The modelling of smart structures with distributed piezoelectric sensor/actuator pair has been investigated in detail for the suppression of mechanical vibration. An earlier investigation of the dynamic equation for piezoelectric electroelasticity was formulated by Allik and Hughes in 1970 using finite solid tetrahedral element and a variational method [88]. Lee analytically modelled a flexible laminated plate with a distribution of piezoelectric sensor/actuator bonded to it in order to achieve the distributed control and sensing of bending, torsion, shearing, shrinking and stretching based on classical laminated thin plate theory [89]. Tzou and Tseng modelled a mechanical structure (plate/shell) with bonded distributed piezoelectric sensor/actuator pair using the finite element method and Hamilton's principle. They proposed a new piezoelectric finite thin solid element model which includes an internal nodal electric degree of freedom [90].

Ha et al studied a laminated composite plate containing distributed piezoelectric ceramics using eight-node brick finite elements to investigate static and dynamic response under mechanical and electrical loading [91]. Detwiler et al modelled a laminated composite plate containing distributed piezoelectric sensor/actuator using the finite element method and a variational principle based on first order shear deformation theory. Quadrilateral isoparametric four node elements with single voltage degree of freedom per piezoelectric layer was used in the modelling [92]. Reddy proposed an analytical formulation, the Navier solution and the finite element models for a composite plate with a distributed piezoelectric sensor/actuator layer based on classical, first and third order shear deformation theories. Simple negative velocity feedback was applied to control the dynamic response of the structure [93].

He et al researched shape and active vibration control of plate material functionally graded in the thickness direction with distributed piezoelectric material using the finite element method based on classical laminated plate theory for shape and vibration control. A constant velocity feedback control scheme was applied to study the dynamic response of a plate [94]. Moita et al investigated a thin laminated structure with integrated piezoelectric sensor and actuator layers based on Kirchhoff's classical laminate theory and finite element analysis. A triangular finite element was proposed with electric voltage single degree of freedom per layer. Negative constant velocity feedback was used to suppress vibration for a composite beam and plate fully covered with discrete sensor/actuator pairs [95]. Kumar et al studied composite plates and shells with a bonded piezoelectric sensor/actuator layer using Hamilton's principle and finite element analysis based on first order shear deformation theory, including an investigation of the effects of mechanical, electrical and thermal loading. Negative velocity feedback control was used for shape control and the suppression of vibration in a cylindrical shell bonded with discrete piezoelectric sensor/actuator pairs. They reported that the controllability depends on the coverage area of sensor/actuator [50]. Recently, multilayers of piezolaminated smart composite shells have been investigated by Balamurugan and Narayanan using higher order shear deformation theory and finite elements. Quadratic variation of electric potential was assumed across the thickness of piezoelectric element. Static and dynamic responses were investigated for various composite shells fully and partially covered with piezoelectric layer. The suppression of the first eight modes of vibration was investigated for a cantilever composite cylindrical shell partially bonded with single sensor and actuator using optimal linear quadratic control. They reported that the vibration reduction achieved just for the second and the

third modes and no reduction for the other modes, but effective vibration control for greater number of modes can be achieved by optimising the size and location of sensors and actuators [80].

There is limited research on the active vibration control of plates and shells stiffened by beams. Researchers [70-73] have investigated plates and shells stiffened by beams bonded with piezoelectric sensor/actuator pair distributed over the whole surface or arbitrarily located at discrete points on the surface, and the details of these studies are explained in section 2.10. High control performance and optimality are achieved by placing discrete piezoelectric sensors/actuators in appropriate locations on a structure. Limited studies have been published concerning optimising the location of piezoelectric sensors and actuators on plates, shells and beams to achieve better responses, higher stability and lower controller power. However, the optimisation of the location for discrete piezoelectric sensors and actuators on a plate stiffened by beams has never been investigated.

3.2. Stiffened Plate Model

Consider a flexible plate stiffened by a number of beams with a number of discrete piezoelectric sensor/actuator pairs bonded to it. The stiffened plate is discretised into finite elements, with each plate element having the possibility of being stiffened at one or more of its edges by between zero and four beam elements, with a piezoelectric sensor/actuator pair bonded to the plate element as shown in Figure 3.1. The assumptions of this model could be listed as follows:

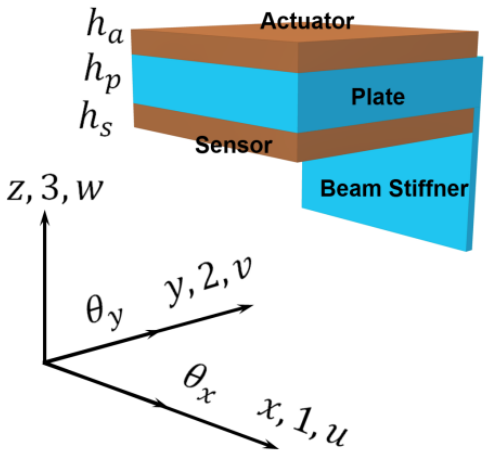

Figure 3.1 Plate element stiffened by beam with a piezoelectric sensor/actuator pair bonded to the surfaces

1. The piezoelectric elements are bonded tightly to the plate element.
2. The beam stiffener elements are fixed to the plate element edges.
3. The element nodal offset between the plate and beam stiffener is taken into consideration, while the nodal offset between the piezoelectric element and plate is very small and is ignored.
4. The plate, beam and piezoelectric patch are analysed according to first order shear deformation theory taking into account the effects of bending, membrane and shear deformation effects.

3.2.1. Plate element

Plate element displacements are a function of the point coordinates and time, as described in equation 3.1, where u, v, w are element displacements in the x, y and z directions respectively as function of x, y, z and time t. However, u_0, v_0, w_0, θ_x and θ_y are displacements and rotations in the mid-plate surface as a function of x, y, t at $z = 0$. Figure 3.2 shows a section in the xz-plane of the plate before and after deformation to clarify the element displacement $u(x, y, z, t)$.

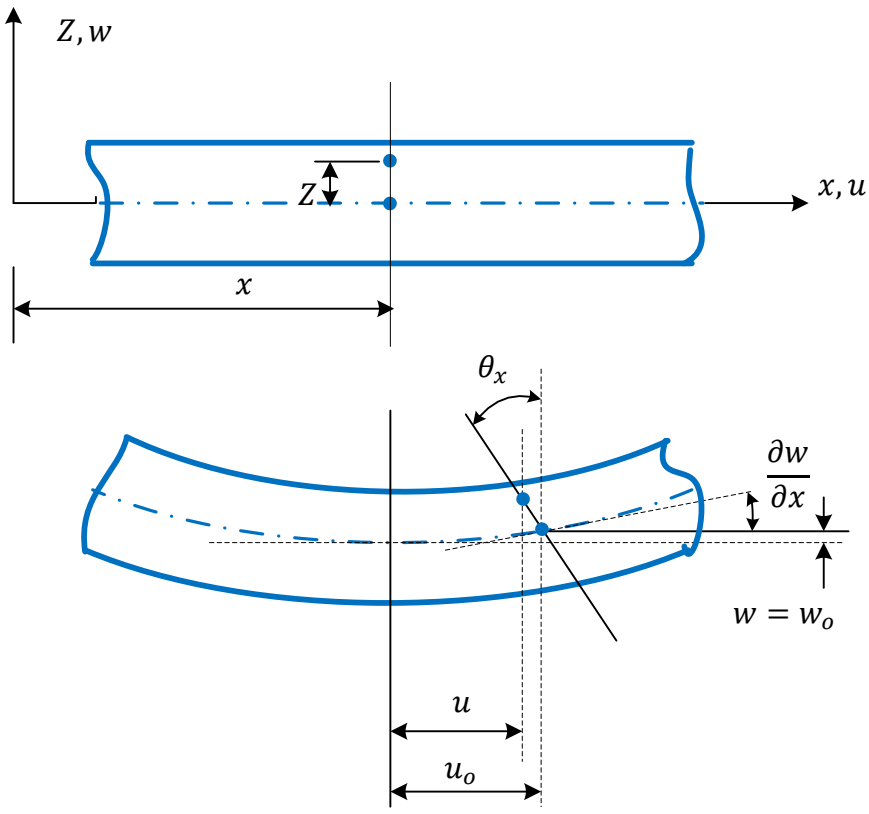

Figure 3.2 Plate section in the x-direction before and after deformation [93]

$$u(x,y,z,t) = u_o(x,y,t) - z\theta_x(x,y,t),$$
$$v(x,y,z,t) = v_o(x,y,t) - z\theta_y(x,y,t)\,, \qquad 3.1$$
$$w(x,y,z,t) = w_o\,(x,y,t)$$

An isoparametric four-node element is chosen for modelling as shown in Figure 3.3. The figure shows a quadrilateral four-node element in the x-y coordinates and its mapping in natural s-r coordinates which vary between 1 and -1.

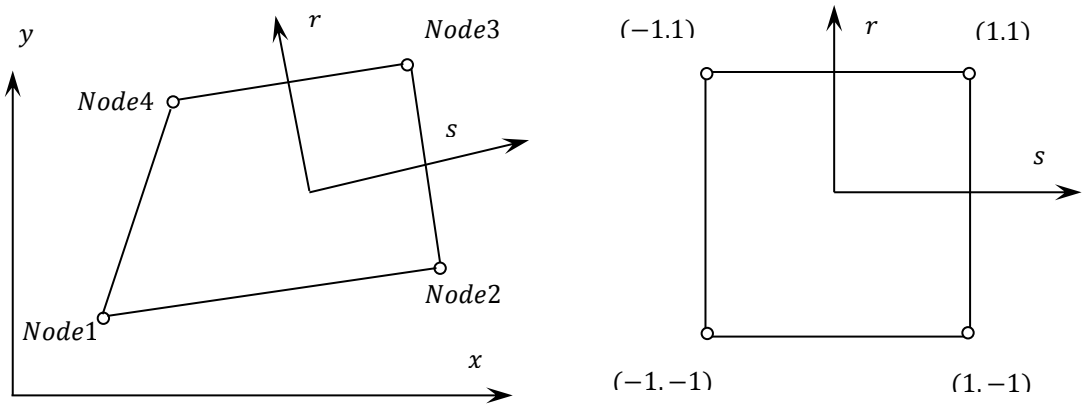

Figure 3.3 Four nodes two-dimensional mapping element from x-y to s-r coordinates [96]

The general element displacements u_0, v_0, w_0, θ_x and θ_y at the mid-plate surface are related to nodal displacements $u_{0i}, v_{0i}, w_{0i}, \theta_{xi}$ and θ_{yi} by a function called the element shape function $N_i(s,r)$, as shown in the following equations.

$$\begin{Bmatrix} u_o \\ v_o \\ w_o \end{Bmatrix} = \sum_{i=1}^{4} N_i(s,r) \begin{Bmatrix} u_{oi} \\ v_{oi} \\ w_{oi} \end{Bmatrix}, \qquad \begin{Bmatrix} \theta_x \\ \theta_y \end{Bmatrix} = \sum_{i=1}^{4} N_i(s,r) \begin{Bmatrix} \theta_{xi} \\ \theta_{yi} \end{Bmatrix} \qquad 3.2$$

$$\begin{Bmatrix} x \\ y \end{Bmatrix} = \sum_{1}^{4} N_i(s,r) \begin{Bmatrix} x_i \\ y_i \end{Bmatrix}$$

$$\begin{Bmatrix} \frac{\partial x}{\partial s} \\ \frac{\partial y}{\partial s} \end{Bmatrix} = \sum_{i=1}^{4} \frac{\partial N_i(s,r)}{\partial s} \begin{Bmatrix} x_i \\ y_i \end{Bmatrix} \quad , \quad \begin{Bmatrix} \frac{\partial x}{\partial r} \\ \frac{\partial y}{\partial r} \end{Bmatrix} = \sum_{i=1}^{4} \frac{\partial N_i(s,r)}{\partial r} \begin{Bmatrix} x_i \\ y_i \end{Bmatrix} \qquad 3.3$$

$$N_i = 0.25(1 + s_i s)(1 + r_i r)$$

$$\frac{\partial N_i}{\partial s} = 0.25(1 + r_i r)\, s_i \qquad , \frac{\partial N_i}{\partial r} = 0.25(1 + s_i s)\, r_i$$

$$N_1 = 0.25(1 - s)(1 - r), \quad N_2 = 0.25(1 + s)(1 - r) \tag{3.4}$$

$$N_3 = 0.25(1 + s)(1 + r), \quad N_4 = 0.25(1 - s)(1 + r)$$

For the isoparametric element, the element displacements and coordinates x, y are related to nodal displacements and coordinates respectively by the same shape function $N_i(s, r)$. The shape function describes the element's geometry in terms of the natural coordinates s, r, which vary between -1 and 1. The strain deformation induced in a plate element as a result of bending, membrane and shear deformation effects could be described by equations 3.5- 3.7:

$$\varepsilon = \begin{Bmatrix} \dfrac{\partial u}{\partial x} \\ \dfrac{\partial v}{\partial y} \\ \dfrac{\partial u}{\partial y} + \dfrac{\partial v}{\partial x} \end{Bmatrix} = \begin{Bmatrix} \dfrac{\partial u_o}{\partial x} - z\dfrac{\partial \theta_x}{\partial x} \\ \dfrac{\partial v_o}{\partial y} - z\dfrac{\partial \theta_y}{\partial y} \\ \dfrac{\partial u_o}{\partial y} + \dfrac{\partial v_o}{\partial x} - z\left(\dfrac{\partial \theta_x}{\partial y} + \dfrac{\partial \theta_y}{\partial x}\right) \end{Bmatrix} \tag{3.5}$$

$$\varepsilon = \sum_{i=1}^{4} (B_{mi}\delta_i + zB_{bi}\delta_i) = B_m\delta \; + zB_b\delta \tag{3.6}$$

$$\gamma = \begin{Bmatrix} \dfrac{\partial w}{\partial x} - \theta_x \\ \dfrac{\partial w}{\partial y} - \theta_y \end{Bmatrix} = \sum_{i=1}^{4} B_{shi}\delta_i \; = B_{sh}\delta \tag{3.7}$$

Here the subscripts b, m, sh and i denote bending, membrane, shear strain and element nodal numbering respectively. It can be seen from equation 3.2 that the element displacements are a function of the natural coordinates s and r. However, the element strain given by equations 3.5-3.7 is a partial differential of the element displacement with respect to the Cartesian coordinates x or y. A matrix called the Jacobian matrix J gives a differential operator solution utilising the chain rule applied to partial differentiation as follows.

$$\frac{\partial N_i}{\partial s} = \frac{\partial N_i}{\partial x}\frac{\partial x}{\partial s} + \frac{\partial N_i}{\partial y}\frac{\partial y}{\partial s} \quad , \quad \frac{\partial N_i}{\partial r} = \frac{\partial N_i}{\partial x}\frac{\partial x}{\partial r} + \frac{\partial N_i}{\partial y}\frac{\partial y}{\partial r} \tag{3.8}$$

$$\begin{bmatrix} \frac{\partial N_i}{\partial s} \\ \frac{\partial N_i}{\partial r} \end{bmatrix} = J \begin{bmatrix} \frac{\partial N_i}{\partial x} \\ \frac{\partial N_i}{\partial y} \end{bmatrix} \quad , \quad J = \begin{bmatrix} \frac{\partial x}{\partial s} & \frac{\partial y}{\partial s} \\ \frac{\partial x}{\partial r} & \frac{\partial y}{\partial r} \end{bmatrix} \tag{3.9}$$

$$\begin{bmatrix} \frac{\partial N_i}{\partial x} \\ \frac{\partial N_i}{\partial y} \end{bmatrix} = J^{-1} \begin{bmatrix} \frac{\partial N_i}{\partial s} \\ \frac{\partial N_i}{\partial r} \end{bmatrix} \tag{3.10}$$

The Jacobian derivative matrix J relates the differentials of the shape function with respect to the Cartesian coordinates x and y to those with respect to the natural coordinates s and r [96].

$$B_{mi} = \begin{bmatrix} \partial N_i/\partial x & 0 & 0 & 0 & 0 \\ 0 & \partial N_i/\partial y & 0 & 0 & 0 \\ \partial N_i/\partial y & \partial N_i/\partial x & 0 & 0 & 0 \end{bmatrix} \tag{3.11}$$

$$B_{bi} = \begin{bmatrix} 0 & 0 & 0 & -\partial N_i/\partial x & 0 \\ 0 & 0 & 0 & 0 & -\partial N_i/\partial y \\ 0 & 0 & 0 & -\partial N_i/\partial y & -\partial N_i/\partial x \end{bmatrix} \tag{3.12}$$

$$B_{shi} = \begin{bmatrix} 0 & 0 & \partial N_i/\partial x & -N_i & 0 \\ 0 & 0 & \partial N_i/\partial y & 0 & -N_i \end{bmatrix} \tag{3.13}$$

$$B_b = [B_{b1} \quad B_{b2} \quad B_{b3} \quad B_{b4}] \tag{3.14}$$

$$B_m = [B_{m1} \quad B_{m2} \quad B_{m3} \quad B_{m4}] \tag{3.15}$$

$$B_{sh} = [B_{sh1} \quad B_{sh2} \quad B_{sh3} \quad B_{sh4}] \tag{3.16}$$

$$\delta = \{\delta_1 \quad \delta_2 \quad \delta_3 \quad \delta_4\}^T \ , \ \delta_i = \{u_{oi} \quad v_{oi} \quad w_{oi} \quad \theta_{xi} \quad \theta_{yi}\}^T \tag{3.17}$$

Here B_b , B_m and B_{sh} are bending, membrane and shear differential matrices which relate element strain to element nodal displacements, and $i = 1, 2, 3, 4$ represent the element local node numbering.

3.2.2. Beam stiffener in the x-direction

The beam stiffener is also analysed according to first order shear deformation theory to include bending, membrane and shear deformation effects. The behaviour of a beam before and after deformation is similar to that of a section of plate in the x-direction, as shown in Figure 3.2. The beam is discretised into isoparametric two-node elements. The element displacements are a function of the point coordinates and time as follows:

$$u_{bx}(x,z,t) = u_{obx}(x,t) - z\theta_{xbx}(x,t),$$
$$w_{bx}(x,z,t) = w_{obx}\,(x,t) \qquad 3.18$$

$$\begin{Bmatrix} u_{obx} \\ w_{obx} \end{Bmatrix} = \sum_{i=1}^{2} N_i(s) \begin{Bmatrix} u_{obxi} \\ w_{obxi} \end{Bmatrix} \quad , \qquad \theta_{xbx} = \sum_{i=1}^{2} N_i(s)\,\theta_{xbxi} \qquad 3.19$$

$$N_i = 0.5(1 + s_i s), \qquad N_1 = 0.5(1 - s)\ , \qquad N_2 = 0.5(1 + s)$$
$$\frac{\partial N_1}{\partial s} = -0.5 \qquad , \qquad \frac{\partial N_2}{\partial s} = 0.5 \qquad 3.20$$

where u_{bx} and w_{bx} are beam element displacements in the x and z directions respectively and as a function of x, z and time t. However, u_{obx}, w_{obx} and θ_{xbx} are displacements and rotations in the mid-plane of the beam surface as a function of x and t at $z = 0$. The element bending, membrane and shear deformation effects are given in the following equations:

$$\varepsilon_{bx} = \frac{\partial u_{bx}}{\partial x} = \frac{\partial u_{obx}}{\partial x} - z\frac{\partial \theta_{xbx}}{\partial x} \qquad 3.21$$

$$\varepsilon_{bx} = B_m \delta_{bx} + z B_b \delta_{bx} \qquad 3.22$$

$$\gamma_{bx} = \frac{\partial w_{bx}}{\partial x} - \theta_{xbx} = B_{sh}\delta_{bx} \qquad 3.23$$

$$B_b = \frac{2}{L_{bx}}\begin{bmatrix} 0 & 0 & 0 & \dfrac{-\partial N_1}{\partial s} & 0 & 0 & 0 & 0 & \dfrac{-\partial N_2}{\partial s} & 0 \end{bmatrix} \qquad 3.24$$

$$B_m = \frac{2}{L_{bx}}\left[\frac{\partial N_1}{\partial s} \quad 0 \quad 0 \quad 0 \quad 0 \quad \frac{\partial N_2}{\partial s} \quad 0 \quad 0 \quad 0 \quad 0\right] \tag{3.25}$$

$$B_{sh} = \left[0 \quad 0 \quad \frac{2}{L_{bx}}\frac{\partial N_1}{\partial s} \quad -N_1 \quad 0 \quad 0 \quad 0 \quad \frac{2}{L_{bx}}\frac{\partial N_2}{\partial s} \quad -N_2 \quad 0\right] \tag{3.26}$$

$$\delta_{bx} = \{u_{obx1} \quad 0 \quad w_{obx1} \quad \theta_{xbx1} \quad 0 \quad u_{obx2} \quad 0 \quad w_{obx2} \quad \theta_{xbx2} \quad 0\}^T \tag{3.27}$$

where the subscript bx refers to the beam stiffener in the x direction. The value of the Jacobian matrix J for the beam element is equal to half the element length ($0.5L_{bx}$) and $J^{-1} = 2/L_{bx}$.

3.2.3. Beam element connection to the plate element

The beam stiffener connection to the plate has a significant role in achieving perfect structure modelling, which depends on the offset elements node points distance between plate and beam. The offset can be ignored if it is very small compared to beam length and the transfer matrix is then considered as unity. However, it requires treatment if the offset is large compared to the plate and beam dimensions. A rough estimation of the offset was used to decide whether to ignore or model its effects based on the beam length L and the offset distance between the beam and the plate mid-plane surface as follows [96]:

1. If $PB < L/100$, the offset can be safely ignored
2. If $L/100 < PB < L/5$, the offset needs to be modelled
3. If $PB > L/5$, ordinary beam, plate and shell elements should not be used. Two or three-dimensional elements should be used instead.

Consider the section shown in Figure 3.4 before and after deformation of a plate stiffened by one beam in the x-direction with an offset distance of PB between two nodes P and B on the mid-plane surface of the plate and beam respectively.

A transformation matrix is developed to relate the degrees of freedom of the beam to those of the plate according to Figure 3.4. It is assumed that the global coordinates and displacements pass through the plate element. It is also assumed that there is an imaginary link connecting the two nodal points P and B. This link is considered before and after deformation in order to determine the relationship between the degrees of freedom of the displacement for the points P and B according to Figure 3.4 as follows:.

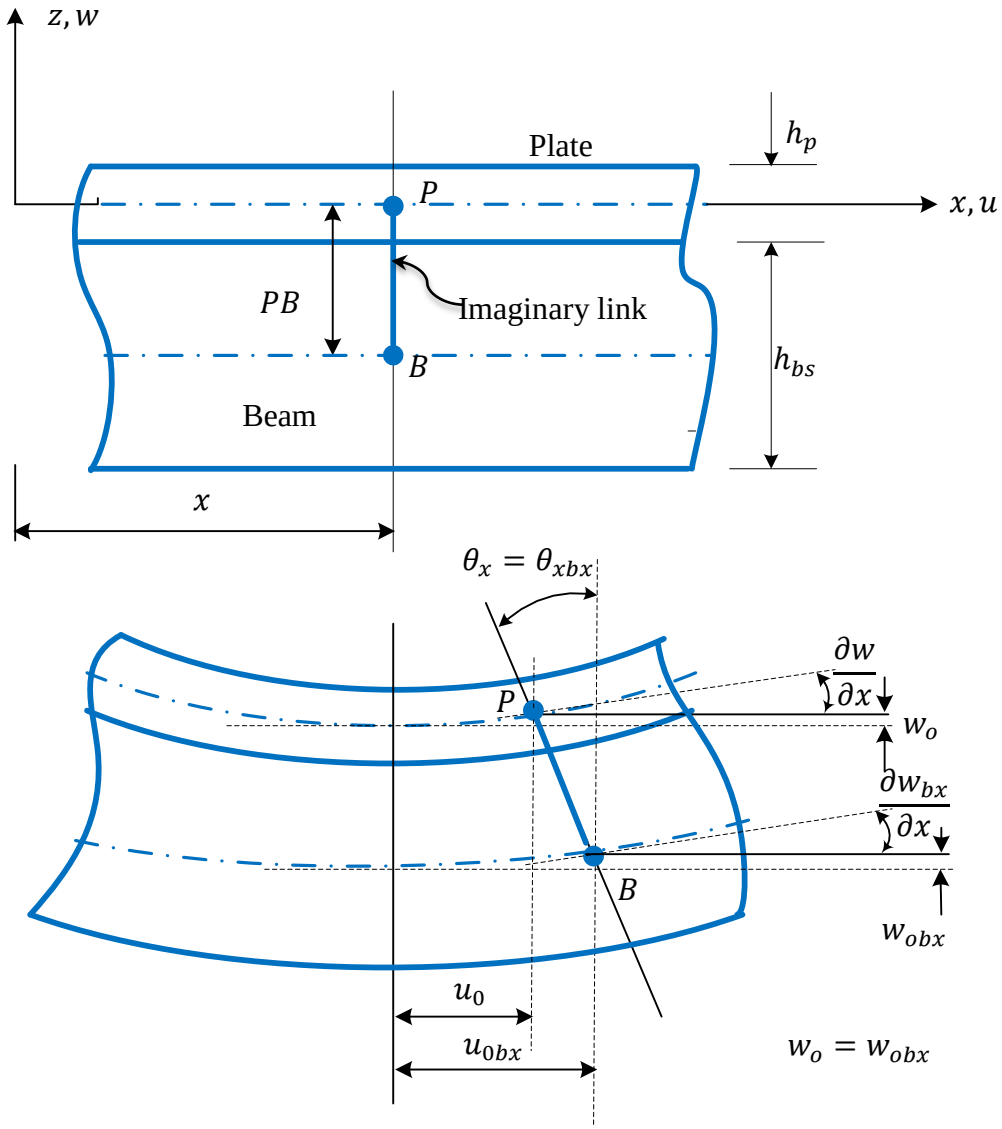

Figure 3.4 section for connection of plate and beam stiffener along the x-direction before and after deformation

$$PB = 0.5(h_p + h_{bs}) \tag{3.28}$$

$$u_o = u_{obx} - BP * \theta_{xbx} \quad , \quad \theta_x = \theta_{xbx} \quad , \quad w_o = w_{obx} \tag{3.29}$$

We rearrange equation 3.29 in matrix form as follows:

$$\begin{Bmatrix} u_o \\ v_o \\ w_o \\ \theta_x \\ \theta_y \end{Bmatrix} = \begin{bmatrix} 1 & 0 & 0 & -BP & 0 \\ 0 & 0 & 0 & 0 & 0 \\ 0 & 0 & 1 & 0 & 0 \\ 0 & 0 & 0 & 1 & 0 \\ 0 & 0 & 0 & 0 & 0 \end{bmatrix} \begin{Bmatrix} u_{obx} \\ 0 \\ w_{obx} \\ \theta_{xbx} \\ 0 \end{Bmatrix} \tag{3.30}$$

$$\delta = T_x \delta_{bx} \quad , \quad T_x = \begin{bmatrix} T_{x1} & 0 \\ 0 & T_{x1} \end{bmatrix} \tag{3.31}$$

$$T_{x1} = \begin{bmatrix} 1 & 0 & 0 & -BP & 0 \\ 0 & 0 & 0 & 0 & 0 \\ 0 & 0 & 1 & 0 & 0 \\ 0 & 0 & 0 & 1 & 0 \\ 0 & 0 & 0 & 0 & 0 \end{bmatrix} \tag{3.32}$$

$$\delta_{bx} = T_x^{-1} \delta = T_{bx} \delta \tag{3.33}$$

$$\delta = \{\delta_1 \quad \delta_2\}^T \tag{3.34}$$

The transformation matrix for the beam stiffener in the y-direction is;

$$v_o = v_{oby} - BP * \theta_{yby} \quad , \quad \theta_y = \theta_{yby} \quad , \quad w_o = w_{oby} \tag{3.35}$$

$$\begin{Bmatrix} u_o \\ v_o \\ w_o \\ \theta_x \\ \theta_y \end{Bmatrix} = \begin{bmatrix} 0 & 0 & 0 & 0 & 0 \\ 0 & 1 & 0 & 0 & -BP \\ 0 & 0 & 1 & 0 & 0 \\ 0 & 0 & 0 & 0 & 0 \\ 0 & 0 & 0 & 0 & 1 \end{bmatrix} \begin{Bmatrix} 0 \\ v_{oby} \\ w_{oby} \\ 0 \\ \theta_{yby} \end{Bmatrix} \tag{3.36}$$

$$\delta = T_y \delta_{by} \quad , \; T_y = \begin{bmatrix} T_{y1} & 0 \\ 0 & T_{y1} \end{bmatrix}, \qquad T_{y1} = \begin{bmatrix} 0 & 0 & 0 & 0 & 0 \\ 0 & 1 & 0 & 0 & -BP \\ 0 & 0 & 1 & 0 & 0 \\ 0 & 0 & 0 & 0 & 0 \\ 0 & 0 & 0 & 0 & 1 \end{bmatrix} \tag{3.37}$$

$$\delta_{by} = T_y^{-1} \delta = T_{by} \delta$$

$$\delta_{by} = \{0 \quad v_{oby1} \quad w_{oby1} \quad 0 \quad \theta_{yby1} \quad 0 \quad v_{oby2} \quad w_{oby2} \quad 0 \quad \theta_{yby2}\}^T \tag{3.38}$$

where T_{bx} and T_{by} are transformation matrices for the beam stiffener in the x and y-directions respectively. So, equation 3.33 is substituted in equations 3.22 and 3.23 to get beam element strain in terms of plate degrees of freedom.

$$\gamma_{bx} = B_{sh} T_{bx} \delta \tag{3.39}$$

$$\varepsilon_{bx} = B_m T_{bx} \delta + z B_b T_{bx} \delta \tag{3.40}$$

3.3. Piezoelectric Constitutive Equations

Various piezoelectric materials and applications have been developed since their original discovery, and they have become a popular and essential part of control system applications. The linear constitutive equation 3.41 describes the coupling relationship between the electrical and mechanical behaviour of piezoelectric material [97].

$$\sigma = C^E\,\varepsilon - e^T E \qquad , \qquad D = e\,\varepsilon + \mu^\sigma\, E \tag{3.41}$$

Where σ, ε, D and E are stress, strain, electrical displacement and electric field vectors respectively. $C, e,$ and μ are elasticity, piezoelectric and permittivity matrices. Superscripts E and σ indicate that measurements are taken under constant electrical displacement and stress respectively. Piezoelectric material coordinates 1, 2, 3 or x, y, z is shown in Figure 3.1. Equation 3.41 can be rearranged into a non-coupled form, according to the assumptions of first order shear deformation theory that the normal stress in the z-direction σ_{zz} is equal to zero and eliminating ε_{zz} by condensation. Also, the polarisation direction of piezoelectric transducer is just in the z-direction, which leads the values of D_x and D_y to be equal to zero. Substituting these values in equation 3.41 we obtain the following [98, 99] .

$$\begin{Bmatrix}\sigma_{xx}\\ \sigma_{yy}\\ \tau_{xy}\end{Bmatrix} = \begin{bmatrix}\bar{C}_{11} & \bar{C}_{12} & 0\\ \bar{C}_{21} & \bar{C}_{22} & 0\\ 0 & 0 & \bar{C}_{33}\end{bmatrix}\begin{Bmatrix}\varepsilon_{xx}\\ \varepsilon_{yy}\\ \gamma_{xy}\end{Bmatrix} - \begin{bmatrix}0 & 0 & \bar{e}_{13}\\ 0 & 0 & \bar{e}_{23}\\ 0 & 0 & 0\end{bmatrix}\begin{Bmatrix}0\\ 0\\ E_z\end{Bmatrix} \tag{3.42}$$

$$\begin{Bmatrix}\tau_{yz}\\ \tau_{xz}\end{Bmatrix} = \begin{bmatrix}\bar{C}_s & 0\\ 0 & \bar{C}_s\end{bmatrix}\begin{Bmatrix}\gamma_{yz}\\ \gamma_{xz}\end{Bmatrix} \tag{3.43}$$

$$D_z = \begin{bmatrix}0 & 0 & 0\\ 0 & 0 & 0\\ \bar{e}_{13} & \bar{e}_{23} & 0\end{bmatrix}\begin{Bmatrix}\varepsilon_{xx}\\ \varepsilon_{yy}\\ \gamma_{xy}\end{Bmatrix} + \bar{\mu}^\sigma_{33}E_z \tag{3.44}$$

$$\bar{C}_{11} = C^{\,E}_{11} - \frac{{C^{\,E}_{13}}^2}{C^{\,E}_{33}} \qquad , \qquad \bar{C}_{12} = C^{\,E}_{12} - \frac{{C^{\,E}_{13}}^2}{C^{\,E}_{33}},$$
$$\bar{C}_{33} = \frac{C^{\,E}_{11} - C^{\,E}_{12}}{2} \qquad , \qquad \bar{C}_s = k(C^{\,E}_{55} - \frac{{e_{15}}^2}{\mu^\sigma_{11}}) \tag{3.45}$$

$$\bar{e}_{13} = e_{31} - \frac{C^{\,E}_{13}}{C^{\,E}_{33}}e_{33} \quad , \quad \bar{e}_{23} = \bar{e}_{13} \quad , \quad \bar{\mu}^\sigma_{33} = \mu^\sigma_{33} + \frac{{e_{33}}^2}{C^{\,E}_{33}} \tag{3.46}$$

3.4. Kinetic and Strain Energy

Hamilton's principle and the finite element method are applied to a plate element with a bonded piezoelectric sensor/actuator pair which is stiffened by a number of beams, in order to obtain the dynamic equilibrium equations and controller state space matrices. The following Hamilton's equation was used by Tzou and Tseng to model a plate fully covered by a distributed piezoelectric sensor/actuator pair [90]:

$$\int_{t1}^{t2} \Delta(\mathcal{L} + \mathrm{VW})\mathrm{dt} = \int_{t1}^{t2} \Delta\,(\mathrm{KE} - \mathrm{SE} + \mathrm{EE} + \mathrm{VW})\mathrm{dt} = 0 \qquad 3.47$$

The total kinetic energy *KE* in a plate element, including the sensor and actuator and beam stiffener is:

$$KE = KE_p + KE_s + KE_a + KE_{bs} \qquad 3.48$$

$$KE_p = 0.5\rho_p \int \left(\dot{u}_o^2 + \dot{v}_o^2 + \dot{w}_o^2 + z^2\dot{\theta}_x^2 + z^2\dot{\theta}_y^2\right) dz dA \qquad 3.49$$

$$KE_p = 0.5\dot{\delta}^T \rho_p \int N^T Z N\, \dot{\delta}\, dz dA \qquad 3.50$$

$$KE_p = 0.5\dot{\delta}^T M_p \dot{\delta} \qquad 3.51$$

$$M_p, M_a, M_s = \sum_{i=1}^{n_g}\sum_{j=1}^{n_g} N^T\Big(\rho_p \int_{-\frac{h_p}{2}}^{\frac{h_p}{2}} Z \quad , \quad \rho_a \int_{\frac{h_p}{2}}^{\frac{h_p}{2}+h_a} Z \quad , \quad \rho_s \int_{-\frac{h_p}{2}-h_s}^{-\frac{h_p}{2}} Z\Big)\, N\, dz\, detJ w_i w_j \qquad 3.52$$

$$Z = \begin{bmatrix} \bar{Z} & & 0 & \\ & \bar{Z} & & \\ & & \bar{Z} & \\ 0 & & & \bar{Z} \end{bmatrix}, \quad \bar{Z} = \begin{bmatrix} 1 & & 0 & \\ & 1 & & \\ & & 1 & \\ 0 & & & z^2 \\ & & & & z^2 \end{bmatrix} \qquad 3.53$$

where $ng, w_i, w_j$and $detJ$ denote the number of Gaussian integration, weighted points and Jacobian determinant respectively, and the subscripts, p, a and s refer to the plate, sensor and actuator respectively.

$$KE_{bx} = 0.5\rho_p \int (\dot{u}_{obx}^2 + \dot{w}_{obx}^2 + z^2\dot{\theta}_{xbx}^2)dxdA = 0.5\dot{\delta}^T M_{bx}\dot{\delta} \quad 3.54$$

$$M_{bx} = 0.5\rho L_{bx} \sum_{i=1}^{n_g} T_{bx}^T N^T Z_{bx} N T_{bx} w_i \quad 3.55$$

$$M_{bx} = 0.5\rho L_{bx} \sum_{i=1}^{n_g} T_{bx}^T N^T Z_{bx} N T_{bx} w_i \quad 3.56$$

$$Z_{bx} = \begin{bmatrix} \bar{Z}_{bx} & 0 \\ 0 & \bar{Z}_{bx} \end{bmatrix} \quad , \quad \bar{Z}_{bx} = \begin{bmatrix} A_{bx} & 0 & 0 \\ 0 & A_{bx} & 0 \\ 0 & 0 & I_{bx} \\ & & & 0 \end{bmatrix} \quad 3.57$$

$$KE = 0.5\dot{\delta}^T \left[M_p + M_a + M_s + \sum_{i=1}^{n_{bs}} M_{bsi} \right] \dot{\delta} = 0.5\dot{\delta}^T M_{uu} \dot{\delta} \quad 3.58$$

The total strain energy SE induced in a plate with beam stiffeners and a piezoelectric sensor/actuator pair can be described by the following equation:

$$SE = SE_p + SE_{bs} + SE_s + SE_a \quad 3.59$$

$$SE_p = \frac{1}{2}\int_v \varepsilon^T \sigma \, dv_p + \frac{1}{2}\int_v \gamma^T \tau \, dv_p \quad 3.60$$

$$SE_p = 0.5\delta^T \int \int_{-\frac{h_p}{2}}^{\frac{h_p}{2}} (z^2 B_b^T D_p B_b + B_m^T D_p B_m + zB_m^T D_p B_b + zB_b^T D_p B_m + B_{sh}^T D_{sh} B_{sh})\delta dz dA \quad 3.61$$

$$D_p = \frac{E}{1-\mu^2}\begin{bmatrix} 1 & \mu & 0 \\ \mu & 1 & 0 \\ 0 & 0 & \frac{1-\mu}{2} \end{bmatrix} \quad , \quad D_{sh} = \frac{kE}{2(1+\mu)}\begin{bmatrix} 1 & 0 \\ 0 & 1 \end{bmatrix} \quad 3.62$$

$$\int dA = \int_{-1}^{1}\int_{-1}^{1} detJ ds dr = \sum_{i=1}^{ng}\sum_{j=1}^{ng} detJ w_i w_j \quad 3.63$$

$$SE_p = 0.5\delta^T K_p \delta \quad 3.63$$

where D_p and D_{sh} denote plate bending and shear elasticity matrices, and E, μ and k refer to modulus of elasticity, Poisson's ratio and shear correction factor respectively. The strain energy induced in the beam stiffener is then:

$$SE_{bs} = 0.5\delta^T T_{bx}^T \sum_{i=1}^{ng} (B_b^T E I_{bx} B_b + B_m^T E A_{bx} B_m + 0.25 B_m^T E h A_{bx} B_b$$
$$+0.25 B_b^T E h A_{bx} B_m + B_{sh}^T \frac{k E A_{bx}}{2(1+\mu)} B_{sh}) T_{bx} \delta 0.5 L_{bx} w_i \quad 3.64$$

$$SE_{bs} = 0.5\delta^T K_{bs} \delta \quad 3.65$$

where T_{bx}, E, A_{bx} and I_{bx} refer to the transformation matrix, modulus of elasticity, area and second moment of area for the beam in the x-direction. K_p and K_{bs} represent the stiffness matrices of the plate and beam element respectively. The strain energy induced in the actuator is then:

$$SE_a = \frac{1}{2} \int_v \varepsilon^T \sigma \, dv_a + \frac{1}{2} \int_v \gamma^T \tau \, dv_a \quad 3.66$$

The electrical potential field distribution E_z varies linearly across the thickness of a piezoelectric element, and the voltage difference across its thickness is constant over its whole area:

$$E_z = -\frac{\Delta\phi}{h} \quad , \quad E_s = -\begin{Bmatrix} 0 \\ 0 \\ 1/h_s \end{Bmatrix} \phi_s = -B_\emptyset^s \phi_s \quad ,$$
$$E_a = -\begin{Bmatrix} 0 \\ 0 \\ 1/h_a \end{Bmatrix} \phi_a = -B_\emptyset^a \phi_a \quad 3.67$$

where ϕ_s and ϕ_a are single voltage degree of freedom over the top centre surface of the sensor and actuator respectively.

$$SE_a = 0.5\delta^T \int \int_{\frac{h_p}{2}}^{\frac{h_p}{2}+h_a} ((z^2 B_b^T \bar{C} B_b + B_m^T \bar{C} B_m + z B_m^T \bar{C} B_b$$
$$+z B_b^T \bar{C} B_m + B_{sh}^T \bar{C}_s B_{sh})\delta + z B_b^T \bar{e}^T B_\emptyset^a \phi_a + B_m^T \bar{e}^T B_\emptyset^a \phi_a) dz dA \quad 3.68$$

$$SE_a = 0.5\delta^T K_{pz}^a \delta + 0.5\delta^T K_{u\emptyset}^a \phi_a \quad 3.69$$

In the same way, the strain energy induced in the sensor can be obtained as represented by equation 3.70;

$$SE_s = 0.5\delta^T K_{pz}^s \delta + 0.5\delta^T K_{u\emptyset}^s \phi_s \quad 3.70$$

where K_{pz} and $K_{u\phi}$ denote piezoelectric sensor/actuator stiffness and electromechanical coupling matrices respectively. The total elastic energy induced in the plate, beam stiffener and piezoelectric element is obtained by substituting equations 3.63, 3.65, 3.69 and 3.70 in equation 3.59, resulting in the following:

$$SE = 0.5\delta^T \left[K_p + K_{bs} + K_{pz}^a + K_{pz}^s\right]\delta + 0.5\delta^T K_{u\emptyset}^s \phi_s + 0.5\delta^T K_{u\emptyset}^a \phi_a \quad 3.71$$

$$SE = 0.5\delta^T \left(K_{uu}\delta + K_{u\emptyset}^s \phi_s + K_{u\emptyset}^a \phi_a\right) \quad 3.72$$

where K_{uu} represents the total mechanical stiffness matrix for a plate, beam stiffener, and piezoelectric sensor/actuator element. The electrical energy induced in a sensor element is then:

$$EE_s = \frac{1}{2}\int_v E^T D \, dv_s = \frac{1}{2}\int_v E^T (\bar{e}\,\varepsilon + \bar{\mu}_{33}^{\sigma} E) \, dv_s \quad 3.73$$

$$EE_s = 0.5\phi_s^T \int \int_{-\frac{h_p}{2}-h_s}^{-\frac{h_p}{2}} -B_{\emptyset}^{sT}((z\bar{e}B_b + \bar{e}B_m)\delta - \bar{\mu}_{33}^{\sigma} B_{\emptyset}^s \phi_s) dz dA \quad 3.74$$

$$EE_s = -0.5\phi_s^T K_{\emptyset u}^s \delta - 0.5\phi_s^T K_{\emptyset\emptyset}^s \phi_s \quad 3.75$$

In the same way, the electrical energy induced in an actuator can be obtained as represented by equation 3.76:

$$EE_a = -0.5\phi_a^T K_{\emptyset u}^a \delta - 0.5\phi_a^T K_{\emptyset\emptyset}^a \phi_a \quad 3.76$$

$K_{\phi\phi}$ is the piezoelectric capacitance matrix, and the virtual work done by external mechanical and electric forces is given by :

$$VW = \delta^T F_u - \phi_a^T F_\phi \quad 3.77$$

where VW, F_u and F_ϕ refer to virtual work, applied mechanical force and electric charge respectively. By substituting equations 3.58, 3.72, 3.75, 3.76 and 3.77 in equation 3.47, we obtain the following equations:

$$M_{uu}\ddot{\delta} + \bar{K}_{uu}\delta = F_u - K^a_{u\emptyset}\phi_a \tag{3.78}$$

$$K^a_{\emptyset u}\delta + K^a_{\emptyset\emptyset}\,\phi_a = F_\phi \tag{3.79}$$

$$K^s_{\emptyset u}\delta + K^s_{\emptyset\emptyset}\phi_s = 0 \tag{3.80}$$

$$\bar{K}_{uu} = K_{uu} - K^s_{u\emptyset}K^s_{\emptyset\emptyset}K^s_{\emptyset u} \tag{3.81}$$

3.4.1. Global assembly

Equation 3.78 represents the dynamic equation for a single plate element with a bonded piezoelectric sensor/actuator pair and stiffened by a number of beam elements. The plate element has the possibility of being bonded with a piezoelectric sensor/actuator pair or stiffened by a number of beam elements, or both or neither of these. The global matrices of the plate need to be assembled, including beams, stiffeners and piezoelectric sensor/actuator pairs, as follows:

$$M_g = \sum_{k=1}^{nel} T_k^T\, M_p T_k + \sum_{k=1}^{nsa} T_k^T\,[M_s + M_a]T_k + \sum_{n=1}^{nbs} T_n^T\, M_{bs} T_n \tag{3.82}$$

$$K_g = \sum_{k=1}^{nel} T_k^T\, K_p T_k + \sum_{n=1}^{nbs} T_n^T\, K_{bs} T_n + \sum_{k=1}^{nsa} T_k^T\left[K^a_{pz} + K^s_{pz} - K^s_{u\emptyset}K^s_{\emptyset\emptyset}K^s_{\emptyset u}\right]T_k \tag{3.83}$$

$$\bar{F}_u = \sum_{k=1}^{nel} T_k^T\, F_u \qquad , \qquad \bar{F}_\emptyset = \sum_{k=1}^{n_{sa}} T_k^T\, K^a_{u\emptyset}\phi_a \tag{3.84}$$

where nel, nsa and nbs are the total numbers of plate, sensors/actuator pairs and beam stiffener elements respectively. M_g and K_g refer to global mass and stiffness matrices for the structure including the plate, piezoelectric pairs and beam stiffeners. T_k and T_n are distributed matrices defined by the following equations [100]:

$$T_k(i,j) = \begin{Bmatrix} 0\ if\ j \neq m_k(i) \\ 1\ if\ j = m_k(i) \end{Bmatrix} \qquad for \qquad \begin{matrix} i = 1,2,\dots,20 \\ j = 1,2,\dots,n_{gdof} \end{matrix} \tag{3.85}$$

$$m_{k\,(1,20)} = \{5n_k - 4 \quad 5n_k - 3 \quad 5n_k - 2 \quad 5n_k - 1 \quad 5n_k\} \tag{3.86}$$

$$T_n(i,j) = \begin{Bmatrix} 0\ if\ j \neq m_n(i) \\ 1\ if\ j = m_n(i) \end{Bmatrix} for \quad \begin{matrix} i = 1,2,\dots,10 \\ j = 1,2,\dots,n_{gdof} \end{matrix} \tag{3.87}$$

$$m_{n\,(1,10)} = \{5n_n - 4 \quad 5n_n - 3 \quad 5n_n - 2 \quad 5n_n - 1 \quad 5n_n\} \tag{3.88}$$

where n_k (four nodes) and n_n (two nodes) are the global element nodal numbering of the plate and beams respectively. The global nodal numbering of sensors, actuators and beam stiffeners elements follow the same global numbering according to their location on the plate. n_{gdof}, m_k and m_n are the global degrees of freedom of entire structure, plate and beam respectively. So, the global dynamic equation for the plate stiffened by a number of beam stiffeners and bonded by number of discrete piezoelectric sensor/actuator pairs, and including structural damping effect, can be written in the following form:

$$M_g\ddot{\delta} + C\dot{\delta} + K_g\delta = \bar{F}_u - \bar{F}_\emptyset \tag{3.89}$$

3.4.2. Dynamic equation in modal coordinates

A flexible structure with low natural damping is typically analysed in the normal mode. The structure produces a normal mode when all points within it vibrate in the same phase at a certain frequency, and all reach the minimum and maximum amplitudes at the same time. Investigating dynamic structures in terms of modal coordinates is considered to be a powerful technique that has advantages in both performing the analysis and in interpreting the results [101]. Low modes of vibration are difficult and costly to analyse using dynamic equations in physical coordinates. The implementation of modal coordinates in the dynamic equations is transferred from a number of coupled equations in terms of physical coordinates δ to uncoupled equations in terms of modal displacement coordinates η . This makes it easier to investigate the individual contribution of each mode by superposition and simplifies the computational effort. The general dynamic equation in terms of modal coordinates provides a powerful method of describing the motion of the system in each individual mode. The relationship between physical and modal displacement is represented by the following equation:

$$\delta = \varphi\,\eta \quad , \quad \dot{\delta} = \varphi\,\dot{\eta} \quad , \quad \ddot{\delta} = \varphi\,\ddot{\eta} \tag{3.90}$$

where φ is an open-loop mass-normalised modal matrix obtained by solving the eigenvalue free damped problem and η is a single vector of the modal coordinates [76].

$$\varphi^T M\varphi = I \quad , \quad \varphi^T K\varphi = \Omega\,, \quad \varphi^T C\varphi = 2\xi\omega \tag{3.91}$$

By substituting equations 3.90 and 3.91 in equation 3.89, a modal non-coupled dynamic equation is obtained:

$$\ddot{\eta} \;+\; 2\xi\omega\dot{\eta} + \;\Omega\,\eta = \varphi^T\,F_u - \varphi^T K^a_{u\emptyset}\phi_a \tag{3.92}$$

$$\phi_s = -\varphi^T {K^s_{\emptyset\emptyset}}^{-1}\,K^s_{\emptyset u}\eta \tag{3.93}$$

In order to put equations 3.92 and 3.93 into state space form and to change from second order to a linear first order equation, the following assumptions are made:

$$X = \begin{Bmatrix} X_1 \\ X_2 \end{Bmatrix} = \begin{Bmatrix} \eta \\ \dot{\eta} \end{Bmatrix} \quad , \quad \dot{X} = \begin{Bmatrix} \dot{X}_1 \\ \dot{X}_2 \end{Bmatrix} = \begin{Bmatrix} \dot{\eta} \\ \ddot{\eta} \end{Bmatrix} \tag{3.94}$$

$$\dot{X} = \begin{bmatrix} 0 & \omega \\ -\omega & -2\xi\omega \end{bmatrix} X + \begin{bmatrix} 0 \\ \varphi^T \end{bmatrix} F_d + \begin{bmatrix} 0 \\ -\varphi^T K^a_{u\emptyset} \end{bmatrix} \phi_a \tag{3.95}$$

$$\dot{X} = AX + B\phi_a + B_{md}F_d \quad , \quad \phi_s \;= C_i\,X_i \tag{3.96}$$

$$\begin{gathered} A_i = \begin{bmatrix} 0 & \omega_i \\ -\omega_i & -2\xi_i\omega_i \end{bmatrix} \quad , \quad B_i = \begin{bmatrix} 0 \\ -\varphi^T K^a_{u\emptyset} \end{bmatrix}, \quad B_{mdi} = \begin{bmatrix} 0 \\ \varphi^T \end{bmatrix} \\ C_i = \left[-\varphi^T \omega_i^{-1}\,{K^s_{\emptyset\emptyset}}^{-1} K^s_{u\emptyset} \quad 0\right] \quad , \quad X_i = \{\omega_i\eta_i \quad \dot{\eta}_\iota\}^T \end{gathered} \tag{3.97}$$

where A_i , B_i , B_{mdi} and C_i are individual modal state and input actuator, mechanical disturbance and output sensor matrices respectively and the subscript (i) refers to mode number. The state matrices for the number of modes n_m and number of actuators r_a are given by:

$$A_{(2n_m \times 2n_m)} = \begin{bmatrix} A_1 & \cdots & 0 \\ \vdots & \ddots & \vdots \\ 0 & \cdots & A_{n_m} \end{bmatrix} \tag{3.98}$$

$$B_{(2n_m \times r_a)} = \begin{bmatrix} (B_1)_1 & \cdots & (B_1)_{r_a} \\ \vdots & \cdots & \vdots \\ (B_{n_m})_1 & \cdots & (B_{n_m})_{r_a} \end{bmatrix} \quad 3.99$$

$$C_{(r_a \times 2n_m)} = \begin{bmatrix} (C_1)_1 & \cdots & (C_{n_m})_1 \\ \vdots & \cdots & \vdots \\ (C_1)_{r_a} & \cdots & (C_{n_m})_{r_a} \end{bmatrix} \quad 3.100$$

$$X_{(2n_m \times 1)} = \{\omega_1 \eta_1 \quad \dot{\eta}_1 \quad \cdots \quad \omega_{n_m} \eta_{n_m} \quad \dot{\eta}_{n_m}\}^T \quad 3.101$$

It is shown in the literature relevant to the active vibration reduction of stiffened plates explained in section2.10 that the optimisation of the location of discrete piezoelectric transducers on a plate stiffened by beams has never been modelled and investigated. In this chapter, the contribution of this finite element model is that it is able to solve and optimise the locations, feedback gain and number of discrete sensors and actuators for unstiffened plates and those stiffened by beams passing through the plate's finite element nodes in any configuration in order to optimise active vibration reduction for these structures.

3.5. Control Law

In this work, optimal linear quadratic control was implemented to attenuate vibration, which is based on the minimisation of the performance index *J*. Moreover, minimisation of the linear quadratic index was used to optimise the locations of sensors and actuators.

$$J = \int_0^\infty (X^T Q X + \phi_a^T R \phi_a) dt \quad 3.102$$

The weighted matrices Q of dimensions $2n_m \times 2n_m$ and R of dimensions $r_a \times r_a$ are positive definite or semi-definite Hermitian or real symmetric matrices. These control the value of the performance index, where n_m and r_a represent the number of modes and actuators respectively. These matrices determine the relative importance of error and controller energy, with high values of Q giving high vibration suppression and controller energy.

Consider the dynamic equation of a system in state space form equation 3.96, but removing the external disturbance part. It is assumed that the system is controllable and observable, and it could then be written as:

$$\dot{X} = AX + B\phi_a \tag{3.103}$$

$$\phi_a = -KX \quad , \quad \phi_s = C_i X_i \tag{3.104}$$

Minimisation of the linear quadratic index J was used to design an optimal feedback control gain K as follows [102]:

$$\dot{X} = (A - BK)X \tag{3.105}$$

It is assumed that the closed loop state matrix $A - BK$ is stable or has negative real part eigenvalues. Substituting the feedback voltage ϕ_a into equation 3.102 gives:

$$J = \int_0^\infty (X^T QX + X^T K^T RKX)dt = \int_0^\infty X^T (Q + K^T RK)Xdt \tag{3.106}$$

$$X^T (Q + K^T RK)X = -\frac{d(X^T PX)}{dt} \tag{3.107}$$

Ogata has shown that it is possible to follow this derivation to design a linear quadratic controller, which leads to the minimum quadratic performance index equation 3.108 and Riccati equations 3.109 and 3.110 [102]:

$$J = X(0)^T PX(0) \tag{3.108}$$

$$A^T P + PA - PBR^{-1}B^T P + Q = 0 \tag{3.109}$$

$$K = R^{-1}B^T P \,, \qquad \phi_a = -KX \tag{3.110}$$

Solution of the reduced Riccati equation 3.109 gives the value of the Riccati matrix P; if matrix P is positive definite then the system is stable or the closed loop matrix $A - BK$ is stable. This means that the real part of the closed loop poles of $A - BK$ are negative on the left hand side. Optimal feedback control gain can be obtained after substitution of the matrix P in equation 3.110.

3.6. Estimator Design

Estimator design is important in the active vibration control of mechanical structures when using optimal control schemes to attenuate the vibration experimentally. However, the system states $X_i = \{\omega_i \eta_i \quad \dot{\eta}_i\}^T$ are impossible to measure experimentally, whereas the feedback controller $\phi_a = -K_i X_i$ is based on measured states as mentioned in section 3.5 and shown in Figure 3.5. The output sensor voltage is the only parameter that could be measured experimentally. Hence, optimal linear quadratic control requires perfect system modelling using state space matrices in order to design an accurate estimator. This involves finding a suitable gain error matrix to reduce the difference in error between the plant and estimator output as much as possible with a response speed higher than that of the system. This section presents the estimator design for feedback gain K and error gain matrices K_e. The error gain matrix K_e forces error quickly between plant and estimator output to zero. For example, if the error converges to zero after a long time, the estimator error gain matrix will increase the speed of convergence and vice versa.

The estimator design is required to determine two types of feedback gain matrices. Firstly, the actuator feedback gain matrix K was designed using the optimal linear quadratic control described in section 3.5; and then the estimator error feedback gain K_e is calculated by pole placement. According to the simulink model of the plant and estimator system shown in Figure 3.5, the plant state, sensor and actuator feedback voltage equations now become:

$$\dot{X} = AX - BK\tilde{X} \tag{3.111}$$

$$\phi_s = CX, \quad \phi_a = -K\tilde{X} \tag{3.112}$$

$$\dot{X} = AX - KB\tilde{X} + KBX - KBX = (A - BK)X + BK\left(X - \tilde{X}\right) \tag{3.113}$$

$$\dot{X} = (A - BK)X + BKe \tag{3.114}$$

where $\tilde{X}$ represents estimator state output and $e = X - \tilde{X}$ is the state error between plant and estimator. The estimator state equation is then:

$$\dot{\tilde{X}} = A\tilde{X} - KB\tilde{X} + K_e(CX - C\tilde{X}) \tag{3.115}$$

Subtracting the estimator equation 3.115 from plant equation 3.111 gives:

$$\dot{X} - \dot{\tilde{X}} = AX - A\tilde{X} - K_e C\left(X - \tilde{X}\right) = (A - K_e C)\left(X - \tilde{X}\right) \quad 3.116$$

$$e = \left(X - \tilde{X}\right) \quad , \quad \dot{e} = \dot{X} - \dot{\tilde{X}} \quad 3.117$$

$$\dot{e} = (A - K_e C)e \quad 3.118$$

The dynamic behaviour of the error vector could be determined from equation 3.118 by determination of the eigenvalues of the matrix $(A - K_e C)$. If the real parts of the eigenvalues are negative, this means that the error matrix $(A - K_e C)$ is stable, and so that error vector converges to zero for any initial error vector value e_0 and the estimator state $\tilde{X}$ will converge to the plant state X at any time t despite the difference between them. Combining the estimator equations 3.114 and 3.118 together gives:

$$\begin{Bmatrix} \dot{X} \\ \dot{e} \end{Bmatrix} = \begin{bmatrix} A - BK & BK \\ 0 & A - K_e C \end{bmatrix} \begin{Bmatrix} X \\ e \end{Bmatrix} \quad 3.119$$

$$\begin{vmatrix} SI - A + BK & -BK \\ 0 & SI - A + K_e C \end{vmatrix} = 0 \quad 3.120$$

$$|sI - A + BK||sI - A + K_e C| = 0 \quad 3.121$$

Equation 3.121 represents the estimator characteristic equation, and the estimator gain matrices K and K_e could be designed independently. In this work, the estimator feedback gain matrix K is firstly designed according to the optimal linear quadratic control scheme, while the estimator error gain matrix K_e is subsequently determined using the pole placement technique. The closed loop poles selected in pole placement are chosen to be close to the location of the poles of the state feedback matrix $(A - BK)$ in order to determine the gain matrix K_e for continuous and discrete control design. The poles of the estimator are usually chosen so that the estimator response is much faster than the system response by the order of two to five times [102].

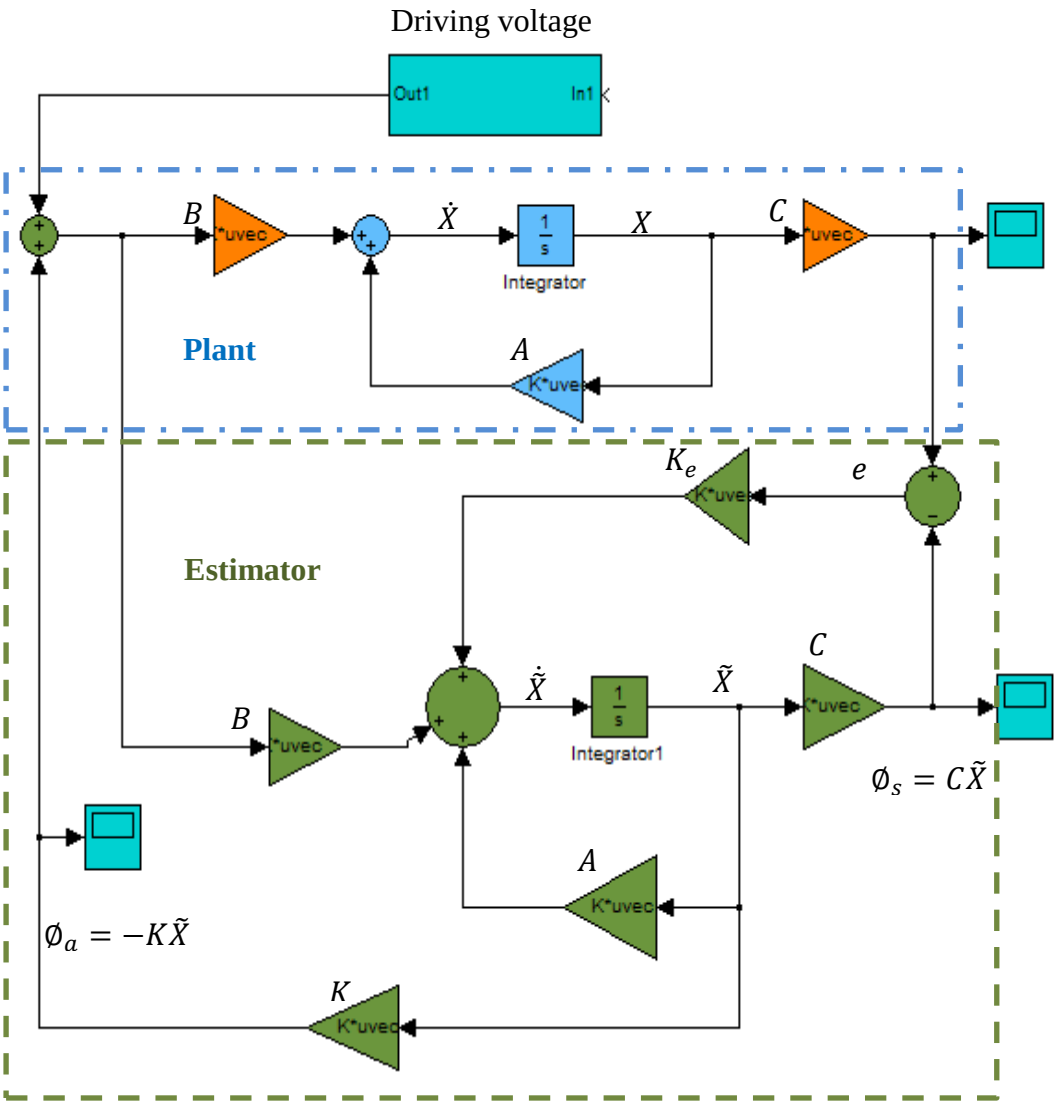

Figure 3.5 Simulink model diagram for a plant and estimator

3.7. Objective Function

Minimisation of the linear quadratic index was implemented by Kondoh as an objective function to optimise actuator location and feedback gain for a flexible beam [57]. The performance index depends on actuator location and initial state conditions according to equation 3.122. The effect of initial state conditions was reduced by taking the average cost function [38, 58, 59, 103], giving:

$$J(x,y) = X(0)^T \mathrm{P}(x,y) X(0) \qquad 3.122$$

$$J(x,y) = Trace\big(\mathrm{P}(x,y)\big) \qquad 3.123$$

$$J_{opt}(x,y) = \min(Trace(\mathrm{P}(x,y)), \mathrm{K}) \qquad 3.124$$

where $x, y \in$ structure dimensions

It can be seen from the Riccati equation 3.109 that the Riccati solution matrix P is a function of the actuator location matrix B, while the matrices R, Q and A are constant for a particular control system. A range of high and low values of P can be gained by changing the location of actuators in matrix B. However, the optimisation of controller gain K and the locations of the actuators require a lower value of P, and it is difficult to find the correct the actuator matrix B using trial and error or simple optimisation methods especially when the optimisation problem has a massive number of candidate solutions. In this context, a genetic algorithm was implemented, which is considered to be a powerful optimisation method depending on fitness and objective functions in finding an optimal solution.

In chapters five and eight, a genetic algorithm placement strategy is developed and a MATLAB program designed to find the optimal actuators location and number of actuators and controller feedback gain. Three placement criteria are implemented; the first based on the minimisation of the linear quadratic index J as explained in this section. The other two placement criteria for fitness and objective functions developed in this work for the determination of optimal feedback gain and the number and location of actuators are explained in chapters six and eight.

3.8. Quality Test Criterion for Optimal Location of Sensors and Actuators

In this work, a criterion is proposed to test the effectiveness of optimal configurations of piezoelectric sensors and actuators based on average closed loop vibration reduction. The criterion is used to measure the average value of closed loop dB gain reduction for all sensors and resonance frequencies as a result of applying a unit amplitude sinusoidal voltage to drive a plate at a single predefined actuator at natural frequencies. Figure 3.6 shows open and closed loop dB gain margins $GO_{j,i}$ and $GC_{j,i}$ for a sensor j as a result of an applied unit amplitude sinusoidal voltage to the predefined actuator at the specified natural mode i using the linear quadratic coefficient matrices R and Q. The system state space and sensor output voltage equations are as follows:

$$\dot{X} = AX + B\phi_a\,, \qquad \phi_s = CX \qquad 3.125$$

The Laplace transform of equation 3.125 is then:

$$sX(s) = AX(s) + B\phi_a(s), \qquad \phi_a(s) = B^{-1}(sI - A)X(s)$$
$$\phi_s(s) = CX(s) \tag{3.126}$$

The open loop transfer function of a system in the s-domain is given as:

$$G(s) = \frac{\phi_s(s)}{\phi_a(s)} = C(sI - A)^{-1}B \tag{3.127}$$

$$G(\omega) = C(j\omega I - A)^{-1}B \tag{3.128}$$

$$GO_{j,i} = 20\log_{10}(|C_i(j\omega_i I - A_i)^{-1}B_i|) \tag{3.129}$$

$$A_{i_c} = A_i - B_i K_i \tag{3.130}$$

$$GC_{j,i} = 20\log_{10}\left(\left|C_i\left(j\omega_i I - A_{i_c}\right)^{-1}B_i\right|\right) \tag{3.131}$$

$$GR_{j,i} = GC_{j,i} - GO_{j,i} \tag{3.132}$$

Where $GR_{j,i}$ is the closed loop gain reduction for the j sensor and i mode as shown in Figure 3.6.

$$MGR = \frac{1}{n_m n_{sa}} \sum_{i=1}^{n_m} \sum_{j=1}^{n_{sa}} GR_{j,i} \tag{3.133}$$

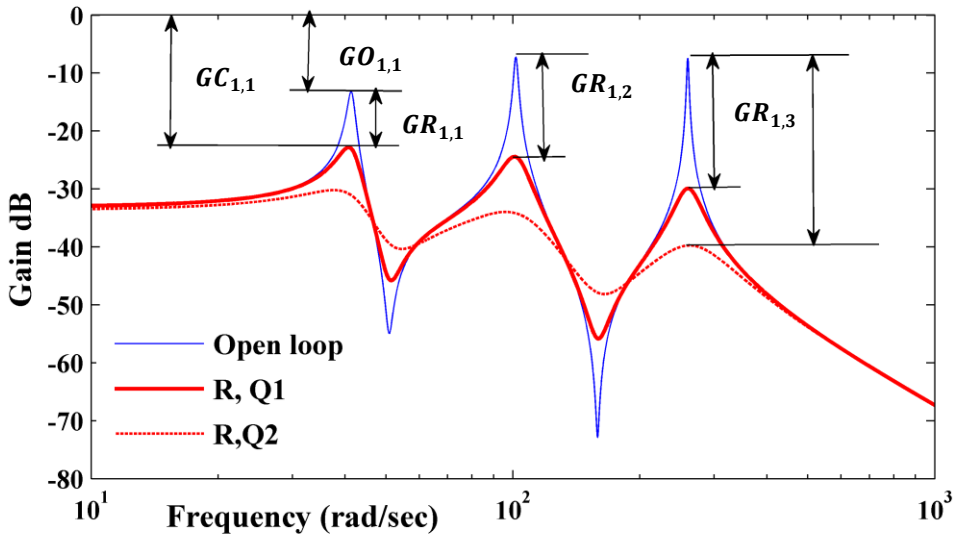

Figure 3.6 Open and closed loop frequency response for the given structure

where MGR refers to the average closed loop dB gain reduction for all sensors n_{sa} as a result of an applied unit amplitude sinusoidal voltage to the predefined actuator at all natural frequencies n_m for the given linear quadratic weighted matrices R and Q.

3.9. Conclusions

Hamilton's principle and finite element analysis are deployed to model a plate stiffened by a number of beam stiffeners and with bonded piezoelectric sensor/actuator pairs. Bending, shear deformation and membrane effects are taken into account based on first order shear deformation theory. Piezoelectric mass, stiffness and electromechanical coupling effects related to sensors and actuators are taken into account. The nodal offset of the beam stiffener with respect to the plate is considered in the model. In section 2.10, the literature review showed that the active vibration reduction was investigated for stiffened plate by beams bonded with either full coverage or arbitrary locating sensor and actuator, and the authors reported that a weak vibration reduction was obtained for some modes no reduction for others. The contribution of the developed finite element model is its ability to be implemented in the genetic algorithms in order to optimise the locations, feedback gain and number of discrete piezoelectric transducers in order to attenuate vibration optimally for flat plates and plates stiffened by beams passing through the plate's finite element nodes in any configuration.

In the next chapter, the model is implemented and tested for flat and stiffened plates with different geometries and boundary conditions, in order to find the first six modes of vibration. The results are then compared with those from the ANSYS finite element package and experimental tests.

Chapter 4. Model Verification

In this chapter, the first six vibration modes and natural frequencies are investigated for unstiffened flat plates and plates stiffened by beams with different geometries and boundary conditions. Firstly, a square flat plate was used in various configurations: fixed along one edge as a cantilever, fixed along two opposite edges (clamped-clamped), and clamped along one edge with one opposite corner fixed. In this way the plate was given one, two and zero axes of symmetry, respectively. Secondly, the cantilever plate was stiffened by two beams arranged as either a cross or T-type to form symmetric and asymmetric plate in geometries, respectively.

A finite element MATLAB program was written to investigate these types of plates based on the model derived in chapter three. The MATLAB results were validated using the ANSYS finite element package and experimentally. The objective of this chapter is to verify the model derived in chapter three for plain and stiffened plates and to prepare the correct data for the next stages of the research. Subsequent chapters then deal with the optimisation of sensor/actuator location, feedback gain and the number of sensor/actuator pairs using the genetic algorithms.

4.1. Problem Description

The various plate configurations are shown in Figure 4.1. These boundary conditions and beam stiffener configurations provided dynamic symmetrical and asymmetrical structures, selected to study the effects of symmetry on mode shapes, modal strain and electric charge in order to optimise the distribution of discrete sensors and actuators. The dimensions of the plate were $500 \times 500 \times 1.9$ mm and of the beam stiffener $500 \times 20 \times 1.9$ mm. The plate and piezoelectric specifications are given in Table 4.1.

Table 4.1 Plate, stiffener and piezoelectric material properties

Properties	Plate	Stiffener	Piezoelectric PIC255
Modulus, GPa	210	210	-------
Density, kg/m^3	7810	7810	7810
Poisson's ratio	0.3	0.3	-------
Thickness, mm	1.9	1.9	0.5
Length, width, mm	500, 500	500, 20	50, 50
e_{31}, e_{32}, e_{33} , C/m^2	---------	---------	-7.15, -7.15,13.7
C_{11}^E, C_{12}^E , C_{13}^E, C_{33}^E, GPa	--------	--------	123,76.7, 70.25, 97.22
μ_{33}^{σ}(F/m)	--------	--------	$1.55x10^{-8}$

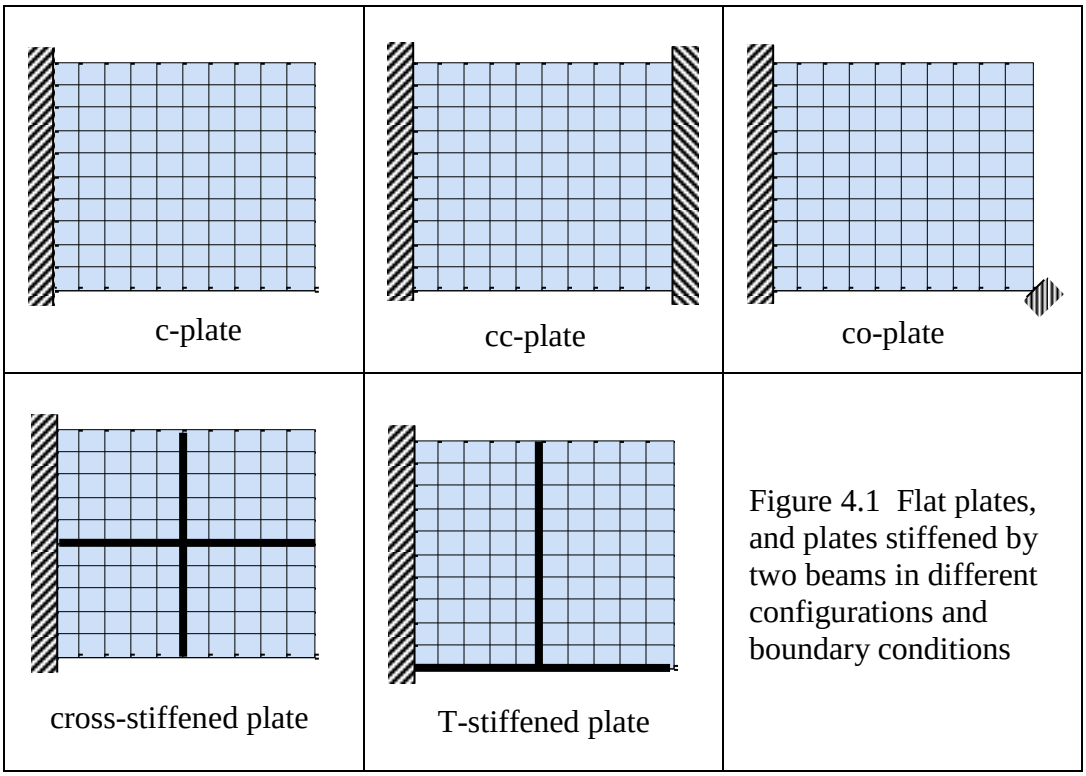

Figure 4.1 Flat plates, and plates stiffened by two beams in different configurations and boundary conditions

4.2. Finite Element Program

In this chapter, a finite element MATLAB m-file program was written for a flat plate and plate stiffened by beams to determine natural frequencies and mode shapes accounting for bending, membrane and shear deformation effects. The program involves automatic mesh generation designed especially for flat plates and plates stiffened by beams. The program is designed to solve flat and beam-stiffened plate with different configurations and boundary conditions according to the modelling derived in chapter three. In this program some standard subroutines dealing with element shape function, shape function derivatives and Gaussian integration points were taken from reference book [104]. The flow chart of the finite element program shown in Figure 4.2 is used to solve natural frequencies and mode shapes for all types of plates used in this study.

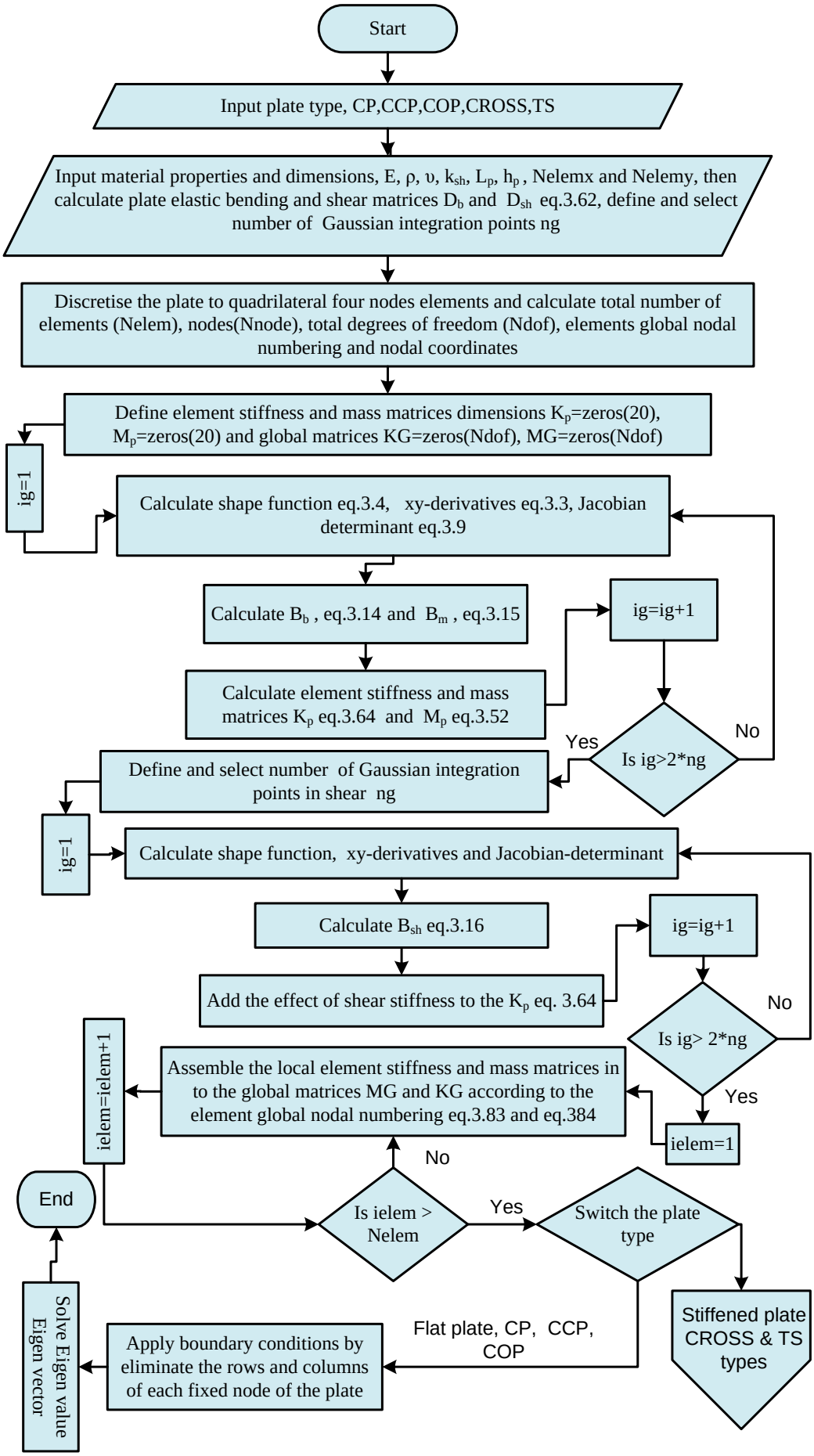
Start
Input plate type, CP,CCP,COP,CROSS,TS
Input material properties and dimensions, E, ρ, υ, k_{sh}, L_p, h_p , Nelemx and Nelemy, then calculate plate elastic bending and shear matrices D_b and D_{sh} eq.3.62, define and select number of Gaussian integration points ng
Discretise the plate to quadrilateral four nodes elements and calculate total number of elements (Nelem), nodes(Nnode), total degrees of freedom (Ndof), elements global nodal numbering and nodal coordinates
Define element stiffness and mass matrices dimensions K_p=zeros(20), M_p=zeros(20) and global matrices KG=zeros(Ndof), MG=zeros(Ndof)
ig=1
Calculate shape function eq.3.4, xy-derivatives eq.3.3, Jacobian determinant eq.3.9
Calculate B_b , eq.3.14 and B_m , eq.3.15
Calculate element stiffness and mass matrices K_p eq.3.64 and M_p eq.3.52
ig=ig+1
Is ig>2*ng
Yes
No
Define and select number of Gaussian integration points in shear ng
ig=1
Calculate shape function, xy-derivatives and Jacobian-determinant
Calculate B_{sh} eq.3.16
Add the effect of shear stiffness to the K_p eq. 3.64
ig=ig+1
Is ig> 2*ng
No
Yes
ielem=1
Assemble the local element stiffness and mass matrices in to the global matrices MG and KG according to the element global nodal numbering eq.3.83 and eq.384
ielem=ielem+1
No
Is ielem > Nelem
Yes
Switch the plate type
Stiffened plate CROSS & TS types
Flat plate, CP, CCP, COP
Apply boundary conditions by eliminate the rows and columns of each fixed node of the plate
Solve Eigen value Eigen vector
End

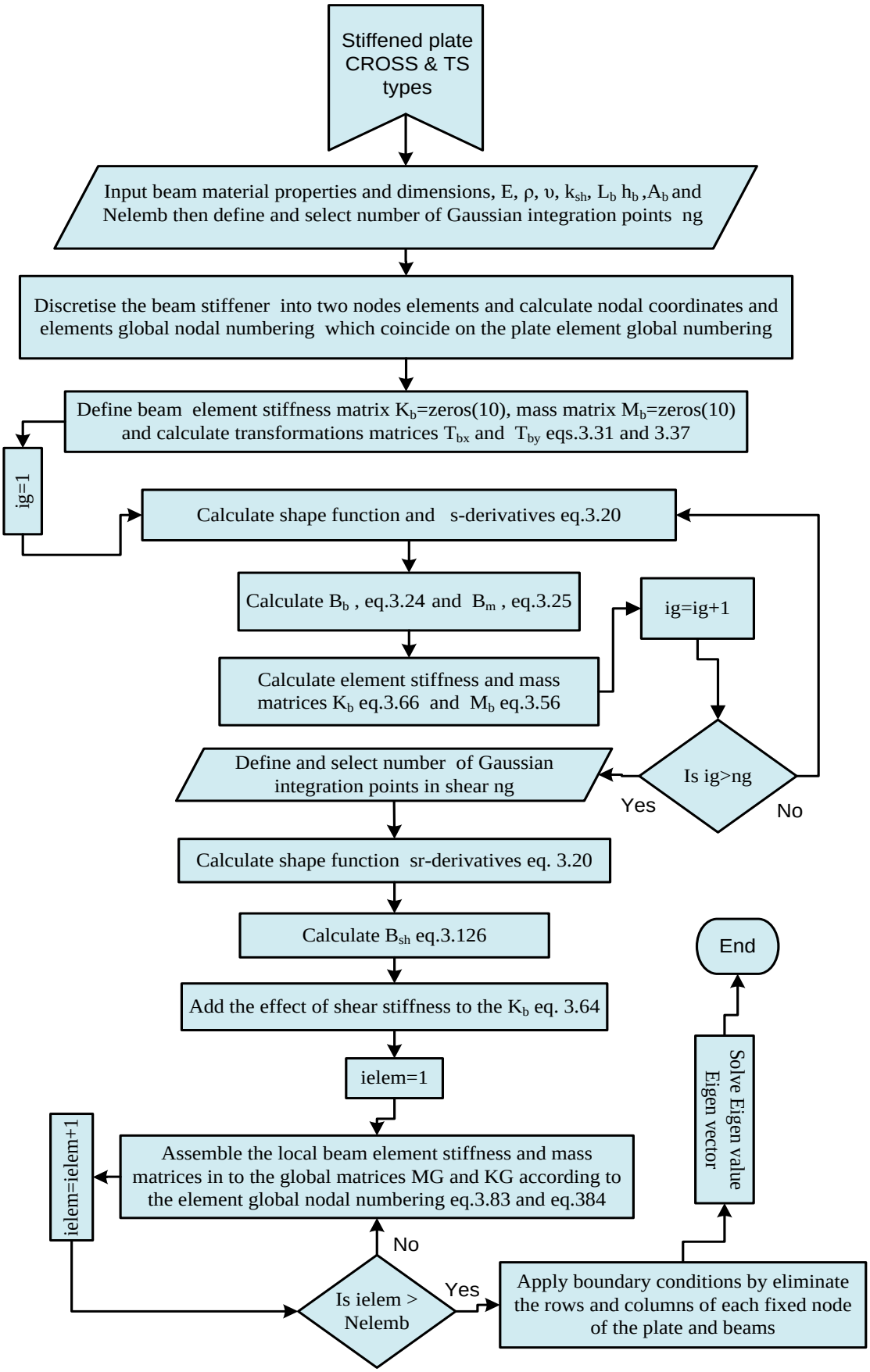

Figure 4.2 Flow chart for finite element program to solve natural frequencies and mode shapes for plates with various geometries and end fixations

4.3. ANSYS Package

In this work, ANSYS Parametric Design Language (APDL) programs were written for flat plates and plates stiffened by beams with different configurations and boundary conditions using a two-dimensional shell63 element and a three-dimensional solid45 element for the plate and beam stiffeners. The APDL programs were written to represent all of the stiffened and unstiffened plates in the ANSYS package and to investigate the first six natural frequencies under the free vibration condition. The APDL program was chosen instead of using workbench in the ANSYS package. This is because APDL has more flexibility to direct the research problem and especially for multiphysics problems such as active vibration control of smart structures, but it requires specialised knowledge about the use of its commands and it takes a long time to write such programs. Examples of these programs are shown Appendix B and C.

4.4. Experimental Rig

The results were tested experimentally using physical flat and stiffened steel plates. They were excited by an impact hammer to obtain the natural frequencies and damping ratios. A single accelerometer located at a point of large displacement in all modes was used to measure the vibration via a Kistler charge amplifier and a National Instruments USB-6215 data acquisition unit, using a lap-top computer running LabVIEW software as the data logger.

The signal was acquired and analysed by the computer using the fast Fourier transform (FFT) facility in the LabVIEW package. Figure 4.3 shows the test rig, comprising a heavy cast iron bed with a vertical cantilever plate with cross-shaped stiffeners mounted on it. In the hammer test, the plate was hit lightly by a small hammer in a number of different locations in order to excite the first six natural vibration modes. The locations of hammer strikes were all on the lower half of the plate near the fixed end in order to excite most modes of vibration.

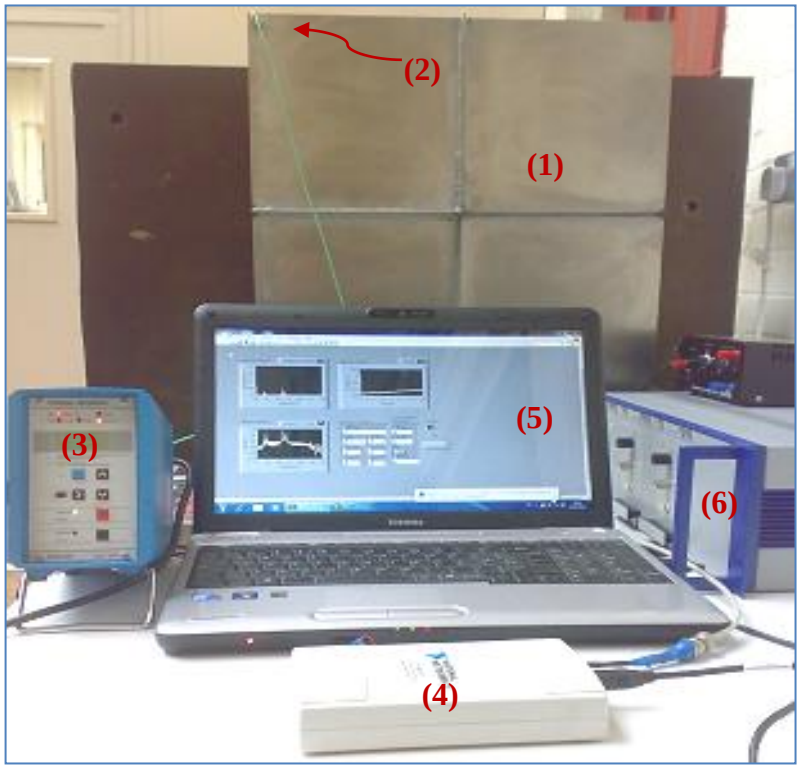

1. Cantilever plate stiffened by two beams in cross configuration, 2. Accelerometer,
3. Charge Amplifier + anti-aliasing filter, 4. USB-6215 data acquisition unit,
5. Lap-top computer running LabVIEW software as the data logger,
6. Piezoelectric high voltage driver for use in active vibration control

Figure 4.3 Test rig showing vertically mounted cantilever plate with cross stiffeners

4.5. Natural Frequencies

The first six natural frequencies and mode shapes for the flat plat and the plate stiffened by beams were investigated using the model described in chapter three, and validated using the ANSYS finite element package and experimental testing. Firstly, the plates were represented in the ANSYS finite element package using two-dimensional shell63 elements and three-dimensional solid45 elements, and the results are shown in Table 4.2 to Table 4.6 for the unstiffened cantilever plate (c-plate), the T-stiffened plate, the cross-stiffened plate, the unstiffened plate clamped on opposite edges (cc-plate) and the cantilever plate with one corner clamped (co-plate) respectively.

The correctness of natural frequencies was tested by convergence study to constant values with increasing mesh refining from 2×2 to 50×50 elements for all the plates. Progressively more elements of type shell63 were used to refine the mesh and the resonant frequency results converged to constant values as shown in the tables. It was found that good convergence was obtained for the first six resonant modes with a 10×10 mesh in all cases, and that further refinement to a 50×50 mesh changed the predicted natural frequencies by 0.45%., 0.58%, 0.6%, 0.3% and 1.2% in the sixth mode for the c-plate, T-type, cross type, cc-plate and co-plate, respectively. For this reason, the optimal placement of sensors and actuators investigated in subsequent chapters made use of a 10×10 mesh.

The results using the three dimensional solid45 elements gave very similar results, but required a much finer mesh of 50×50 to provide an appropriate aspect ratio for the thin plate, beams and piezoelectric sensors and actuators. The greatest discrepancies between the soli45 and shell63 results were 0.3%., 1.2%, 0.54%, 0.44% and 0.57% in the sixth mode for the c-plate, T-type, cross type, cc-plate and co-plate respectively.

The MATLAB m-code model results are also listed in Table 4.2 to Table 4.6. These were close to the ANSYS results for all plate types in all cases. The maximum percentage discrepancy between the model and ANSYS results was 4.7% at the first mode for the stiffened cross-type plate and in all other cases it was less than 2.5%.

Table 4.2 ANSYS natural frequencies compared with MATLAB model and experiment for an unstiffened flat cantilever plate

Element type	Mode (Hz)					
	1^{st}	2^{nd}	3^{td}	4^{th}	5^{th}	6^{th}
ANSYS shell63 (2×2)	6.53	16.73	39.98	50.71	57.30	88.49
ANSYS shell63 (4×4)	6.58	16.37	40.76	51.75	59.67	104.51
ANSYS shell63 (8×8)	6.59	16.21	40.53	51.67	59.13	103.54
ANSYS shell63 (10×10)	6.59	16.19	40.49	51.66	59.01	103.34
ANSYS shell63 (20×20)	6.59	16.15	40.42	51.63	58.83	103.00
ANSYS shell63 (50×50)	6.58	16.14	40.40	51.62	58.76	102.87
ANSYS solid45(50×50)	6.59	16.15	40.44	51.68	58.86	103.18
Present model(20×20)	6.57	16.12	40.54	51.72	58.87	103.12
Error between model and ANSYS%	0.30	0.18	0.29	0.17	0.06	0.11
Experimental Frequency	5.90	16.90	37.30	51.60	58.20	101.00
Error between model and experiment %	10.19	4.83	7.99	0.23	1.13	2.05
Damping ratio $\times 10^{-4}$	124.4	46.2	25.6	23.1	21.2	14.9

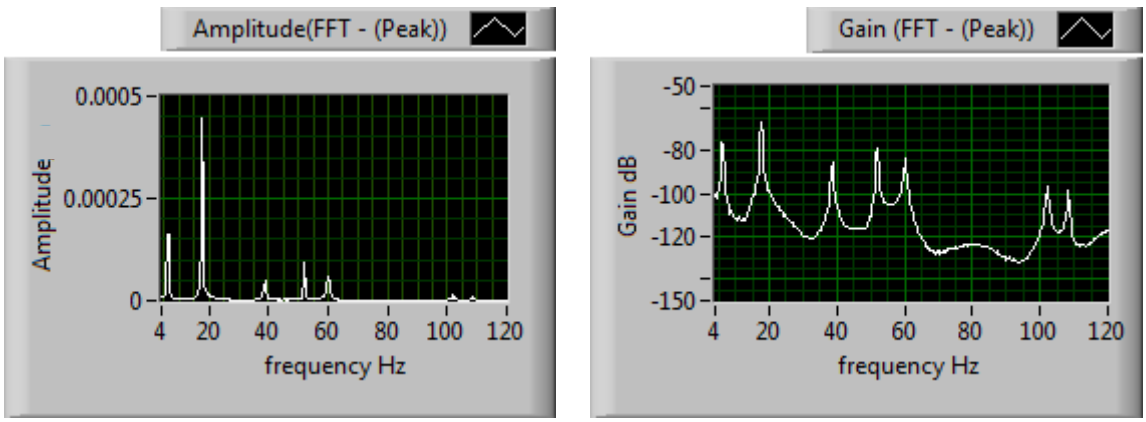

Figure 4.4 Experimental Lab VIEW graph showing frequency response for the flat cantilever plate

Finally, the results were also validated experimentally using physical cantilever plates with and without stiffening. The experimental frequency responses are given in the tables and are also shown graphically in Figure 4.4 to Figure 4.6. It may be seen that the

finite element analysis gave resonant frequencies in the correct range, though with some significant discrepancies.

Table 4.3 ANSYS Natural frequencies compared with present model and experimentally for stiffened plate T-type

Element type	Mode (Hz)					
	1^{st}	2^{nd}	3^{td}	4^{th}	5^{th}	6^{th}
ANSYS shell63 (2 × 2)	10.27	39.91	46.18	75.35	99.44	143.78
ANSYS shell63 (4 × 4)	10.18	39.55	46.38	80.03	120.09	128.05
ANSYS shell63 (8 × 8)	10.14	39.27	46.15	78.77	120.69	126.93
ANSYS shell63 (10 × 10)	10.13	39.21	46.12	78.57	120.64	126.62
ANSYS shell63 (20 × 20)	10.13	39.12	46.07	78.26	120.51	126.09
ANSYS shell63 (50 × 50)	10.13	39.10	46.05	78.16	120.44	125.88
ANSYS solid45(50 × 50)	10.19	39.57	46.23	78.65	120.97	127.51
Present model(20 × 20)	09.88	39.97	46.40	79.83	121.52	127.00
Error between model and ANSYS %	2.4	2.1	0.71	2.0	0.80	0.72
Experimental Frequency	09.85	36.96	45.67	74.67	114.90	120.0
Error between model and experiment %	0.30	7.5	1.57	6.4	5.4	5.5
Damping ratio $\times 10^{-4}$	224.2	44.1	55	43.1	19.9	19.3

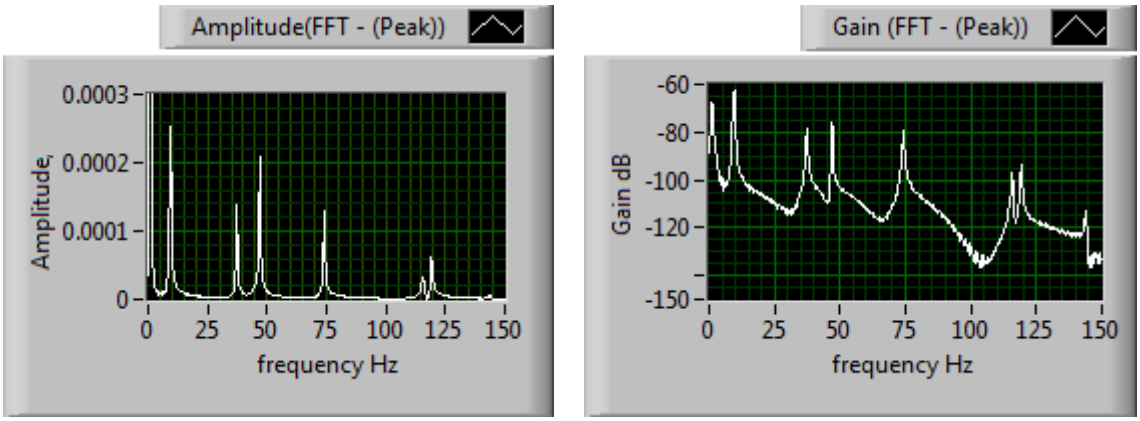

Figure 4.5 Experimental Lab VIEW graph showing frequency response for the T-type stiffened plate by two beams

Table 4.4 ANSYS Natural frequencies compared with present model and experimentally for a cantilever plate stiffened by two beams in the cross-type

Element type	Mode (Hz)					
	1^{st}	2^{nd}	3^{td}	4^{th}	5^{th}	6^{th}
ANSYS shell63 (2 × 2)	7.11	25.89	56.75	69.81	99.51	130.47
ANSYS shell63 (4 × 4)	16.75	24.55	58.59	72.16	126.05	133.89
ANSYS shell63 (4 × 4)	16.59	24.24	57.98	70.55	121.79	133.83
ANSYS shell63 (10 × 10)	16.56	24.19	57.84	70.33	121.11	133.51
ANSYS shell63 (20 × 20)	16.53	24.12	57.68	70.02	120.04	132.88
ANSYS shell63 (50 × 50)	16.52	24.09	57.62	69.91	119.60	132.63
ANSYS solid45(50 × 50)	16.62	25.46	57.84	71.02	125.11	133.36
Present model (20 × 20)	15.90	25.32	56.96	70.62	125.35	132.16
Error between model and ANSYS%	3.81	4.7	1.2	0.85	4.4	0.54
Experimental Frequency	15.10	19.70	58.50	66.90	120.00	128.40
Error between model and experiment%	5.0	22.2	2.70	5.26	4.26	2.84
Damping ratio $\times 10^{-4}$	320.1	177.8	110	57.4	52.5	22.9

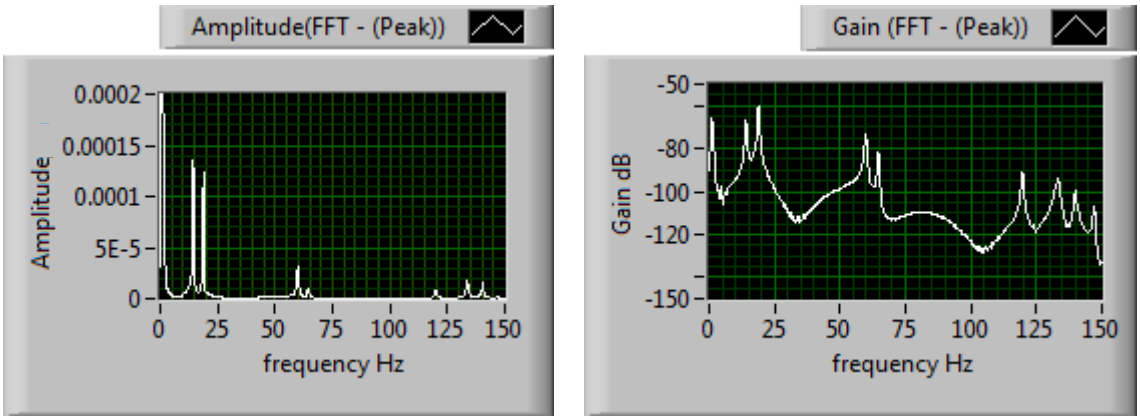

Figure 4.6 Experimental Lab VIEW graphs showing frequency response for the cross-type stiffened plate by two beams

The calculated resonant frequencies for the flat and stiffened plates were consistently higher than the experimental results, probably due to the imperfect bonding of the stiffeners and plate fixation which reduced the stiffness of the physical structure. The cantilever flat and asymmetrical T-shaped stiffened plate shows better agreement with no systematic discrepancy. The maximum discrepancy was 10.19% for the cantilever flat plate at the first mode and 7.5% for the stiffened plate T-type and 22.2% for the cross type at the second mode. The bigger discrepancy in the second mode for the cross-stiffened plate is due to their close coupling, which distorts the individual peaks.

Table 4.2 to Table 4.4 also show the damping ratio for each mode obtained from the half power bandwidth determined using the frequency response graph. The frequency difference $\Delta\omega$ between the half power (-3dB) points on each modal peak ω_n was measured and the damping ratio calculated as $\Delta\omega/2\omega_n$. The value of damping ratio was assumed to be 0.01 for all the first six modes of vibration for the cc-plate and co-plate types.

Table 4.5 ANSYS natural frequencies compared with present model for the clamped-clamped plate "cc-plate"

Element type	Mode (Hz)					
	1^{st}	2^{nd}	3^{td}	4^{th}	5^{th}	6^{th}
ANSYS shell63 (2 × 2)	39.77	47.64	76.73	156.2	158.6	161.7
ANSYS shell63 (4 × 4)	42.04	50.95	83.19	115.11	126.01	150.17
ANSYS shell63 (8 × 8)	42.13	50.51	82.97	116.22	128.27	150.82
ANSYS shell63 (10 × 10)	42.12	50.38	82.90	116.2	128.10	151.03
ANSYS shell63 (20 × 20)	42.09	50.19	82.78	116.17	127.72	151.36
ANSYS shell63 (50 × 50)	42.07	50.12	82.74	116.12	127.53	151.47
ANSYS solid45(50×50)	42.13	50.24	83.01	116.17	128.09	152.15
Present model (20 × 20)	42.39	50.40	83.04	118.50	129.83	153.16
Error between model and ANSYS%	0.71	0.41	0.31	2.00	1.65	1.18

Table 4.6 ANSYS natural frequencies compared with present model for the clamped-one point fixed plate "co-plate"

Element type	Mode (Hz)					
	1^{st}	2^{nd}	3^{td}	4^{th}	5^{th}	6^{th}
ANSYS shell63(2×2)	12.92	35.37	47.02	59.94	82.73	144.34
ANSYS shell63(4×4)	12.15	35.75	45.84	60.15	90.87	112.59
ANSYS shell63(8×8)	11.67	34.79	44.51	58.66	89.77	111.45
ANSYS shell63(10×10)	11.56	34.467	44.23	58.34	89.29	111.09
ANSYS shell63(20×20)	11.30	33.60	43.64	57.70	87.93	110.26
ANSYS shell63(50×50)	11.07	32.81	43.20	57.26	86.62	109.70
ANSYS solid45(50×50)	11.26	33.40	43.62	57.71	87.78	110.33
Present model (20×20)	11.17	33.33	43.33	57.54	87.88	111.05
Error between model and ANSYS %	1.15	0.81	0.71	0.27	0.05	0.71

4.6. Conclusions

Square flat plates with and without stiffeners have been tested in various configurations to achieve dynamically symmetric and asymmetric structures. These structures have been used to test the MATLAB m-code program described in chapter three against two separate equivalent ANSYS models and against experimental measurement and found to give acceptable agreement for the first six vibration modes in all cases. This gives a confidence level for the using the model to prepare the state space matrices used in subsequent chapters to optimise the location and feedback gain and number of sensors and actuators.

Chapter 5. The Optimal Placement of Actuators for Flat Plate

This chapter concerns the active vibration reduction of flexible plates with low natural damping using discrete piezoelectric patches bonded to the plate surface in the optimal locations. The optimisation of the location of these transducers can be approached using the genetic algorithm, but the search space is very large for complex structures with many transducers needed to suppress several modes of vibration. A placement strategy including conditional filtering is proposed to reduce the search time, and to achieve a global optimal solution along with the genetic algorithm program stability, and hence to increase the efficiency of the optimisation process. This filter works by eliminating repeated genes in the chromosome and exploring the global optimal configuration of sensors and actuators. An isotropic plate is investigated using Hamilton's principle and the finite element method based on first order shear deformation theory to account for the effects of piezoelectric mass, stiffness and electromechanical coupling according to the model derived in chapter three. In this study, an APDL program was written for the cantilever plate bonded with a single piezoelectric pair covering the whole plate using a three dimensional solid45 element for passive structure and solid5 element for piezoelectric active structure and represented in the ANSYS finite element package in order to study the distribution of mode shape, modal strain intensity and electric charge over the piezoelectric surface for the first six modes in a free vibration test. The distributions were found to be symmetrical about the plate’s dynamic axis of symmetry for the first six modes of vibration.

The genetic algorithm placement strategy was programmed in MATLAB and applied for a cantilever plate so as to locate combinations of two, four and ten sensor/actuator pairs based on the minimisation of the linear quadratic index as an objective function, suppressing the first six vibration modes. The optimal placement of discrete sensor/actuator pairs was found to be symmetrically distributed and in accordance with the dynamic axis of symmetry of the plate. The reliability of the placement strategy and the effectiveness of the conditional filter were tested by running the genetic algorithm program multiple times for the same cantilever plate to locate ten and four actuators. The same optimal distribution of actuators was found in all of the computer program tests. The results are compared with those previously published for optimal actuators distribution. It is shown that the placement strategy using the conditional filter greatly reduces the run time needed to find the global optimal solution, and that the vibration

reduction achieved over the first six modes is an improvement on previously published optimal distributions of piezoelectric actuators.

The correctness and effectiveness of the optimal location and modelling for ten actuators was also tested in the ANSYS finite element package using two types of control schemes. The APDL code was written which utilised the optimal linear quadratic control and estimator which is based on the modelling and interacting with the cantilever plate by sensors and actuators. Another APDL code was written that implemented the proportional differential control scheme and, again interacting with the cantilever plate by sensors and actuators. The closed loop time response at steady state was close for the two control schemes and gave a percentage reduction of 94% for the first three modes. Finally, the robustness of the estimator was tested under a complex rang of conditions and was found to give high stability and vibration suppression.

5.1. Introduction

The genetic algorithm is a powerful optimisation method which is used in this work to determine efficient locations for discrete sensors and actuators for the active vibration control of smart structures. The complexity of the genetic algorithm when applied to the sensor and actuator placement problem depends on the number of candidates in the search space, which is the statistical combination of the numbers of sensors or actuators and their possible positions on a structure. The search space may have many locally optimal solutions but just one unique global optimal solution. When using a genetic algorithm, it is difficult and costly to find the global optimal solution when the search space is large. A local or suboptimal solution often gives acceptable vibration suppression. However, the configuration of a global optimal solution could have significantly better properties than those of local and suboptimal solutions and more than vibration reduction optimisation.

Flexible smart structures with a distributed piezoelectric sensor/actuator pair have been investigated thoroughly in attempting to suppress mechanical vibration, as explained in the introduction to chapter three. In active vibration control, researchers have paid attention to discrete piezoelectric sensors and actuators and their optimal locations in order to achieve high sensing and actuating effects [38, 50, 73, 76-79, 82, 83]. The optimal placement of discrete piezoelectric sensors and actuators on flexible structures has been investigated by many researchers using genetic algorithms based on different types of objective functions and placement strategies.

The optimisation of feedback gain and the locations of three piezoelectric sensor/actuator pairs was investigated by Zhang et al for a cantilever beam to suppress the first four modes of vibration, taking the maximisation of energy dissipation as an objective function. A novel floating-point coded chromosome was proposed instead of binary coding in order to reduce the computer memory storage and to increase the genetic algorithm search speed. They wrote that the difference between genetic algorithm based on a floating-point coding chromosome and that using a binary-encoded chromosome was that the latter caused major difficulties during the decoding process. Parents for the next generation were chosen based on the rank selection process which is carried out by ordering the individuals according to their fitness values and then the selection process is based on their position in that order. They stated that the use of rank selection can support a steady selective pressure and avoid early convergence to suboptimal solutions. They also showed that the optimisation method using a quasi-Newtonian algorithm utilised in a previous study [105] does not guarantee finding the global optimal solution and the final optimal solution was based on seven local optimal solutions. They found the optimal solution with fitness improvement of 40.35% compared with the previous study [105] using the floating-point coded chromosome [27].

Sadri et al investigated vibration reduction of a simply supported plate by the optimal placement of two actuators using a genetic algorithm based on modal and grammian controllability as objective functions. The chromosome was encoded by binary numbers and the parent individuals were selected randomly. Different optimal actuator configurations were found for each placement criterion and asymmetrical distribution of actuators on the symmetrical plate [25]. The use of the binary-encoded chromosome and random selection could be considered as weak points in this study and the alternatives are the integer-encoded chromosome and rank selection method in order to increase the efficiency of the genetic algorithm search.

Han and Lee investigated the placement of two actuators and six piezofilm sensors optimised for a cantilever plate using grammian controllability and observability as objective functions to suppress the first three modes of vibration, and spillover effect reduction was also considered for the fourth and fifth modes as a residual. The plate dimensions were $22 \times 18 \times 0.082$ cm discretised to 99 elements, and total numbers of possible combinations of the locations of six sensors were found to be equal to 11.2×10^{11}. Chromosome string length was forty-eight based on the number of sensors using

binary coding and the parent individuals were selected for the next generation via the tournament method. Crossover was carefully implemented between individual words instead of between bits in order to give correct locations on the structures. The optimal configuration of six sensors was found to be symmetrically distributed about the plate axes of symmetry [26]. This method of crossover meant that the chromosome binary-encoding behaves as an integer.

Peng et al studied the optimal placement of four sensor/actuator pairs using genetic algorithms to attenuate the first five modes of vibration based on the maximisation of the grammian controllability index as an objective function. In the placement strategy, a binary-encoded chromosome was used and the parent individuals were selected according to their fitness to form the next generation. The genetic algorithm program was run ten times and they found different suboptimal solutions for each run. They selected twelve solutions from these computer runs and the final optimal solution of the distribution of four sensor/actuator pairs was selected based on the scores of repeated individual genes of nine sensor/actuator pairs which were found in the twelve solutions for each individual mode [35]. However, the best placement strategy gave the same optimal solution for each computer run, but here there was no relationship between the scores of repeated individual genes and the final optimal solution. The optimal solution based on the suppression of modes collectively is more efficient than individual suppression.

Kumar and Narayanan investigated the optimal placement of ten sensor/actuator pairs for a cantilever plate using the minimisation of the linear quadratic index as an objective function to suppress the first six modes of vibration. The plate was discretised to one-hundred elements and the chromosome string length was equal to the number of finite elements of the plate. The chromosome was binary-encoded and marked by one for an element bonded to a sensor/actuator pair and otherwise marked as zero. Random parent selection was implemented to form the next generation [38]. Basing chromosome string length on the total number of finite elements of a structure however, could cause problems and misguide the convergence to the optimal solution for such plates or larger structures discretised to thousands of finite elements. Alternative effective chromosome string length is based on the number of sensor/actuators required to be optimised. The binary method of encoding the chromosome also adds extra problems and distorts the guidance to the optimal solution. The parents of the next generation were selected based on a random method, which achieves a very low genetic pressure engine by giving the

same probability to the chromosomes of the highest and lowest fitness. Selection based on the principle of the "survival of the fittest" gives a high probability of survival to the most-fit individual which is against random selection based individual genetic code. This type of selection requires a massive number of generations to find suboptimal or optimal solution.

Roy and Chakraborty investigated active vibration reduction in a composite beam and shell by optimally placed sensor/actuator pairs using an integer-coded genetic algorithm and the maximisation of controllability index as an objective function. A comparison of two case studies based on binary-encoded and integer-encoded chromosomes was conducted for a cantilever beam discretised to 20 finite elements in order to optimise four actuators and to suppress the first mode of vibration. The number of generations for convergence to the optimal solution was greatly reduced from 246 using binary-encoding to 31 using integer-encoded chromosome with string length equal to the number of actuators. The parents for the next generation were selected according to the roulette wheel [40]. The selection of individual parents based on the roulette wheel is better than random selection in order to follow the principle of "survival of the fittest".

The genetic algorithm program was run multiple times to get the optimal piezoelectric configuration and different optimal configurations were found for each run [35, 105]. Also the optimal placement selected was based on the scores of individual genes for efficient locations, while in other studies the optimal configuration was based on best and average fitness value [25, 30]. However the optimal configuration should be selected by the genetic algorithm program based on optimal fitness taking into account the effects of modes collectively so as to give the same optimal configuration in each run.

Different placement strategies have been implemented [25-27, 30, 34, 35, 38, 67] using genetic algorithms to locate sensors and actuators, without the robustness of these placement strategies being tested or the global optimum being searched. Most previous studies showed the results of optimal solution for just one computer program run. Of those studies reporting a number of genetic algorithm computer program runs, two found different optimal solutions for each run [35, 105] and one found same optimal solutions for each run, but only after 5000 generations, much longer than taken by other method [49].

In this chapter a new optimal placement strategy is proposed which includes a conditional filter in the genetic algorithm to reduce the search space and to explore

global optimal actuator location using integer-coded chromosomes. An isotropic plate with bonded discrete piezoelectric sensor/actuator pairs was investigated according to the model derived in chapter three. The optimal placement of two, four and ten piezoelectric actuators and optimal feedback gain were investigated for a cantilever plate to attenuate the first six modes of vibration using the minimisation of linear quadratic index as an objective function. Active vibration suppression was also investigated for a cantilever plate with ten sensor/actuator pairs using optimal linear quadratic and proportional differential control schemes.

5.2. Modelling

The full modelling derived in chapter three for a plate stiffened by beams and bonded with discrete sensors and actuators is used in this chapter to investigate a flat plate by assuming that the mass and stiffness of the beam are equal to zero. Controller state space matrices were prepared according to equations 3.97 to 3.100.

5.3. Control Scheme and Objective Function

In this chapter, the minimisation of the linear quadratic index is used as an objective function to locate the actuators according to the discussion in section 3.7. An optimal linear quadratic control scheme is implemented to attenuate the first six vibration modes, as explained in sections 3.5 and 3.8. A proportional differential control scheme was also used for comparison and validation.

5.4. Modified Genetic Algorithm for Piezoelectric Placement on Structures

In 1975, Holland invented the genetic algorithm, which is a superior guided random method based on the principle of survival of the fittest or natural evolution theory used to find optimal solutions. It has been continuously improved and is now a powerful method for searching for optimal solutions. An optimisation problem consists of a large number of possible solutions, which is called the search space, and each of these solutions can be marked by a fitness value depending on a problem definition or fitness function. An exhaustive search in which every element of the search space is evaluated is very costly. For example, the work described here involves the optimal location of ten sensor/actuator pairs on a plate discretised into 100 elements, so that the size of the search space is the statistical combination of 10 items from 100, which gives 1.73×10^{13} possible solutions. The genetic algorithm represents an efficient method to search for

the global optimal solution and is largely immune to the problem of becoming "stuck" at a local optimum.

The fundamental unit in the genetic algorithm is a population of individuals, each defined by a chromosome containing a number of genes. The effectiveness or "fitness" of each individual is calculated according to some rule using the values of the genes. The members of the population with the highest fitness values are allowed to "breed" to form the next generation, and the process continues until convergence is achieved. In this case, the ten "genes" are the locations of the ten sensor/actuator pairs defined by an integer number (1-100), and the fitness function is the linear quadratic index. This process is directly analogous to the survival of the fittest concept in Darwinian natural selection, in which the more successful individuals in a population are inclined to breed and so form the next generation. By this means the genes that code for desirable characteristics, and so give the individuals possessing them a high degree of fitness, are transmitted down the generations at the expense of less useful genes, which die out.

The working mechanism of the genetic algorithm is represented by two stages: firstly the selection of the breeding population from the current whole population, and secondly reproduction. The process is started by defining a population of individuals at random from the search space, the chromosome of each being made up of ten random numbers in the range (1-100, of the finite element global numbering on the plate), representing the locations of the ten sensor/actuator pairs on the plate. This is the population in the first generation. In the selection process, the fitness function value for each individual is calculated using these genetic values as data, and the breeding population is defined as those with the highest values of fitness. The reproduction process is closely based on sexual reproduction. Pairs of the best individuals from the breeding population share their genetic material to produce offspring containing a combination of their parents' genes.

Many strategies have been developed to apply the reproduction process, but all involve "crossover" and "mutation". In crossover, the chromosome of each parent is broken and two new chromosomes formed from the pieces. In mutation, one or more genes in a child's chromosome are changed randomly. In this way crossover is used to explore the known regions of the search space by testing different combinations of genes that have been shown to promote high fitness, while mutation helps to maintain diversity in the population and so to explore new regions of the search space. The process then continues for many generations until the population converges on a single optimal

solution, which is to say that the chromosomes of all members of the breeding population are almost identical.

The plate is divided into 100 elements encoded by sequential integer numbers 01, 02, , , 100; each representing a possible location of a sensor/actuator pair as shown in Figure 5.1(a). As implemented in this work, chromosome length contains ten genes for sensor/actuator locations and the chromosome is marked with its fitness value as shown in Figure 5.1(b) which also illustrates the reproduction process.

Suppose two chromosomes are selected from the search space: the first is coded 01 54 27 93 41 60 67 72 15 99 and the second is coded 87 70 03 56 76 22 24 06 81 30 marked by their fitness value Fit1 and Fit2 calculated from the chromosome gene properties. These chromosomes represent the two parents. For the case illustrated, crossover occurs randomly at some point along the chromosomes to produce the two child chromosomes. In addition, the tenth gene of the second child has undergone mutation.

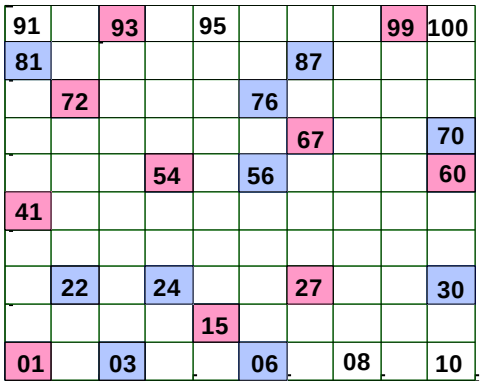

(a) Search space

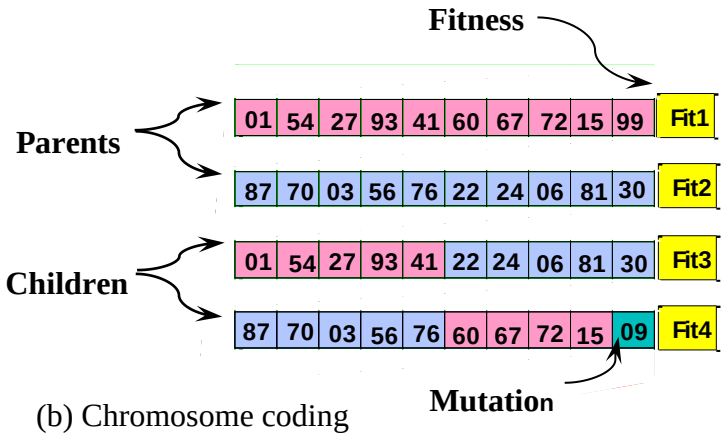

(b) Chromosome coding

Figure 5.1 Search space, chromosome integer number coding, crossover and mutation give off-spring of two children with new fitness values

5.5. Placement Strategy

In this work, the strategy for the placement of piezoelectric actuators is proposed and programmed in MATLAB m-code according to flowchart shown in Figure 5.2. Its main features are:

1. Suitable values of $Q = 10 \times 10^{11} \times I_{2n_m,2n_m}$ and $R = 1 \times I_{r_a,r_a}$ are set by the user. The weighted matrix Q controls the level of vibration suppression of flexible structures. Increasing the value of the weighted matrix Q gives the optimal locations of sensor/actuator pairs on a structure in order to achieve higher vibration suppression, and this may require higher external energy and vice versa.
2. The state matrix A of dimension $(2n_m, 2n_m)$ is prepared for the first six modes of vibration according to equation 3.98.
3. One hundred chromosomes are chosen randomly from the search space to form the initial population.
4. The input (actuators) matrix is calculated for each chromosome and for the first six modes of vibration according to equation 3.99.
5. A fitness value is calculated for each member of the population based on the fitness function, according to equation 3.123, and stored in the chromosome string to be saved for future recalculation.
6. The chromosomes are sorted according to their fitness value and the 50 chromosomes (less than or equal to the initial population depending on the problem size) with the lowest fitness values (i.e. the most fit) are selected to form the breeding population. These are called parents. The remaining, less fit, chromosomes are discarded.
7. The members of the breeding population are paired up in order of fitness and 50% crossover is applied to each pair; the crossover point being selected randomly and is different for each parent. This gives two new offspring (child) chromosomes with new properties.
8. A mutation rate of 5% is used on the child chromosomes.
9. The new chromosomes are filtered for repeated genes. It is a physical requirement of this work that there be ten sensor/actuator pairs, so more than one gene for a particular location would be meaningless and disrupts the path to the optimal solution. The filter tests for repeated genes, and if one is detected it

is replaced with a gene from the search space. For example, if a child chromosome has the code [01 72 33 54 65 80 01 45 100 17], the gene 01 is

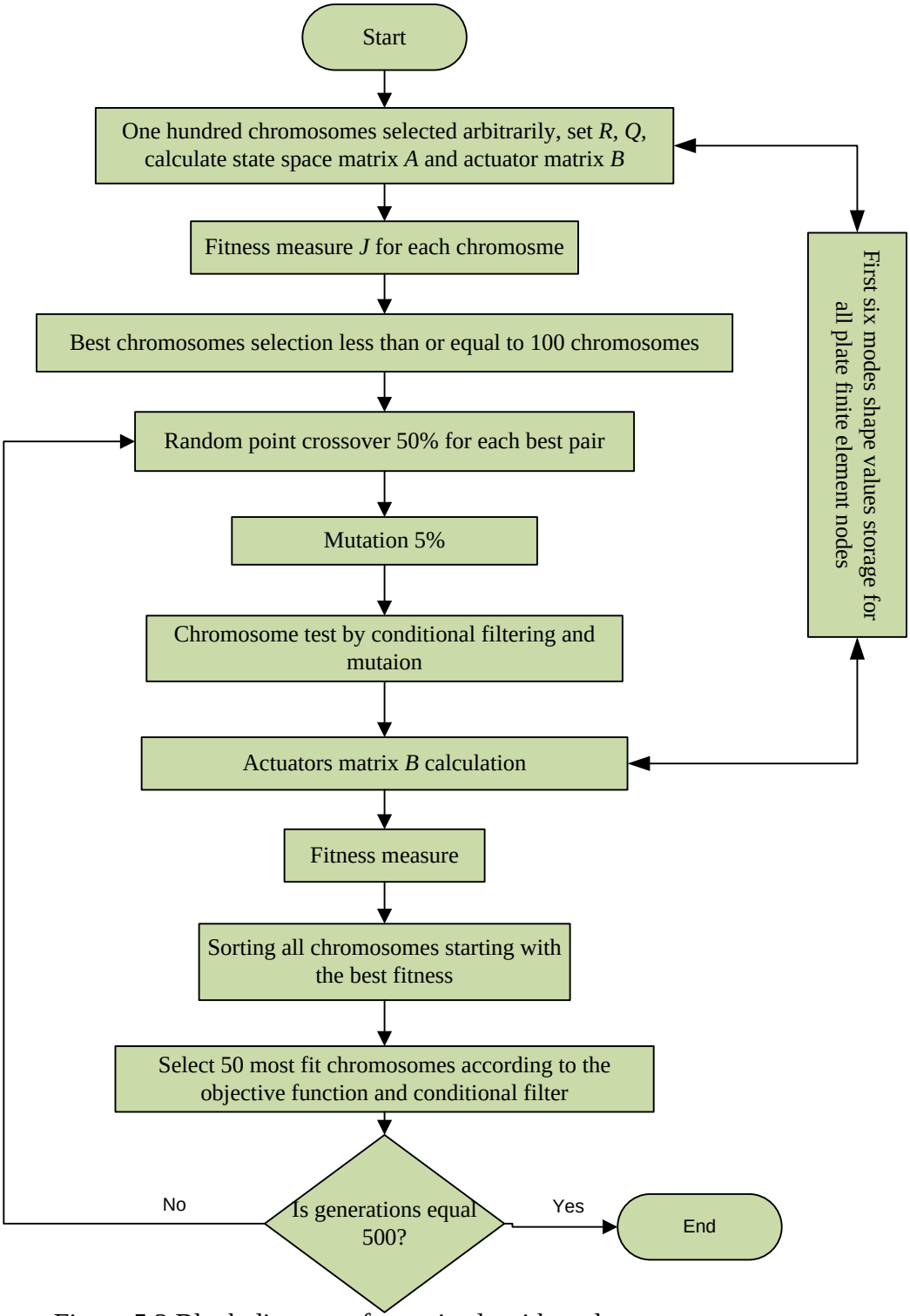

Figure 5.2 Block diagram of genetic algorithm placement strategy

repeated as a result of crossover or mutation. Replacing this one occurrence with a random value serves the same purpose as mutation, that of preserving diversity in the gene pool and preventing premature convergence to a local solution.

10. The input (actuators) matrix is calculated for each child chromosome according to equation 3.99 (see section 3.4.2) and thereafter the process is repeated from step 5 for a preset number of generations.

5.6. Results and Discussion

5.6.1. Research problem

A cantilever flat plate of dimensions $500 \times 500 \times 1.9$mm was mounted rigidly from the left hand edge as shown in Figure 5.3. The plate is discretised to one hundred 10×10 elements sequentially numbered from left to right and bottom to top as shown in the Figure. The global optimal placement of two, four, six and ten piezoelectric sensor/actuator pairs is investigated to suppress the first six modes of vibration. These four cases are chosen to give direct comparisons with previously published work [35, 38, 49, 54] . The plate and piezoelectric properties were listed in Table 4.1.

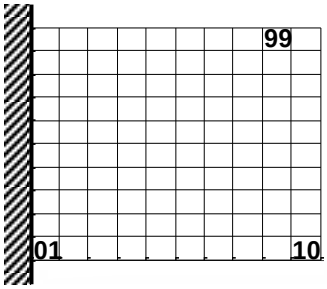

Figure 5.3 Cantilever plate mounted rigidly from the left hand edge discretised to one hundred elements sequentially numbered from left to right and bottom to top

5.6.2. Natural frequencies

The first six natural frequencies and mode shapes for the cantilever plate were determined using a MATLAB m-code program based on the present model and validated by the ANSYS finite element package using two-dimensional shell63 and three-dimensional solid45 elements and were also validated experimentally as explained in section 4.5 and with the results listed in Table 4.2.

5.6.3. Mode shape, modal strain and electric charge distribution

An APDL computer program was written for the flat plate and represented in the ANSYS finite element package to investigate the mode shape, modal strain and electric

charge distributions in the first six modes. Three-dimensional solid45 and solid5 elements are used respectively for the passive structure and the active piezoelectric sensor/actuator pair. The results are shown in Figure 5.4 to Figure 5.6 for the distribution of mode shape, modal strain and electric charge respectively.

Firstly, it can be seen from Figure 5.4 that the shapes of first six modes are symmetrically distributed about the axis of symmetry of the plate, which is perpendicular to its fixed end.

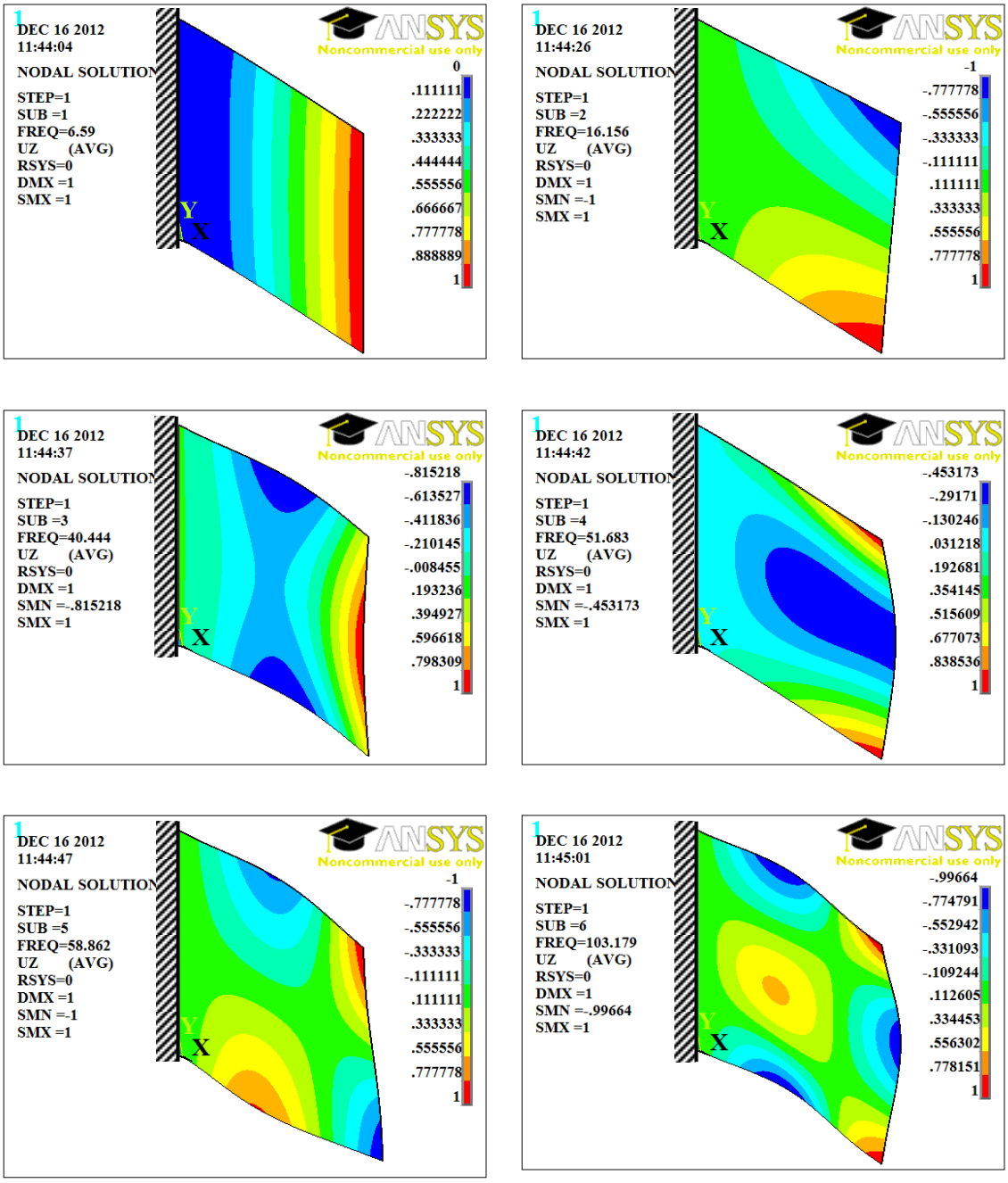

Figure 5.4 Distribution of the first six modes shape in z-direction for a cantilever plate mounted rigidly from the left-hand side

Secondly, Figure 5.5 shows the distribution of the modal strain intensity in the first six modes. It can be observed that the distribution is also symmetrically distributed about the plate's axis of symmetry. The concentration of modal strain is higher on the fixed end of the plate than the free end, and the opposite is true in case of the mode shape distribution. Moreover, the modal strain concentrations shared the same location at the corners of the root of the plate for all the first six modes.

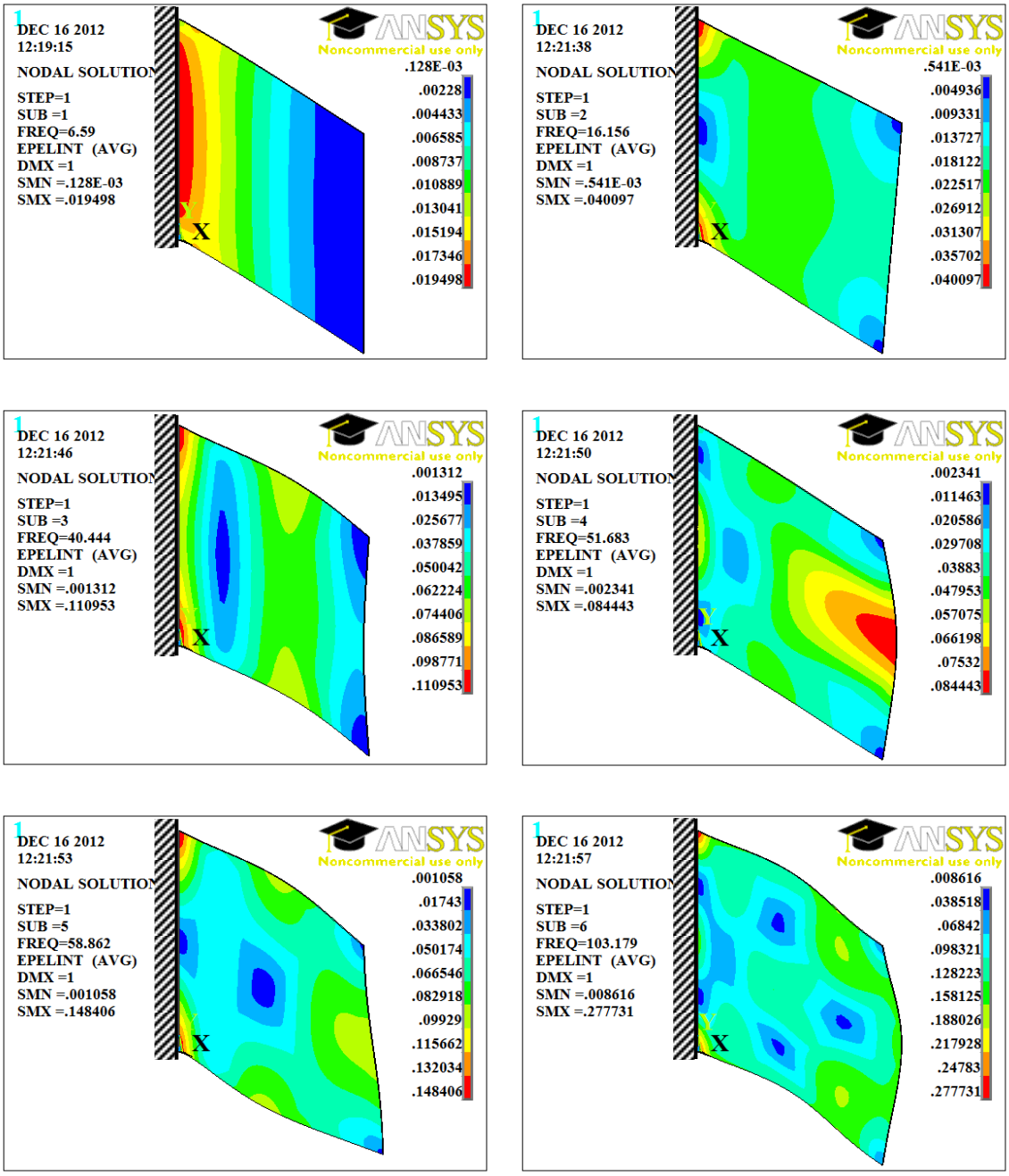

Figure 5.5 Distribution of the modal strain intensity in the first six modes for a cantilever plate mounted rigidly from the left hand side

Finally, the cantilever plate is fully bonded to a single piezoelectric sensor/actuator pair which covers the whole plate and is represented in the ANSYS package using an APDL program to investigate the distribution of electric charge over the sensor and actuator surfaces. The modal electric charge is also distributed symmetrically over the piezoelectric sensor and actuator surfaces for all of the first six modes, as shown in Figure 5.6. The following conclusions can be drawn from this section.

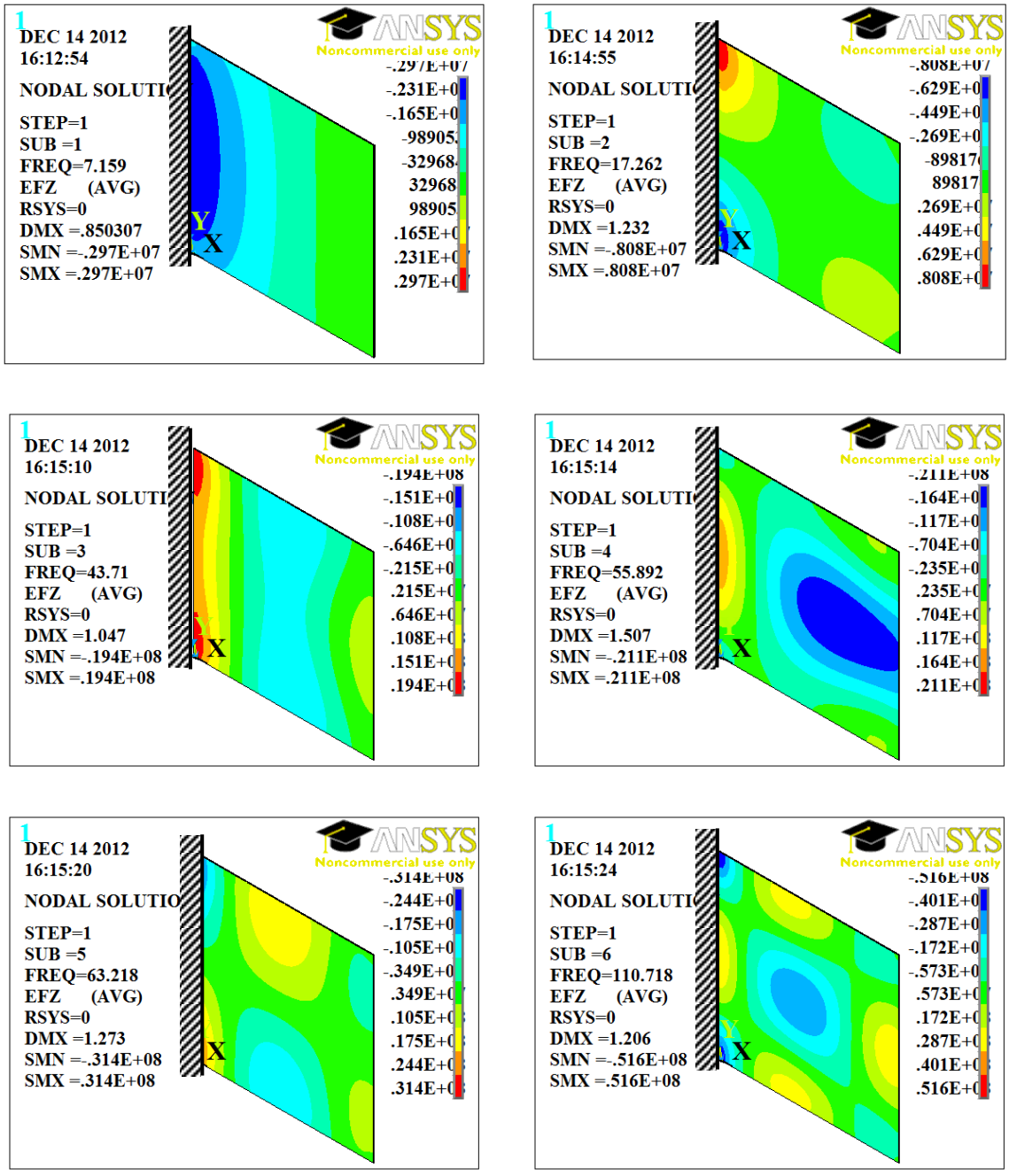

Figure 5.6 Distribution of the modal electric field in z-direction through piezoelectric in the first six

The evidence concerning the distribution of mode shapes, modal strain and electric charge distribution indicates that the global optimal location of discrete piezoelectric sensors and actuators is also likely to be symmetrically distributed also.

It is observed from the distribution of electric charge in the first six modes shown in Figure 5.6 that the collective effect of electric charge over the piezoelectric surface approximately sums to zero for each mode. Therefore, it could be said that the sensing and actuating effects are nearly cancelled out for a mechanical structure fully covered by a single sensor/actuator pair. However, discrete sensor/actuator pairs give high sensing and actuating effects if they are appropriately located.

5.6.4. Optimisation of piezoelectric actuator location

The genetic algorithm and placement strategy described in sections 5.4 and 5.5 were implemented to find the optimal locations of ten piezoelectric actuators on a cantilever plate measuring 0.5m square mounted rigidly from the left hand edge, as shown in Figure 5.3. The progressive convergence of the population onto an optimal solution is shown in Figure 5.7**,** in which the population is distributed around the circle with radius ***r*** which represents the fitness value to be minimised. At the first generation shown in Figure 5.7(a) the population is very diverse with representatives of high and low fitness and a range in between. After twenty generations, as in Figure 5.7(b), the population is much less diverse, made up of individuals of high, though not yet optimal, fitness. After 500 generations, shown in Figure 5.7(c), the population has completely converged to a level of fitness higher than any individual in the first or twentieth generations.

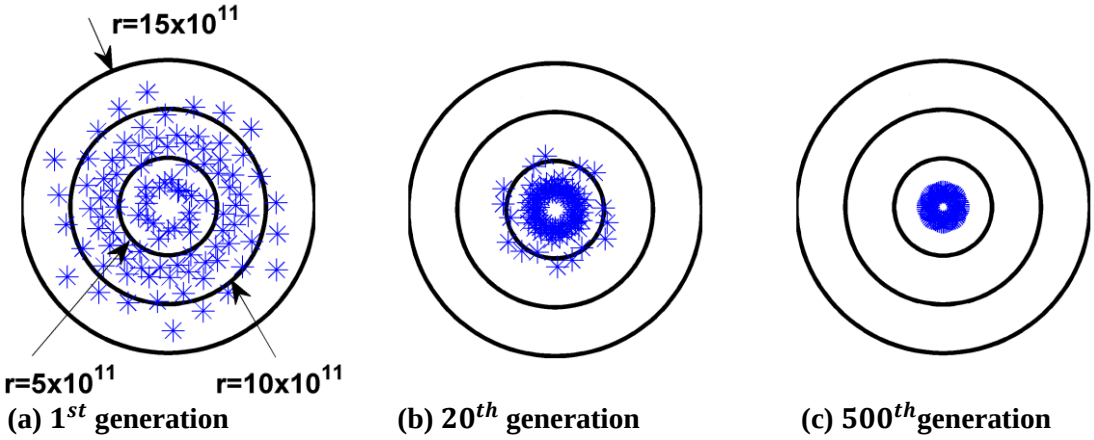

Figure 5.7 Population fitness progression over 500 generations. Each individual is represented as one of the points distributed around the circle, with its fitness value, obtained from its chromosome, defining its distance from the centre.

This convergence is shown in another form in Figure 5.8. Each point represents the location of a sensor/actuator pair for one of the individuals in a particular generation. In the first generation these locations are widely distributed, having been selected at random, as shown in Figure 5.8(a). After twenty generations they have begun to cluster in a few locations, as shown in Figure 5.8(b) and after five hundred generations the clustering is mostly complete with most individual chromosomes coding for sensor/actuator pairs at the ten most effective sites, as in Figure 5.8(c). The optimal arrangement was found to be symmetrically distributed about the x-axis, which is the axis of dynamic symmetry for this structure.

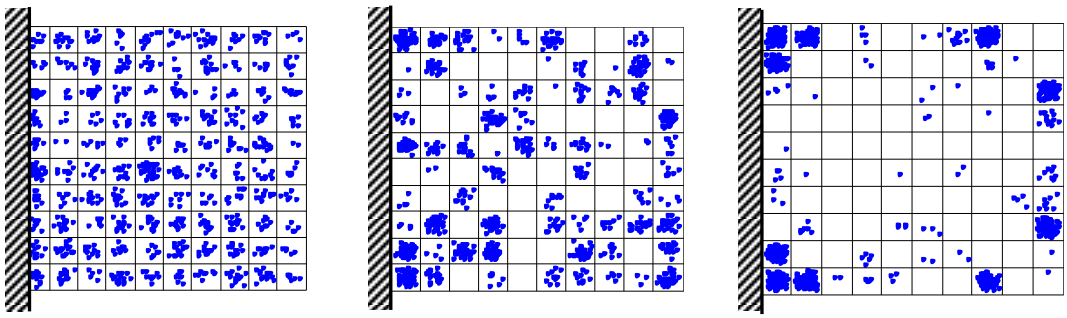

(a) 1^{st} generation **(b) 20^{th} generation** **(c) 500^{th} generation**

Figure 5.8 Sensor/actuator placement for the cantilever plate. Each dot shows the location of a sensor/actuator pair in one of the 100 breeding individuals in each generation. Initially they are randomly distributed. After 20 generations they have begun to group in efficient locations. After 500 generations they have mostly converged on ten sites, symmetrically distributed on the plate.

5.6.5. Test of robustness of the placement strategy and conditional filter

The reliability of the genetic algorithm placement strategy described in section 5.5 was tested by running it multiple times on a single problem, optimising the location of actuators on a square cantilever plate. It was found that in all cases there was convergence toward a minimum fitness value, and this convergence is speeded up considerably by the use of the conditional filter described in section 5.5.

The results shown in Figure 5.9 and Figure 5.10 (blue colour curves) give an indication of the progress of each run by plotting the fitness value for the fittest member of each generation. It can be seen that the final fitness value is the same in each run, though the path by which it is reached is different. This indicates that the process is robust in repeatedly finding the optimal solution.

The same test and placement strategy were implemented without the conditional filter, as also shown in Figure 5.9 and Figure 5.10 (red colour curves). It can be observed for off-conditional filter case that the final fitness value is different for each run, but these might converge to the same global fitness level after many hundreds of generations. Figure 5.9 and Figure 5.10 also show the equivalent results from published sources [35, 38]. It is evident that these do not represent the global optimum since their fitness values are higher than those obtained in this work with or without the filter.

The present placement strategy including the conditional filter gave a global optimal distribution of piezoelectric actuators with higher fitness which converged quickly to the optimal solution after fewer generations. This improvement was obtained as a result of placement strategy developed in this study which differed from those in published sources [35, 38] by the following points:

Firstly, the present placement strategy defined chromosome length clearly based on the number of actuators to be optimised which were encoded by integer numbers, whereas previously chromosome length was based on the total number of finite elements of the plate [38] and number of actuators [35] which were both binary-encoded. The implementation of integer-encoded instead of binary chromosome was investigated by Roy and Chakraborty, who reduced the number of generations from 246 to just 31 to get the same optimal solution for a cantilever beam where the total number of possible candidate solutions was 4845 [40].

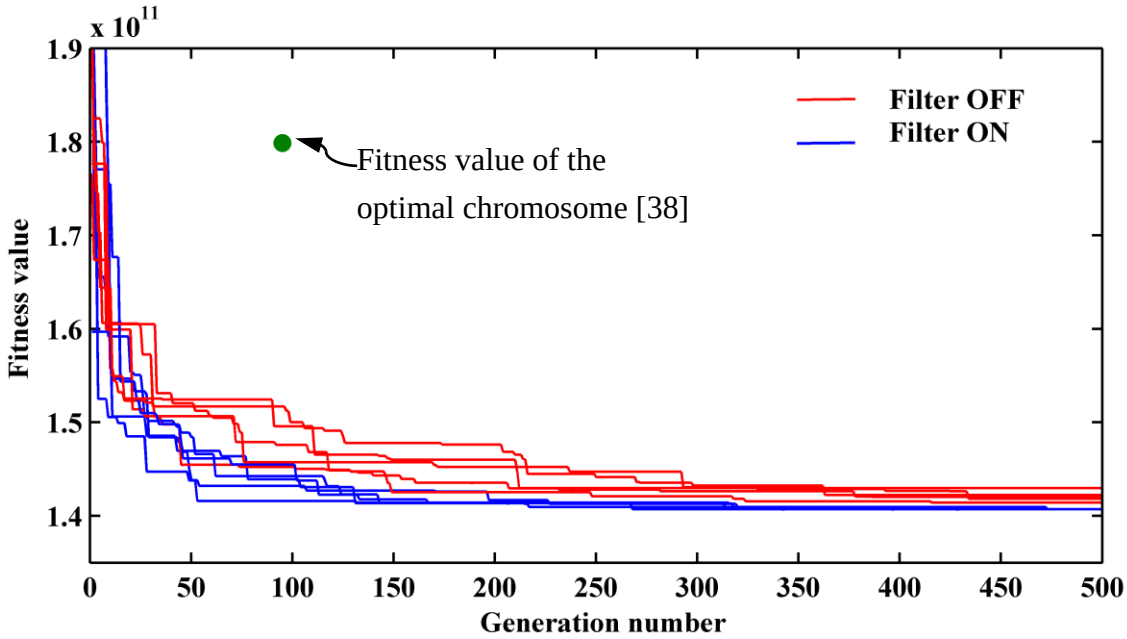

Figure 5.9 Fitness value of the best member in each generation with and without conditional filter to locate ten piezoelectric actuators on the cantilever plate, six times computer program run

Secondly, the parent individuals of the next generation were selected based on the rank of their chromosomes fitness. This gives high genetic pressure to converge to the optimal solution within fewer generations, whereas the parent selection was previously carried out using the random method [38] and a method based on individuals of high fitness having a better chance of being selected [35].

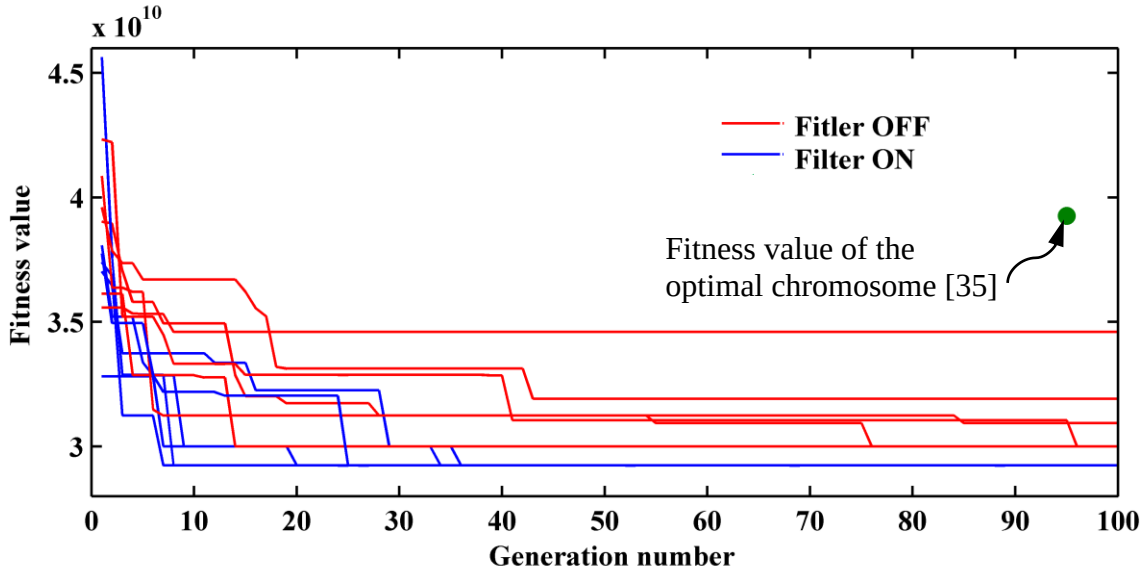

Figure 5.10 Fitness value of the best member in each generation for two cases with and without conditional filter to locate four piezoelectric actuators on the cantilever plate, six times computer program run

Thirdly, a conditional filter was proposed to filter all individuals by replacing any two identical genes in the chromosome as a result of crossover or the mutation process which is carried out before measuring their fitness. This filter significantly increased the speed of progression and prevented early convergence to local or suboptimal solutions, and to sustain the guidance of the progression convergence by the fitness function to the global optimal solution. Roy and Chakraborty applied the mutation operator under a condition of picking different gene from the old one [40]. However, the process does not check for the replacement gene being different from the other genes in the chromosome. The conditional filter solves this problem and observes the individual genes under conditions of limited number of genes inside the individual and dissimilarities between them during crossover and mutation operators.

The conditional filter considerably reduced the number of generations needed to reach the global optimal solution as shown in Figure 5.10 comparing results with those in the

study by Roy and Chakraborty [40] and other published sources [35, 38]. The total numbers of solution candidates in the optimisation problem solved in Figure 5.10 is more than 3.921×10^6 (statistical combination of 4 items from 100 equal to 3.921×10^6) and the progression converged to the global optimal solution between 8 and 37 generations. Roy and Chakraborty used an integer chromosome instead of binary-coding to reduce the number of generations from 246 to just 31 to get same optimal solution for a cantilever beam with a total number of possible candidate solutions of 4845 (statistical combination of 4 items from 20 equal to 4845). This indicates that the problem solved in Figure 5.10 is much more complicated with such a big difference in the total number of candidate solutions, but achieves the optimal solution within fewer generations.

Finally, the determination of the global optimal locations of sensor/actuator pairs reported in this section and represented in Figure 5.9 and Figure 5.10 was also investigated in the same way by Liu et al [49]. They investigated a clamped-clamped plate to optimise four nodal locations for accelerometer sensors and point force actuators using genetic algorithms. The plate was discretised to 162 finite elements and 460 nodes, which gives 1.84×10^9 candidate solutions. A binary-coded chromosome was used with a string length equal to the total number of nodes and the population size of 50 chromosomes. Random selection was implemented and fitter individuals had a higher possibility of selection. The optimisation computer program was run five times for 10,000 generations at each run, and these runs converged to the same fitness value after 5,000 generations. The authors reported that the optimal solution obtained represented the global optimal distribution. However, the case study investigated by Liu et al had a total number of candidate solutions of 1.84×10^9 which is much lower than for the cantilever plate investigated in this work which has a total number of candidates of 1.73×10^{13}. Nevertheless, their method was slow to converge and computationally less efficient compared to the work presented here.

5.6.6. Optimal piezoelectric distribution mapping on the plate

The global optimal configurations of ten, six, four and two piezoelectric actuators obtained in section 5.6.4 were mapped on the cantilever plate and found to be symmetrically distributed about the axis of symmetry of the plate as shown in Figure 5.11 and Figure 5.13. In this study, the identification of the global optimal actuator distribution was found to be symmetrical and to follow the plate's dynamic

axes of symmetry. This agrees with ANSYS results for electric charge distribution on the piezoelectric surface shown in Figure 5.6 and the optimal distribution obtained in previous studies [26, 54]. This property will be tested in the next chapters with different objective function and structures.

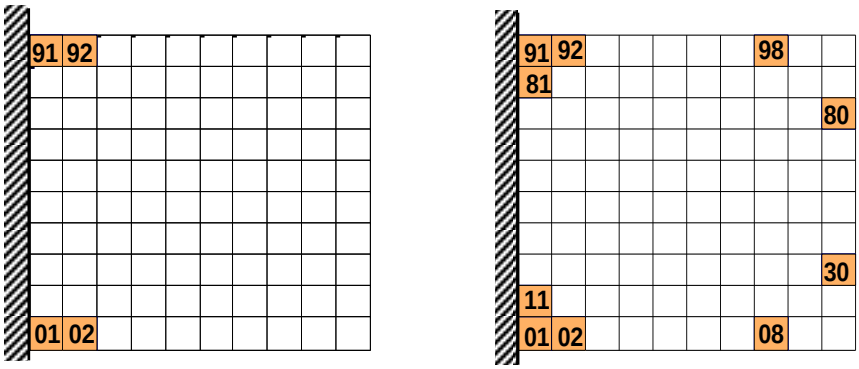

Figure 5.11 Global optimal placement configuration in the present study of four and ten piezoelectric pairs bonded to the cantilever plate

From previous studies, the optimal placement of ten piezoelectric sensor/actuator pairs [38] based on the minimisation of optimal linear quadratic index as an objective function to attenuate the first six modes, and four optimal piezoelectric pairs [35] based on maximisation of grammian controllability as an objective function to attenuate the first five modes for a cantilever plate are shown in Figure 5.12

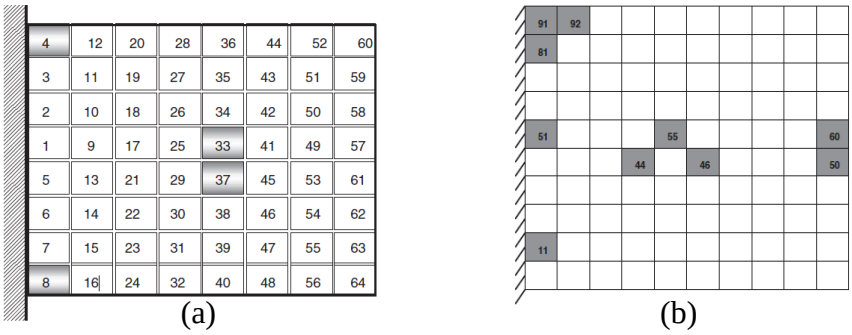

(a) (b)

Figure 5.12 Optimal placement configuration in the previous studies [35, 38] of four and ten piezoelectric pairs bonded to the cantilever plate

Figure 5.12 (a) shows the optimal placement of four sensor/actuator pairs, where the authors found twelve suboptimal solutions in nine computer runs. Locations 8 and 4 on the plate were found in all solutions; however, the other two locations were found to be different in each solution and locations 33 and 37 were chosen according to their scores

order in the suboptimal solutions. The study shown in Figure 5.12 (b) found an asymmetrical optimal distribution of ten sensor/actuator pairs for a cantilever plate.

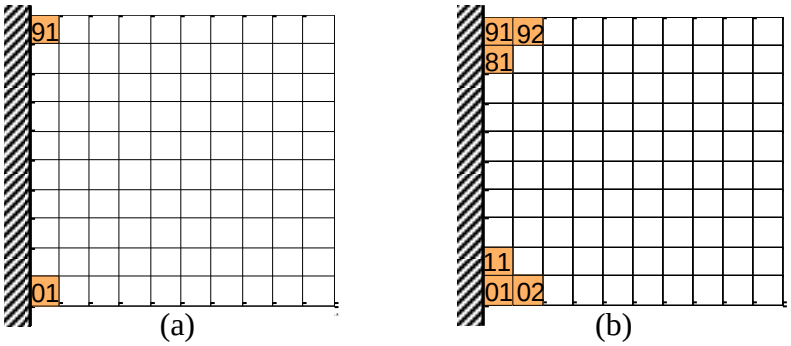

(a) (b)

Figure 5.13 Global optimal placement configuration in the present study of two and six piezoelectric pairs bonded to the cantilever plate

In other previous studies, the optimal placement of two sensor/actuator on a cantilever plate was investigated by Quek et al, who found them to be symmetrically distributed about the axis of symmetry. He used a simple search method to suppress the first two modes of vibration based on the maximisation of modal or system controllability as an objective function. The result is shown in Figure 5.14 (a) [54], which agrees with the present optimal distribution shown in Figure 5.13(a).

The optimal locations of six sensors to suppress the first five modes using genetic algorithm was investigated by Han and Lee, who also found them to be symmetrically distributed about the axis of symmetry of a cantilever plate as shown in Figure 5.14(a) [26]. This is also in agreement with the present distribution shown in Figure 5.13(b).

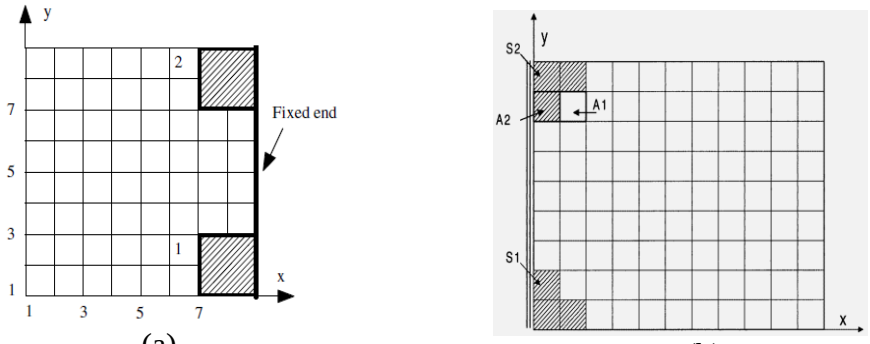

(a) (b)

Figure 5.14 Optimal placement of two actuators and six sensors for a cantilever plate investigated by [54] and [26] respectively.

5.6.7. State space and controller gain matrices.

The state space matrices can be determined for the cantilever plate bonded with ten sensor/actuator pairs in optimal locations. The state space matrices were calculated based on equations 3.98 to 3.100. Then the optimal feedback control gain matrix was calculated using optimal linear quadratic control with weighted matrices R=1 and Q=10^7 and 10^8. MATLAB commands lqr and dlqr were used to determine the optimal feedback gain matrices. Subsequently, the estimator gain matrix was determined using pole placement and the MATLAB command place. The matrices are shown in Appendix A for the state, ten actuators, ten sensors, control feedback and estimator gain matrices for the first six modes of vibration. The state space matrices are used in section 5.6.10 and implemented in simulink as shown in Figure 5.17 and Figure 5.18.

Table 5.1 shows the effects of piezoelectric mass and stiffness on the first six natural frequencies for the cantilever plate. Adding piezoelectric sensors and actuators to the plate has the two passive effects of adding stiffness and mass. These will both affect the natural frequencies, tending to increase and reduce them respectively. The effects of plate stiffening from the addition of piezoelectric sensors and actuators is more than the effects of piezoelectric mass and caused a slight increase in the natural frequencies as shown in Table 5.1.

Table 5.1 Effects of ten and four piezoelectric mass and stiffness on the natural frequencies of the cantilever plate

Case	1st	2ed	3th	4th	5th	6th
Without PZT	6.59	16.15	40.44	51.68	58.86	103.18
Ten PZT present study	6.76	16.50	41.63	51.33	61.00	106.85
Percentage effects %	2.57	2.17	2.94	0.677	3.63	3.56
Ten PZT [38]	6.81	16.93	41.29	52.68	61.14	103.41
Percentage effects %	3.33	4.82	2.10	1.93	3.87	0.22
Four PZT present study	6.80	16.74	41.45	51.94	60.39	105.01
Percentage effects %	3.18	3.65	2.49	0.5	2.6	1.77
Four PZT [35]	6.69	16.68	41.50	51.87	60.41	104.73
Percentage effects %	1.51	3.28	2.62	0.36	3.04	1.50

5.6.8. Frequency response

The closed loop average vibration reduction using an optimal linear quadratic control scheme for the cantilever plate with four and ten sensor/actuator pairs optimally located and shown in Figure 5.11 was compared with that of optimal piezoelectric configurations in previously published studies [35, 38] as shown in Figure 5.12. The calculation is performed as shown in section 3.8. The plates were actuated with a sinusoidal voltage of constant unit amplitude at actuator locations 11 and 01 for plates bonded with ten and four sensor/actuator pairs respectively. Optimal linear quadratic control was implemented with different values of the weighted matrix of 10^7 and 10^8, and the final results are reported in Table 5.2 and Table 5.3. It is clear that the present global optimal four and ten piezoelectric pairs give an average improved vibration reduction of 56.49% and 45.84% at R=1 and Q=10^8 compared to those in the previously published optimal sensor/actuator pairs configurations. An increase in the weighted matrix Q to a value higher than 10^8 causes noise and locations divergence of the poles of the closed loop system on the s-plane.

Table 5.2 Closed loop average dB gain reduction for the cantilever plate bonded with four sensor/actuator pairs over the first five modes

Four S/A pairs	Closed loop dB gain reduction		
	Present study	Ref [35]	Improvement %
$Q = 10^7$	21.02dB	18.77dB	29.5%
$Q = 10^8$	30.11dB	26.22dB	56.49%

Table 5.3 Closed loop average dB gain reduction for the cantilever plate bonded with ten sensor/actuator pairs over the first six modes

Ten S/A pairs	Closed loop dB gain reduction		
	Present study	Ref [38]	Improvement %
$Q = 10^7$	23.0722dB	21.4369dB	20.71%
$Q = 10^8$	30.9426dB	27.6645dB	45.84%

The open and closed loop frequency responses were tested for the cantilever plate bonded with ten sensor/actuator pairs according to the present work using optimal linear quadratic control scheme. The plate was driven by a sinusoidal unit voltage amplitude at actuator location 02 on the plate and the frequency responses are shown in Figure 5.15(a), (b) and (c) for sensors locations 01, 02 and 11 on the plate respectively.

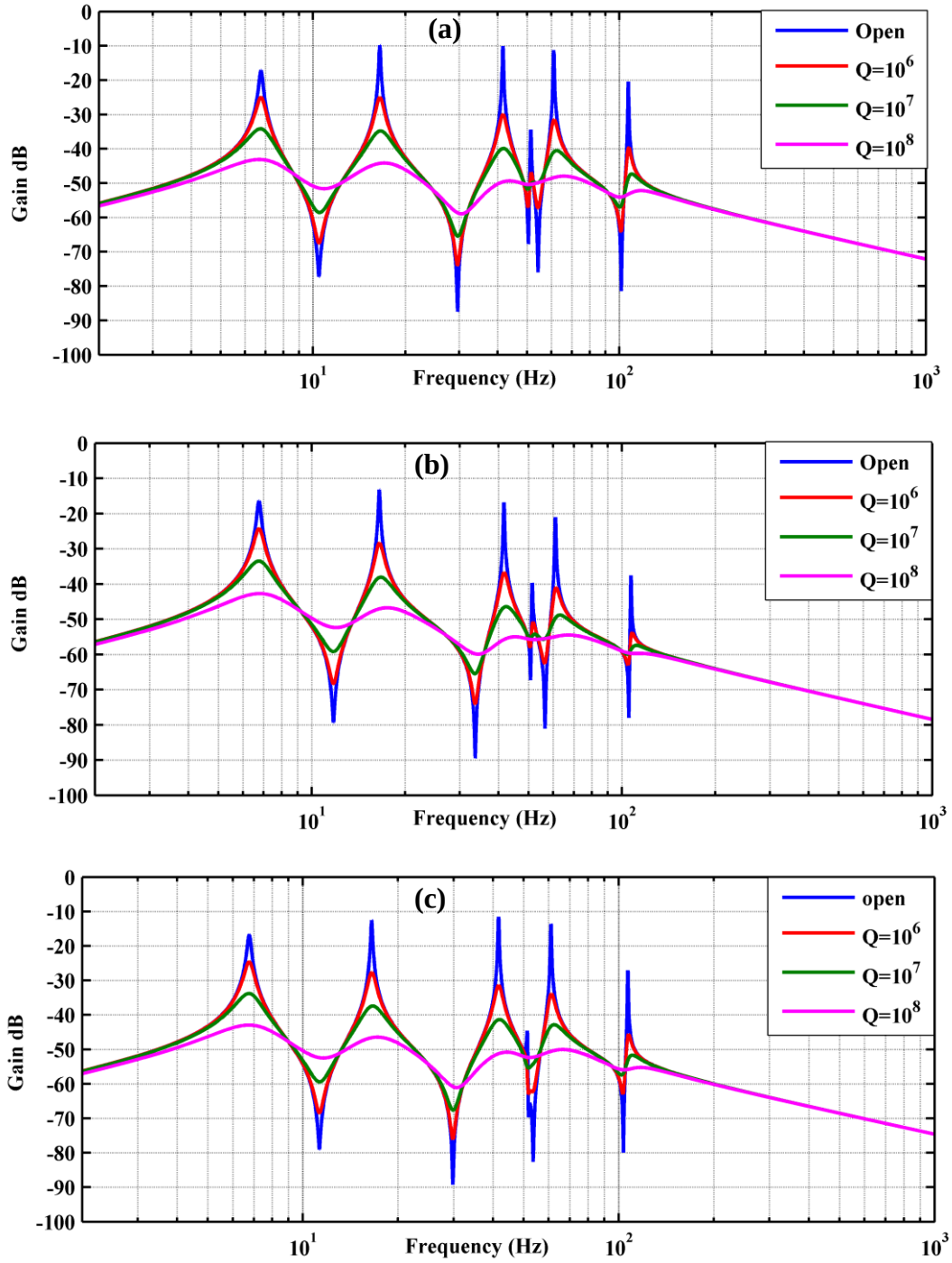

Figure 5.15 Open and closed loop frequency response for the cantilever plate bonded with ten piezoelectric pairs, showing the response at sensor locations on the plate **(a)** 01 , **(b)** 02 and **(c)** 11 as a results of driving unit sinusoidal voltage at actuator location 02.

5.6.9. Open and closed loop pole location

Pole locations in open and closed loop system were investigated for the cantilever plate with ten sensor/actuator pairs in the locations optimised using the optimal linear quadratic control scheme as shown in Figure 5.16. It can be seen that the open loop poles are moved to the left-hand side with increasing values of the weighted matrix *Q*, and the closed loop damping ratios are increased for all the first six modes as shown in Table 5.4.

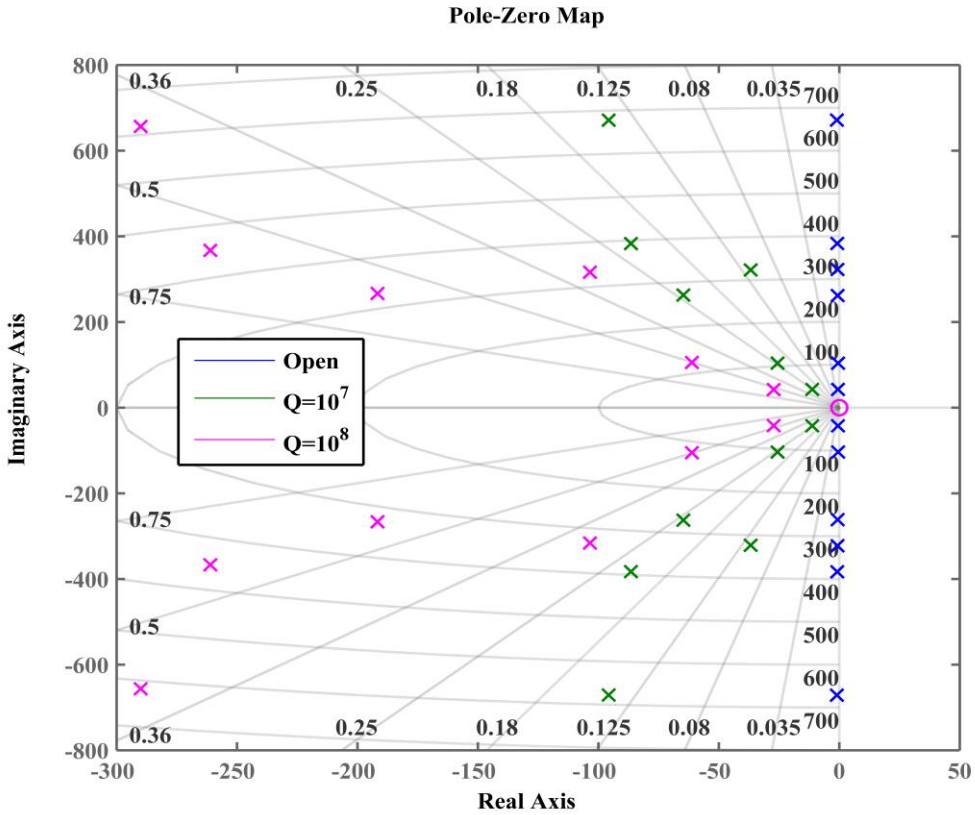

Figure 5.16 Open and closed loop pole-map for the cantilever plate using LQR control scheme

Table 5.4 Open and closed loop modal damping ratio for the cantilever plate using LQR control scheme

Case	1st	2ed	3th	4th	5th	6th
Open loop damping ratio	0.0124	0.0046	0.0025	0.0023	0.0021	0.0014
Closed loop damping ratio $Q=10^7$	0.256	0.240	0.114	0.239	0.22	0.141
Closed loop damping ratio $Q=10^8$	0.544	0.582	0.311	0.584	0.58	0.404

5.6.10. Time response

Open and closed loop time responses were also investigated for the cantilever plate bonded with ten piezoelectric pairs in the optimal locations. Firstly, the optimal linear quadratic control and estimator were designed based on the model as shown in Figure 5.17, and the matrices of this simulink model are shown in Appendix A.

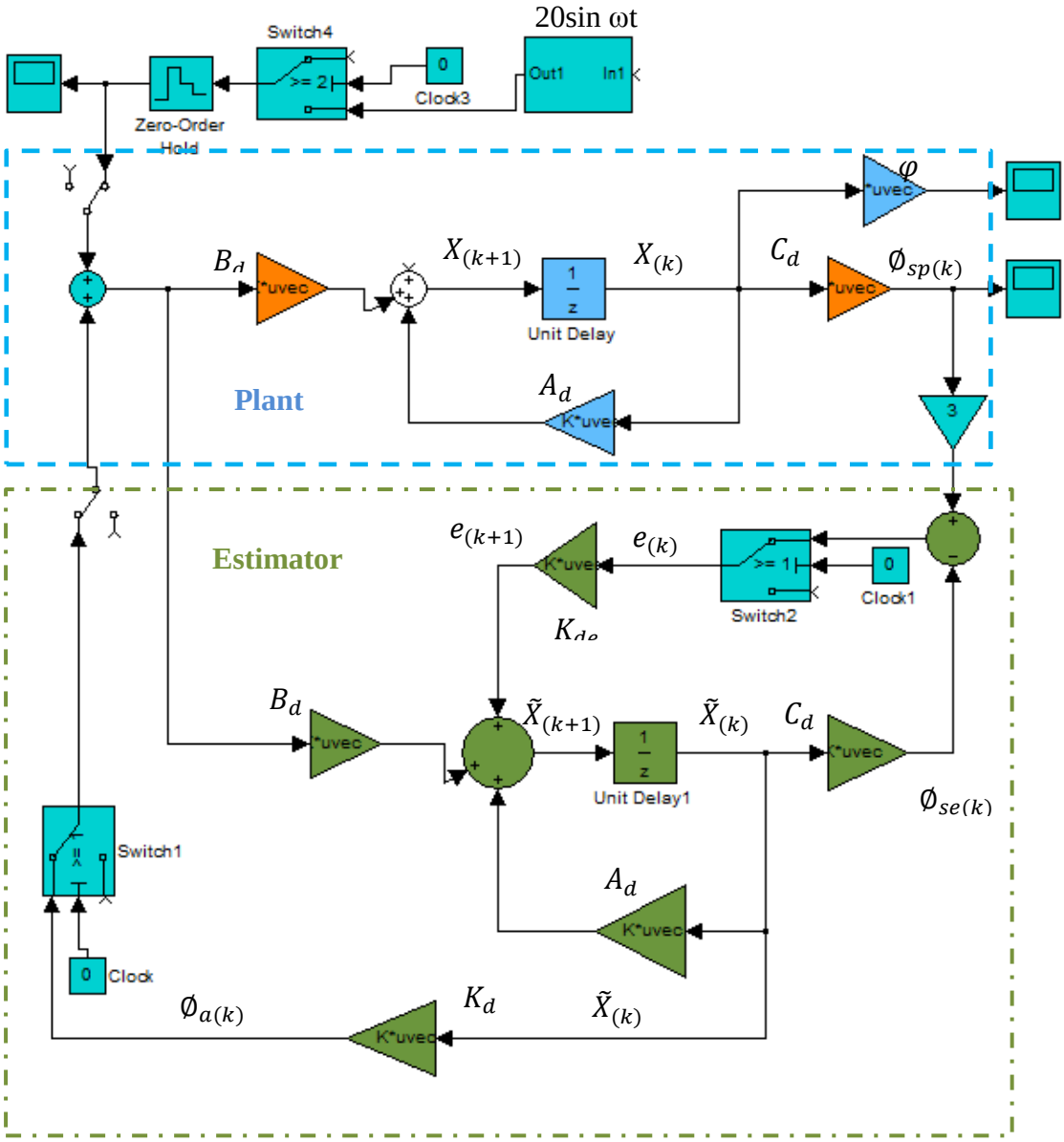

Figure 5.17 Simulink diagram for the plant (plate) and estimator

Secondly, the optimal linear quadratic controller and estimator designed in the first step were coupled with the cantilever plate and represented in the ANSYS finite element package as shown in Figure 5.18. In this step, an APDL program code was written for the cantilever plate bonded with ten piezoelectric pairs using three dimensional finite elements solid45 and solid5 as the plant and interacted to the controller and estimator. The APDL program for the Figure 5.18 can be seen in Appendix C.

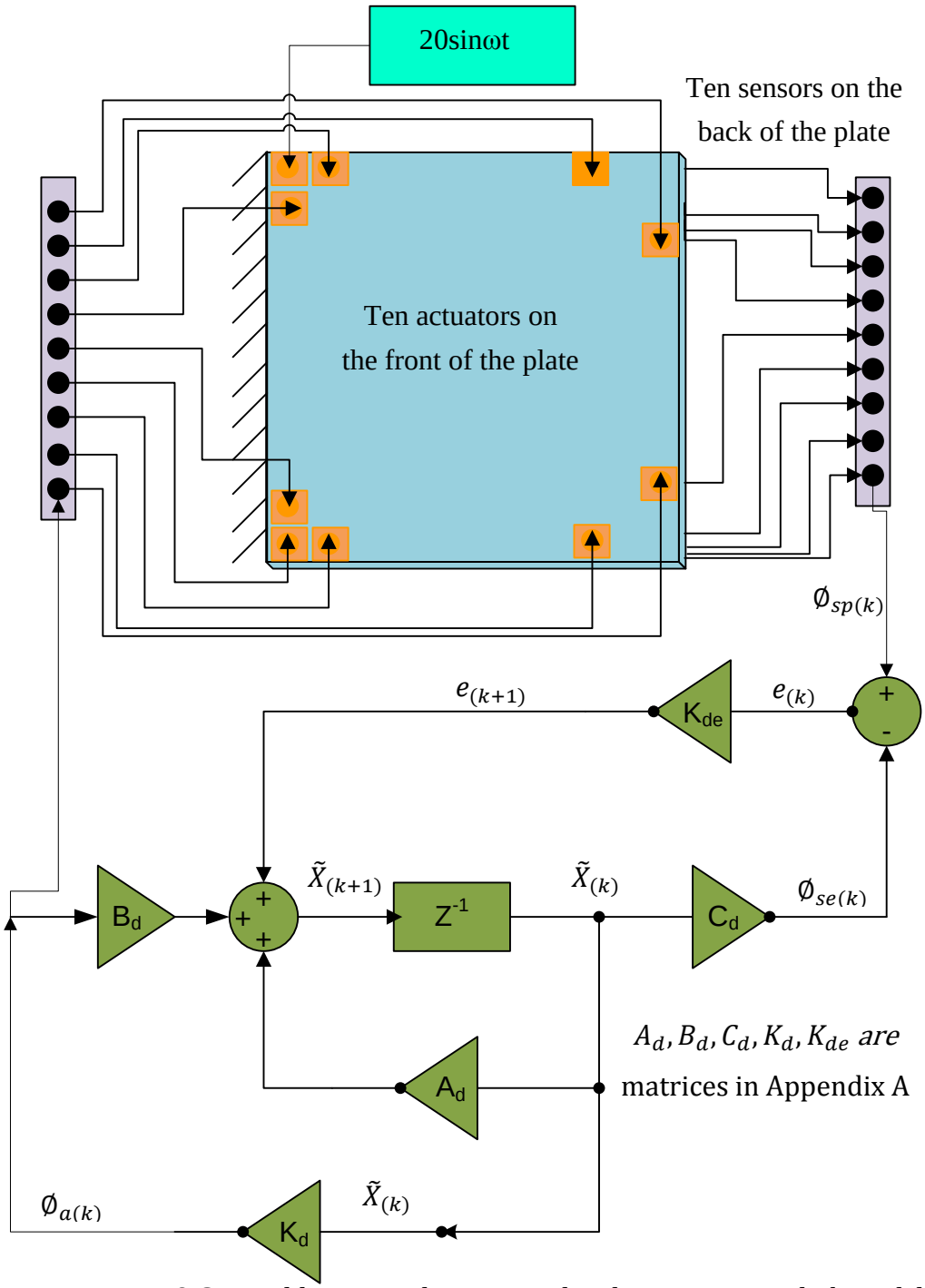

Figure 5.18 Optimal linear quadratic control and estimator simulink model interacting with the cantilever plate bonded with ten sensor/actuator pairs in the optimal location

Thirdly, proportional differential control scheme was connected to the cantilever plate and another APDL program code was written for the same cantilever plate and implementing the proportional differential control scheme as shown in Figure 5.19. In the second and third cases, the cantilever plate was driven by a sinusoidal constant amplitude voltage at actuator location 91 at the first, second and third modes and represented in the ANSYS finite element package in order to test the correctness and effectiveness of the optimal location of ten sensor/actuator pairs.

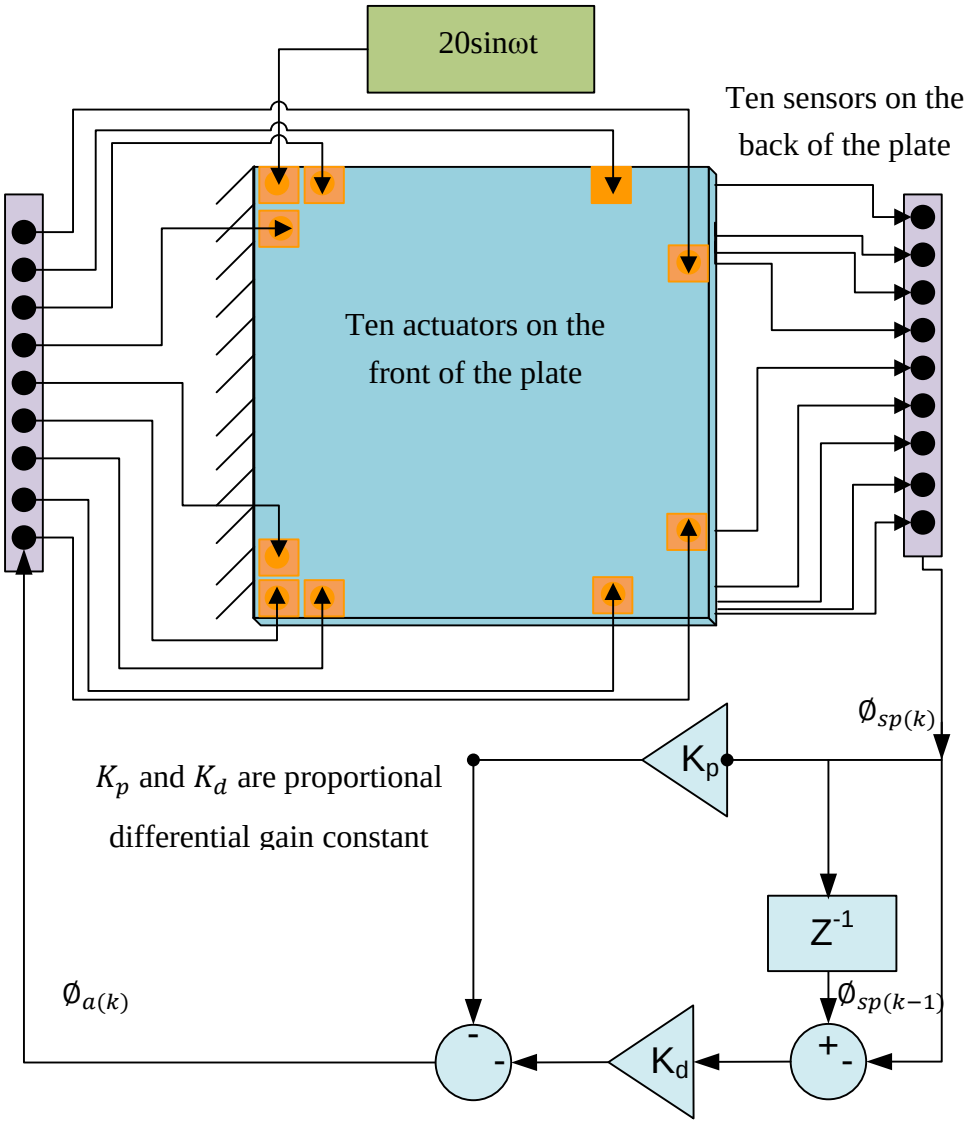

Figure 5.19 PD control scheme interacted with the cantilever plate bonded with ten sensor/actuator pairs in the optimal location

The ANSYS finite element package results for the open and closed loop time responses can be seen in Figure 5.20 to Figure 5.22 for the first, second and third modes. The open and closed loop voltage time responses are shown for the first five sensors and actuators at locations 01, 11, 02, 08, and 30 on the lower part of the plate. The responses of the other five sensor/actuator pairs at locations 91, 92, 81, 98, and 80 on the upper part of the plate are found to have the same responses as the lower part for the two controller types. The open and closed loop acceleration time responses are also investigated at a finite element node located at the top of the central area of each sensor (sensor tip acceleration). However, the acceleration time response at the node located on the top area of the first sensor 01 is always close to zero, and is replaced by a finite element node located at the free-end plate corner. The time response curve at steady state was magnified as shown on the right-hand sides of the figures.

Figure 5.20 (a1, a2, a3 and a4) shows open and closed loop voltage time responses for the five sensors at locations 01, 11, 02, 08 and 30 at the first mode. The average closed loop sensors voltage responses were reduced by 87.1% using optimal linear quadratic control at $Q=10^7$, and the reduction was increased to 91.1% at $Q=10^8$, and the average closed loop sensor voltage reduced by 87.68% using proportional differential control scheme as shown in Figure 5.20 (a1, a2, a3 and a4). Further details are given in Table 5.5**.**

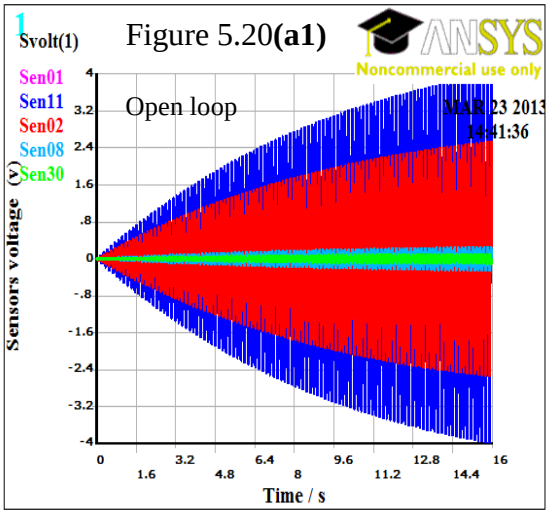

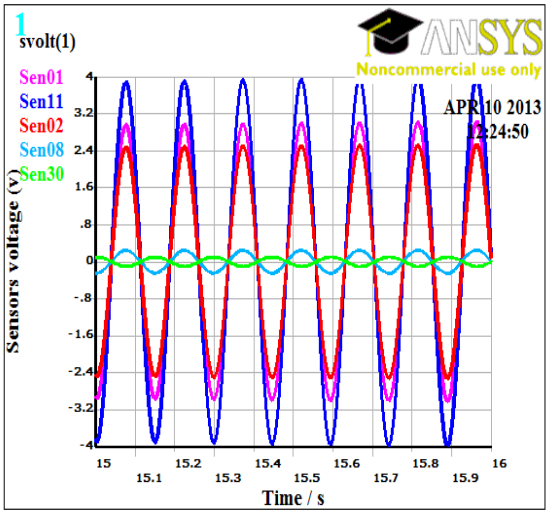

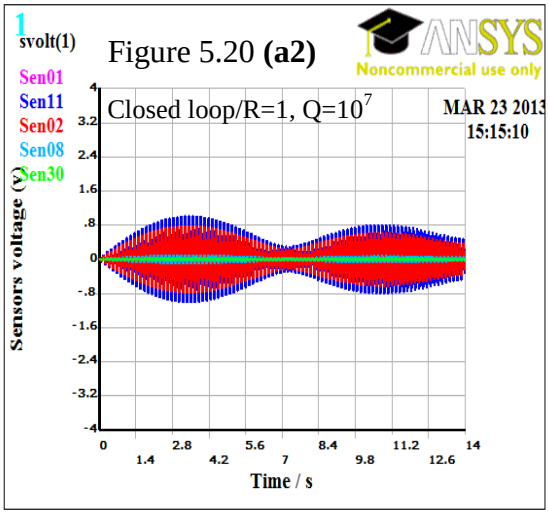

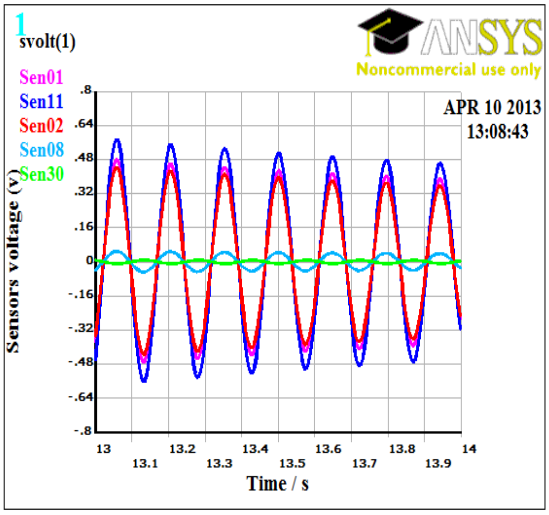

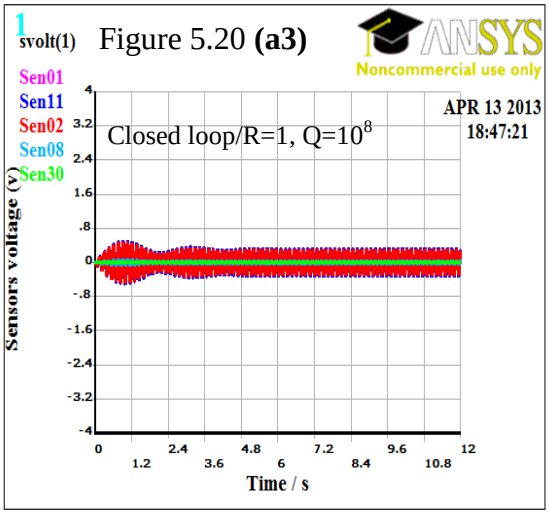
svolt(1)
Figure 5.20 (a3)
Noncommercial use only
Sen01
Sen11
Sen02
Sen08
Sen30
Closed loop/R=1, Q=10^8
APR 13 2013
18:47:21
Sensors voltage (v)
Time / s

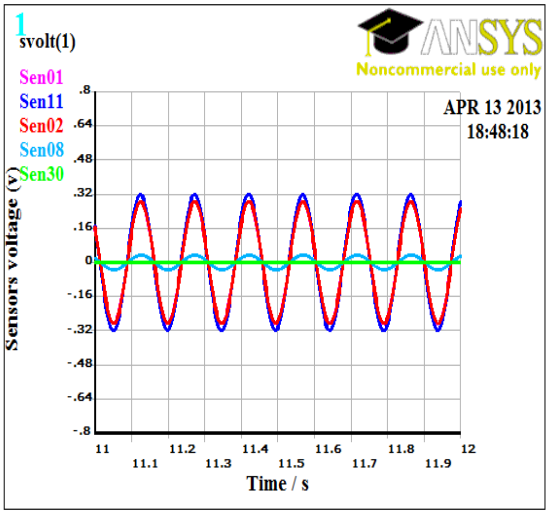
svolt(1)
Noncommercial use only
Sen01
Sen11
Sen02
Sen08
Sen30
APR 13 2013
18:48:18
Sensors voltage (v)
Time / s

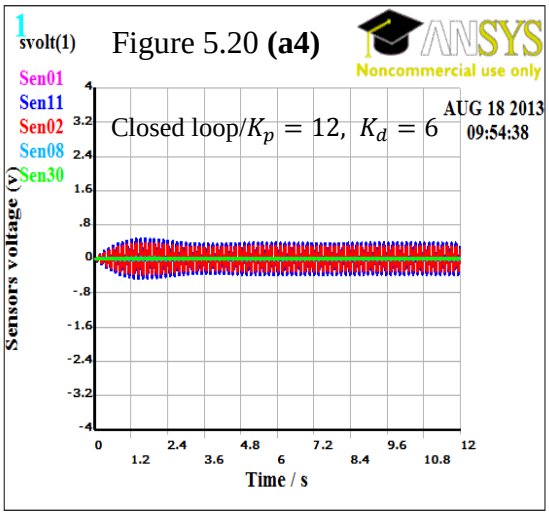
svolt(1)
Figure 5.20 (a4)
Noncommercial use only
Sen01
Sen11
Sen02
Sen08
Sen30
Closed loop/$K_p = 12,\ K_d = 6$
AUG 18 2013
09:54:38
Sensors voltage (v)
Time / s

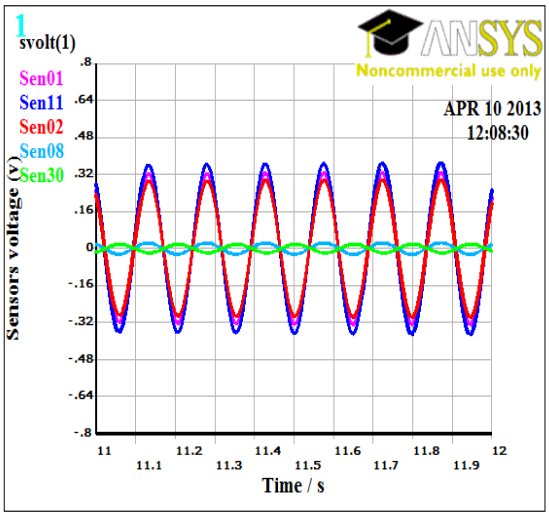
svolt(1)
Noncommercial use only
Sen01
Sen11
Sen02
Sen08
Sen30
APR 10 2013
12:08:30
Sensors voltage (v)
Time / s

Figure 5.20 (b1, b2, b3 and b4) shows open and closed loop acceleration time responses at the first mode for a finite element node located at the top centre area of the each sensor at the locations of Free-end,11, 02, 08 and 30 and a finite element node located at the free-end plate corner.

The average closed loop acceleration responses were reduced by 88.63% using optimal linear quadratic control at $Q=10^7$, and the reduction increased to 92.54% at $Q=10^8$, and the average closed loop closed loop acceleration was reduced by 87.68%, using proportional differential control scheme as shown in Figure 5.20 (b1, b2, b3 and b4). More details can be found in Table 5.5**.**

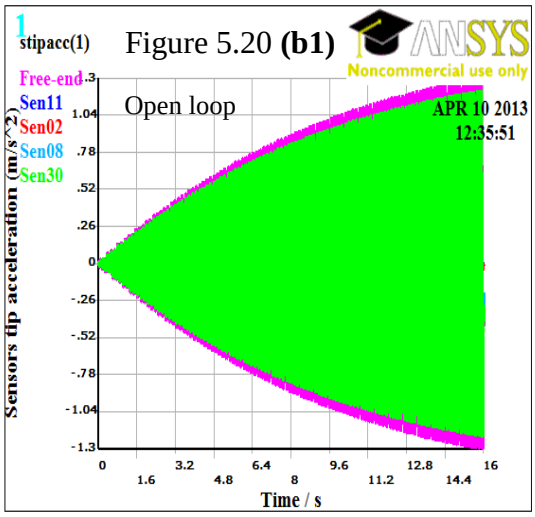

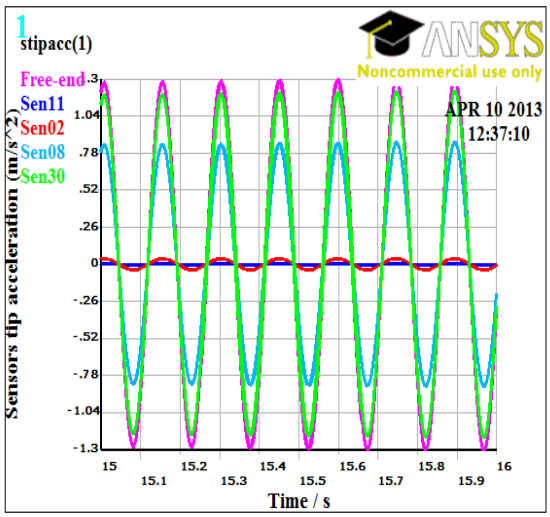

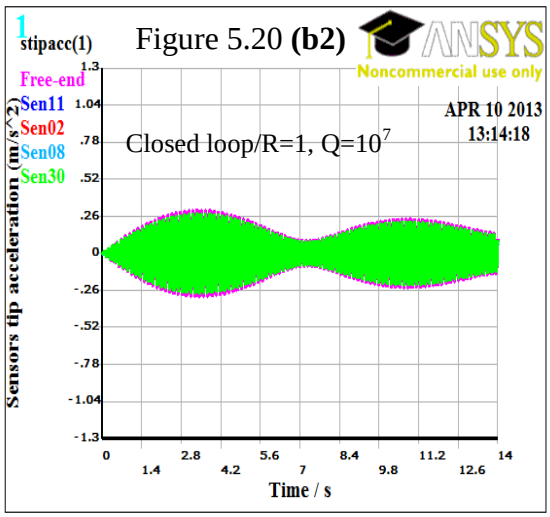

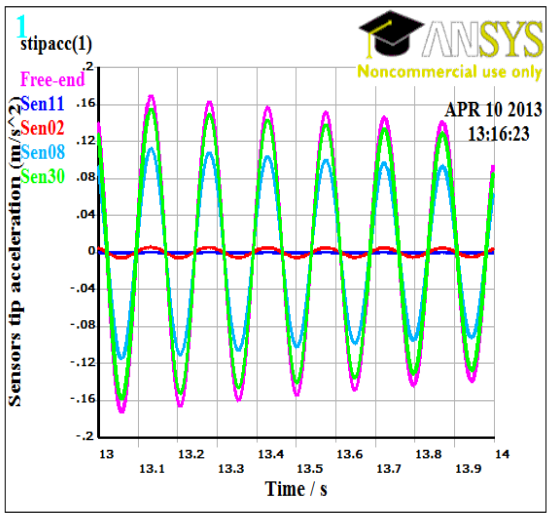

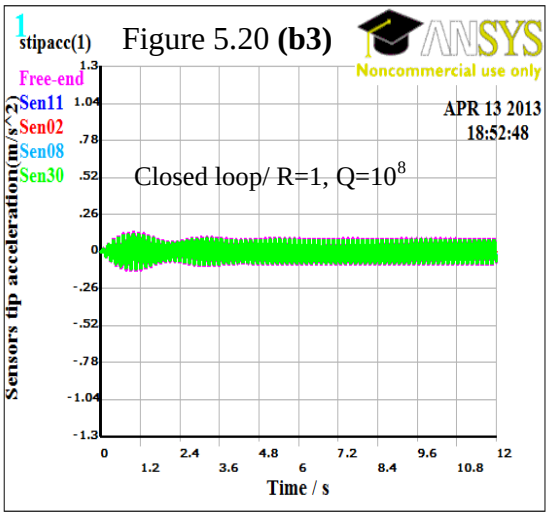

Figure 5.20 **(b3)**

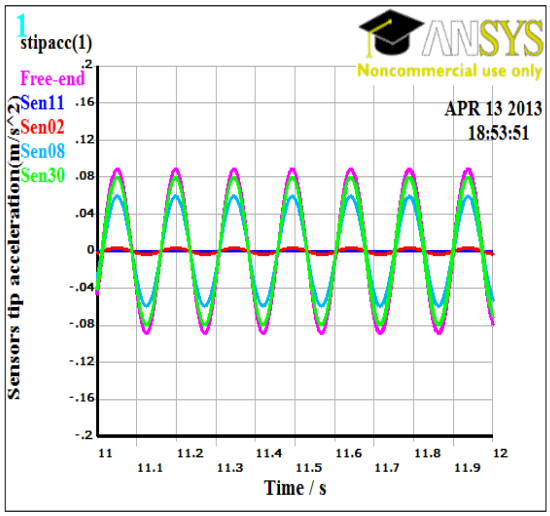

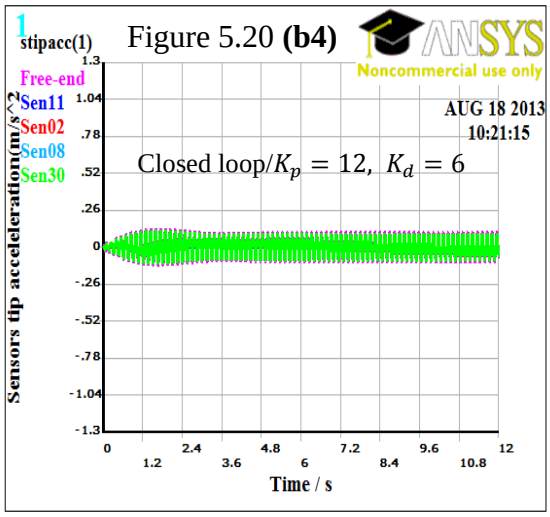

Figure 5.20 **(b4)**

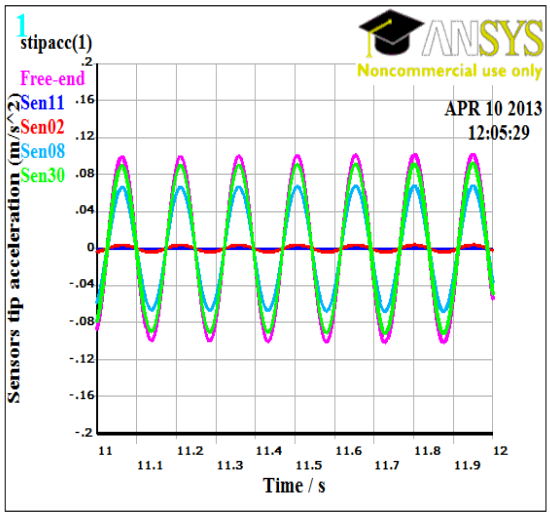

Figure 5.20 (c1, c2 and c3) shows closed loop actuator feedback voltage responses at the first mode for the actuators at locations 01, 11, 02, 08 and 30. The summations of all actuators feedback voltage were 15.96V and 20.92V using optimal linear quadratic control at $Q=10^7$ and $Q=10^8$ respectively, and 21.24V using the proportional differential controller. Again more details are given in Table 5.5**.**

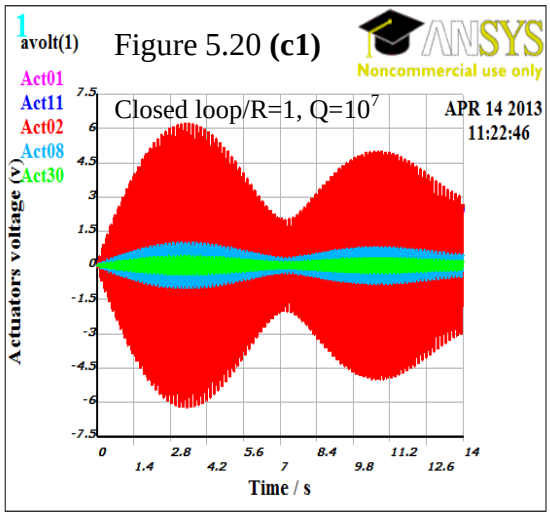

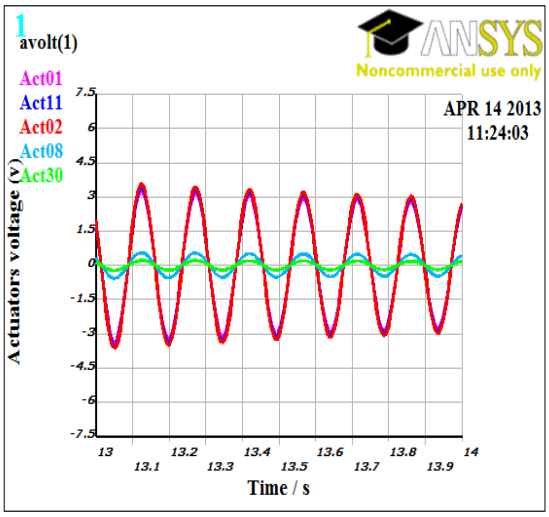

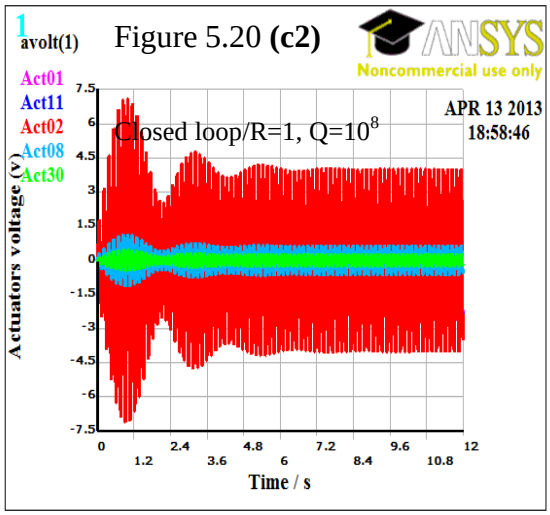

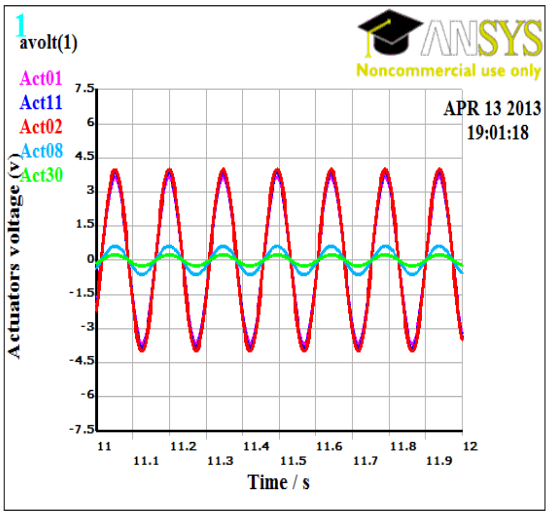

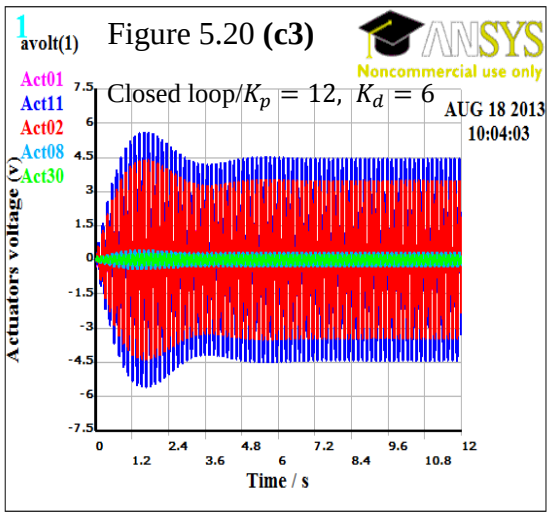

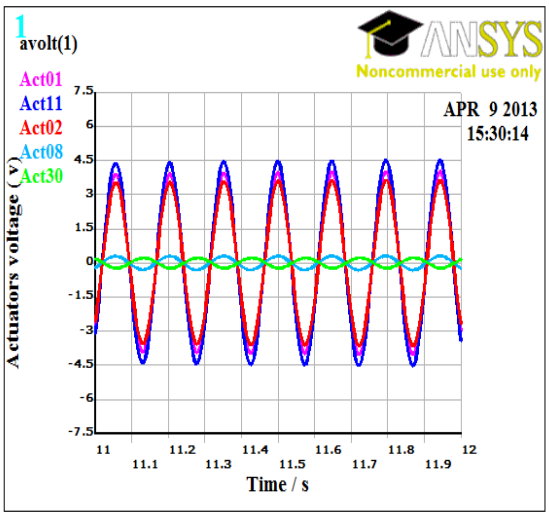

Figure 5.20 **(a, b and c)** ANSYS results for the open and closed loop time responses at the first mode using LQR and PD control schemes for the present model, the figures on the right hand side was a magnification of the steady state response

Table 5.5 Open and closed loop sensor and actuator voltage and acceleration maximum amplitude responses at steady state for the first mode of vibration

Steady state sensor voltages for various control schemes (V)						
Case	Sen01	Sen11	Sen02	Sen08	Sen30	Average
Open loop sensor voltage	2.9	3.9	2.4	0.25	0.1	-----
Closed loop $Q=10^7$	0.38	0.48	0.36	0.04	0.008	0.25
Percentage reduction %	86.89	87.69	85	84	92	87.11
Closed loop $Q=10^8$	0.285	0.32	0.285	0.034	0.00095	-----
Percentage reduction %	90.17	91.79	88.12	86.4	99.05	91.10
Closed loop P=12, D=6	0.32	0.34	0.3	0.024	0.02	-----
Percentage reduction %	88.96	91.28	87.5	90.4	80	87.62
Actuator feedback voltages for various control schemes (V)						
Case	Act01	Act11	Act02	Act08	Act30	sum
R=1 and $Q=10^7$	2.8	2.9	3.0	0.48	0.20	9.32
R=1 and $Q=10^8$	3.6	3.8	4.0	0.62	0.24	12.26
P=12, D=6	4.0	4.5	3.6	0.30	0.22	12.26
Steady state sensor tip accelerations for various control schemes ($m.s^{-2}$)						
Case	Free-end	Sen11	Sen02	Sen08	Sen30	Average
Open loop	01.3	0.003	0.04	0.86	01.20	-----
Closed loop $Q=10^7$	0.14	0.0003	0.005	0.095	0.13	-----
Percentage reduction %	89.23	88.33	87.5	88.95	89.16	88.63
Closed loop $Q=10^8$	0.098	0.00022	0.0035	0.06	0.08	-----
Percentage reduction %	92.46	92.66	91.25	93.02	93.33	92.54
Closed loop P=12, D=6	0.10	0.00024	0.004	0.068	0.091	-----
Percentage reduction	92.30	92	90	92.09	92.41	91.7

Figure 5.21 (a1, a2, a3 and a4) shows the open and closed loop voltage time responses for the five sensors at locations 01, 11, 02, 08 and 30 at the second mode. The average closed loop sensors voltage responses were reduced by 88.79% using optimal linear quadratic control at $Q=10^7$, and the reduction was increased to 94.39% at $Q=10^8$, as shown in Figure 5.21(a2 and a3)

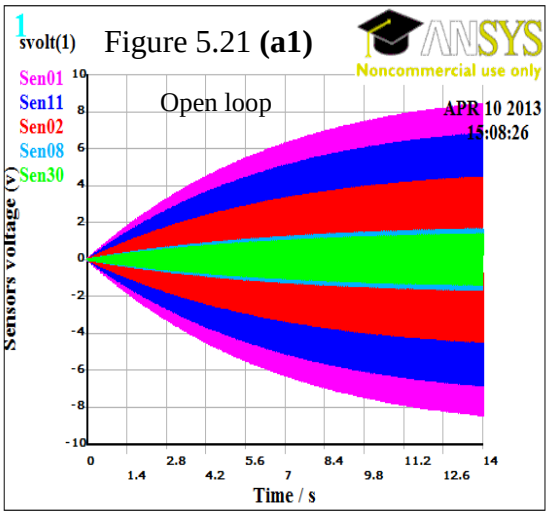

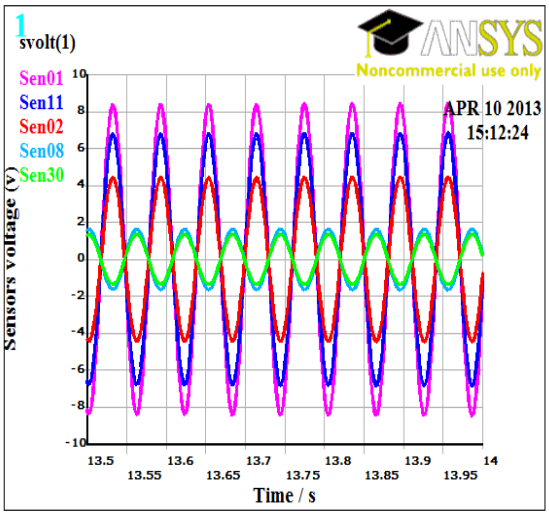

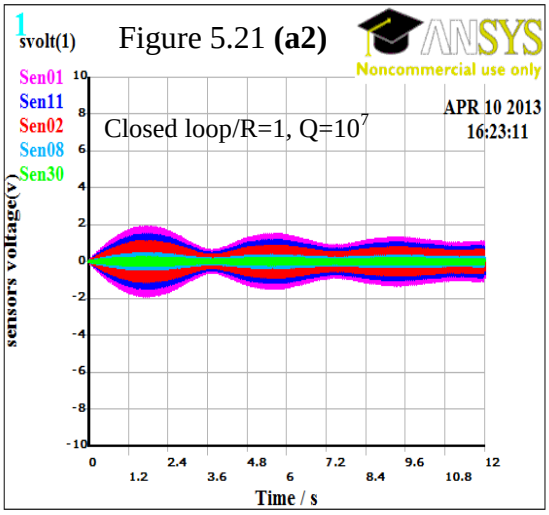

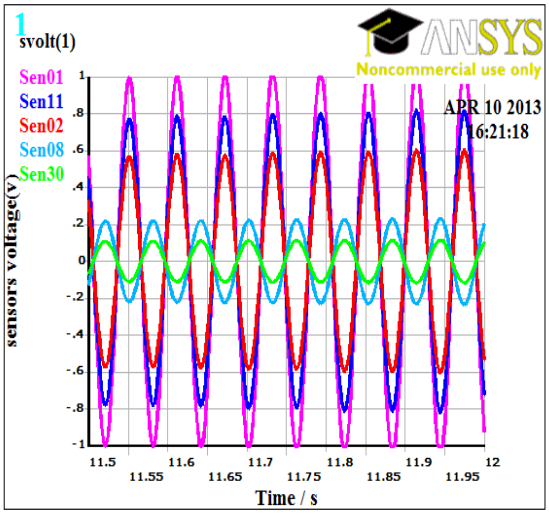

The average closed loop sensor voltage responses were reduced by 92.9%, using proportional differential control at $K_P = 12$ and $K_d = 6$, as shown in Figure 5.21 (a4).

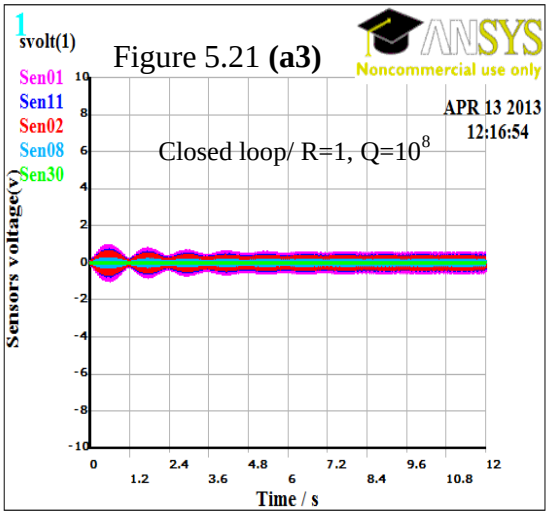

Figure 5.21 **(a3)**

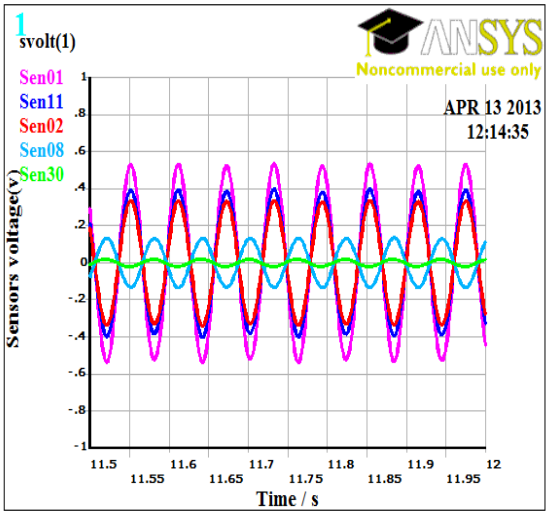

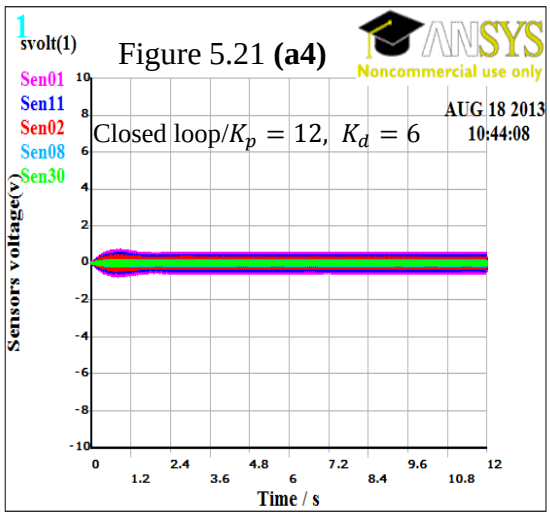

Figure 5.21 **(a4)**

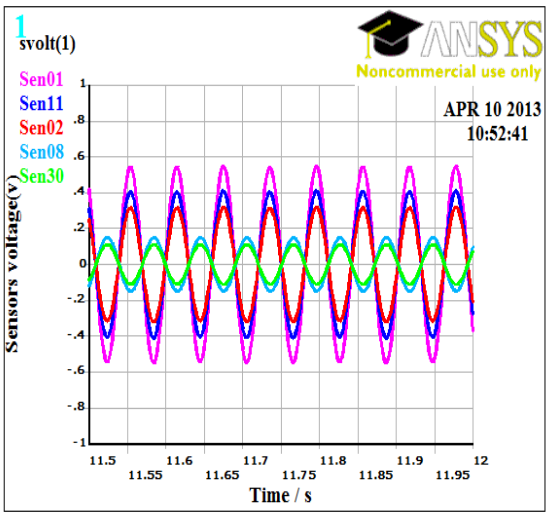

Figure 5.21(b1, b2, b3 and b4) shows the open and closed loop acceleration time responses at the second mode for a finite element node located at the top centre area of each sensor at locations free-end, 11, 02, 08 and 30 and a finite element node located at the free-end plate corner. The average closed loop acceleration responses were reduced by 89.49%, using optimal linear quadratic control at $Q=10^7$. The acceleration reduction was increased to 94.39%, at $Q=10^8$ as shown in Figure 5.21 (b2 and b3)

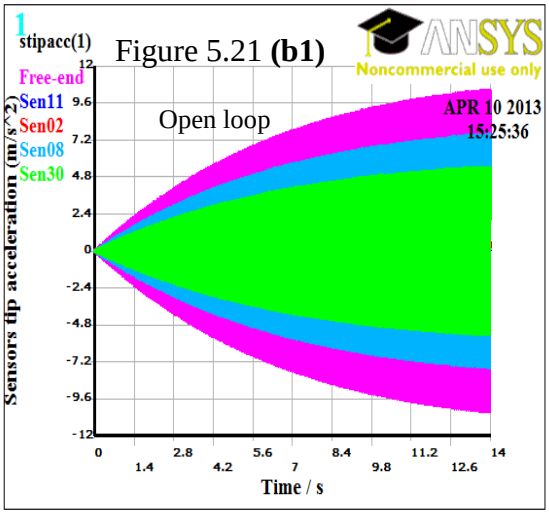

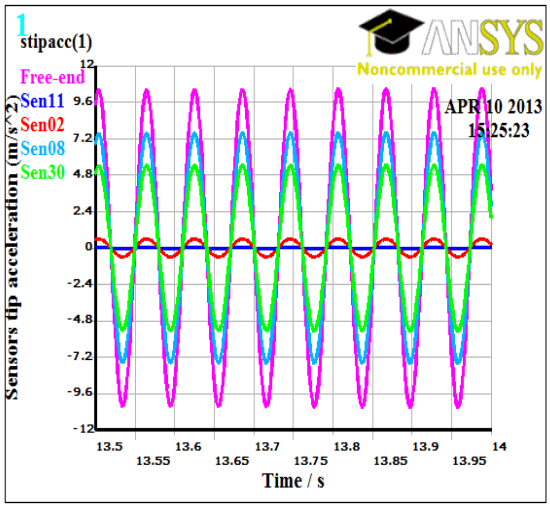

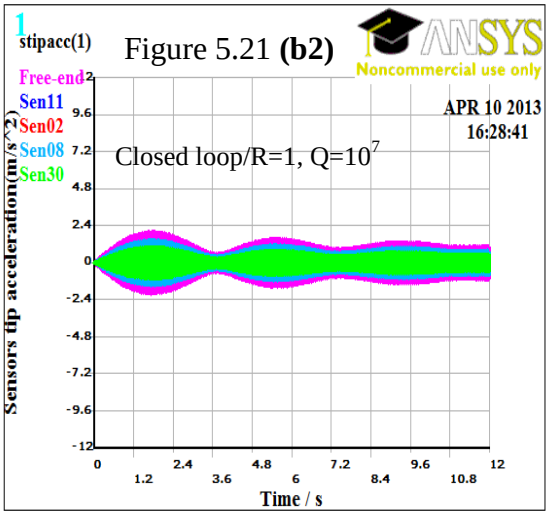

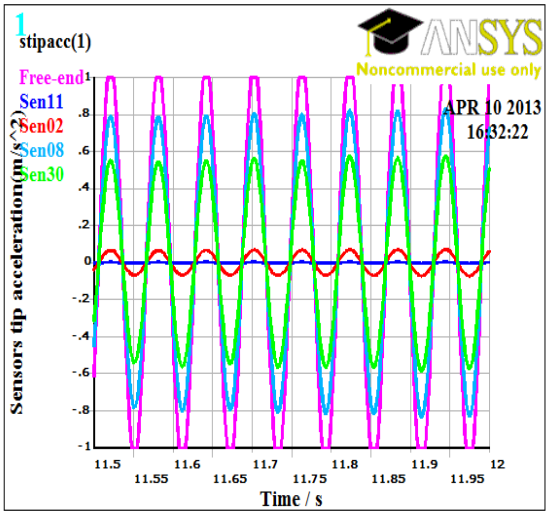

The average closed loop acceleration responses were reduced by 95.34% using proportional differential control at $K_P = 12$ and $K_d = 6$ as shown in Figure 5.21 (b4).

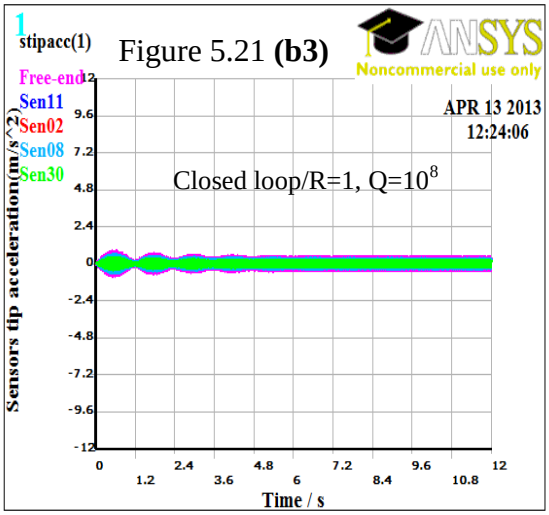

Figure 5.21 **(b3)**

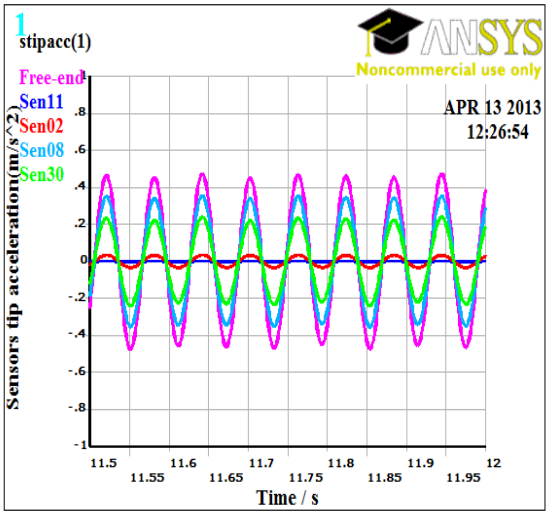

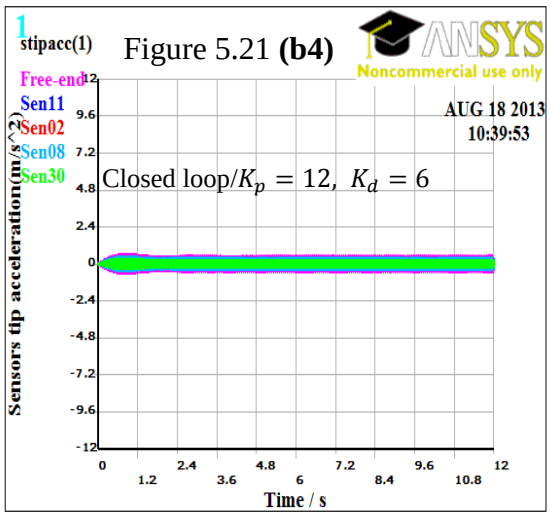

Figure 5.21 **(b4)**

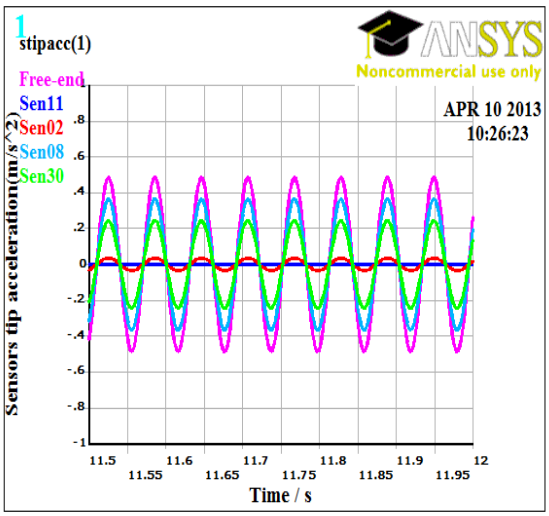

Figure 5.21 (c1, c2 and c3) shows the closed loop actuator's feedback voltage time responses at the second mode for the actuators at locations 01, 11, 02, 08 and 30. The summations of the all actuators feedback voltage were 25.04Vand 31.6V, using optimal linear quadratic control at $Q=10^7$ and $Q=10^8$, as shown in Figure 5.21(c1 and c2) respectively, and 30.9V, using proportional differential controller, at $K_P=12$ and $K_d=6$, as shown in Figure 5.21(c3)

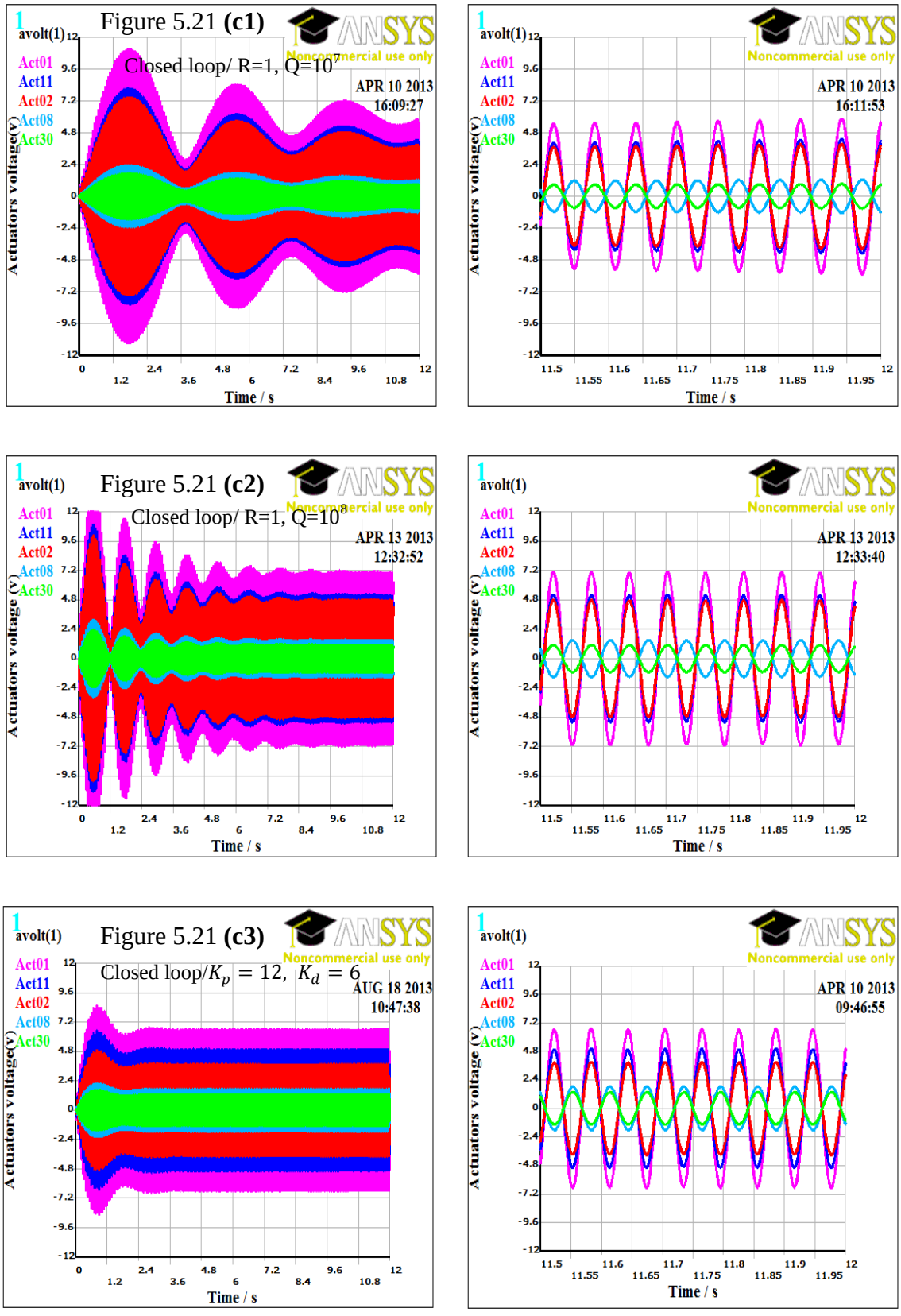

Figure 5.21 **(a, b and c)** ANSYS finite element package results for the open and closed loop time responses at the second mode using LQR and PD control schemes for the present model, the figures on the right hand side are a magnification of the steady state response

Table 5.6 Open and closed loop sensor and actuator voltage and acceleration maximum amplitude responses at steady state for the second mode of vibration

Steady state sensor voltages for various control schemes (V)						
Case	Sen01	Sen11	Sen02	Sen08	Sen30	Average
Open loop sensor voltage	8.5	6.8	4.5	1.7	1.35	-----
Closed loop $Q=10^7$	1.0	0.80	0.60	0.20	0.10	-----
Percentage reduction %	88.23	88.23	86.66	88.23	92.59	88.79
Closed loop $Q=10^8$	0.50	0.39	0.33	0.13	0.019	-----
Percentage reduction %	94.11	94.26	92.66	92.35	98.59	94.39
Closed loop P=12, D=6	0.52	0.40	0.32	0.14	0.11	-----
Percentage reduction %	93.88	94.11	92.88	91.76	91.85	92.90
Actuator feedback voltages at various control schemes (V)						
Case	Act01	Act11	Act02	Act08	Act30	sum
R=1 and $Q=10^7$	5.6	4.0	3.8	1.12	0.8	15.3
R=1 and $Q=10^8$	7.0	5.2	4.7	1.4	1.0	19.3
P=12, D=6	6.6	5.0	3.95	1.8	1.4	18.7
Steady state sensor tip accelerations at various control schemes ($m.s^{-2}$)						
Case	Free-end	Sen11	Sen02	Sen08	Sen30	Average
Open loop	10.50	0.03	0.60	7.70	5.50	-----
Closed loop $Q=10^7$	1.10	0.003	0.065	0.8	0.56	-----
Percentage reduction %	89.52	90	89.16	89.61	89.81	89.49
Closed loop $Q=10^8$	0.50	0.39	0.33	0.13	0.019	-----
Percentage reduction %	94.11	94.26	92.66	92.35	98.59	94.39
Closed loop P=12, D=6	0.46	0.0015	0.032	0.35	0.22	-----
Percentage reduction	95.61	95.00	94.66	95.45	96.00	95.34

Figure 5.22 (a1, a2 and a3) shows the open and closed loop time responses at the third mode using the proportional differential controller. The controller was activated after four seconds and gave high reduction and fast responses, which prove the effectiveness of the optimal piezoelectric sensor/actuator locations.

Figure 5.22 (a1) shows the open and closed loop voltage time responses for the five sensors at locations 01, 11, 02, 08 and 30 at the third mode. The average sensor voltage responses were reduced by 92.86% at K_P=12 and K_d=6.

Figure 5.22 **(a1)**

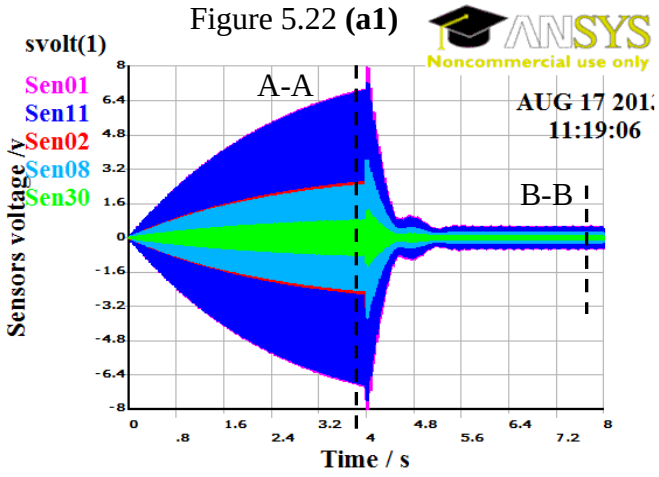

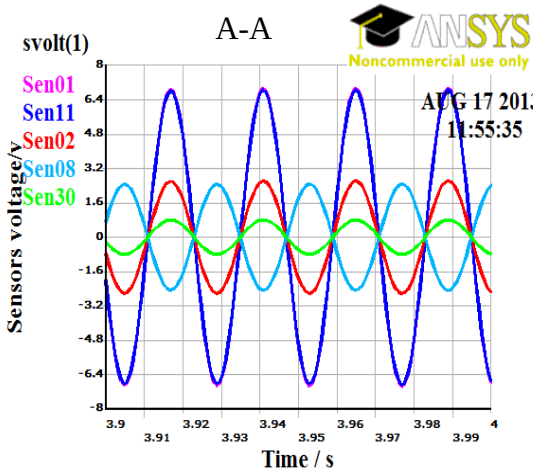

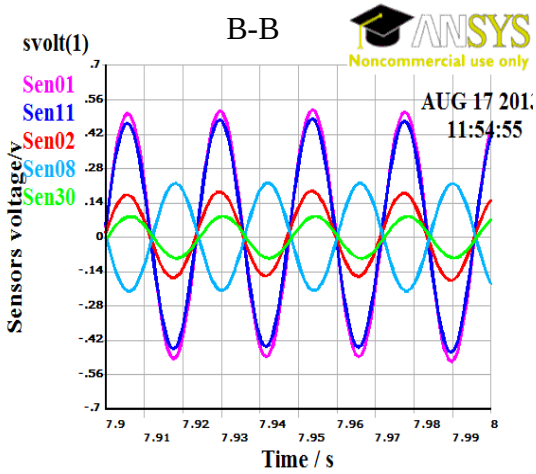

Figure 5.22 (**a2**) shows the open and closed loop acceleration time responses at the third mode for a finite element node located at the top centre area of each sensor at locations free-end, 11, 02, 08 and 30 and a finite element node located at the free-end plate corner. The average acceleration time response was reduced by 93.71%.

Figure 5.22 **(a2)**

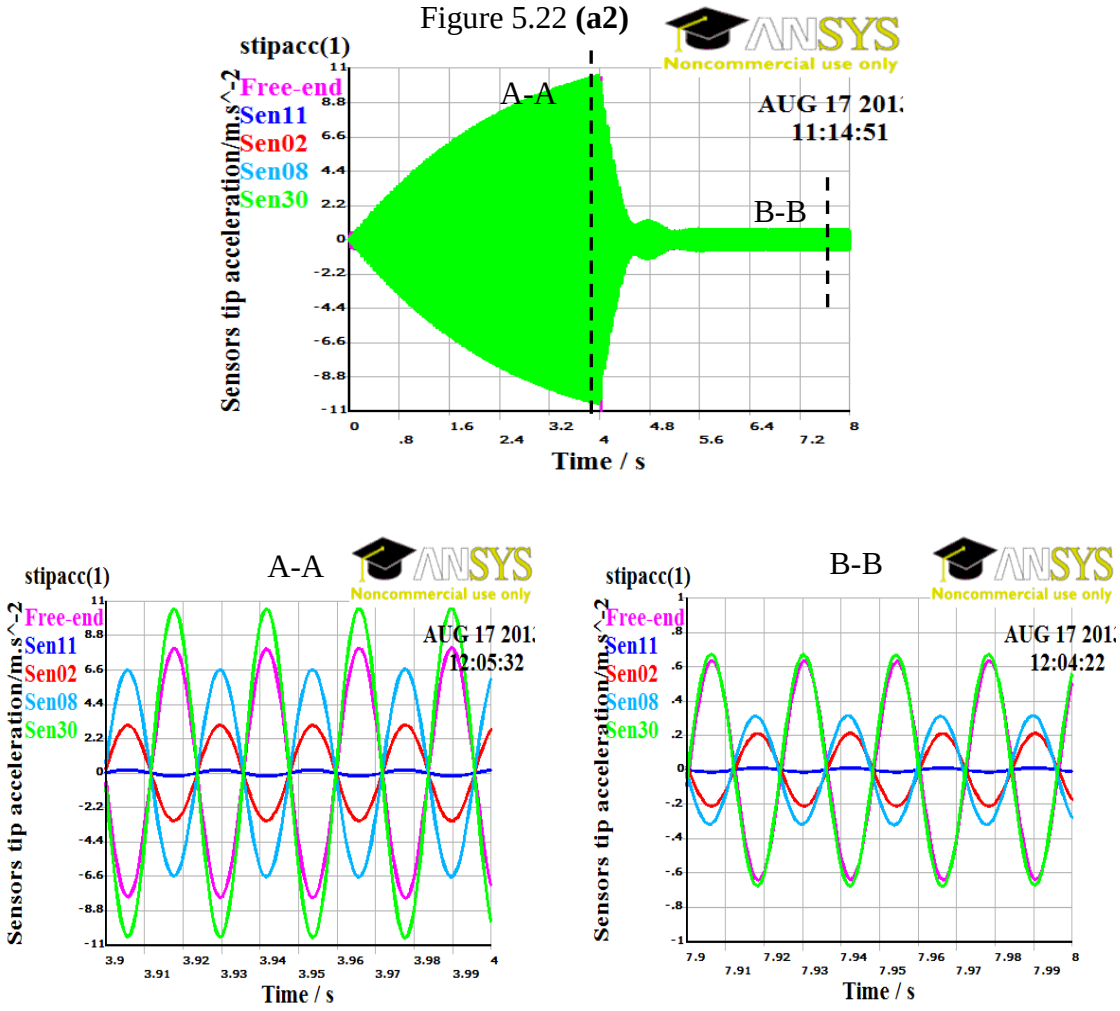

Figure 5.22 (a3) shows the open and closed loop actuator feedback voltage time responses at the third mode for the actuators at locations 01, 11, 02, 08 and 30. The summation of all actuator feedback voltage was 29V at the steady state. The peak of actuator feedback voltage was higher than the steady state value for a short time as a result of controller activation after four second. However, in real situations the controller should always be active in order to increase structure stability, speed of response and suppress vibration within minimum feedback voltage and to maintain piezoelectric effectiveness for a long time; but this case was chosen to test the effectiveness of the piezoelectric locations.

Figure 5.22 **(a3)**

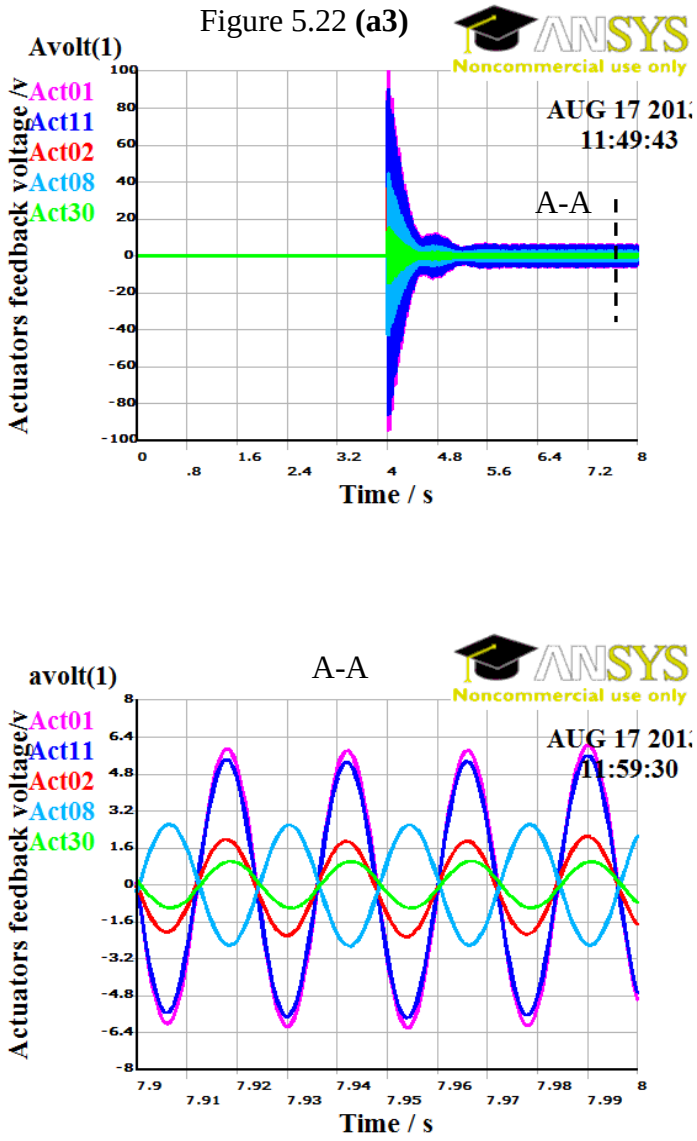

Figure 5.22 ANSYS results for the open and closed loop time responses at the third mode using PD control scheme K_p=12, K_d=6, sections A-A and B-B are magnification of results at the steady state

The differential feedback gain K_d was doubled from 6 to 12 to test its effect on the closed loop transient response as shown in Figure 5.23. It was shown a significant improvement in the closed loop transient responses and the same responses at the steady state compared to results obtained in Figure 5.22.

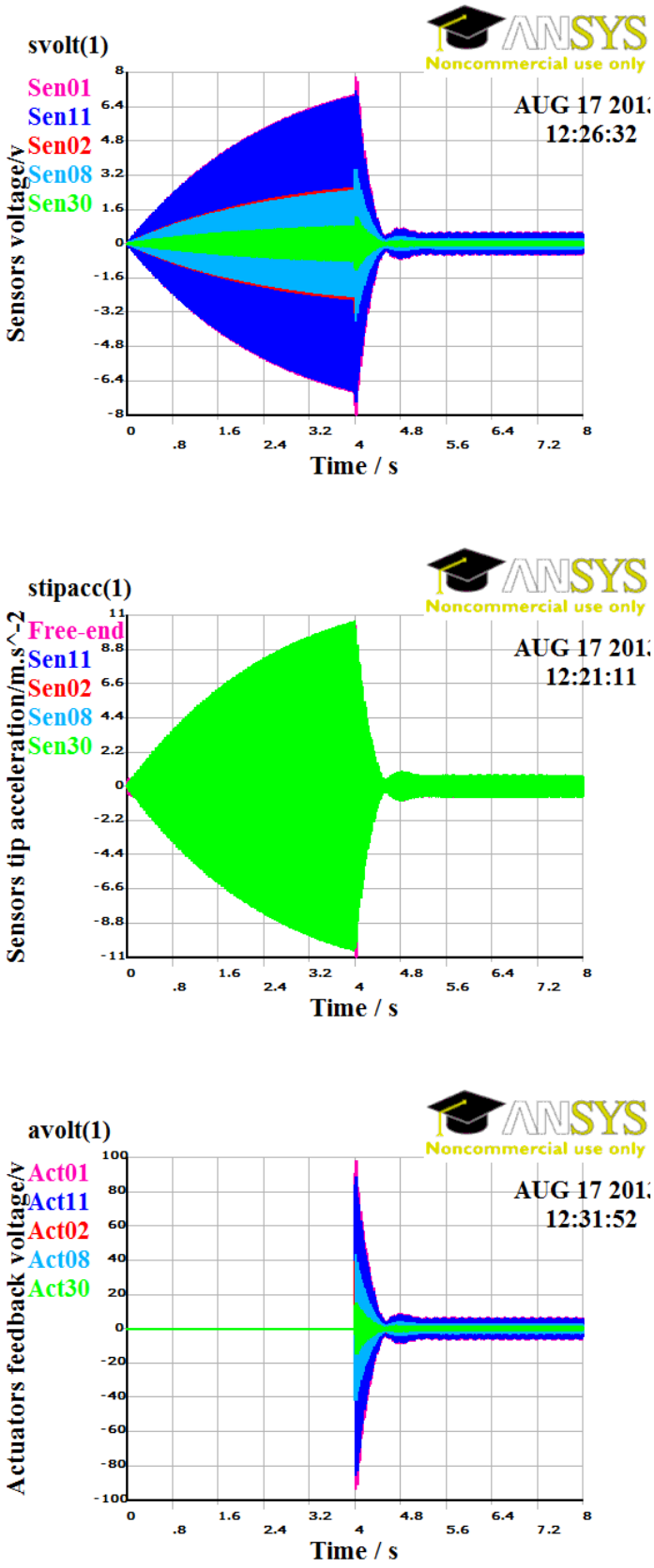

Figure 5.23 ANSYS results for the open and closed loop time responses at the third mode using PD control scheme K_p=12, K_d=12

It can be seen from the figure that the steady state closed loop time responses are quite similar for all sensors and actuators despite using different controllers which operate with different principles. In the LQR estimator shown in Figure 5.18 the estimator produces feedback voltage to the actuators based on the estimator states, which is impossible to measure states directly from the plate. However, the proportional differential controller shown in Figure 5.19 produces feedback voltage to the actuators based on the sensor output voltage.

5.6.11. Estimator robustness test

Estimator robustness was tested for the fifth mode of vibration. The driven sinusoidal voltage was applied at actuator 02 and the response measured for the sensor at location 01. The plate and estimator were tested under two conditions: firstly, it is assumed that the plate sensor voltages and state responses are the same as the estimator responses, and that the disturbance voltage drives the plate and estimator as an ideal environment. The results are shown in Figure 5.24 (a1, a2, a3, and a4).

Secondly, in a real environment it would be impossible to feed a disturbance from the plate to the estimator. Therefore, the disturbance voltage was applied to the plate only, which causes a difference in error between the plate and the estimator responses. Moreover, the open loop plate sensors output voltages might be higher or lower than the estimator sensors voltage. Therefore, in the second case, the sensor output voltages are multiplied by three in order to make the difference error between them higher. The results for the second case are shown in Figure 5.24 (b1, b2, b3 and b4). The controller was activated after one second for an interval of one second while the disturbance was activated for the first two seconds and then removed at the last half-second.

In the first case, the sensor voltage error between plate and estimator was zero for the ideal environment, as shown in Figure 5.24 (a3). In the second case, the sensor voltage error was higher than in the first case by three before controller activation, but this error was forced to zero after controller activation as shown in Figure 5.24 (b3). The sensor voltage and plate free end displacement responses were the same responses in the two cases and gave higher reduction than in the first case, as shown in Figure 5.24 (a1, a2, b1, and b2).

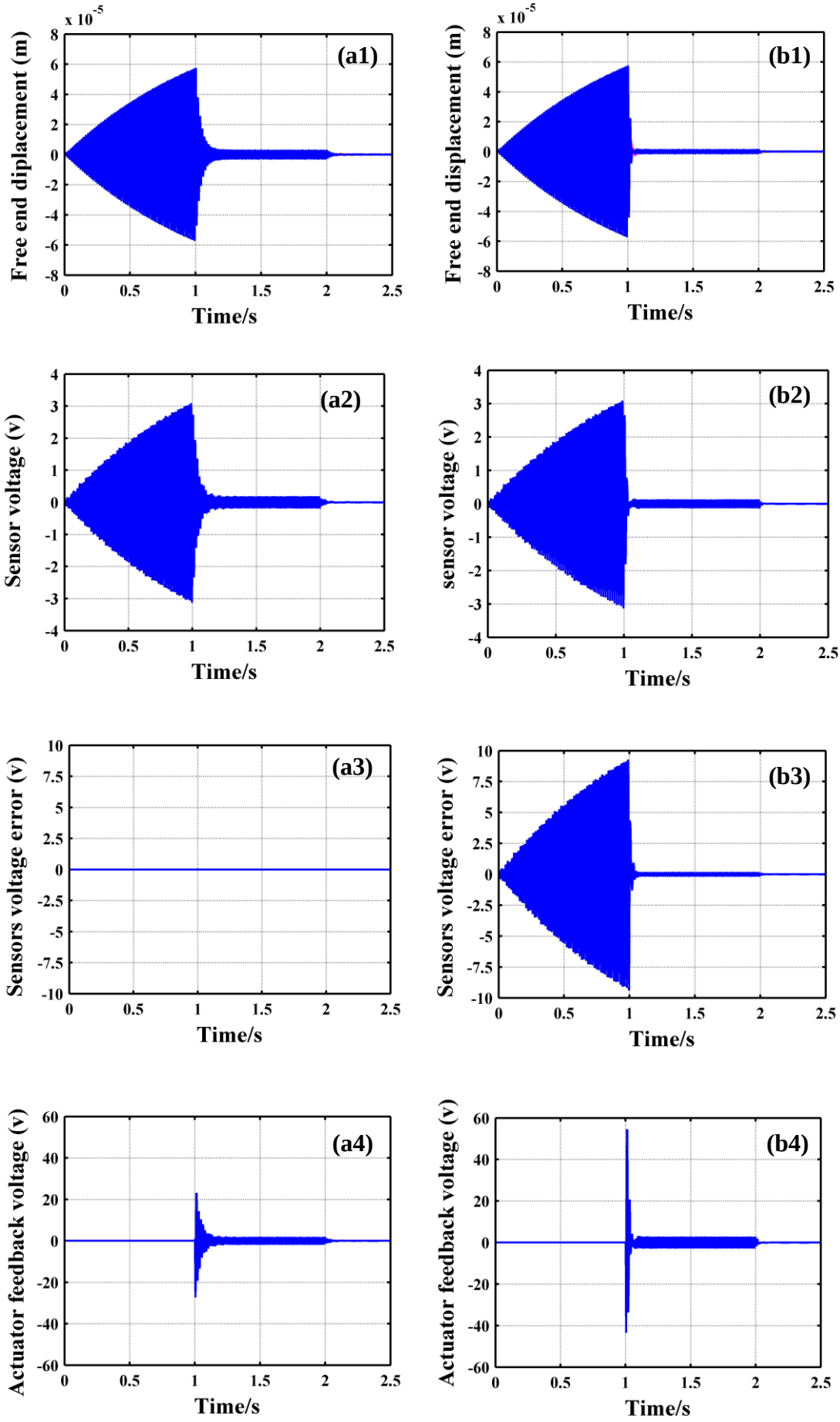

Figure 5.24 Open and closed loop responses at sensor/actuator 02 and the driven voltage at actuator 02, for the fifth mode, for an ideal **(a)** and real **(b)** environment

For a short time, the peak of the actuator feedback voltage was three times higher in the second case than in the first case, then reduced at the steady state to being slightly higher than the first case, as shown in Figure 5.24 (a4 and b4). The increase in actuator feedback voltage was used to force the error difference between the estimator and the plate to zero.

5.7. Conclusions

In this chapter, a new placement strategy which includes a conditional filter was developed to locate piezoelectric sensors and actuators on a flexible structure using a genetic algorithm. The optimal placement and feedback gain of two, four, six and ten piezoelectric actuators was investigated for an isotropic cantilever plate to attenuate the first six natural modes of vibration. The optimal configuration of discrete piezoelectric sensors and actuators has been found to be symmetrically distributed about the plate's axis of symmetry, which gives agreement with the ANSYS results for mode shape, modal strain and electrical charge distributions over the piezoelectric surface. The present optimal piezoelectric configuration agrees with the previous published studies [26, 54] and disagrees with others [35, 38]. The robustness of the placement strategy was tested by running the computer program multiple times. The same optimal fitness was achieved via different routes in each run, which demonstrates the correctness and robustness of the placement strategy.

The closed loop average vibration reduction was investigated for the cantilever plate with four and ten optimally placed piezoelectric pairs using an optimal linear quadratic control scheme. The present optimal piezoelectric sensor/actuator configurations gave average reductions in sensor output of 56.49% and 45.84% higher than those published previously [35, 38], clearly demonstrating the effectiveness of the placement strategy.

An optimal linear quadratic controller and estimator were designed for the cantilever plate bonded to ten optimally located piezoelectric pairs and this was represented in the ANSYS finite element package using the APDL program as a new method for a modelling control scheme test and to compensate for any lack of experimental testing. Another control scheme test using a proportional differential controller was designed for the same plate and APDL code was written in order to represent the system in the ANSYS package. The two controller schemes gave a reduction of nearly 94% in the sensor tip acceleration at the steady state for the first three modes of vibration. The ANSYS finite element test is a highly trust worthy test and gave results close to those of

experimental test. The ANSYS test gave further confirmation of the effectiveness of the optimal actuator location and the correctness of the theoretical model by connecting the estimator to the plate.

The robustness of the estimator was tested with a complex set of conditions by feeding the driven voltage only to the plate, and the plate sensor output voltage was multiplied by three to increase the error between the plate and estimator, with the controller activated after one second. The estimator gave high performance by forcing the error quickly to zero.

The placement strategy, including the conditional filter, symmetric global optimal sensor/actuator configuration and implementation of the optimal linear quadratic control and estimator in the ANSYS finite element package, are the most significant achievements reported in this chapter. The symmetrical optimal configuration of actuators is confirmed in chapters six and seven using flat and stiffened plates with different boundary conditions and geometries as well as by implementing the fitness and objective functions developed in this study.

Chapter 6. Development of New Fitness and Objective Functions

This chapter is concerned with the active vibration reduction of a square isotropic plate, mounted rigidly along one edge to form a cantilever. The optimal combination of six and ten piezoelectric sensor/actuator pairs is investigated using genetic algorithms to suppress the first six modes of vibration collectively. A new objective function based on H_∞ is proposed to find the optimal locations for the sensors based on the minimisation of open loop absolute average dB gain for all sensors and modes. The purpose of this chapter is to test the new fitness and objective functions based on the optimisation of sensor location and to compare the results with those from chapter five and previously published work. The placement strategy involving the new fitness function reduces the computational costs and converges faster to reach the optimal solution. The present optimal sensor/actuator configuration was given greater vibration reduction than in previously published optimal configurations.

6.1. Introduction

The reduction of vibration in a flexible structure can be optimised by locating piezoelectric sensors and actuators in the most efficient locations using optimisation methods such as genetic algorithms. The complexity of the optimisation process is directly proportional to the type of fitness function used, the number of modes to be controlled and the number of possible solutions in the search space. The latter is equal to the statistical combination of finite element discretisation and the number of sensors or actuators to be optimised. The complexity of optimisation problem in the active vibration control of flexible structures has led researchers to try to reduce the search space and computational effort and to explore global optimal sensor and actuator location in order to optimise controller performance. The studies of the optimal placement of sensors and actuators described in previous chapters are mainly based on the maximisation of grammian observability and controllability and the minimisation of the linear quadratic index as objective functions in genetic algorithms. Only a few studies [49, 62-64, 106] have investigated the placement of sensors and actuators in optimal positions on flexible structures using H_∞ and H_2 norms as objective functions.

The optimal placement of individual accelerometer sensors and point force actuators was investigated by Gawronski for a fixed-ended beam, cantilever truss and the

international space station truss based on the use of the H_∞, H_2 and H_s norms under open loop control to suppress the first modes individually and then grading them collectively. He reported that the placement of small numbers of sensors or actuators can be determined through a search procedure, while the search for the possible combinations of numbers of sensors or actuators for large structures requires high computational effort and does not necessarily give the optimal solution. The proposed placement strategy was implemented by optimising the location of each sensor or actuator according to their optimal norms for each mode which was required to be suppressed, and then grading them according to their participation in their modes in order to reduce the computational effort needed. The placement strategy was started by selecting a sub-search space from the total search space based on engineering experience, technical requirements and physical constraints. The optimal number was determined by reducing the sub-search space step by step according to the fitness value of the required numbers of sensors or actuators. The placement strategy based on simple search methods and placement indices for sensors and actuators has been explained thoroughly with modelling based on the H norms in chapter seven of the original study [52], and this chapter includes a number of papers for the same author and subject. The method of determination of the optimal locations of sensors or actuators for each individual mode and then their grading does not give the optimal combination of sensors or actuators needed to suppress a number of modes collectively. This is because the optimal location varied from one mode to another. To find combinations between them is not easy and may require more sensors and actuators to be added to achieve that aim. Furthermore, the process of choosing a sub-search space from the total search space does not achieve the global optimal solution. These aspects can be improved by using an efficient placement strategy and search algorithm, such as a genetic algorithm to find the minimum combinations of sensors or actuators needed to attenuate a number of modes collectively.

The optimal placement of two sensor/actuator pairs on a beam was investigated by Hiramoto et al using an H_∞ controller based on the use of simple addition and multiplication matrices to reduce the computational effort required compared to using the standard solution of Riccati equation. The proposed method found the optimal locations based on the minimisation of the closed loop H_2 norm as an objective function using a quasi-Newton optimisation method [62].

Specific configurations of the placement of finite numbers of sensors and actuators on a continuous flexible structure were investigated by Chemishkian and Arabyan in order to

reduce structural deformation to a minimum in the H_∞ sense. The computational overhead can be reduced by evaluating the minimum H_∞ norm for each step in the genetic algorithm, and the controller H_∞ is designed only when the lower limit is below a predefined value [63, 64]. The spatial H_2 norm was developed by Liu et al to optimise the location of sensors and actuators in controlled flexible structures based on dominant modes which have significant effects on the structure. The positions of four finite element nodes was optimised for sensors and actuators on a clamped-clamped plate using a genetic algorithm [49].

These studies [49, 62-64] have investigated the optimal locations of sensors and actuators under closed loop control using optimisation algorithms to find the optimal combinations of sensors and actuators needed to suppress a number of modes collectively, and open loop control [65] is based entirely on a search method using a small search space and sub-search spaces for large-scale structures to find the optimal locations of sensors or actuators to suppress individual modes and then grading them.

In this chapter, the combination of locations of six and ten sensor/actuator pairs on a cantilever plate is optimised using a genetic algorithm to attenuate the first six modes of vibration collectively. A new objective function is proposed based on H_∞ to minimise an average summation of the absolute dB gain for the open loop transfer function for all sensors and modes as a result of applying a unit sinusoidal voltage at the location of a predefined or arbitrary single actuator through all generations in the genetic algorithms placement progression. The method is implemented for the same cantilever plate investigated in chapter five.

6.2. Modelling

The full modelling derived in chapter three for a plate stiffened by beams bonded with discrete sensors and actuators is used in this chapter to investigate a flat plate by considering that the mass and stiffness of the beam are zero. Controller state space matrices were then prepared according to equations 3.97 to 3.100.

6.3. Control Scheme

In this chapter, an optimal linear quadratic control scheme is implemented to attenuate the first six modes, as explained in section 3.5 and section 3.8.

6.4. Objective Function

A new objective function has been developed in this study to find the optimal configuration of sensors based on minimisation of the H_∞ norm. The fitness function is a measure of the open loop average dB gains for all sensors at all the required modes to be attenuated, as a result of a sinusoidal unit voltage applied at a single predefined actuator. This actuator was selected at large modal strain or at an arbitrary location and is fixed for all chromosomes and generations.

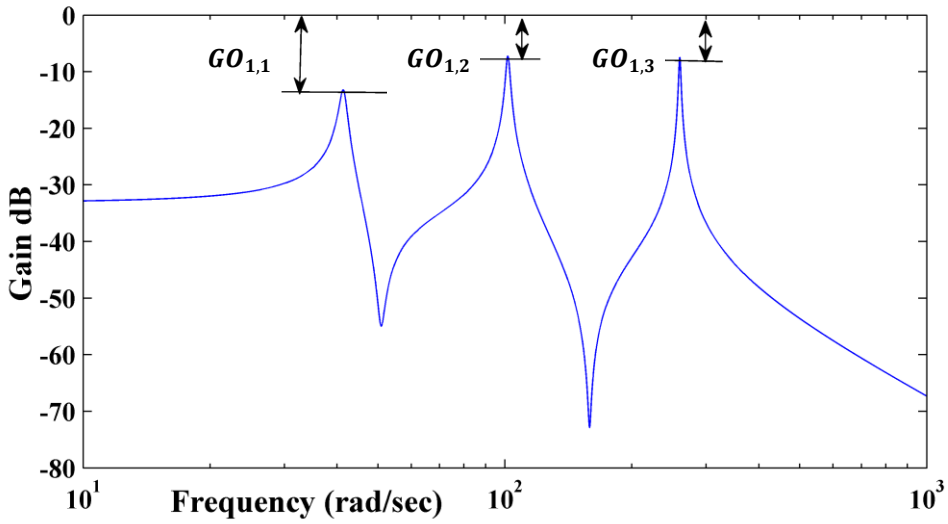

Figure 6.1 Open loop frequency response for a asystem

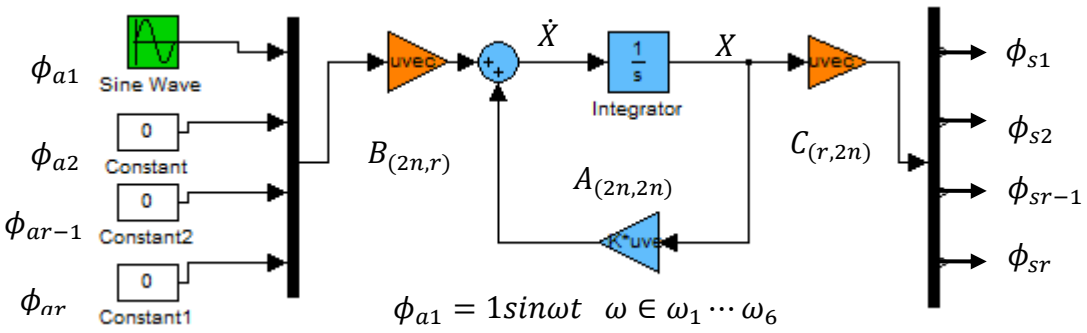

Figure 6.2 Simulink graph to demonstrate the fitness function

Consider a system state space and sensor output voltage equations are:

$$\dot{X} = AX + B\phi_a\,, \qquad \phi_s = CX \tag{6.1}$$

Then take the Laplace transform of equation 6.1, which gives:

$$\begin{gathered} sX(s) = AX(s) + B\phi_a(s), \quad \phi_a(s) = B^{-1}(sI - A)X(s) \\ \phi_s(s) = CX(s) \end{gathered} \tag{6.2}$$

The open loop transfer function of the system in the s-domain is then:

$$G(s) = \frac{\phi_s(s)}{\phi_a(s)} = C(sI - A)^{-1}B \tag{6.3}$$

$$G(\omega) = C(j\omega I - A)^{-1}B \tag{6.4}$$

According to Figure 6.1 and Figure 6.2, the peak magnitude of the transfer function is the H_∞ norm of the single sensor i as a result of applying a unit sinusoidal voltage at the first actuator for a single mode ω_j .

$$H_\infty = GO_{i,j} = max\big(20Log_{10}G(\omega)\big) = 20Log_{10}G_i\big(\omega_j\big) \tag{6.5}$$

$$J(x,y) = \frac{1}{n_m n_{sa}} \left| \sum_{i=1}^{n_{sa}} \sum_{j=1}^{n_m} GO_{i,j} \right|_{predifined\ actuator} \tag{6.6}$$

$$J_{opt}(x,y) = \min\big(J(x,y)\big) \tag{6.7}$$

where $\boldsymbol{x}, \boldsymbol{y} \in$ plate dimensions of 50×50 cm. Use of the fitness and objective function equations 6.6 and 6.7 involve much lower computational costs and have simpler mathematical forms than the matrices of the standard H_∞ placement indices. The minimisation of the objective function increases the observability of the structure.

6.5. Genetic Algorithm and Sensors Placement Strategy

The strategy for the placement of actuators using a genetic algorithm, including a conditional filter, is implemented in this chapter according to the new objective and fitness functions, as explained in sections 5.4 and 5.5 respectively.

The new sensor placement strategy using the fitness and objective functions developed in the previous section can be summarised in the following points concerning the

optimisation of sensor location, while the actuators will be paired with the sensors in their optimal locations.

In this work, the strategy of the placement for piezoelectric sensors is proposed and programmed in MATLAB m-code. Its main features are as follows:

1. The state matrix A of dimension $(2n_m, 2n_m)$ is prepared for the first six modes of vibration according to equation 3.99.
2. One-hundred chromosomes are chosen randomly from the search space to form the initial population.
3. An actuator location is predefined for the application of the disturbance voltage, selected either at a high modal strain location (for example, actuator location 01 is chosen in this work) or at any location in the structure which will be cancelled at the end of the optimisation process. In this case the chromosome length must be increased by one sensor/actuator pair.
4. The actuator B matrix is prepared for location 01 according to equation 3.100.
5. A sinusoidal disturbance with unity voltage amplitude is applied at the predefined actuator while the other actuators at are zero voltage throughout all generations, as shown in Figure 6.2.
6. The output sensor matrix C is calculated for each chromosome and for the first six modes of vibration according to equation 3.100.
7. A fitness value is calculated for each member of the population based on the fitness function according to equation 6.6, and this is stored in the chromosome string to be saved for future recalculation.
8. The chromosomes are sorted according to their fitness values and the 50 chromosomes (less than or equal to the initial population depending on the size of the problem) with the lowest fitness values (i.e. the most fit; see equation 6.7) are selected to form the breeding population. These are called parents, and the remaining less fit chromosomes are discarded.
9. The members of the breeding population are paired up in order of fitness and 50% crossover is applied to each pair. The crossover point is selected randomly and is different for each parent. This gives two new offspring (child) chromosomes with new properties.
10. A mutation rate of 5% is used on the child chromosomes.
11. The new chromosomes are filtered for repeated genes through the conditional filter.

12. The output sensor matrix C is calculated for each child chromosome according to equation 3.100, and thereafter the process is repeated from step 7 for a preset number of generations.

6.6. Results and Discussion

The cantilever flat plate tested in section 5.6 was also investigated in this section in order to optimise the locations of ten and six sensors using the developed sensors placement strategy. This case is chosen to give a direct comparison with the actuator placement strategy described in section 5.5 and in previously published work [26, 38, 49] and to test the reliability and robustness of the present study.

The genetic algorithm and placement strategy described in section 6.5 were used to find optimal locations for ten piezoelectric sensors on this cantilever plate. The progressive convergence of the population onto an optimal solution is shown in Figure 6.3**,** where the population is distributed around the circle with a radius representing its fitness value which needs to be minimised. A sinusoidal unit voltage disturbance is applied at actuator location 01 according to the third point in section 6.5. The optimisation results proceeded in a similar way to that described in section 5.6.4, with good convergence occurring by the 500th generation as shown in Figure 6.3 and Figure 6.4. The optimal distribution of ten sensors was also found to be symmetrical about the plate's dynamic axis of symmetry as shown in Figure 6.4 (c), in spite of using different objective functions based on sensor placement. This indicates that the optimal configuration of sensors or actuators follows the dynamic axes of symmetry of a mechanical structure. This finding will be proved in the next chapter using different types of structure with various geometries and types of fixations.

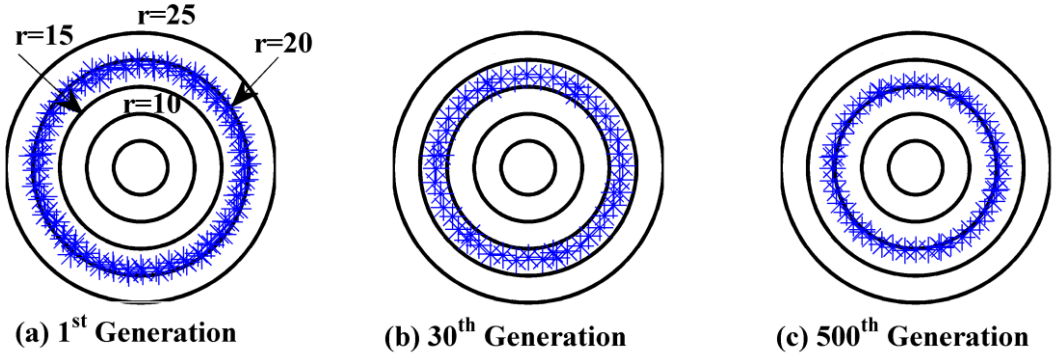

Figure 6.3 Population fitness progression over 500 generations: each individual is represented as one of the points distributed around the circle, with fitness value shown

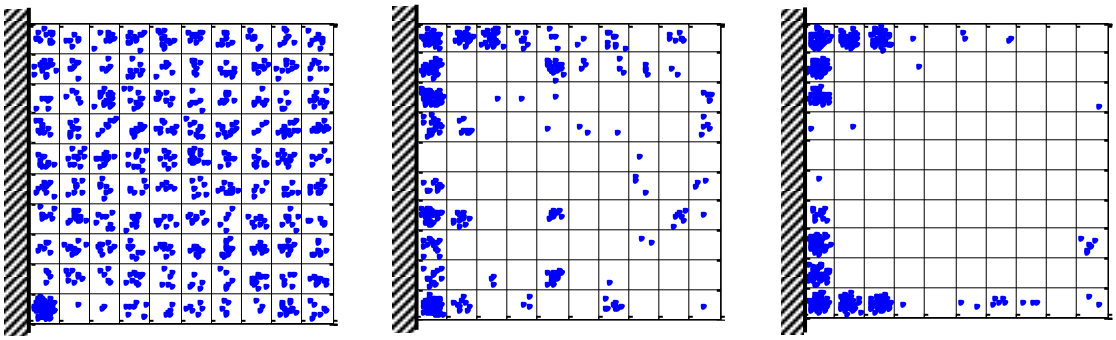

(a) 1st Generation (b) 30th Generation (c) 500th Generation

Figure 6.4 Sensor/actuator placement for the cantilever plate, each dot showing the location of a sensor/actuator pair in one of the 50 breeding individuals at each generation. Initially they are randomly distributed. After 30 generations they have begun to group in efficient locations. After 500 generations they have mostly converged at ten sites symmetrically distributed about axis of symmetry.

The computer program was run again to optimise six sensors on the same cantilever plate for the purpose of comparison with another published study [26]. Figure 6.5 (a, b and c) shows the progression of the placement of six sensors. After 300 generations they had completely converged at six sites symmetrically distributed about the plate's axis of symmetry.

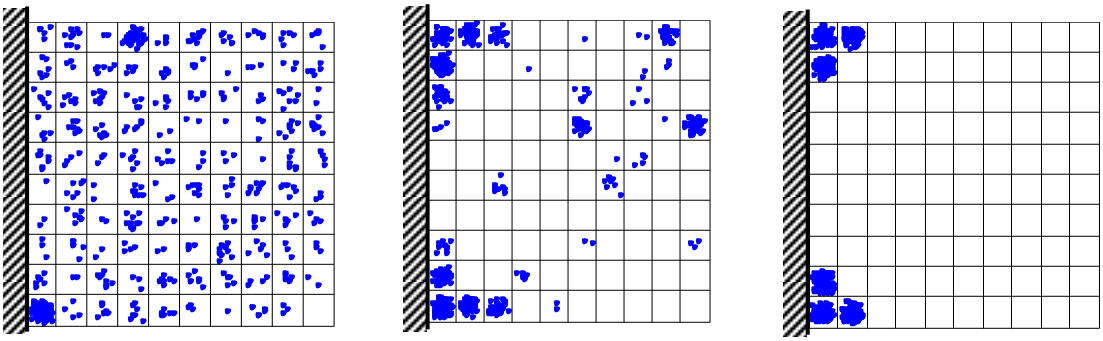

(a) 1st Generation **(b) 30th Generation** **(c) 300th Generation**

Figure 6.5 Sensor/actuator placement for the cantilever plate, each dot showing the location of a sensor/actuator pair in one of the 100 breeding individuals at each generation. Initially they are randomly distributed. After 30 generations they have begun to group in efficient locations. After 300 generations they have completely converged at six sites symmetrically distributed about axis of symmetry.

The developed sensor placement strategy was validated by running the genetic algorithm program six times to locate ten sensor/actuator pairs on a cantilever plate. The results for the six runs are shown in Figure 6.6. The figure shows convergence progressing to the optimal solution by plotting the best member at each generation and the results gave the same behaviour as that described in section 5.6.5. The results indicate that the optimal solution is global and the optimisation process is robust in finding repeatedly the global optimal solution .

Liu et al investigated a clamped-clamped plate to optimise four sensors and actuator locations using the closed loop H_2 norm as an objective function. A binary-encoded chromosome was used with string length equal to the total number of finite element nodes. The computer program was run five times to get the global optimal solution as shown in Figure 6.7 [49].

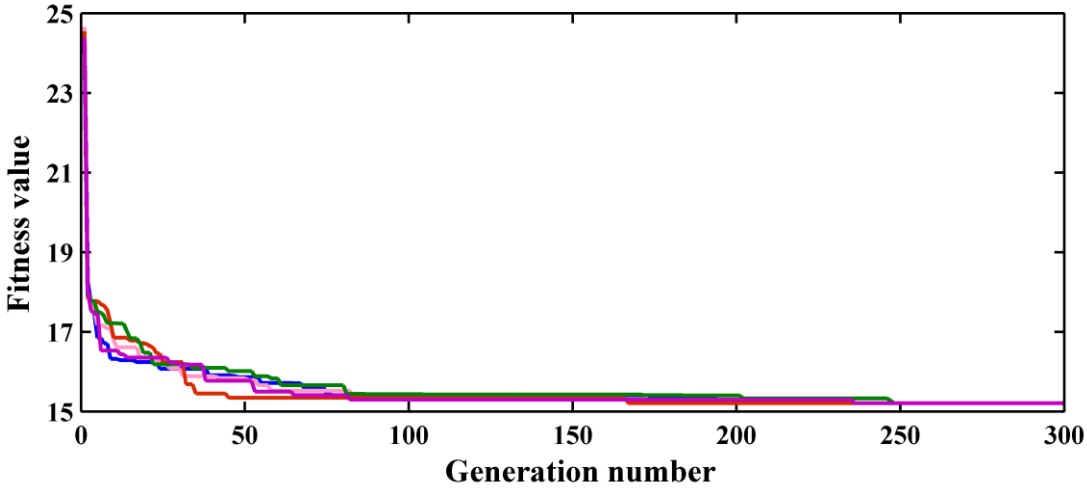

Figure 6.6 Fitness value for the best member in each generation for the cantilever plate. six runs of computer program gives the same optimal fitness value.

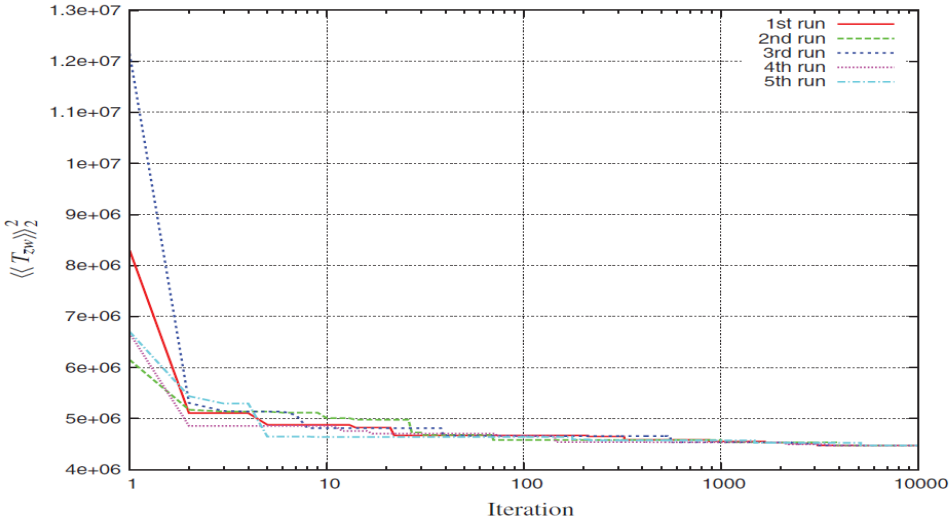

Figure 6.7 The performance index vs the GA iteration steps [49]

Table 6.1 shows a comparison between the present work and Liu et al's study [49]. It can be seen from the table that the search space of the present study involves 17310×10^9 candidate solutions, which is much more complicated than the previous study's 1.83×10^9 candidate solutions. The global optimal solution found within 250 generations , which is much faster than than Liu et al's 5000 generations.

Table 6.1 Comparison study between the present work and reference [49]

Case	Reference [49]	Present work
Number of sensors and actuators	4	10
Chromosome encoding type	Binary	Integer
Mutation based on	One or two bits inside gene	One gene inside chrom.
Population size	50	100
Number of modes to be controlled	4	6
Optimisation algorithms/fitness function	Genetic/H_2	Genetic/H_∞
Chromosome selection	Random based on fitness	Truncation
Search space total number of candidates	1.84×10^9	17310×10^9
Number of generations to reach the optimal solution	5000	250

The optimal distribution of six sensors determined in this section (see Figure 6.5) was mapped onto the cantilever plate as shown in Figure 6.8(a). The optimal configuration agreed with that in the study by Han and Lee where six sensors were optimised for a cantilever plate using genetic algorithms based on grammian observability as an objective function, as shown in Figure 6.8(b) [26].

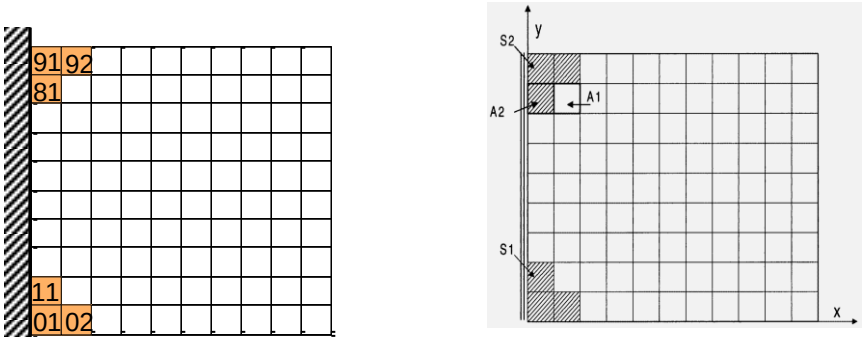

(a) (b)

Figure 6.8 Optimal configuration of six sensors on a cantilever plate mounted rigidly on the left edge, **(a)** present work of this chapter, **(b)** reference study [26]

The present optimal placement configuration was tested to measure the average closed loop dB gain reduction for all sensors over the first six modes using the optimal linear quadratic control scheme. The results are compared with those from chapter five and a previous study, as shown in Figure 6.9. In this section, the criterion used to compare the quality of the three systems of optimal configurations of the piezoelectric sensor/actuator pairs was explained in section 3.8.

The optimal locations of sensor/actuator pairs for the three systems shown in Figure 6.9 are obtained according to various objective functions. In Figure 6.9 (a) and (b), the optimisation was based on the minimisation of the quadratic cost function in placing the actuators, and the sensors were paired with the actuators. However, the optimal configuration shown in Figure 6.9 (c) was based on the minimisation of the average open loop dB gain to locate the sensors, and the actuators were then paired with them, as explained in section 6.5. A sinusoidal disturbance of unit amplitude was applied at actuator location 11 at the plates for all three cases. The present configuration gives an improvement of 38.60% reduction at $Q = 10^8$ compared to the optimal piezoelectric configuration in the previous study[38] , as shown in

Table 6.2.

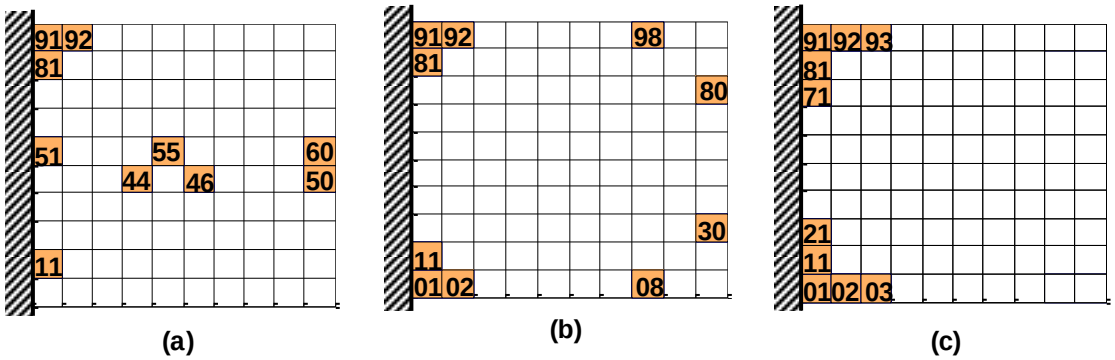

Figure 6.9 Optimal configuration of sensor/actuator pair for a cantilever plate mounted rigidly on the left edge, **(a)** Kumar and Narayanan [38] **(b)** optimal distribution determined in chapter five **(c)** this chapter

Table 6.2 Closed loop average dB gain reduction and percentage improvement compared to [38]

Case	[38]	Chapter five	This chapter	Improvement
$Q = 10^7$	21.4369dB	23.0722dB	22.70dB	15.65%
$Q = 10^8$	27.6645dB	30.9426dB	30.50dB	38.60%

6.7. Conclusions

In this chapter, new fitness and objective functions have been developed to optimise the locations of six and ten sensors for a cantilever plate using the genetic algorithm. The objective function is the minimisation of an absolute average open loop dB gain for all sensors as a result of applying a sinusoidal disturbance unit voltage amplitude at a predefined or arbitrary actuator. The locations of sensors were optimised, and the actuators were then paired with the sensors.

It has been found that the optimal configurations of six and ten sensors were symmetrically distributed about the plate's axis of symmetry, and this finding is in complete agreement with that in a previous study [26] and with the findings in chapter five. Thus it is clear that the global optimal distribution of sensor/actuator on a

symmetrical structure is itself symmetrical. This indicates that this finding is general and is not dependent on the objective function used.

The robustness of the placement strategy and objective function was tested by running the computer program six times, and the results converged to the same optimal solution within much fewer generations, 250, than the previous study's [49] 5000 generations, even though the present optimisation problem is much more complicated. The optimal sensor configuration is then compared with optimal actuators determined in chapter five and a previously published study [38] using optimal linear quadratic control. It is found that the present optimal configuration gives an average reduction 38.60% better than the published optimal piezoelectric sensor/actuator distribution using optimal linear quadratic control with weighted matrices $R = 1$ and $Q = 10^8$.

The contribution of this chapter is its development of new objective function and genetic algorithm placement strategy which optimises a combination of various numbers of discrete sensors on a flexible structure in order to attenuate number of modes collectively. This new objective function achieved the optimal combination of ten sensors in far fewer generations and for a much more complex optimisation problem than previously published work [49] and gave higher vibration reduction than other published optimal sensor/actuator configuration [38]. This holds great potential for use with large-scale structures to determine the global optimal distributions of discrete sensors in fewer generations.

Chapter 7. Plates Stiffened by Beams

In this chapter, the optimal placement of ten sensor/actuator pairs on plates stiffened by beams is studied according to the theory presented in chapters three and five. Symmetrical and asymmetrical geometries and methods of plate fixation were investigated to study their effects on the optimal distribution of sensors and actuators. Firstly, the optimal placement of ten sensor/actuator pairs and the feedback gain matrix were found for plates stiffened by two beams arranged in the form either of a cross or T-type, which were chosen because they provide symmetrical and asymmetrical dynamic geometries of the structures. Secondly, the placement of the sensor/actuator pairs was optimised for a symmetrical flat plate mounted with different boundary conditions to produce symmetrical and asymmetrical plates. The upper surface areas of all plates were fully covered by the piezoelectric layer and represented in the ANSYS finite element package using the APDL program in order to study the distributions of modal electric charge over the piezoelectric surface in free vibration tests at the first six modes. It was found that the mode shape, modal strain energy and electric charge distribution followed the dynamic axes of symmetry of the plates.

The genetic algorithm explained in chapter five was utilized to determine the optimal placement of eight and ten piezoelectric sensor/actuator pairs to suppress the first six modes of vibration, and the effects of plate boundary conditions and geometry on the optimal distribution of piezoelectric actuators was investigated. It was shown that for the structures with symmetrical geometries and boundary conditions, optimal transducer locations were distributed with the same axes of symmetry. This agreed with the results of the ANSYS test.

The open and closed loop time responses of the plate stiffened by two beams in the cross type were investigated in order to validate the optimal locations of the ten sensor/actuator pairs. The cross-type stiffened plate was driven by a sinusoidal voltage at actuator location 91 to investigate the time response at the first mode, and at actuator location 70 to study the time response at the third and fifth modes. The stiffened plate was represented in the ANSYS finite element package using APDL programming and the proportional differential control scheme was implemented in order to suppress vibration in the normal modes. The steady state closed loop time response gave average reductions in the sensor tip acceleration of 65%, 80%, 78% at the first, third and fifth modes respectively. A comparison study was also investigated for stiffened plate cross-

type using two types of piezoelectric configurations: the optimal configuration of ten sensor/actuator pairs; and "full coverage" with a single sensor/actuator pair covering the whole surfaces of the stiffened plate. The plates are actuated with an out of plane sinusoidal concentrated force of constant amplitude at the free-end plate corner. The closed loop time responses for sensor voltages and vibration amplitude were reduced by 90% for the optimal configurations and no reduction for the full coverage piezoelectric case at the first and third modes.

7.1. Introduction

Plates and shells stiffened by beams are widely used to construct mechanical structures with increased specific strength and stiffness, and they have been investigated extensively for improvements in static and dynamic properties. However, only a limited number of papers have been published on research into the active vibration control of such plates and shells. It was reported in section 2.10 that researchers have investigated plates and shells stiffened by beams with a piezoelectric sensor/actuator pair distributed over the whole surface or arbitrarily located at discrete points about the surface [70-73]. Conversely, many studies described in section 2.10 have drawn attention to the importance of discrete sensors and actuators and their locations in achieving high sensing and actuating effects with low feedback voltage, and high response and stability. The previous studies presented in section 2.10 reveal that the optimisation of the locations of discrete piezoelectric sensors and actuators on plates stiffened by beams has yet to be investigated.

Genetic algorithms have been utilized by many researchers for the optimal location of piezoelectric sensors and actuators on flat plates and shells, as demonstrated in chapters three, five and six. In many studies of the optimal placement of discrete piezoelectric sensors and actuators on a plate symmetrical in geometry and boundary conditions [25, 38, 43, 49, 66], a completely asymmetrical distribution of piezoelectric sensors and actuators was found, whereas in others symmetrical optimal configurations were found [26, 30, 35, 54] or distributions which were close to symmetrical [40, 66]. However, the effect of symmetrical and asymmetrical boundary conditions and geometry on the optimal configuration of sensors and actuators, and the impact of these variables on the genetic algorithm problem reduction, has never been investigated for flexible structures.

In this chapter, two research points were investigated concerned with the optimal placement of actuators on plates stiffened by beams according to the theory presented in

chapters three and five, and the effects of the structure's dynamic symmetry on optimal actuator configurations.

7.2. Modelling

The full modelling derived in chapter three for plates stiffened by beams bonded to discrete piezoelectric sensors and actuators is used in to investigate the effects of symmetrical and asymmetrical geometries and boundary conditions on the optimal locations of discrete piezoelectric sensors and actuators.

7.3. Control Law, Objective Function and Genetic Algorithm

The proportional differential control scheme was implemented to study the open and closed loop time responses of the plate stiffened by two beams in the cross formation. The minimisation of the linear quadratic index was used as an objective function to locate the actuators, as explained in section 3.7. The use of the genetic algorithm and placement strategy applied in this chapter was conducted according to the explanations in sections 5.4 and 5.5 respectively.

7.4. Results and Discussion

7.4.1. Problem description

A flat plate of dimensions $500 \times 500 \times 1.9\,\text{mm}$ was arranged with four types of fixation and geometry, as shown in Figure 7.1. Firstly, a flat plate was fixed as a clamped-clamped cc-plate, and stiffened by two beams in a cross-type configuration and mounted rigidly from the left-hand side as a cantilever, to achieve two axes and one axis of symmetry respectively as shown in Figure 7.1 (a) and (b). Secondly, an asymmetric configuration was arranged by mounting a flat plate rigidly at the left-hand edge and at one lower corner point on the free end. This is the co-plate shown in Figure 7.1 (c). Finally, a flat plate was stiffened by two beams of dimensions $500 \times 20 \times 1.9\text{mm}$ arranged in the form of an inverted T and mounted as a cantilever giving geometrical asymmetry, called the T-stiffened plate as shown in Figure 7.1(d).

These types of fixation are expected to affect the plate's mode shape, modal strain and hence the modal electrical charge distribution induced on the surface of the piezoelectric sensors and actuators bonded to the plates. In addition, the symmetrical and asymmetrical boundary conditions and different geometries might be expected to

affect the optimal configuration of the piezoelectric sensors and actuators and so might help to explain the conflicting findings in the literature noted in section 2.9.

The plates were discretised to a number of finite elements numbered from 01 to100 as shown in Figure 7.1(a). An optimal placement of eight actuators was investigated for the cc-plate and ten actuators were used for the other configurations because it was expected that the optimal configuration of actuators would have two axes of symmetry in the cc-plate, with one axis of symmetry in the cross plate and none for others. The properties of the mild steel plate and piezoelectric layers (PZT type PIC255) are listed in Table 4.1.

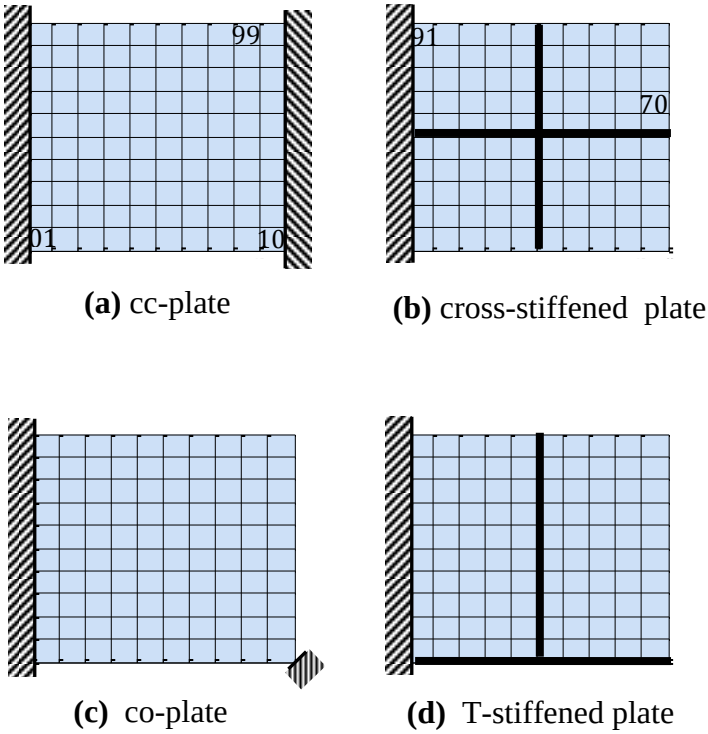

(a) cc-plate **(b)** cross-stiffened plate

(c) co-plate **(d)** T-stiffened plate

Figure 7.1 Symmetrical and asymmetrical plates in boundary conditions and geometries to achieve **(a)**, two axes of symmetry, **(b)**, one axis of symmetry, **(c)** and **(d)** completely asymmetrical dynamic structure

7.4.2. Mode shape modal strain and electric charge distribution

In this section, ANSYS finite element programs were written in APDL for all symmetric and asymmetric plates shown in Figure 7.1 to investigate mode shape and modal strain distribution for the first six modes, and then for all plates a single piezoelectric sensor/actuator pair was bonded to the plate so as to cover the whole plate surface in order to investigate the electric charge distribution over the piezoelectric

surface. Three dimensional solid45 and solid5 elements were deployed for the passive structure and the active piezoelectric sensor and actuator respectively.

Figure 7.2 shows the mode shape distributions in the first, third and fifth modes for a plate stiffened by two beams in the cross- and T-type. It can be seen that all the amplitudes of the mode shapes are symmetrically distributed about the plate's axis of symmetry, which is perpendicular to the fixed end for the cross-type while the distribution is asymmetrical for the T-type.

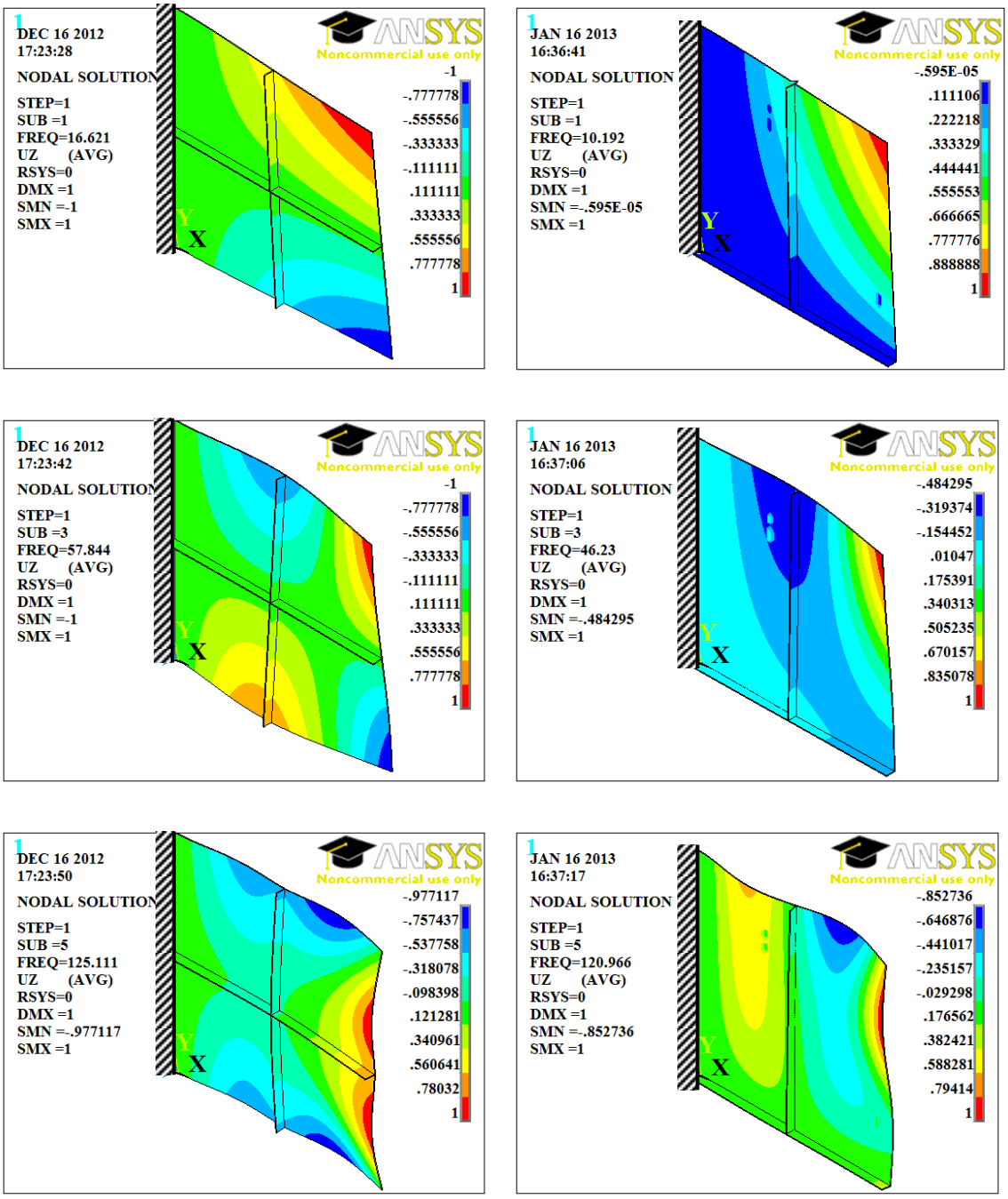

Figure 7.2 First, third and fifth mode shape distribution in the z-direction for the plates stiffened by two beams in the cross and T-type

Figure 7.3 shows the distributions of the amplitude of modes shape at the first, third and fifth modes for the cc-plate and co-plate. It can be seen that the distribution of all mode shapes are symmetrical about two axes of symmetries for the cc-plate while being completely asymmetrical for the co-plate.

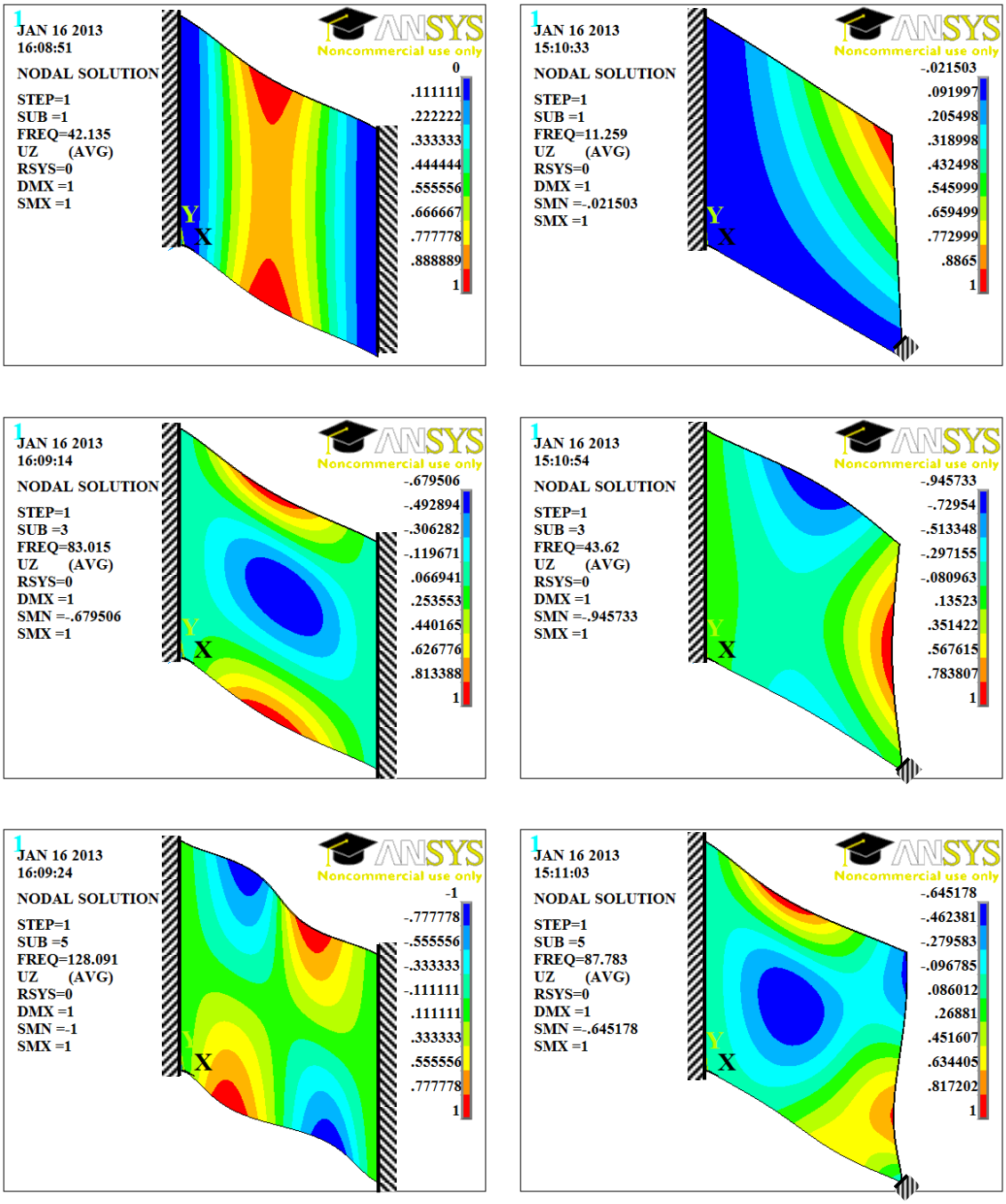

Figure 7.3 First, third and fifth mode shape distribution in the z-direction for the cc-plate and the co-plate

Figure 7.4 demonstrates the distribution of the modal strain intensity for the first, third and fifth modes of vibration for the stiffened plate in the cross- and T-type. It can be observed that the modal strain intensity is distributed in the same pattern as the symmetries of mode shape amplitude. Modal strain intensity is distributed symmetrically about one axis for the cross type and asymmetrically for the T-type which is completely asymmetrical in geometry.

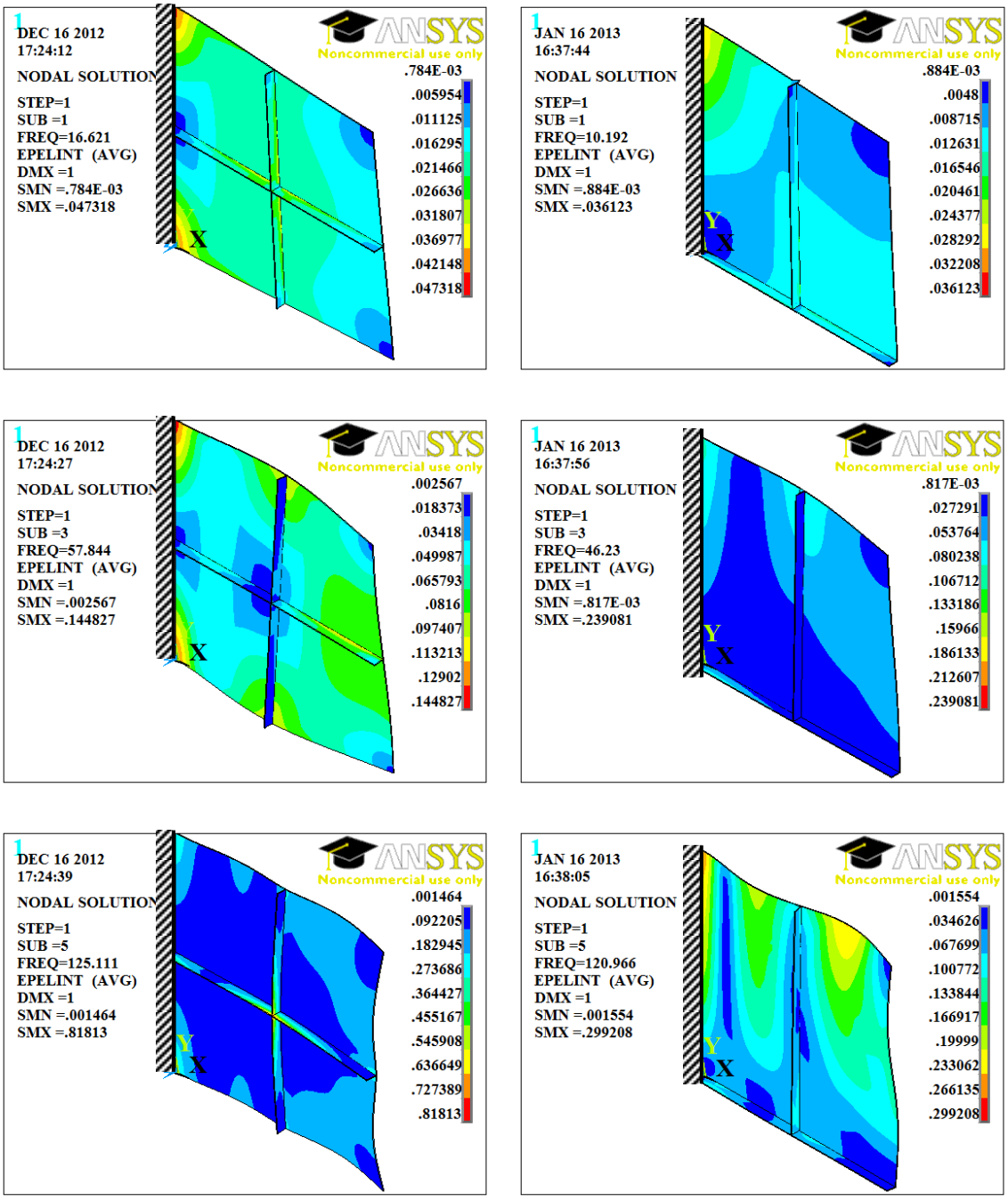

Figure 7.4 First, third and fifth modal strain intensity distribution for the plates stiffened by two beams on the cross and T-type

Figure 7.5 shows the first, third and fifth modal strain intensity distributions for the cc-plate and co-plate. It can be seen that the distribution of all modal strain intensities are symmetrical about two axes of symmetries for the cc-plate while being completely asymmetrical for the co-plate. This is because the latter has two axes of symmetry in geometry and boundary conditions, while the co-plate is asymmetrical in the boundary conditions.

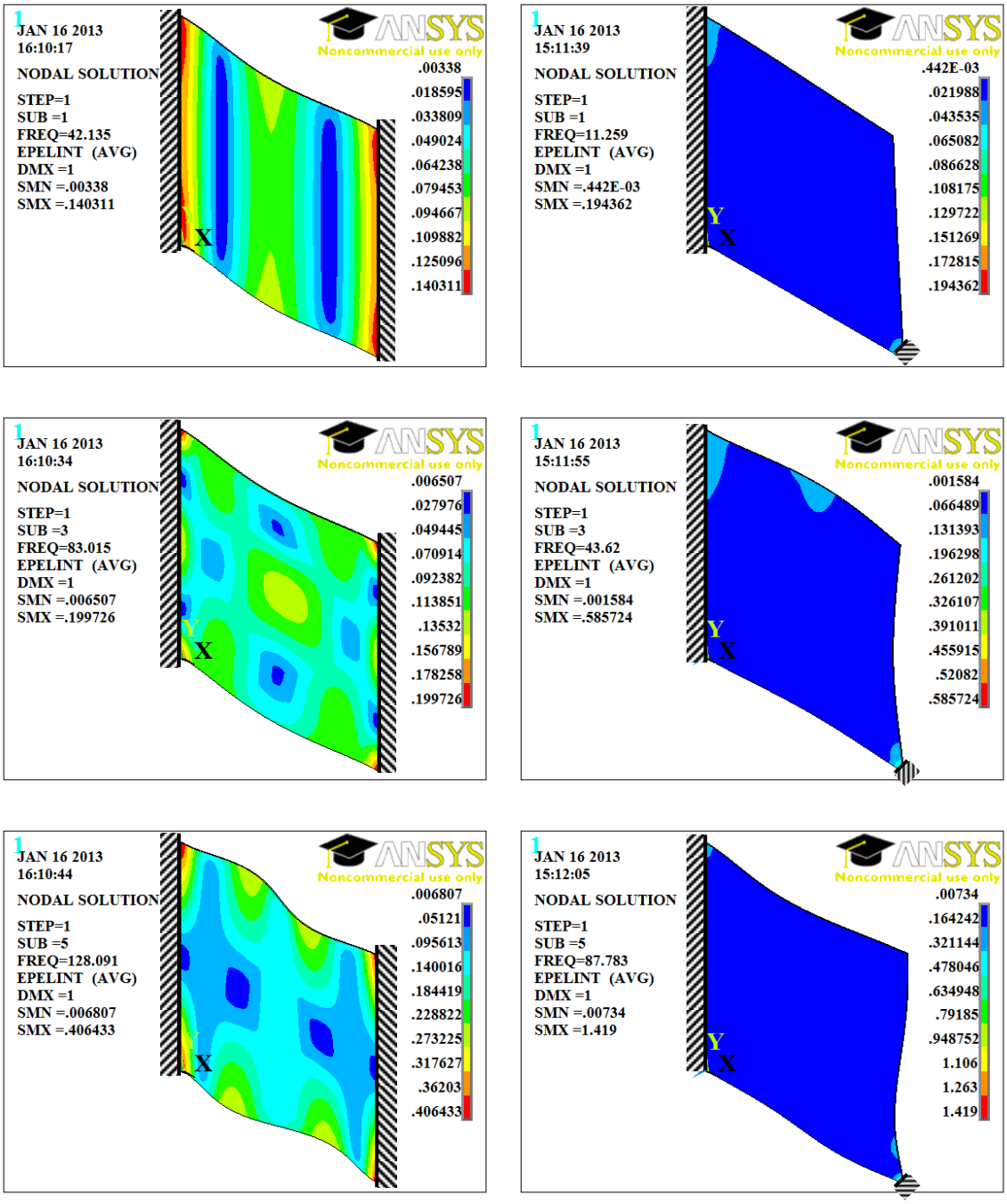

Figure 7.5 First, third and fifth modal strain intensity distribution for the cc-plate and co-plate

Each type of plate was bonded to a single piezoelectric sensor/actuator pair covering the whole plate and modelled using a solid45 element for the plate and a solid5 element for the piezoelectric pair before being represented in the ANSYS finite element package to determine the modal electric charge distribution over the piezoelectric surface, as shown in Figure 7.6 and Figure 7.7. The figures show the modal electric field distribution between upper and lower piezoelectric surfaces, which directly relates to the modal electric charge distribution over the piezoelectric surface.

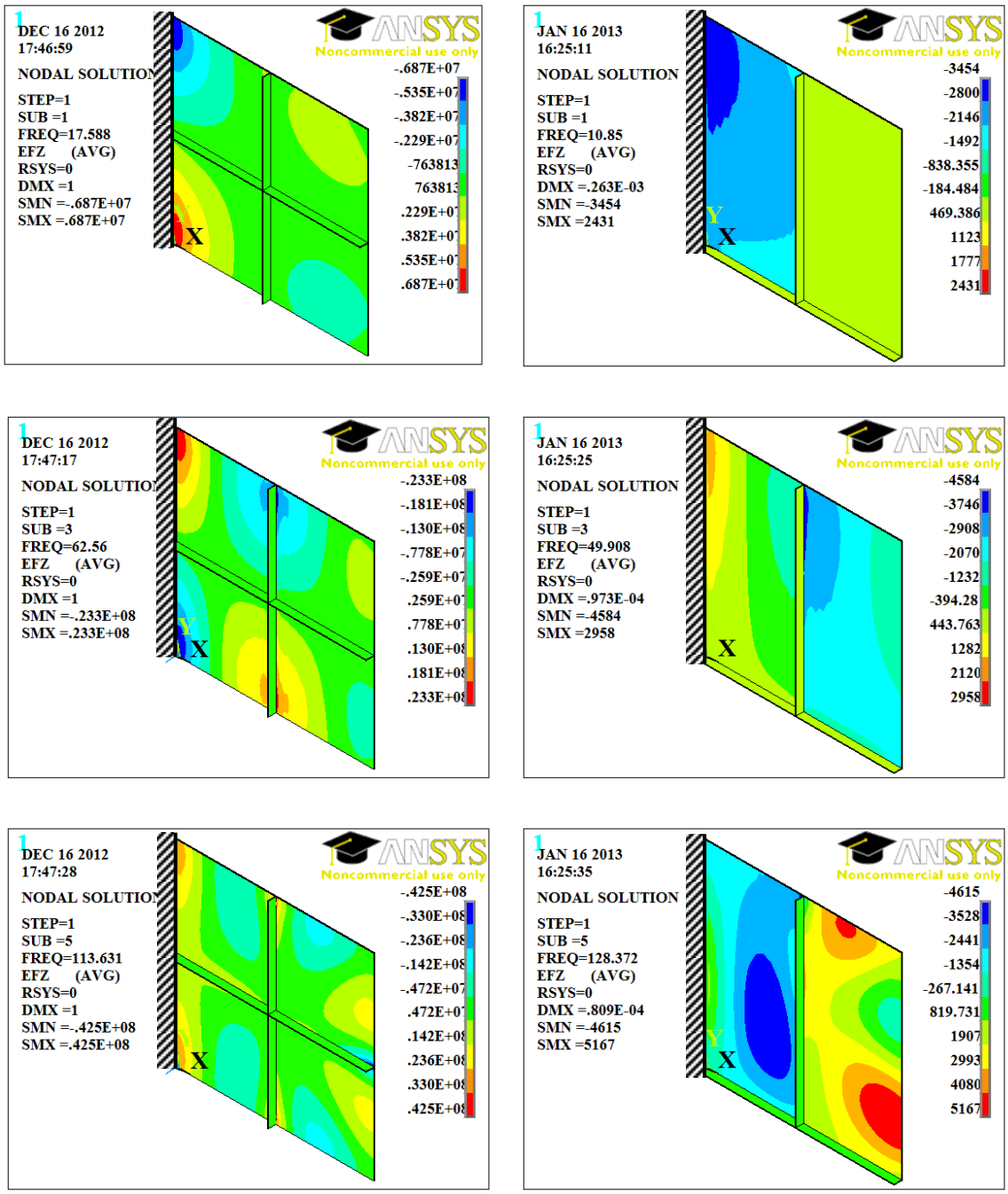

Figure 7.6 First, third and fifth modal electric field distributions in the z-direction for the plates stiffened by two beams in the cross and T-type

It can be seen from Figure 7.6 and Figure 7.7 that the distribution of the modal electric field is symmetrical for plates symmetrical in geometry and boundary conditions but asymmetrical for plates which are asymmetrical in geometry or boundary conditions. It could be expected that the global optimal distribution of discrete piezoelectric sensors and actuators would be symmetrical for plates symmetrical in geometry and boundary conditions and asymmetric for plates asymmetrical in geometry or boundary conditions.

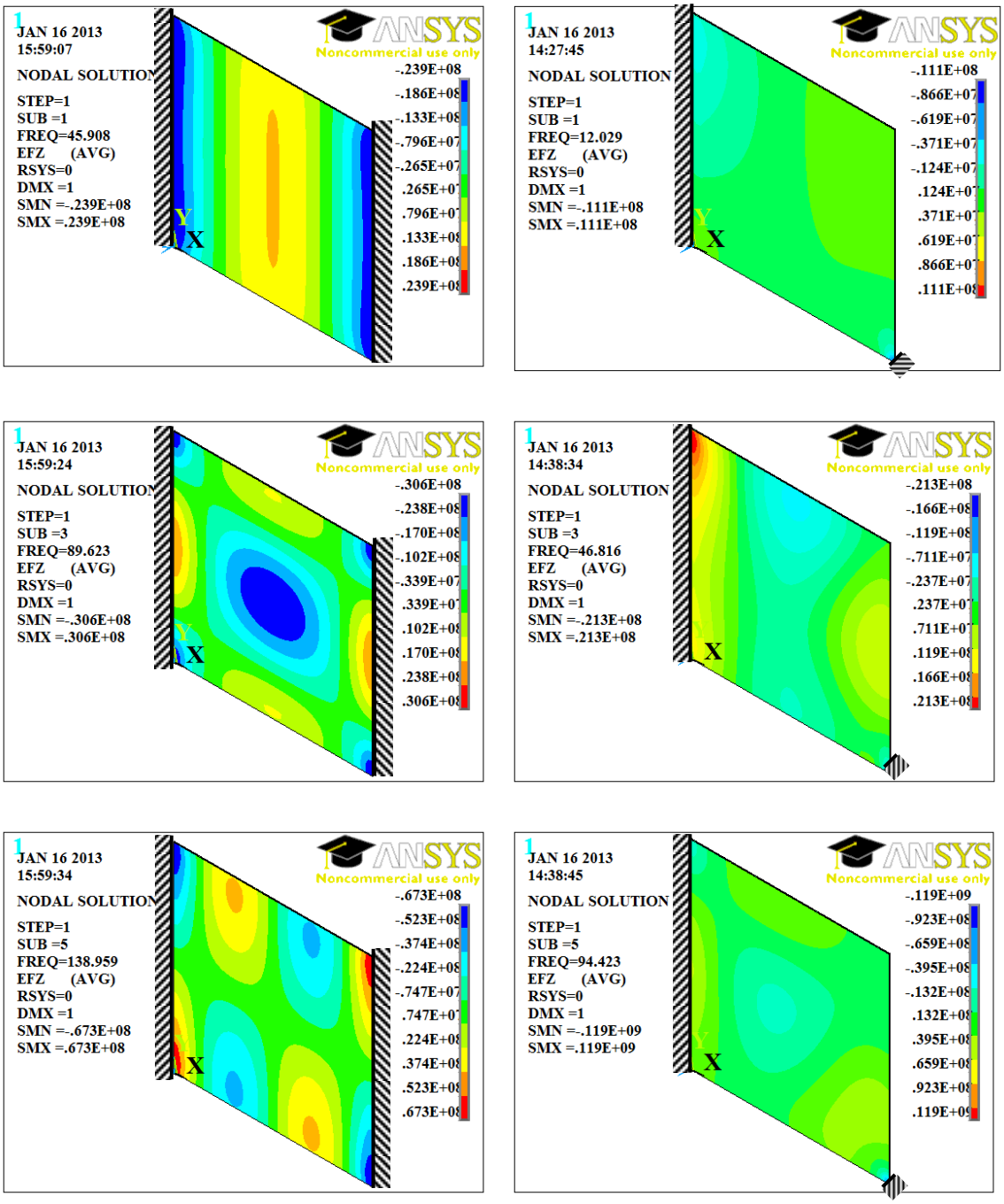

Figure 7.7 First, third and fifth modal electrical field distributions in the z-direction for the cc-plate and co-plate

It can be observed from this section that the evidence concerning the distribution of mode shapes, modal strain and electric charge distribution indicates that the global optimal location of discrete piezoelectric sensors and actuators is likely to be symmetrically distributed also for symmetrical structures and asymmetrical for asymmetrical structure.

It is also observed from the distribution of electric charge in the first and third modes for the stiffened cross-type plate, and for the third mode of the T-type, as shown in Figure 7.6 , as well as the first, third and fifth modes for the cc-plate as shown in Figure 7.7, that the collective effect of electric charge over the piezoelectric surface approximately sums to zero for these modes and some of the even modes (the second, fourth and sixth modes are not displayed in this section). Therefore, it could be said that the vibration detection and actuating effects nearly cancel out for a mechanical structure fully covered by a single sensor/actuator pair for most modes. However, discrete sensor/actuator pairs give high sensing and actuating effects if they are properly located.

7.4.3. Optimisation of sensor/actuator location

The genetic algorithm and placement strategy described in sections 5.4 and 5.5 were used to find optimal locations for ten sensor/actuator pairs on a 0.5m square cantilever plate with cross-type stiffeners. The progressive convergence of the population onto an optimal solution is shown in Figure 7.8(a), Figure 7.9(a) and Figure 7.10(a), where the population is distributed around the circle with a radius representing the fitness value to be minimised. At the first generation (Figure 7.8(a)), the population is very diverse with representatives of high and low fitness and a range in between. After fifty generations (Figure 7.9 (a)) the population is much less diverse, made up of individuals of high, though not yet optimal, fitness. After 500 generations (Figure 7.10 (a)) the population has almost converged to a level of fitness higher than any individual in the first or 50^{th} generations.

This convergence is shown in another form in Figure 7.8(b), Figure 7.9(b) and Figure 7.10(b). Each point represents the location of a sensor/actuator pair for one of the individuals in a particular generation. In the first generation these locations are widely distributed, having been selected at random. After 50 generations they have begun to cluster in a few locations and after 500 generations the clustering is almost complete with all individual chromosomes coding for sensor/actuator pairs at the ten most effective sites, plus a few at less effective sites distributed around the plate. It can be

seen from Figure 7.10(b) that the optimal piezoelectric actuator locations are symmetrically distributed about the x-axis, which is the only axis of symmetry for the plate fixed along the left-hand edge.

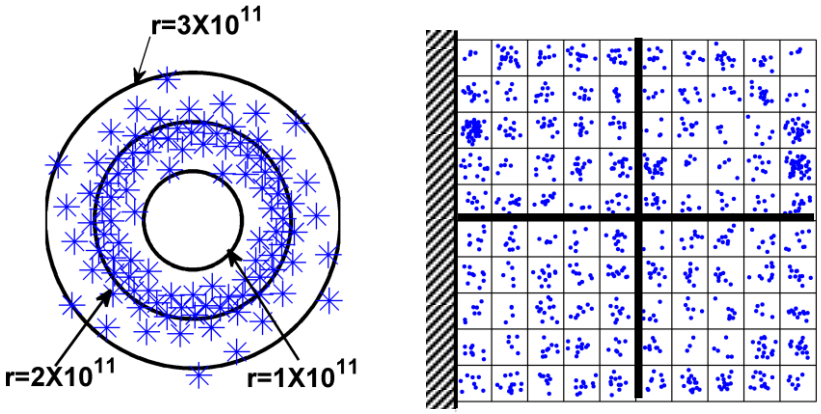

(a) Chromosomes fitness **(a) Genes distribution**

Figure 7.8 Distribution of one hundred chromosomes for the first random population of chromosomes and genes (actuators) on the stiffened cantilever plate surface, where **r** refers to circle radius which is the fitness value

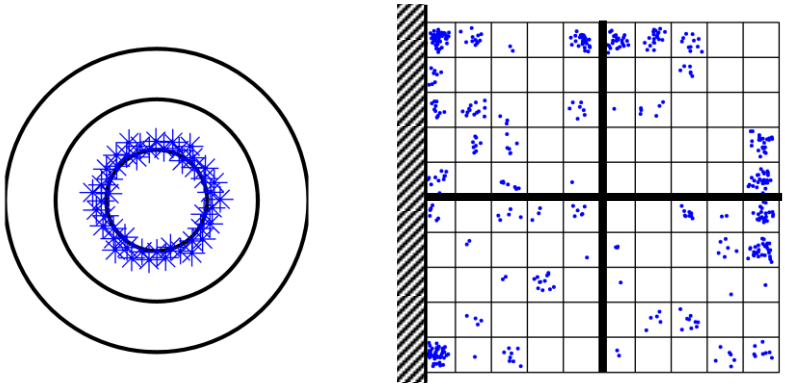

(a) Chromosomes fitness **(a) Genes distribution**

Figure 7.9 Progression in chromosomes fitness and locations of gene (actuators) after 50 generations on the stiffened cantilever plate surface

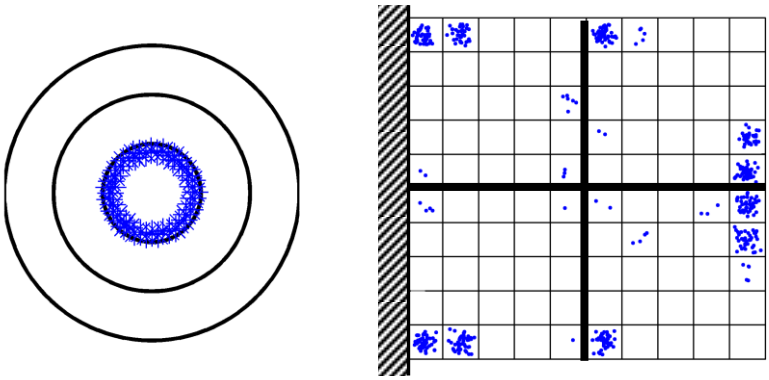

(a) Chromosomes fitness **(b) Genes distribution**

Figure 7.10 Progression of chromosomes fitness and locations of gene (actuators) after 500 generations on the stiffened cantilever plate surface

The same genetic algorithm program was run to optimise eight actuators for the flat cc-plate as shown in Figure 7.11. After 300 generations the clustering is almost complete with all individual chromosomes coding for sensor/actuator pairs at the eight most effective sites, plus a few at less effective sites distributed around the plate. It can be seen from Figure 7.11 that the optimal piezoelectric actuator locations are symmetrically distributed about the x-axis and y-axis, which are the axes of symmetry for the cc-plate.

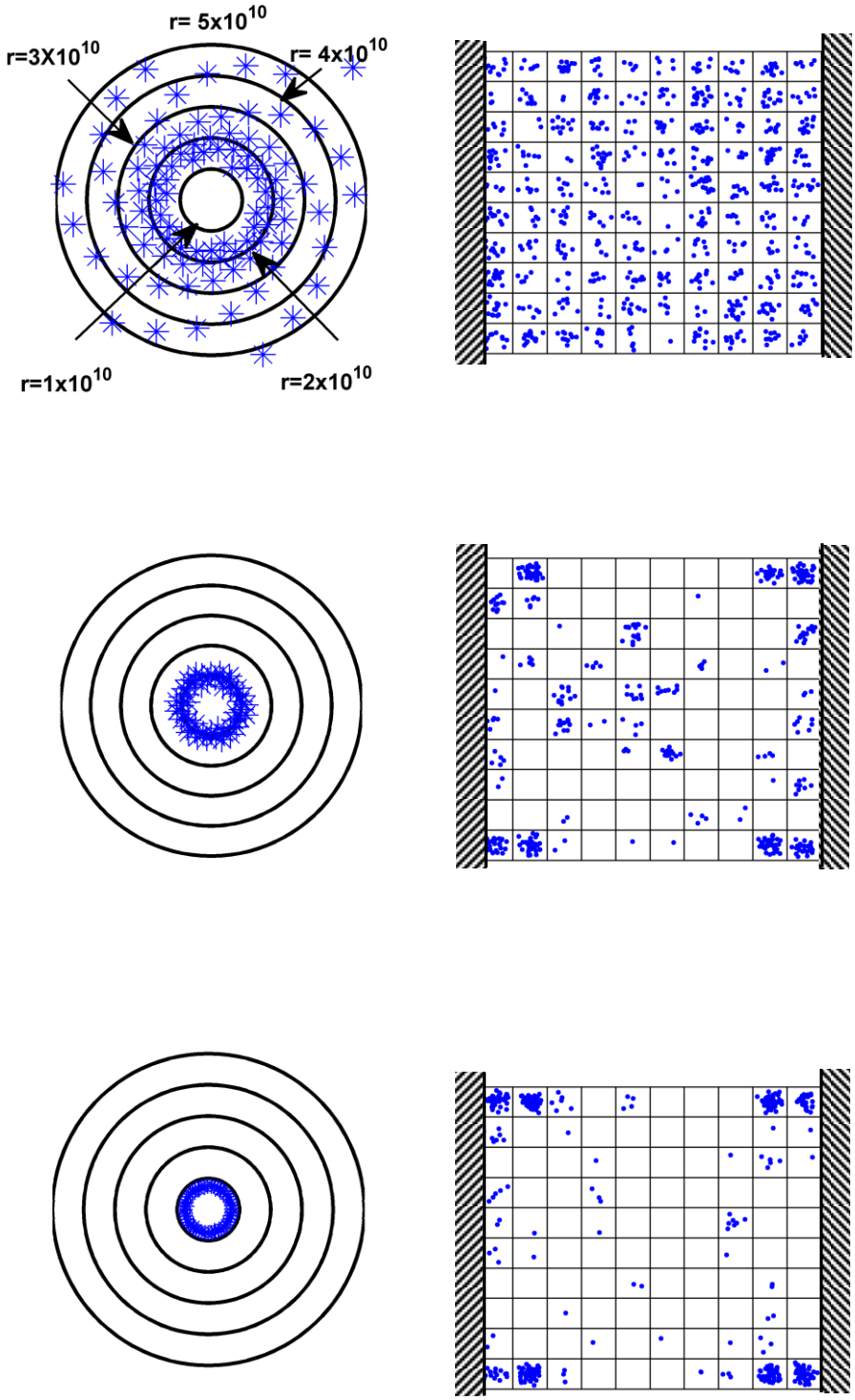

(a) Chromosomes fitness **(b) Genes distribution**

Figure 7.11 Progression of chromosomes fitness value and actuator distribution on the cc-plate for the first random population, and after 30 and 300 generations respectively

7.5. Optimal Piezoelectric Configurations for all Plates

The optimal locations for vibration reduction of sensor/actuator pairs for various symmetrical and asymmetrical plates as set out in section 7.4.3 are represented in Figure 7.12 and Figure 7.13. The distributions of the optimal sensor/actuator pairs for the plates which are symmetrical in geometry and boundary conditions are shown in Figure 7.12. The optimal configurations agree with the symmetrical distributions of mode shapes, modal strain and electric field distribution over the plates shown in section 7.4.2

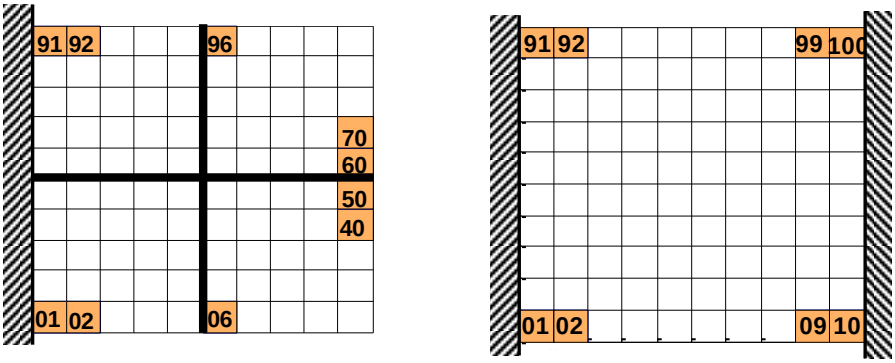

Figure 7.12 Global optimal sensor/actuator configurations for the cantilever plate stiffened by two beams in the cross type and the cc-plate

The same optimisation process described in section 7.4.3 was applied to optimise ten actuators for the plate stiffened by two beams in the T-type and the co-plate. The actuators started to cluster after 30 generations and after 500 generations there is a clear dominance of ten optimal locations. These optimal configurations are asymmetrically distributed about the plate's axes, as shown in Figure 7.13. The optimal configurations agree with the distribution of mode shape, modal strain and electric field distribution over the plates shown in section 7.4.2.

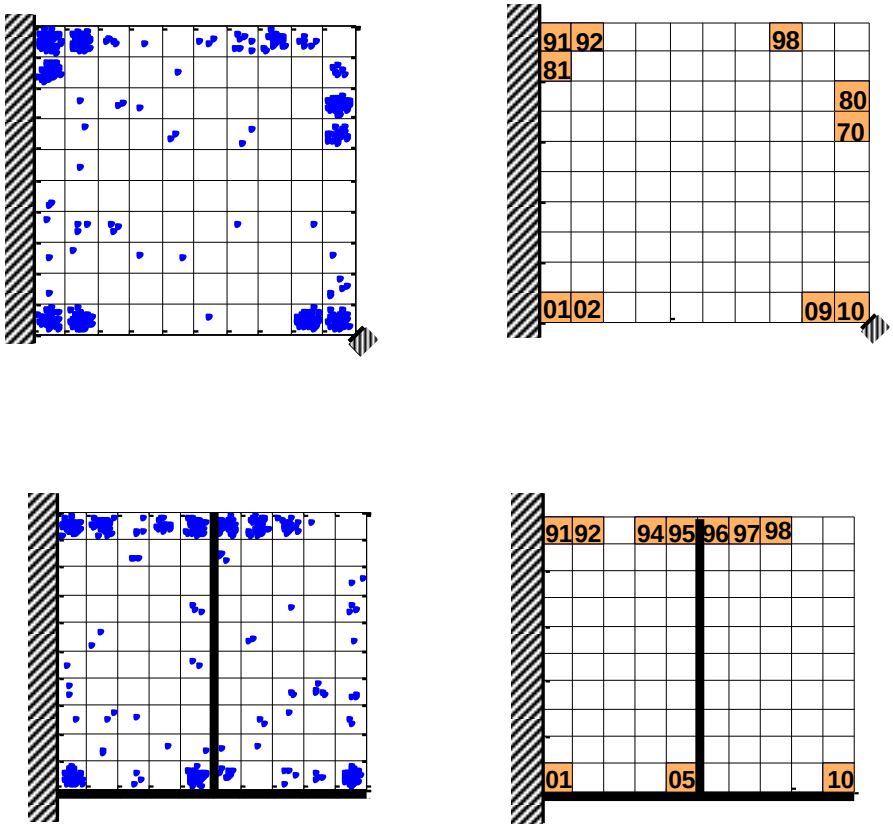

Figure 7.13 Optimal distribution of ten piezoelectric pairs on co-plate and stiffened plate by two beams T-type.

7.6. Validation of Location Optimisation

7.6.1. Validation by convergence

The genetic algorithm program was run multiple times to test the repeatability of the optimised sensor/actuator locations for the plates. The results are shown in Figure 7.14, which gives an indication of the progress of each of five runs by plotting the fitness value for the fittest member of the breeding population at each generation. It can be seen that the final fitness value is the same in each case, although the path by which it is reached is different for each run. This indicates that the process is robust in repeatedly finding the global optimal solution.

The search space of the stiffened plate is more complex than that of the cc-plate which gives the global optimal solution withn 150 to 350 generations while between 40 to 90 generations are needed for the cc-plate.

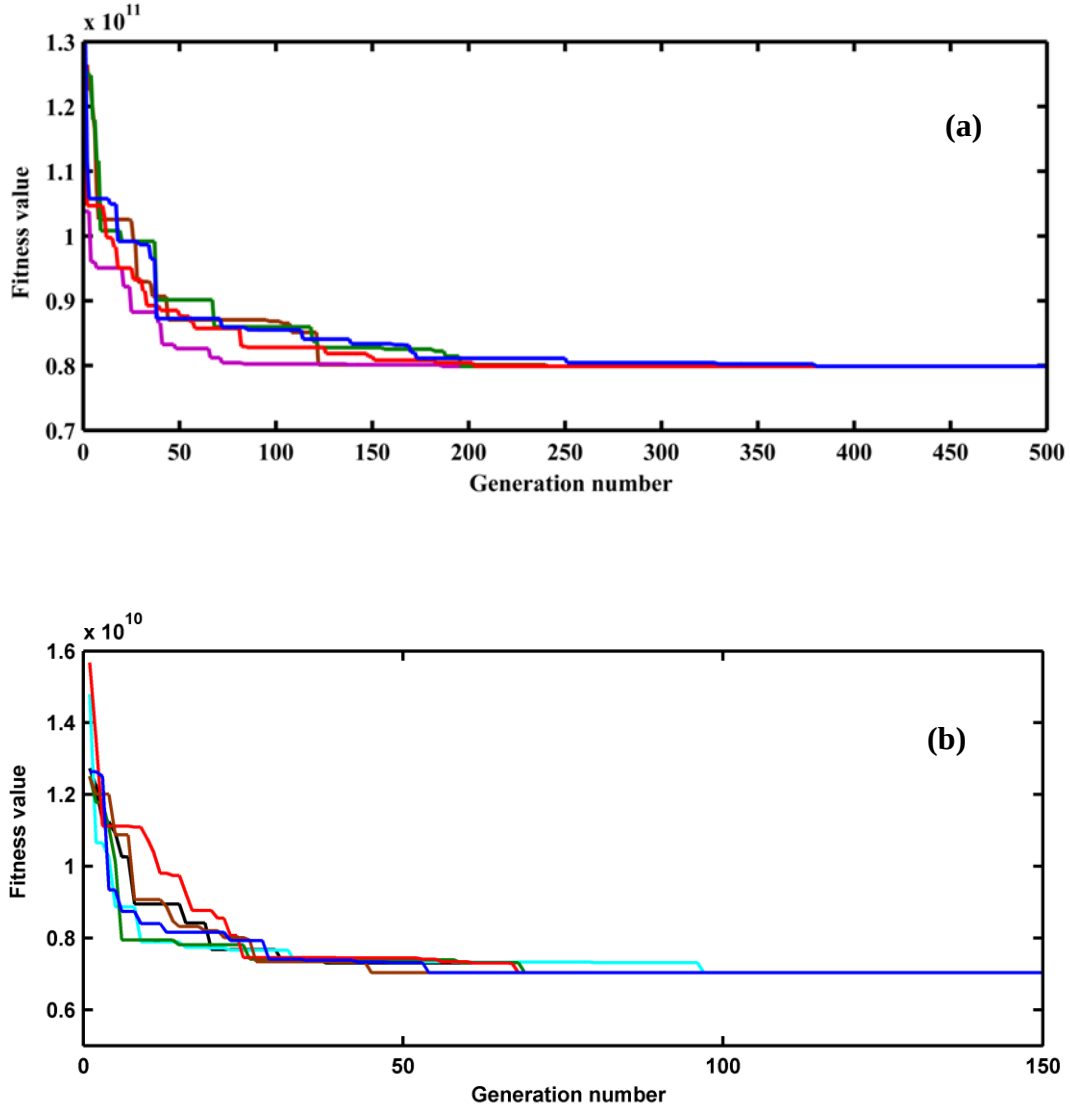

Figure 7.14 Fitness value for the best individual in each generation, repeated for five runs for (**a**) plate stiffened by two beams in the cross-type and (**b**) the cc-plate

7.6.2. Piezoelectric mass and stiffness effects

Adding piezoelectric sensor and actuator layers to the plate has the two passive effects of adding stiffness and adding mass. These will both affect the natural frequencies, tending to increase and reduce them respectively. This effect was represented in ANSYS using three dimensional solid45 elements for the main structure and solid5 elements for the piezoelectric pairs. Trials were conducted on the cross-type stiffened plate for three cases: no piezoelectric components; 100 sensor/actuator pairs, giving complete coverage of both surfaces of the plate; and 10 sensor/actuator pairs in the optimal locations. The configurations were tested and the results are shown in

Table 7.1. It may be seen that there is a small but significant effect, but no simple relationship between the added layers and changes in the natural frequencies of the various modes. These results are used in the analysis of vibration reduction for sensor/actuator pair configurations described in section 7.6.3.

Table 7.1 Piezoelectric mass and stiffness effects on natural frequencies

Solid45/solid5 elements	1^{st}	2^{nd}	3^{td}	4^{th}	5^{th}	6^{th}
Neglecting piezoelectric effects	16.6	25.4	57.8	71.0	125.1	133.3
100 s/a pairs cover whole plate	17.6	22.3	62.5	73.5	114.0	142.3
10 s/a pairs in optimal location	17.1	25.1	59.7	73.6	122.0	135.7

7.6.3. Open and closed loop time responses: first test

The open and closed loop time responses of the cross-type stiffened plate bonded with ten sensor/actuator pairs in optimal locations were tested in the ANSYS finite element package. An ANSYS APDL program was built to implement the proportional differential control scheme for the stiffened plate and sensor/actuator pairs, as shown in Figure 7.15. The stiffened plate is driven by a sinusoidal voltage of $30 \times \sin(\omega t)$ applied at actuator location 91 on the stiffened plate in order to test vibration suppression at the first mode and at actuator location 70 on the stiffened plate in order to test vibration attenuation at the third and fifth modes.

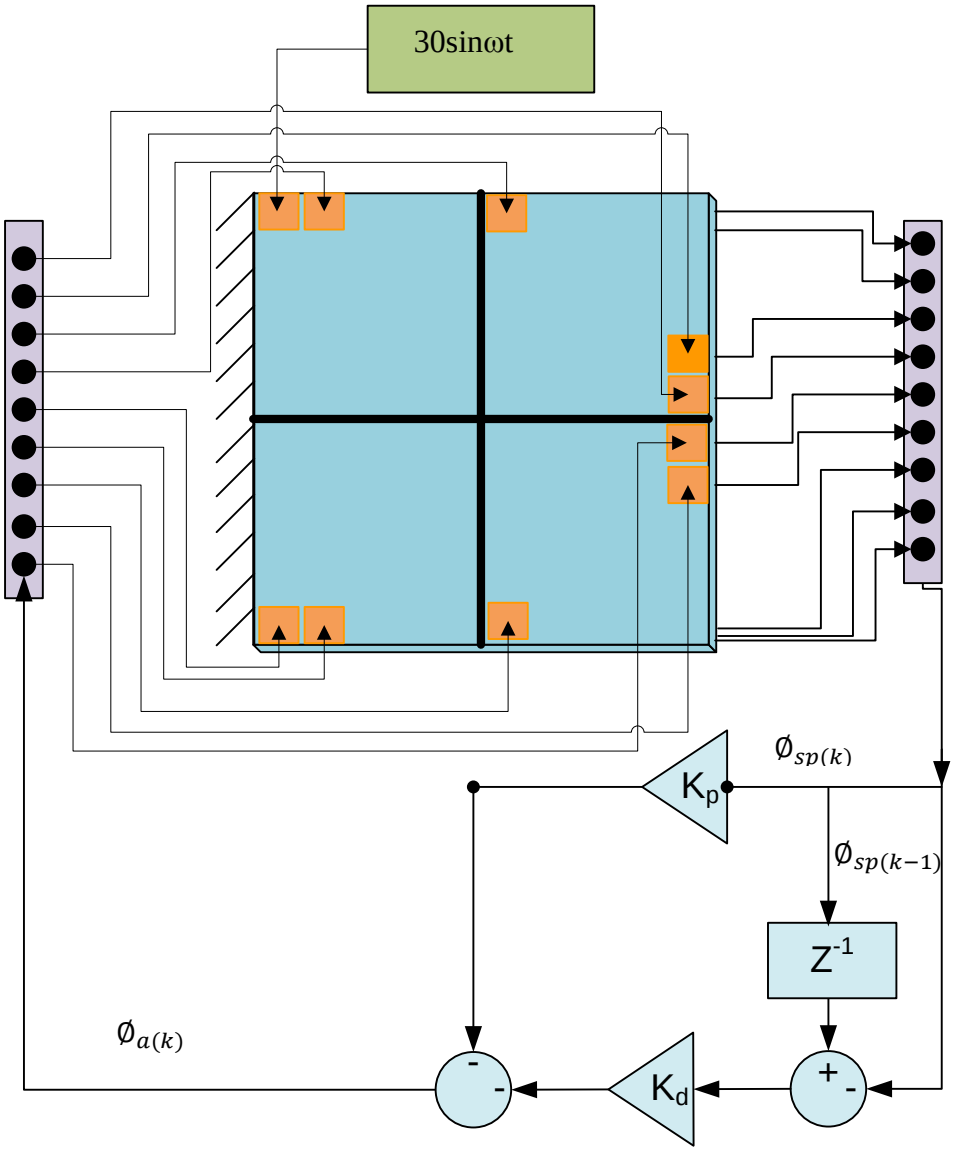

Figure 7.15 Plate stiffened by two beams in the cross type bonded to ten sensor/actuator pairs in optimal locations connected to PD control scheme and represented in the ANSYS package using the APDL program

Figure 7.16 (a1, a2, a3, a4, a5, a6, a7 and a8) shows the open and closed loop voltage and acceleration time responses at the first mode for the sensor/actuator pairs at locations 01, 02, 06, 40 and 50 at the lower part of the stiffened plate. The open and closed loop acceleration time responses were investigated at a finite element node located at the top centre of each sensor. The stiffened plate was driven by a sinusoidal voltage of $30 \times \sin(\omega_1 t)$ to the actuator by location 91 on the plate.

Figure 7.16 (a1, a2 and a3) shows the open and closed loop sensors voltage responses. The average closed loop sensor voltage responses were reduced by 52.4% and the reduction increased to 61.3% as the feedback gain increased.

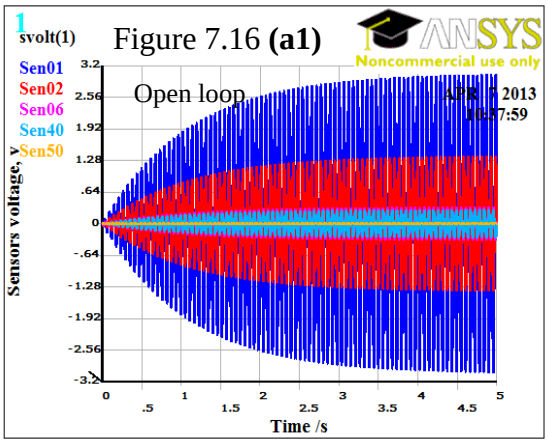

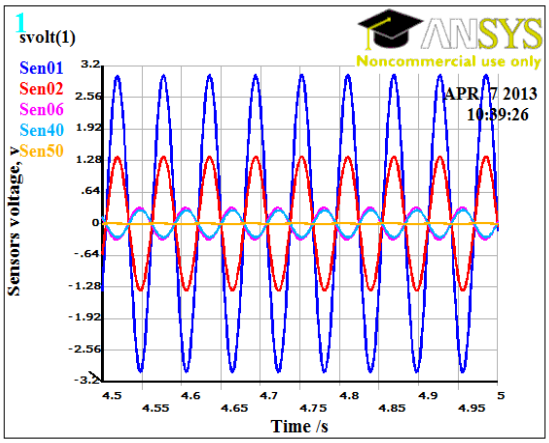

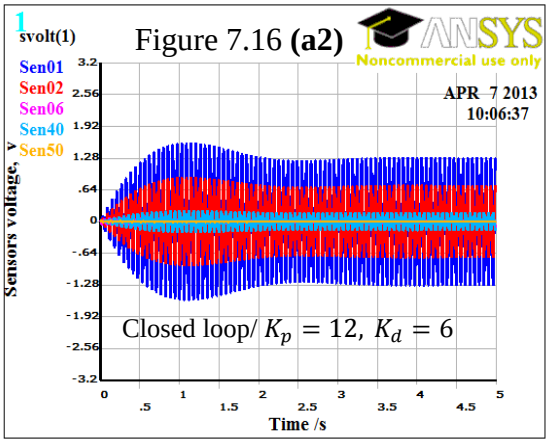

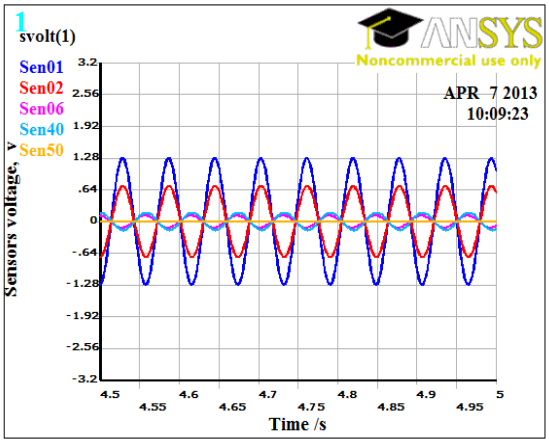

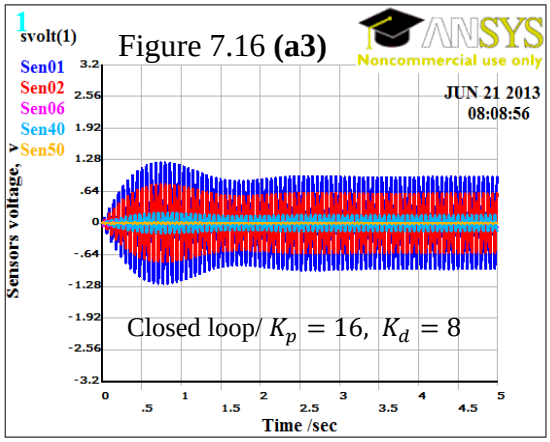

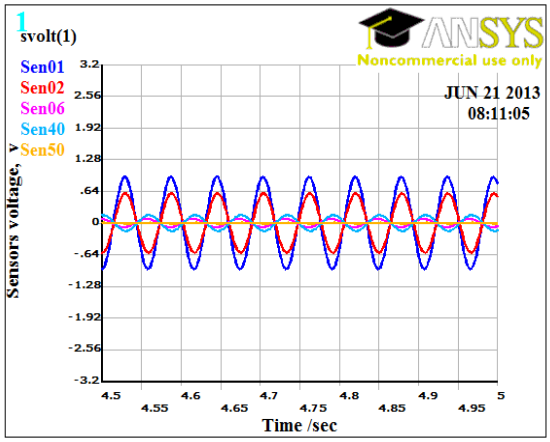

Figure 7.16 (a4, a5 and a6) shows the open and closed loop sensor tip acceleration time responses. The closed loop sensor tip acceleration responses were reduced by 64.97% and the reduction increased to 77.14% as the feedback gain increased.

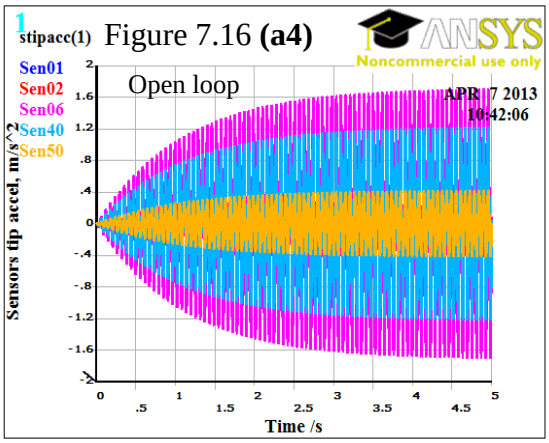

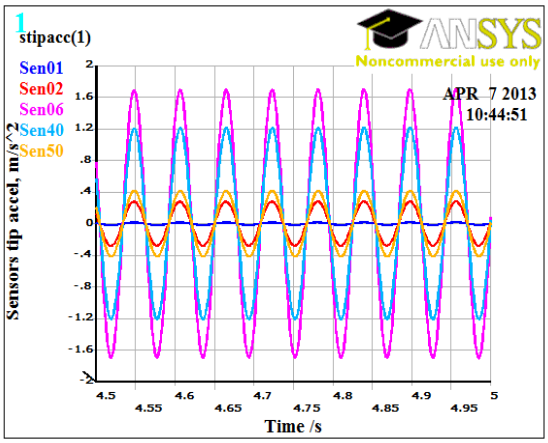

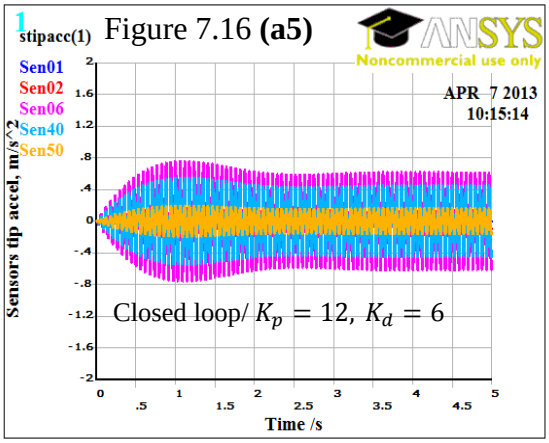

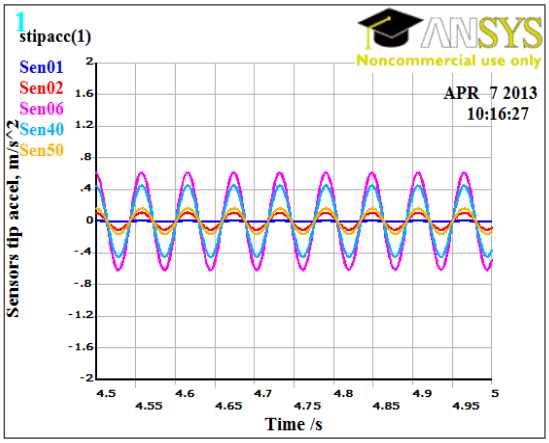

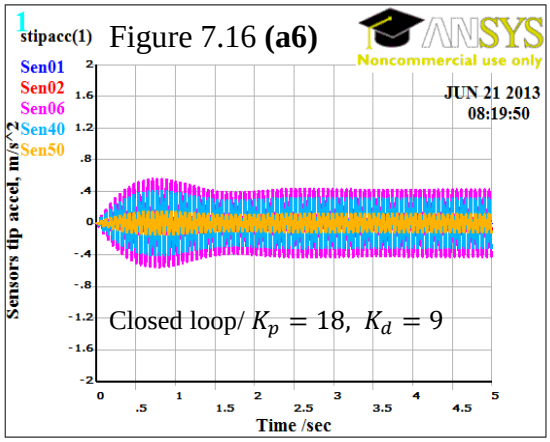

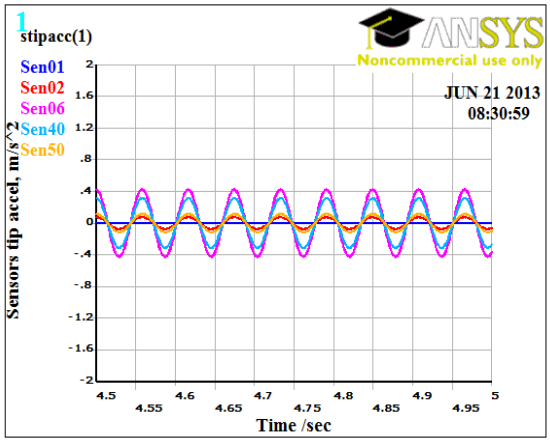

Figure 7.16 (a7 and a8) shows the closed loop actuator feedback voltage time responses. The summation of feedback voltage for the five actuators on the lower part of the plate was 27.4V which slightly increased to 28.4V as the feedback gain increased. The increase in the feedback gain at the first mode gives percentage improvement of 18.7% in the average vibration reduction with little percentage increased in feedback voltage of 3.6%.

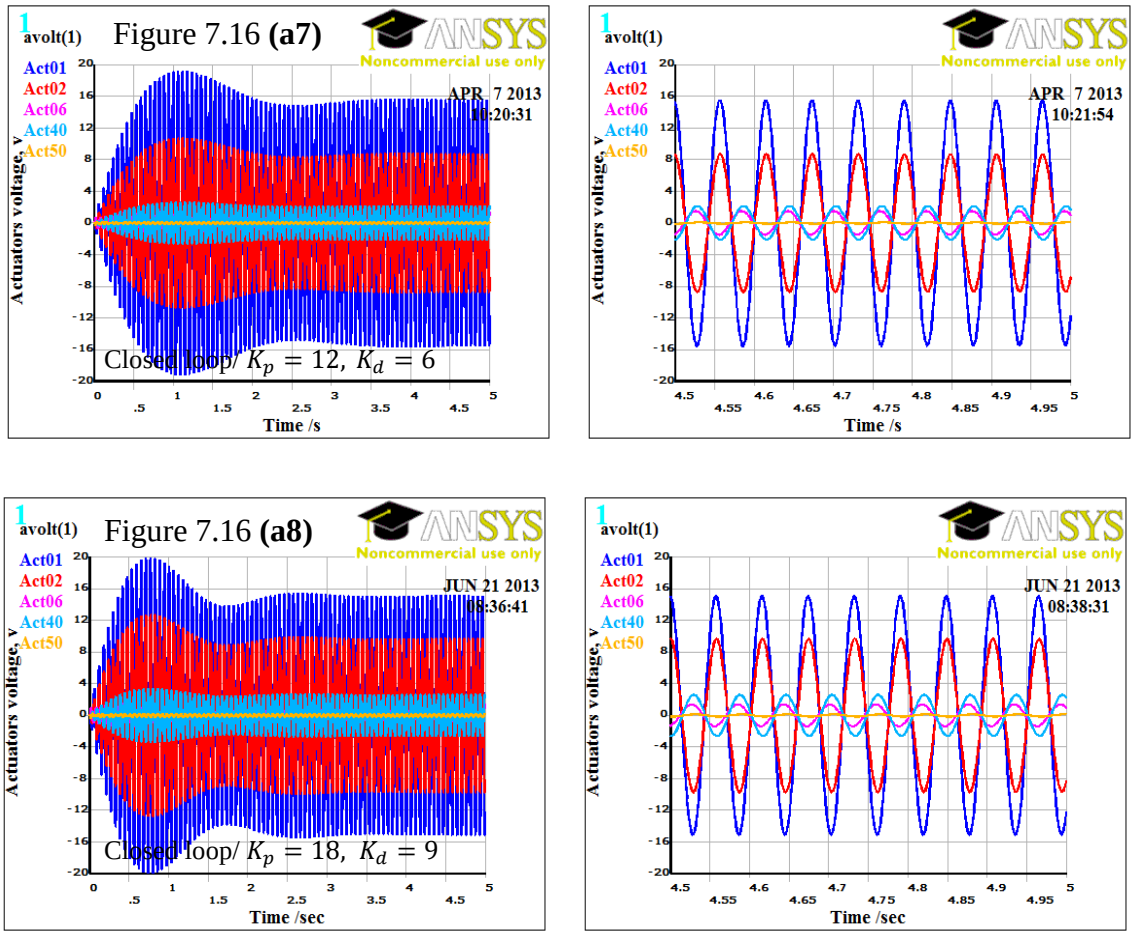

Figure 7.16 Open and closed loop time responses at the first mode for the sensor/actuator pairs at locations 01,02,06,40 and 50 on the lower part of the stiffened plate in the cross type. The plate was driven by sinusoidal voltage at actuator location 91 and the vibration reduced using the PD control scheme and the APDL program in the ANSYS package

Figure 7.17 (a1, a2, a3, a4 and a5) shows the open and closed loop time responses of voltage and sensor tip acceleration in the third mode as a result of applying a sinusoidal voltage of $30 \times \sin(\omega_3 t)$ to the actuator at location 70 on the plate. Figure 7.17 (a1, a2 and a3) shows the open and closed loop sensor and actuator voltage responses. The average closed loop sensor voltage responses were reduced by 78.13% and the summation of feedback voltage for the five actuators on the lower part of the plate was 3.182V as shown in Figure 7.17 (**a3**).

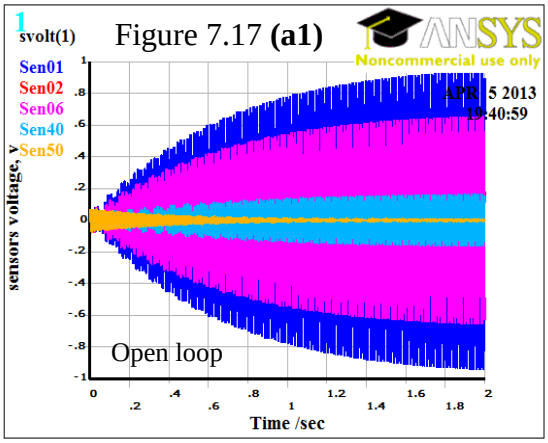

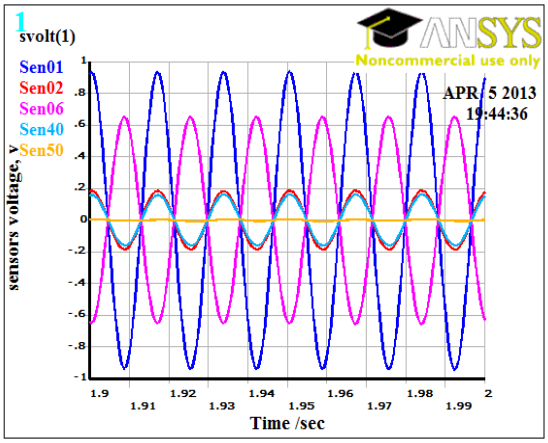

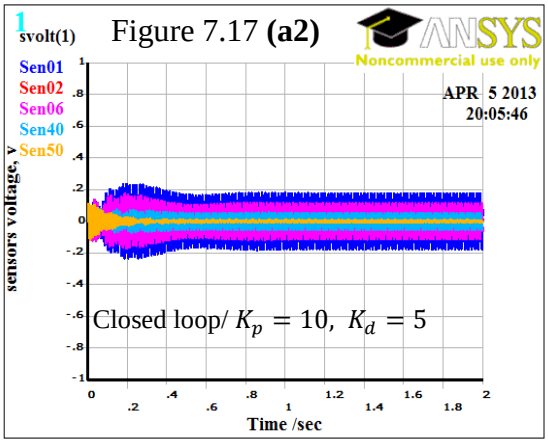

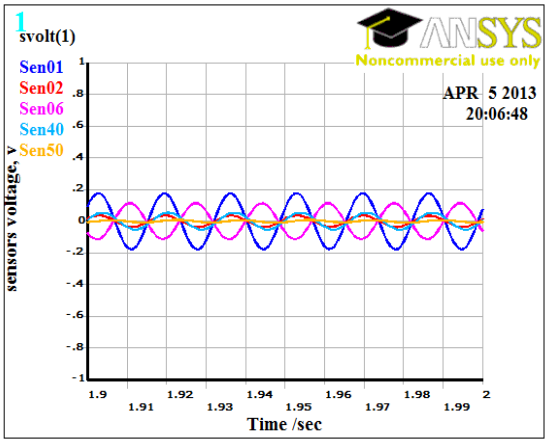

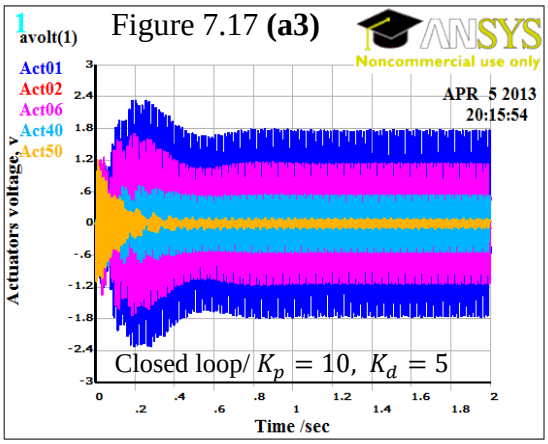

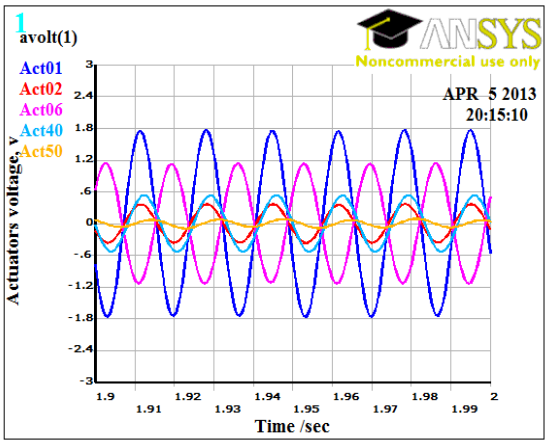

The actuator feedback voltage is low compared to that in the first and fifth mode, because the plate was driven by the actuator at location 70 on the plate, and this actuator and its pair was used for driving, sensing and actuating. However, in the tests at the first and fifth modes, the plate was driven by the actuator at location 91, and this actuator and its pair was used only to drive the plate.

Figure 7.17 (a4 and a5) shows the open and closed loop sensor tip acceleration time responses. The average closed loop sensors tip acceleration responses were reduced by 80.2%.

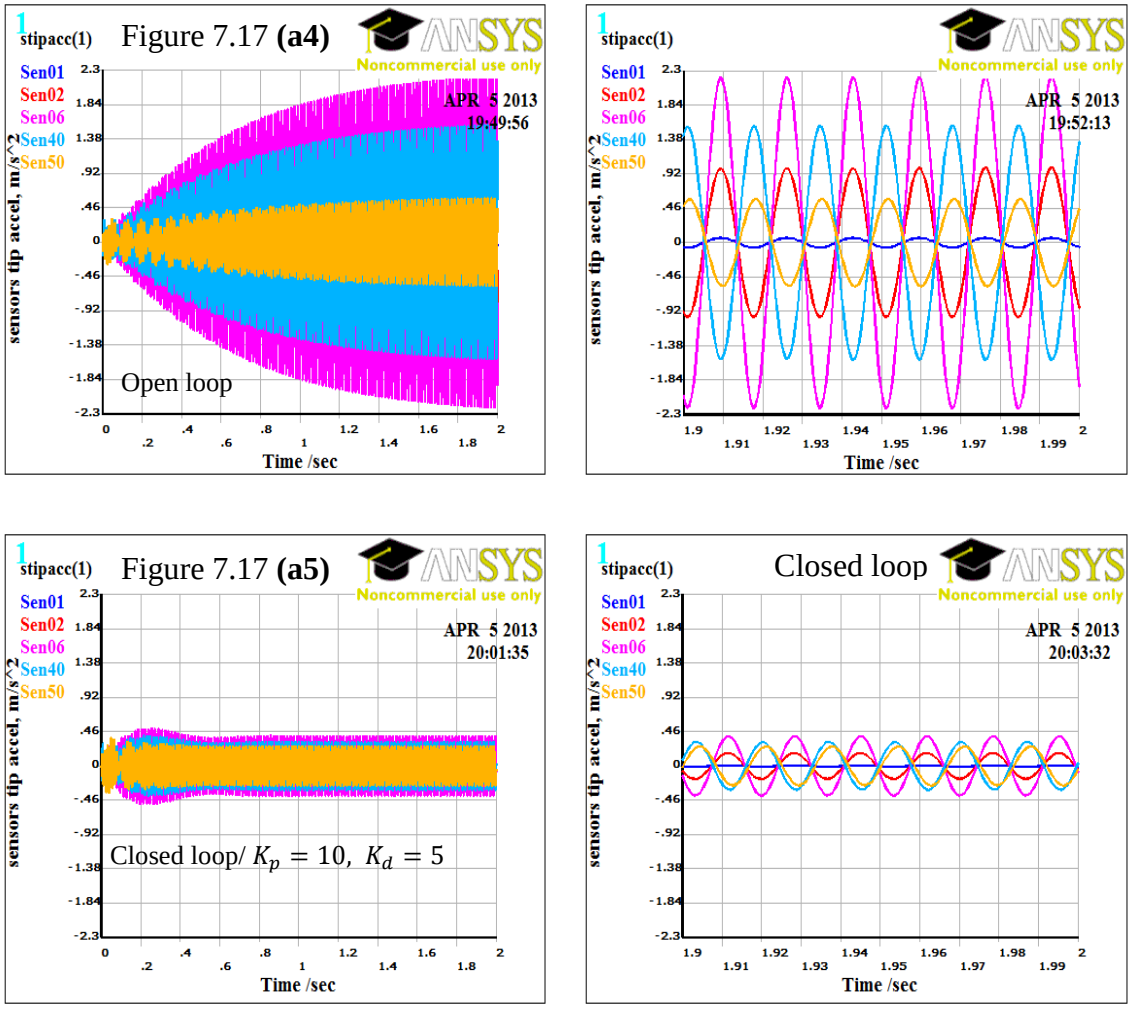

Figure 7.17 Open and closed loop time responses at the third mode for the sensor/actuator pairs at locations 01,02,06,40 and 50 for the lower part of the stiffened plate in the cross type. The plate was driven by a sinusoidal voltage at actuator location 70 using the PD control scheme and the APDL program in the ANSYS package

Figure 7.18 (a1, a2, a3, a4 and a5) shows the open and closed loop time responses of the sensor and actuator voltage and sensor tip acceleration at locations 01, 02, 06, 40 and 50 at the fifth mode, as a result of applying a sinusoidal voltage of $30 \times \sin(\omega_5 t)$ to the actuator at location 70 on the stiffened plate.

Figure 7.18 (a1 and a2) shows the open and closed loop sensor voltage responses. The average closed loop sensors voltage responses were reduced by 66.63% .

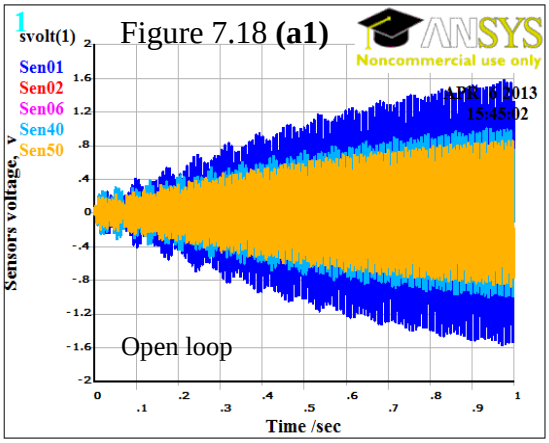

Figure 7.18 **(a1)**

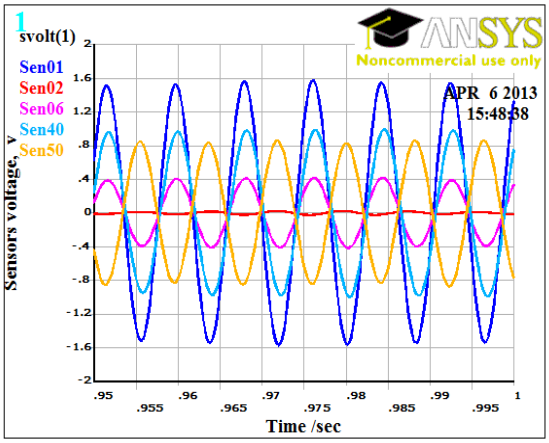

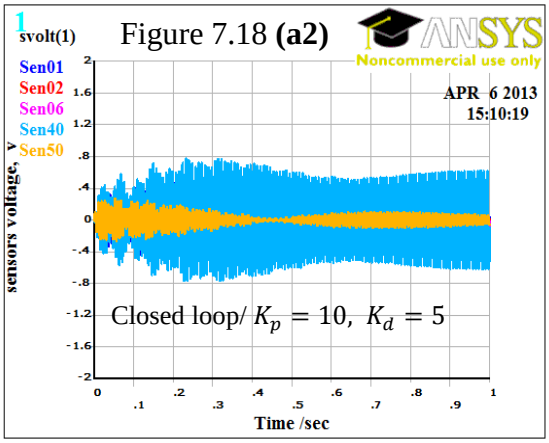

Figure 7.18 **(a2)**

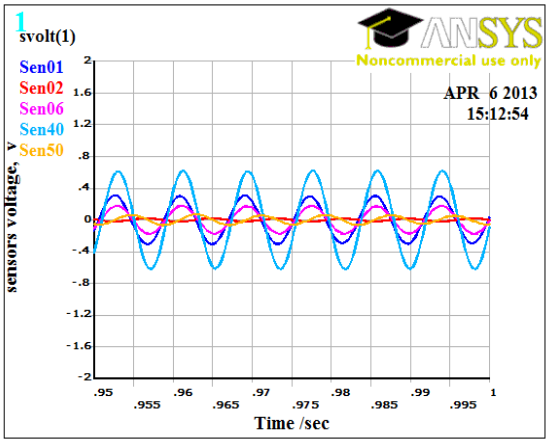

Figure 7.18 (**a3, a4** and **a5**) shows the open and closed loop sensor tip acceleration and actuator feedback voltage responses. The average sensor tip acceleration responses were reduced by 78% and the collective feedback voltage for the five actuators on the lower part of the plate was 11.75V.

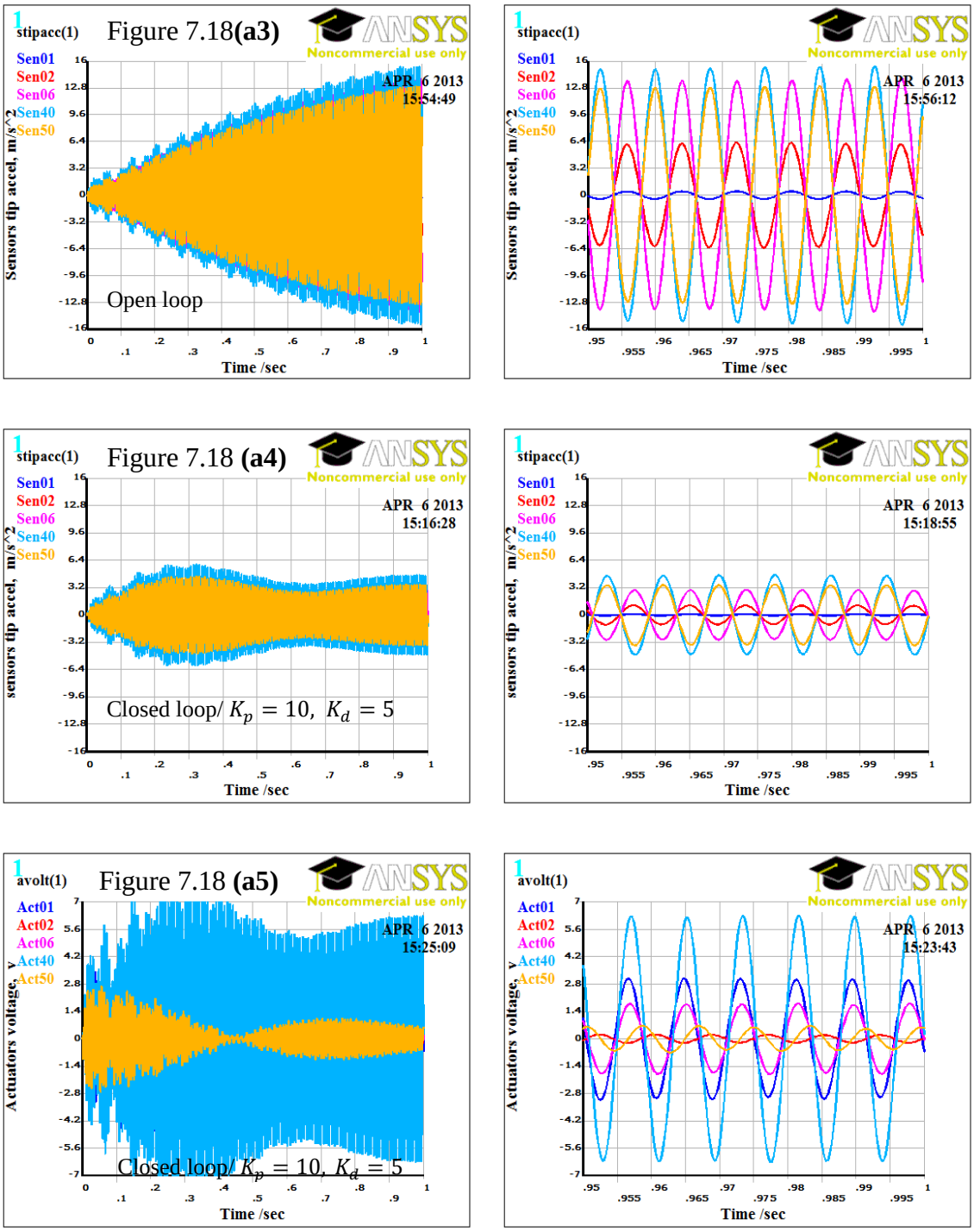

Figure 7.18 Open and closed loop time responses at the fifth mode for the sensor/actuator pairs at locations 01,02,06,40 and 50 for the lower part of the cross-type stiffened plate. The plate was driven by a sinusoidal voltage at actuator location 70 using the PD control scheme and the APDL program in the ANSYS package, P=10, D=5

7.6.4. Open and closed loop time responses: second test

The effectiveness of the optimal sensor/actuator locations was investigated for the cross-type cantilever stiffened plate. The open and closed loop time responses at the first and third modes were determined using two separate sensor/actuator configurations: the optimal configuration of ten sensor/actuator pairs as shown in Figure 7.19(a), and "full coverage" with a single sensor/actuator pair covering the whole surfaces of the stiffened plate as shown in Figure 7.19(b). The plates are actuated with an out of plane sinusoidal concentrated force of constant amplitude at the free-end plate corner, and the responses are measured at the location of maximum amplitude at the other side of the free-end plate corner, as shown in Figure 7.19. The plates were connected to the proportional differential control scheme and represented in the ANSYS package using the APDL program according to section 7.6.3 (Figure 7.15).

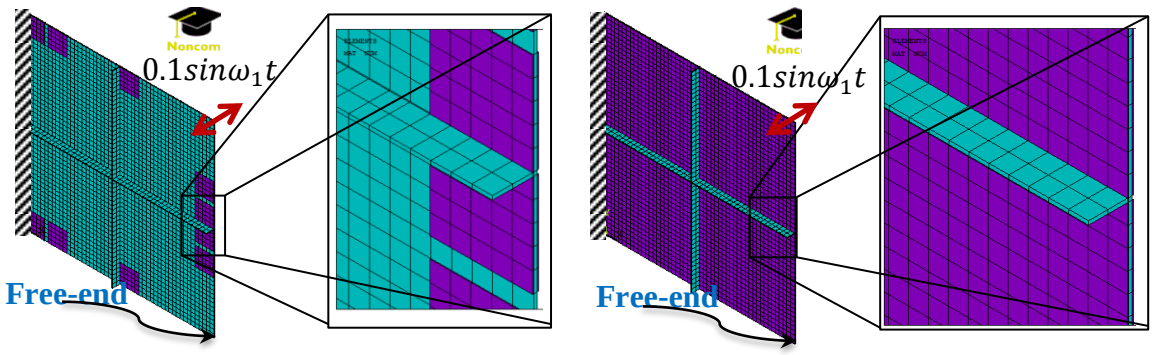

Figure 7.19 (**a**) Cantilever stiffened plate cross-type bonded with ten discrete sensor/actuator pairs in the optimal locations, and (**b**) single sensor/actuator cover whole the stiffened plate

The results of the open and closed loop time responses at the first mode are shown in Figure 7.20 (a and b) for the two configurations. Figure 7.20 (a1, a2, a3, a4, and a5) shows the open and closed loop time responses for the first case bonded with ten pairs in the optimal locations. The open loop maximum vibration amplitude for the full coverage stiffened plate was lower than that for the first case as shown in Figure 7.20 (b2) and Figure 7.20 (a2) respectively. This is because the piezoelectric sensor and actuator layers increased the stiffness and structural damping of the stiffened plate.

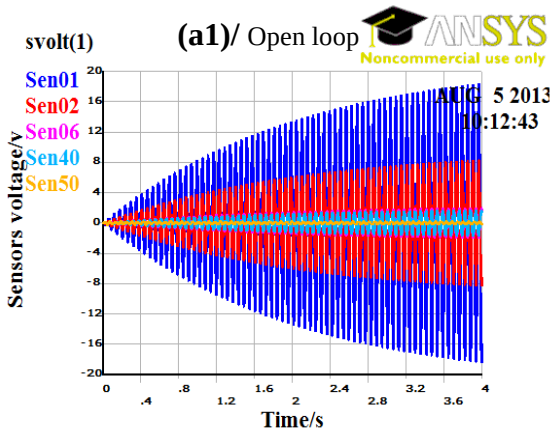
svolt(1)
(a1)/ Open loop
Noncommercial use only
Sen01
Sen02
Sen06
Sen40
Sen50
AUG 5 2013
11:12:43
Sensors voltage/v
Time/s

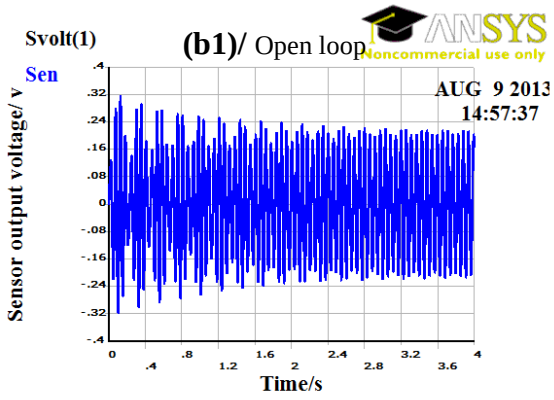
Svolt(1)
(b1)/ Open loop
Noncommercial use only
Sen
AUG 9 2013
14:57:37
Sensor output voltage/ v
Time/s

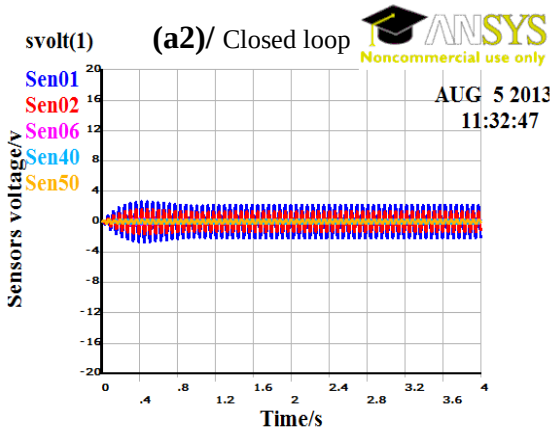
svolt(1)
(a2)/ Closed loop
Noncommercial use only
Sen01
Sen02
Sen06
Sen40
Sen50
AUG 5 2013
11:32:47
Sensors voltage/v
Time/s

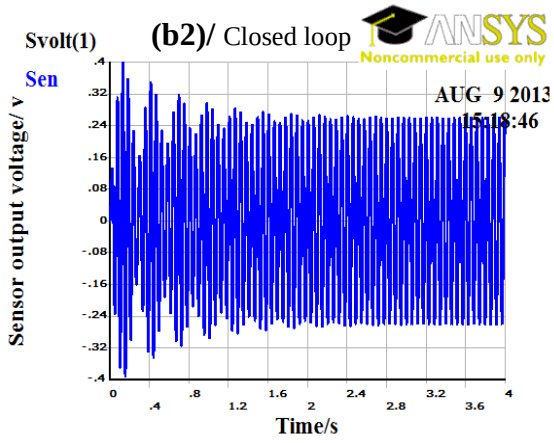
Svolt(1)
(b2)/ Closed loop
Noncommercial use only
Sen
AUG 9 2013
15:18:46
Sensor output voltage/ v
Time/s

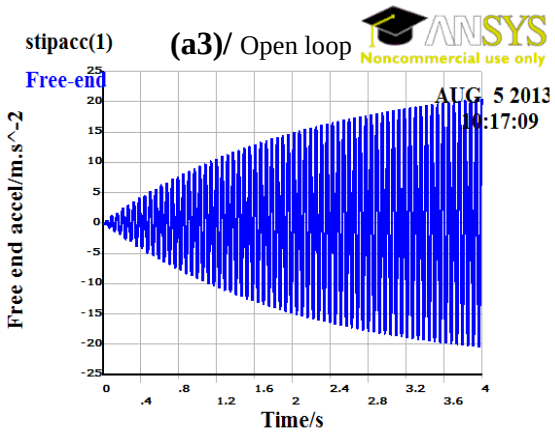
stipacc(1)
(a3)/ Open loop
Noncommercial use only
Free-end
AUG 5 2013
11:17:09
Free end accel/m.s^-2
Time/s

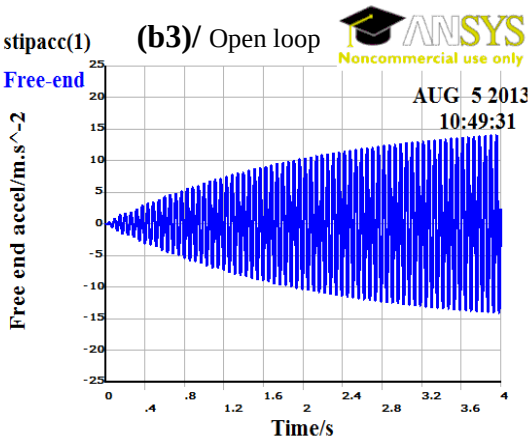
stipacc(1)
(b3)/ Open loop
Noncommercial use only
Free-end
AUG 5 2013
10:49:31
Free end accel/m.s^-2
Time/s

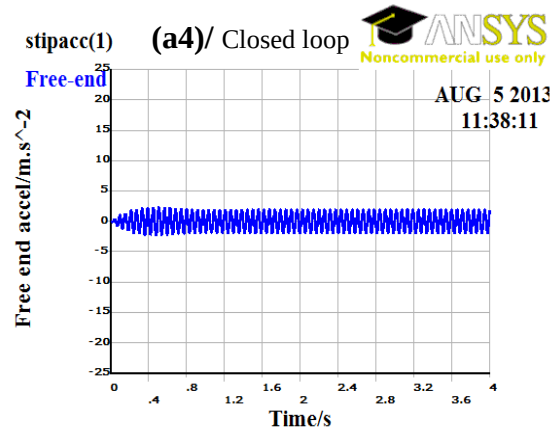
stipacc(1)
(a4)/ Closed loop
Noncommercial use only
Free-end
AUG 5 2013
11:38:11
Free end accel/m.s^-2
Time/s

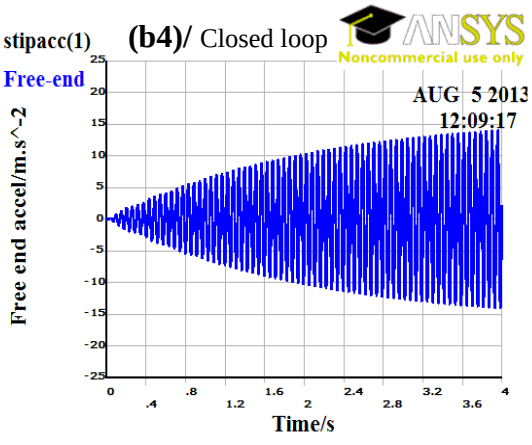
stipacc(1)
(b4)/ Closed loop
Noncommercial use only
Free-end
AUG 5 2013
12:09:17
Free end accel/m.s^-2
Time/s

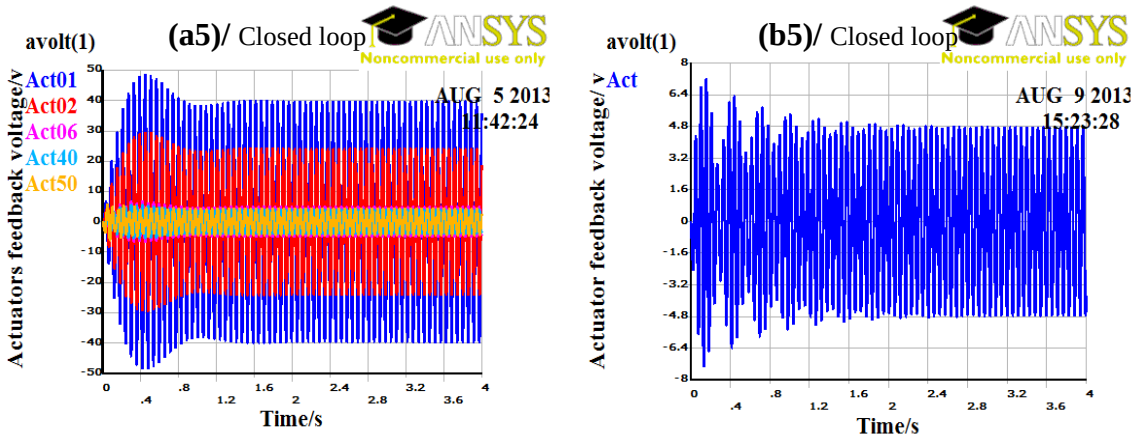

Figure 7.20 Open and closed loop time responses at the first mode for the cantilever stiffened plate cross-type bonded with (**a**),ten sensor/actuator pairs in the optimal locations and (**b**),single pair cover whole the stiffened plate, respectively using feedback gain $K_p = 18,\ K_d = 9$

The closed loop sensor voltage and free-end plate amplitude was reduced by 90% with total actuator feedback voltage of 160V as shown in Figure 7.20(a1, a2, a3, a4 and a5), no reduction was obtained in the second full coverage case, as shown in Figure 7.20 (b1, b2, b3, b4, and b5). It was shown that the extra increase in feedback gain led to unstable responses, as shown in Figure 7.20 (b2), where the maximum closed loop sensor voltage at steady state is larger than that for the open loop shown in Figure 7.20 (b1).

The results of the open and closed loop time responses at the third mode are shown in Figure 7.21 (a and b) for the two piezoelectric configurations. The closed loop sensor voltage and free-end amplitude responses were also reduced by 90% with a total feedback voltage 70V for the first case, as shown in Figure 7.21(a1, a2, a3, a4 and a5) and no reduction at the second full coverage case as shown in Figure 7.21(b1, b2, b3, b4 and b5). Unstable closed loop responses were shown at gain values $K_p = 18,\ K_d = 9,$ and then the gain was reduced to $K_p = 12,\ K_d = 6$ during the test of full coverage case. In the full coverage test, no detection of vibration or actuation was found.

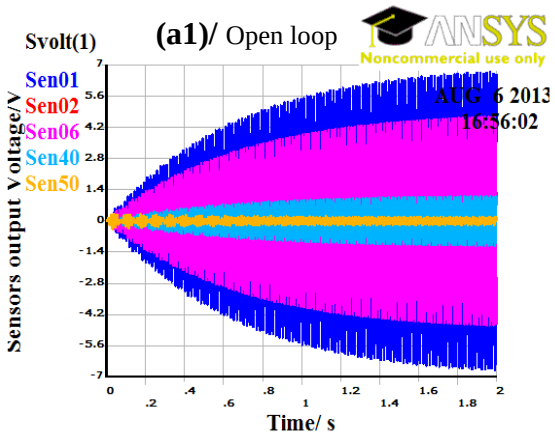
Svolt(1)
(a1)/ Open loop
Noncommercial use only
Sen01
Sen02
Sen06
Sen40
Sen50
AUG 6 2013
16:56:02
Sensors output voltage/V
Time/ s

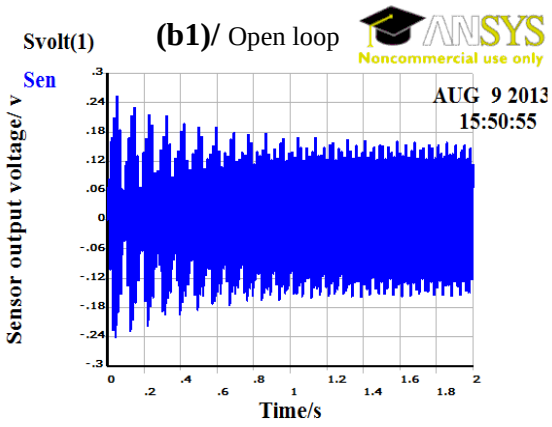
Svolt(1)
(b1)/ Open loop
Noncommercial use only
Sen
AUG 9 2013
15:50:55
Sensor output voltage/ v
Time/s

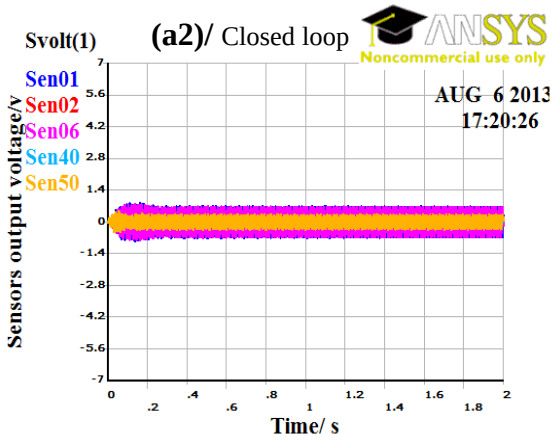
Svolt(1)
(a2)/ Closed loop
Noncommercial use only
Sen01
Sen02
Sen06
Sen40
Sen50
AUG 6 2013
17:20:26
Sensors output voltage/v
Time/ s

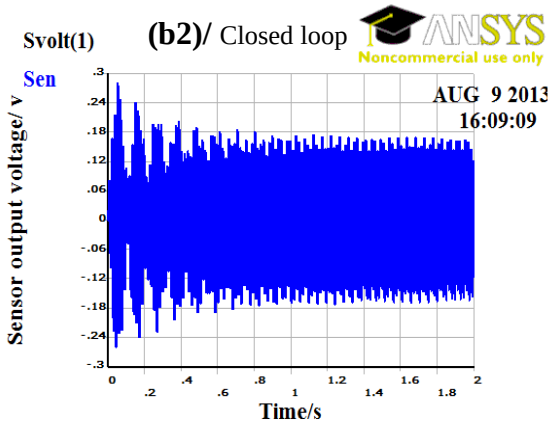
Svolt(1)
(b2)/ Closed loop
Noncommercial use only
Sen
AUG 9 2013
16:09:09
Sensor output voltage/ v
Time/s

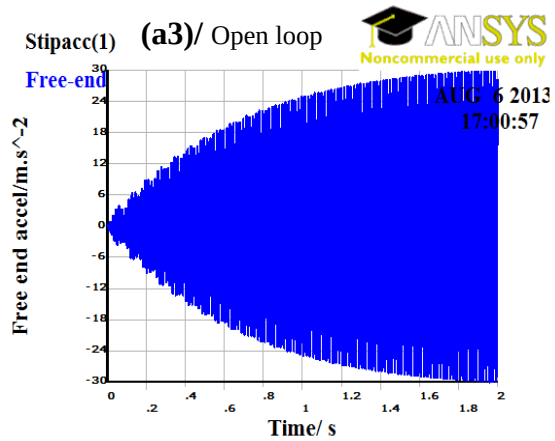
Stipacc(1)
(a3)/ Open loop
Noncommercial use only
Free-end
AUG 6 2013
17:00:57
Free end accel/m.s^-2
Time/ s

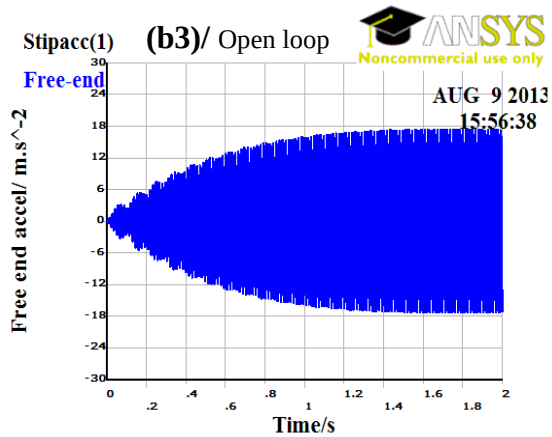
Stipacc(1)
(b3)/ Open loop
Noncommercial use only
Free-end
AUG 9 2013
15:56:38
Free end accel/ m.s^-2
Time/s

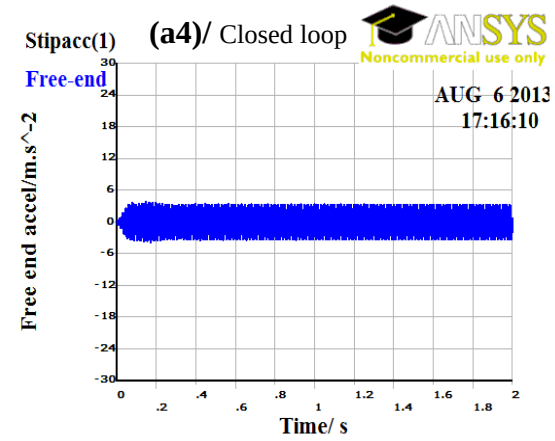
Stipacc(1)
(a4)/ Closed loop
Noncommercial use only
Free-end
AUG 6 2013
17:16:10
Free end accel/m.s^-2
Time/ s

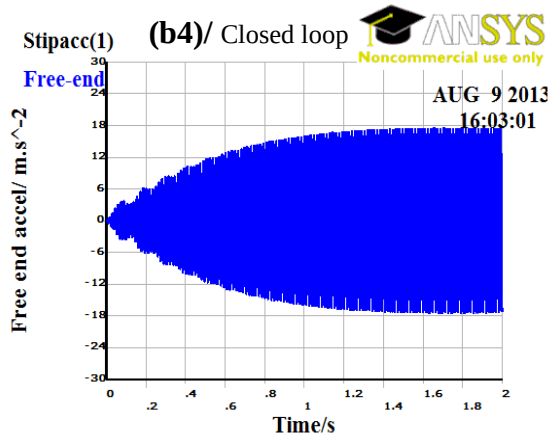
Stipacc(1)
(b4)/ Closed loop
Noncommercial use only
Free-end
AUG 9 2013
16:03:01
Free end accel/ m.s^-2
Time/s

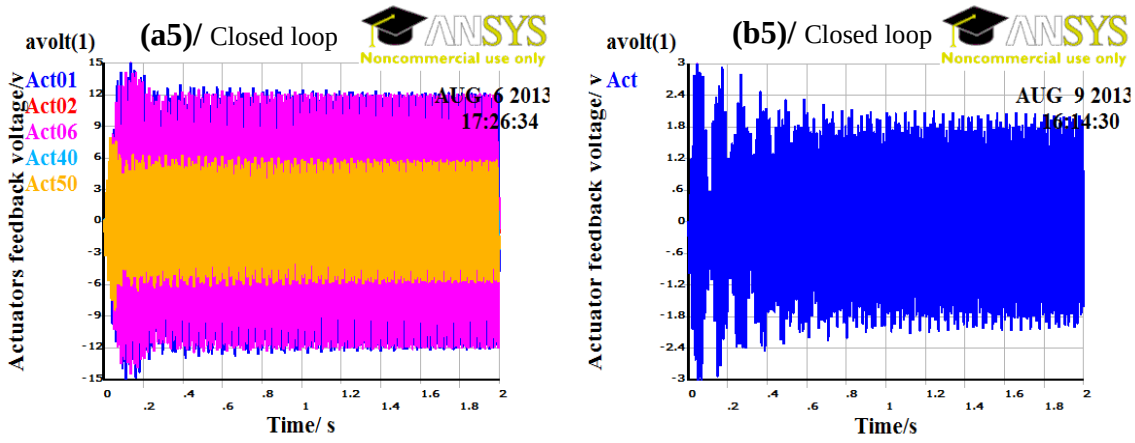

Figure 7.21 Open and closed loop time responses at the third mode for the cantilever stiffened plate cross-type bonded with (**a**),ten sensor/actuator pairs in the optimal locations feedback gain $K_p = 18,\ K_d = 9$ and (**b**),single pair cover whole the stiffened plate, respectively using feedback gain $K_p = 12,\ K_d = 6$

The results of the large vibration reduction obtained for the case of the optimal distribution of ten piezoelectric pairs proved the effectiveness and correctness of the placement strategy and the global optimal configurations of sensor/actuator pairs. However, the results of no vibration reduction obtained for the full coverage piezoelectric case agreed with and validated the correctness of the newly developed analysis represented by the modal electric field distribution over the piezoelectric surface as explained in sections 5.6.3 and 7.4.2.

7.7. Conclusions

Isotropic plates with different symmetrical and asymmetrical boundary conditions and stiffening geometries are investigated to find the optimal configuration of eight and ten piezoelectric sensor/actuator pairs using the genetic algorithm. APDL programs were built for all types of plates and executed in the ANSYS finite element package. It was found that the first six mode shapes, modal strain and electric charge were distributed according to the same symmetry (if any) of the plates.

A genetic algorithm program was written in MATLAB m-code in order to optimise the locations of actuators based on the minimisation of the linear quadratic index as an objective function and taking the effects of the first six modes collectively. The optimal configuration of sensors and actuators was shown to be symmetrically distributed about the axes of symmetry of symmetrical plates, and to be asymmetrical for asymmetrical plates. The solutions obtained were tested for robustness by running the program

repeatedly. It was found that the same optimal locations were obtained in every case, despite following different evolutionary paths. The symmetrical global distribution of sensors and actuators for structures symmetrical in geometry and boundary conditions as determined in chapters five, six and seven had a strong effect in reducing the genetic algorithm search problem and guaranteed the global optimal solution within fewer generations, and this effect is investigated in the next chapter.

The reliability and correctness of the optimal configuration of sensor/actuator pairs for the cross-type stiffened plate was tested in the ANSYS package using the APDL program and implementing a proportional differential control scheme. The stiffened plate was driven by a sinusoidal voltage at actuator locations 91 and 71 . The average closed loop steady state time response were reduced by 77.14%, 78% and 80.27% at the first, third and fifth modes respectively.

A comparison study was conducted for two separate sensor/actuator configurations: the cross-type cantilever stiffened plate with ten sensor/actuator pairs bonded in the optimal locations; and a single sensor/actuator pair covering the whole surface of the stiffened plate. The closed loop time responses for the sensor voltage and free-end plate amplitude were reduced by 90% for the first case at the first and third modes, and no reduction was found for the full coverage case under same feedback gain values. Unstable closed loop time responses were shown at higher values of feedback gain for the full coverage case.

The closed loop time responses of zero reduction for the full coverage case were found to be in agreement with the newly developed analysis represented by the modal electric field distribution over the piezoelectric surface explained in sections 5.6.3 and 7.4.2.

Chapter 8. Genetic Algorithm Problem Reduction

The determination of the optimal placement of sensors and actuators for active vibration control is limited by the number of candidates in the search space. The search space to optimise the location of ten actuators for a small structure discretized to one-hundred elements gives 1.73×10^{13} possible solutions, only one of which is the global optimum.

In this chapter, a new half- and quarter-chromosome technique is developed based on the findings reported in chapters five, six and seven that the global optimal distribution of sensors and actuators is symmetrical about the axes of symmetry for structures which are symmetrical in geometry and fixation. This technique based on symmetry is developed so that the search space for the optimisation of sensor/actuator locations in the active vibration control of flexible structures may be greatly reduced. The technique is applied to the optimisation of the location of eight and ten actuators on a 500×500mm square plate, and the search space is reduced by up to 99.99%, allowing the global optimal solution to be found after a greatly reduced number of generations. An isotropic plate with piezoelectric sensor/actuator pairs bonded to its surface was investigated using the finite element method and Hamilton's principle based on first order shear deformation theory as described in chapter three. The placement and feedback gain of ten and eight sensor/actuator pairs were optimised for a cantilever and clamped-clamped plate to attenuate the first six modes of vibration, using the minimisation of the linear quadratic index as an objective function.

8.1. Introduction

The complexity of the genetic algorithm used to solve the placement problem is defined by the total number of candidate solutions in the search space, which is the statistical combination of the numbers of sensors and actuators and the total number of possible locations on the structure. The reduction of the total numbers of candidate solutions in the genetic algorithm search space simplifies the complexity of the problem of obtaining the global optimal solution within fewer generations.

In chapters five, six and seven, optimal locations for two, four, six, eight and ten sensors and actuators have been investigated for flat plates and plates stiffened by beams with both symmetrical and asymmetrical geometries and boundary conditions. Symmetrical configurations of actuators for symmetrical structures and asymmetrical actuator configurations for asymmetrical structures were found to be optimal using the minimisation of the linear quadratic index as an objective function. Furthermore, these symmetrical configurations gave higher vibration attenuation than previously published asymmetrical configurations. In chapter seven, the global optimal configurations obtained using a new fitness function based on H_∞, also gave a symmetrical sensor/actuator distribution with higher vibration reduction than in earlier studies.

This chapter complements the work done in chapters five to seven by reducing the search space of the genetic algorithms and obtaining global optimal sensor and actuator locations after fewer generations using a developed half- and quarter-chromosome technique. The optimal placement of ten and eight sensor/actuator pairs on cantilever and clamped-clamped plates is investigated based on the minimisation of the optimal linear quadratic index as an objective function.

8.2. Modelling

The full modelling derived in chapter three for plates stiffened by beams bonded with discrete piezoelectric sensors and actuators is used in this chapter to investigate flat plates by substituting zero mass and stiffness for the beam stiffener in equations 3.80-3.87. Controller state space matrices were prepared according to equations 3.94-3.99.

8.3. Genetic Algorithm

In chapters five to seven, flat plates and plates stiffened by beams were considered with different boundary conditions based on the minimisation of the linear quadratic index and H_∞ using a full-length chromosome. This showed that the global optimal distribution of piezoelectric sensors and actuators has the same axes of symmetry as the structure itself. In this chapter, the chromosome is reduced in length to a quarter and a half of its size based on the symmetry of the structure, using a quarter of the chromosome length for a structure having two axes of dynamic symmetry and a half-length for a structure having one axis of dynamic symmetry. The placement strategy using the genetic algorithm comprising the conditional filter proposed in chapter five is used in this chapter.

8.4. Full, Half and Quarter Chromosome Lengths

New quarter- and half-chromosome and a reduced genetic algorithm search space are proposed by this work based on the findings reported in previous chapters. Figure 8.1 demonstrates all three types of chromosome length and the resulting search spaces. The numbers of candidates are greatly reduced with half- and quarter-length chromosomes (2,117,860 and 300 candidates respectively) compared with the full chromosome (1.730309×10^{13}). It may be expected that, using this technique, a global optimal solution can be found after a smaller number of generations.

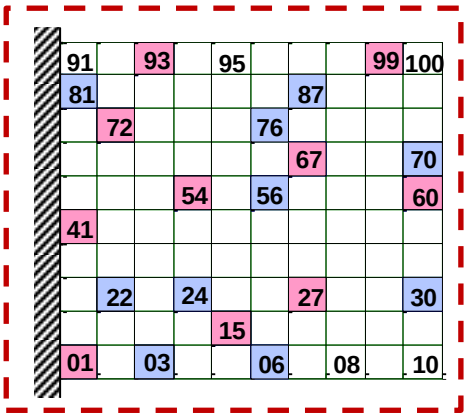

Search space numbered from 01-100

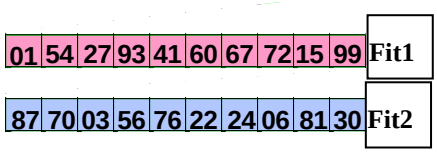

Full chromosomes

Possible solutions= $100!/(10! \times 90!)$

1.73×10^{13}

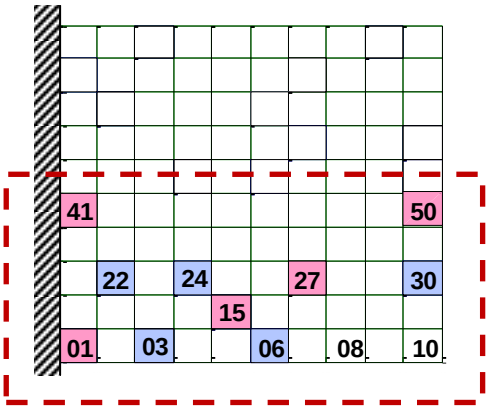

Search space numbered from 01-50

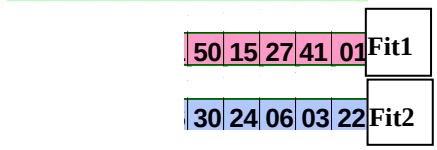

Half chromosomes

Possible solutions= $50!/(5! \times 45!)$

=2117860

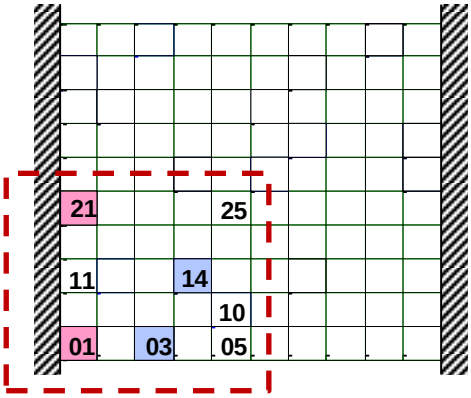

Search space numbered from 01-25

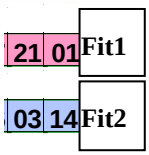

Quarter chromosomes

Possible solutions= $25!/(2! \times 23!)$

=300

Figure 8.1 Full, half and quarter chromosomes with search space for a plate discretised to one hundred elements, demonstrating search space selection and numbering and chromosome coding along with calculation of the total numbers of possible candidates

8.5. Results and discussion

8.5.1. Research problem

A flat plate of the dimensions $500 \times 500 \times 1.9$mm was mounted rigidly on the left hand edge to form a cantilever and from the left and right hand edges to form a clamped-clamped plate. The plates are discretised into one hundred elements 10×10 sequentially numbered from left to right and down to up as shown in Figure 8.2. These two plate arrangements same as in those chosen in chapters five and seven, to allow the direct comparison of results.

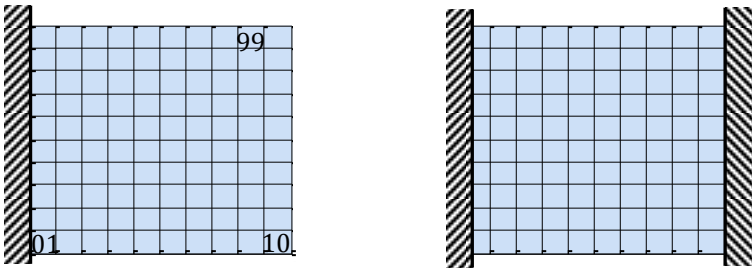

(a) Cantilever plate **(b)** cc- plate

Figure 8.2 Cantilever and clamped –clamped plates

8.5.2. *Actuator optimisation using half–length chromosome*

The genetic algorithm described in chapter five was used based on a half-chromosome length to find the optimal locations of ten piezoelectric actuators on the cantilever plate. The progressive convergence of the population to an optimal solution is shown in Figure 8.3**,** in which the population is distributed around the circle with radius **(r)** representing the fitness value to be minimised. The convergence to the global optimal solution shown in Figure 8.3 and Figure 8.4 (a, b and c) is similar to that obtained with the full chromosome as shown in the section 5.6.4, but the optimal solution occurs after less than 50 generations. The optimal solutions found are the same, which is as expected.

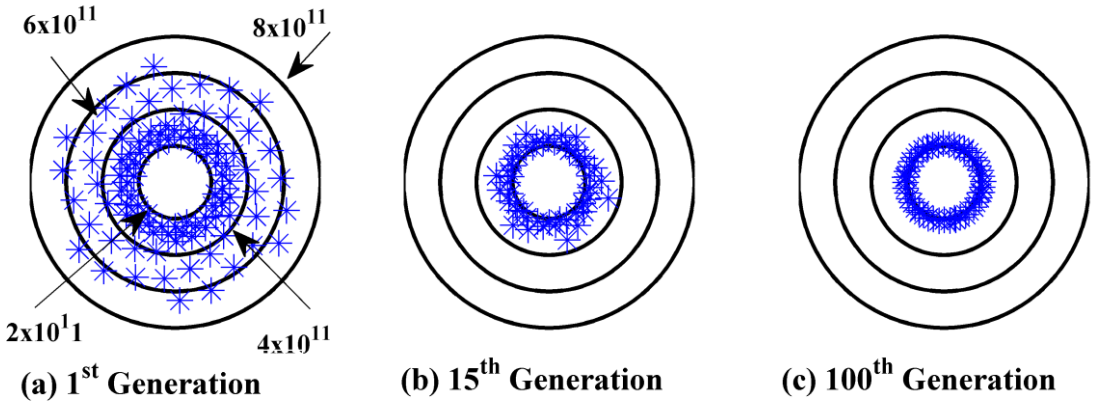

Figure 8.3 Population fitness progression over 100 generations using half-chromosome length. Each individual is represented as one of the points distributed around the circle with radii **r** which represent its fitness value to be minimised

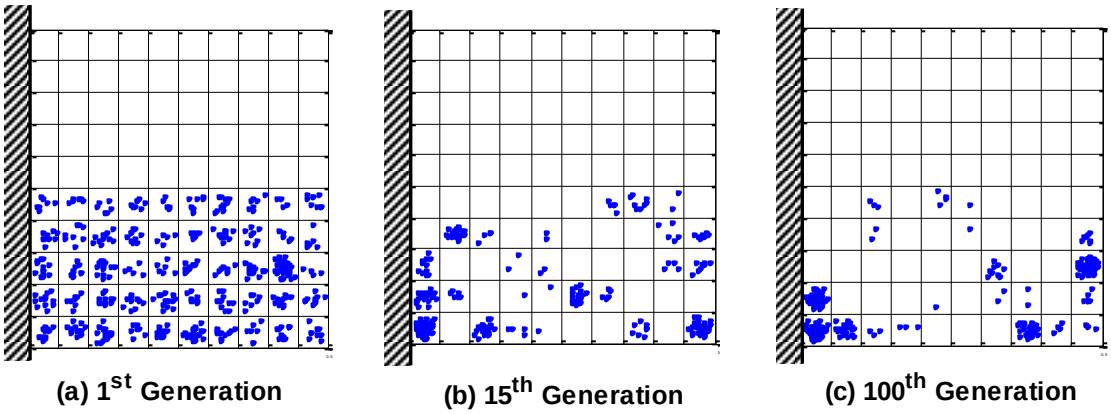

Figure 8.4 Sensor/actuator placement using half chromosome length for the cantilever plate. Each dot shows the location of a sensor/actuator pair in one of the 50 breeding individuals in each generation. Initially they are randomly distributed. After 15 generations they have begun to group in efficient locations. After 100 generations they have mostly converged on five sites.

8.5.3. Actuator optimisation using quarter-length chromosome

The same scenario as that in the previous section is applied to locate eight discrete piezoelectric actuators for a clamped-clamped plate using a quarter-chromosome length. The convergence on the global optimal solution shown in Figure 8.5 and Figure 8.6 (a, b and c) is similar to that obtained with the full chromosome shown in the section 7.4.3,

but the optimal solution occurs in less than 10 generations. The optimal solutions found are again the same, as expected.

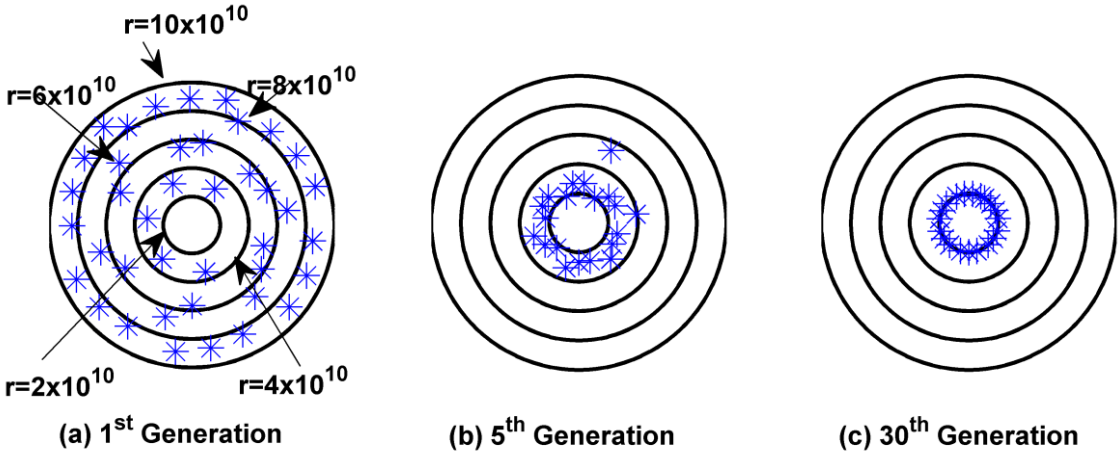

Figure 8.5 Population fitness progression over 30 generations using 40 chromosomes as first population and the progression is implemented for 20 chromosomes. Each individual is represented as one of the points distributed around the circle, with its fitness value obtained from chromosome defining its distance from the centre.

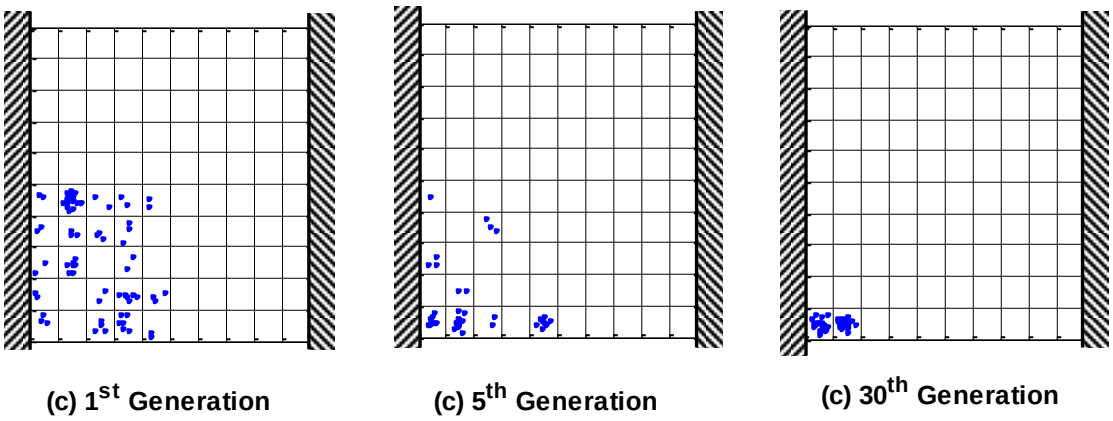

Figure 8.6 Sensor/actuator placement using quarter chromosome length for the clamped-clamped plate. Each dot shows the location of a sensor/actuator pair in one of the 20 breeding individuals in each generation. Initially they are randomly distributed. After 5 generations they have begun to group in efficient locations. After 30 generations they have completely converged on two sites.

The optimal placement of two, four, six, eight and ten discrete piezoelectric actuators has been investigated for unstiffened plates and plates stiffened by beams with different boundary conditions and geometries. It has been found that the optimal configuration of actuators is always symmetrically distributed about the axes of the symmetry of the plate, as shown in chapters five to seven.

The present optimal piezoelectric actuator distribution using half- and quarter-length chromosomes is in agreement with this previous studies, as shown in Figure 8.7 (b) and (d). This technique therefore holds great promise for application to large mechanical structures in order to determine global optimal locations without unacceptably large computational costs.

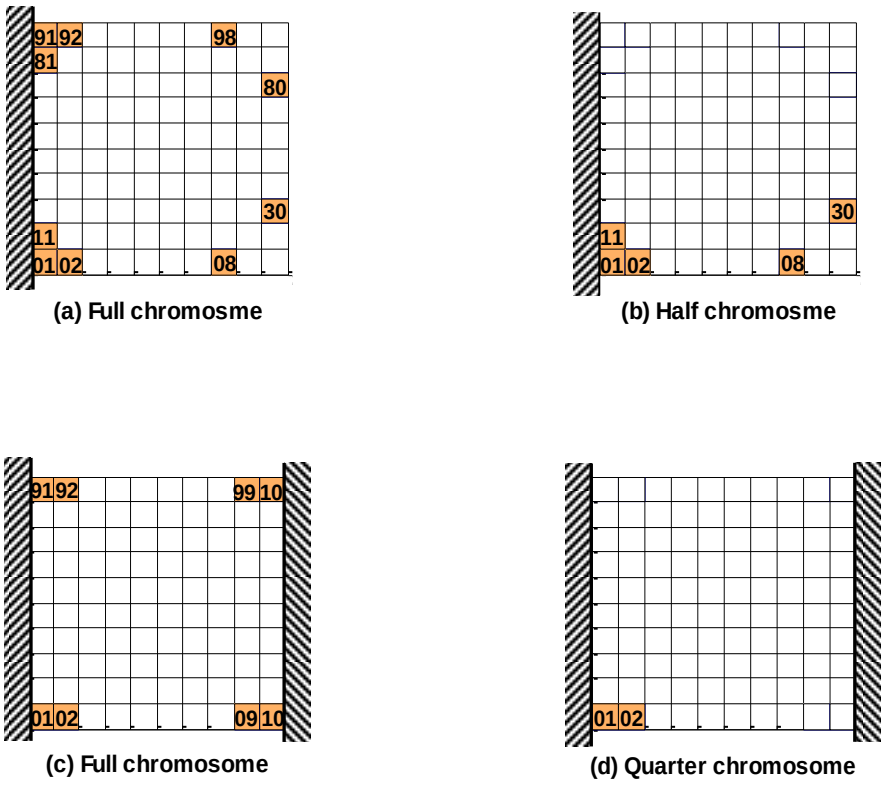

Figure 8.7 Optimal piezoelectric sensor/actuator configuration for a cantilever plate using **(a)** full-length chromosome (chapter five) , **(b)** this chapter using half-length chromosome. Clamped-clamped plate **(c)** full chromosome (chapter seven), **(d)** this chapter quarter chromosome

8.6. Validation by Convergence Study

The genetic algorithm program was run many times for both the cantilever and clamped-clamped plates to test the reliability of the optimised actuator locations using half- and quarter-chromosome lengths. The results are shown in Figure 8.8 and Figure 8.9, which give an indication of the progress of each run by plotting the fitness value for the fittest member of each generation. It can be seen from the results that the level of fitness converges to the same optimal value at each run and the same curves behaviour are observed as that obtained in sections 5.6.5 and 7.6.1 using the full-length chromosome, but with far fewer generations.

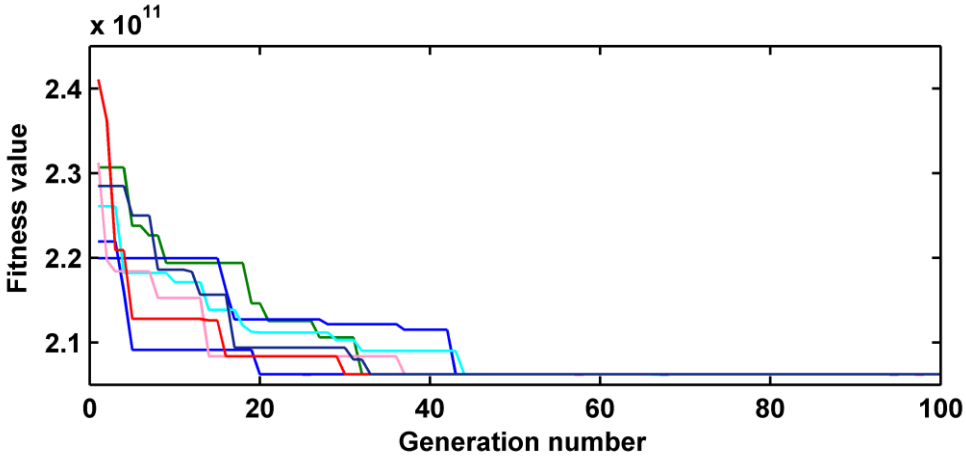

Figure 8.8 Fitness value for the best member in each generation for the cantilever plate using half chromosome length

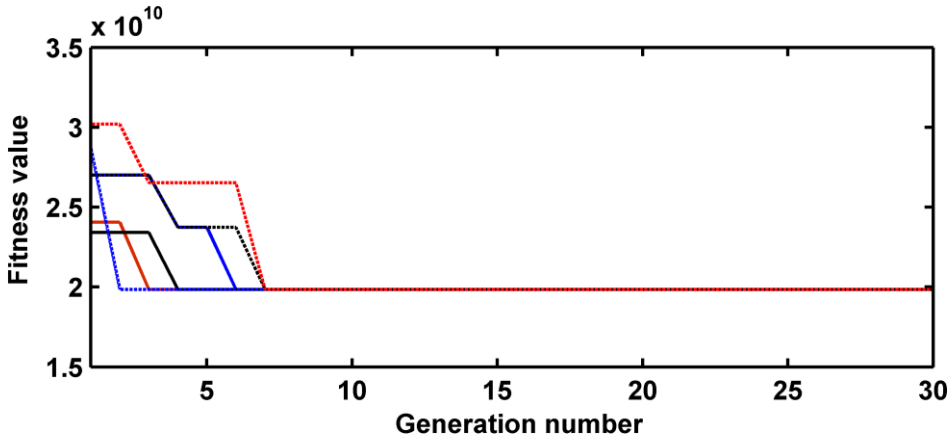

Figure 8.9 Fitness value for the best member at each generation for the clamped-clamped plate using quarter chromosome length

8.6.1. Genetic algorithm problem reduction

The percentage genetic algorithm problem reduction is calculated using half and quarter chromosomes compared to the full-length chromosome. The results are shown in Table 8.1 and Table 8.2 for the cantilever and clamped-clamped flat plates respectively.

Two measures of reduction are calculated: the size of the search space and the average number of fitness calculations required to find the optimal solution. The total search space, or the number of candidate chromosomes, is the statistical combination of the number of actuators to be optimised and the number of possible locations on the structure. This gives a reduction in the number of candidates equal to 99.99% for the half-length and 99.99% for the quarter-chromosome length compared with the full chromosome.

The second measure of reduction is calculated on the basis of the actual computational effort required to obtain the optimal solutions. Table 8.1 shows that the half-length chromosome technique requires 700 fitness solutions compared with 31,900 for the full chromosome, representing a 97.80% reduction in computation. Similarly, Table 8.2 shows that the quarter chromosome requires only 25 calculations, compared with 3,350 for the full chromosome, which is equal to a 99.25% reduction in computation.

Table 8.1 Percentage genetic algorithm reduction obtained using half-chromosome length

Case	Number of candidates	Number of solved chromosomes
Full Chromosome chapter 5	$\frac{100!}{10! \times 90!} = 1.73 \times 10^{13}$	$319 \times 100 = 31900$
Half-chromosome	$\frac{50!}{5! \times 45!} = 2.1 \times 10^{6}$	$28 \times 50 \times 0.5 = 700$
Reduction obtained	**>99.99%**	**97.80%**

Table 8.2 Percentage genetic algorithm reduction obtained using quarter-chromosome length

Case	Number of candidates	Number of solved chromosomes
Full chromosome chapter 7	$\frac{100!}{8! \times 92!} = 1.86 \times 10^{11}$	$67 \times 50 = 3350$
Quarter-chromosome	$\frac{25!}{2! \times 23!} = 300$	$5 \times 20 \times 0.25 = 25$
Reduction obtained	**>99.99%**	**99.25%**

8.7. Conclusions

A technique using half- and quarter-length chromosomes has been developed to optimise the feedback gain and the location of discrete piezoelectric actuators on a flat plate fixed as a cantilever and clamped-clamped, giving one and two axes of symmetry respectively. The minimisation of the linear quadratic index is used as an objective function to locate ten and eight discrete piezoelectric actuators and to attenuate the first six modes of vibration.

The technique has been developed based on the findings in chapters five to seven, It was observed that the optimal configuration of discrete sensors and actuators is symmetrical for a structure symmetrical in geometry and fixation and asymmetrical for structures asymmetric in geometry or fixations. The optimisations obtained exploiting these symmetries were found to be in complete agreement with the full calculations, but requiring as little as 0.01% of the computational effort for the double symmetry case.

This technique holds great promise for application to large mechanical structures in which there are often symmetries that can be exploited in this way, allowing for the determination of global optimal locations without unacceptably large computational costs.

Chapter 9. Optimisation of the Number of Sensors and Actuators

This chapter is concerned with the active vibration reduction of a square isotropic plate, mounted rigidly along one edge to form a cantilever. The number of piezoelectric sensor/actuator pairs, their location and controller gain are optimised using a genetic algorithm based on the linear quadratic index and closed loop dB gain reduction as objective functions. A new fitness function is developed to determine the optimal number of actuators based on variations in average closed loop dB gain reduction for all optimal piezoelectric pairs and the modes which required to be attenuated using the optimal linear quadratic control scheme. The aim of this work is to find the minimum number of optimally located discrete sensor/actuator pairs which can achieve the same vibration reduction as when more piezoelectric patches are used, in order to reduce the weight of the structure, costs, the equipment required for experimental testing and real-time control calculations. It is shown that two sensor/actuator pairs located in optimal locations give almost the same vibration reduction as ten pairs in their optimal locations. The results based on the modelling are validated by investigating the open and closed loop time responses of one finite element node and actuator feedback voltages against the number of piezoelectric pairs in the first and the second modes, using the ANSYS finite element package and a proportional differential control scheme. It is found that just two sensor/actuator pairs in optimal locations give as much vibration attenuation as larger numbers. Moreover, the summation of all actuator voltage feedback increased with increases in the number of sensor/actuator pairs, compared to one or two pairs. The sensor and actuator feedback voltages were more widely distributed as the number of sensor/actuator pairs increased.

9.1. Introduction

Control optimality can be achieved by locating discrete sensors and actuators optimally on a structure. In addition, limiting the number of optimal sensors and actuators could reduce costs, weight and real-time control calculations, and achieve the same vibration reduction as greater numbers. Han and Lee reported that the increased numbers of sensors and actuators leads to increasing the complexity of control system design, costs and weight [26].

A limited amount of work has been published concerning the optimal location of piezoelectric sensors and actuators on a flexible structure, as explained in the previous

chapters. Subsequently, a few papers have been published which investigate the optimal size and number of sensors and actuators. In this area, the optimal placement and size (length) of piezoelectric sensor/actuator pairs [53, 107] and feedback gain [34] were investigated for a beam based on the minimisation of the optimal linear quadratic index and the maximisation of the controllability index and energy dissipation as objective functions respectively. The optimal number and placement of piezoelectric actuators has been investigated for the active vibration control of trusses [28, 33, 108] and plates [32]. Here, the eigenvalue distribution of the energy correlative matrix of control input force was presented to determine the required number of actuators, and a genetic algorithm found their optimal placement based on active vibration control effects as an objective function [28, 32]. The optimal location and number of discrete actuators has been determined by a fitness function based on energy degree of controllability and arbitrarily weighted factors using the genetic algorithm [108]. A two level genetic algorithm, as proposed by Li et al was based on the minimisation of the maximum top floor displacement as an objective function for the optimal placement and number of actuators in multi-storey buildings [33].

In this chapter, the optimal placement, gain and number of piezoelectric patches on a cantilever plate is investigated using the genetic algorithm. Placement and feedback gain are optimised based on the minimisation of the linear quadratic index as an objective function, while their number is optimised based on the new fitness and objective functions developed in this study by measuring the average variations of closed loop dB gain reduction for all piezoelectric pairs and modes using the optimal linear quadratic control scheme.

9.2. Modelling

The modelling derived in chapter three to formulate controller state space matrices and the genetic algorithm explained in chapter five are used in this chapter .

9.3. Development of Fitness and Objective Functions

A second stage of optimisation is based on the development of new fitness and objective functions in order to find the optimal number of actuators by measuring the variation of closed loop average dB gain reduction for all optimal sensor/actuator pairs

and for all the required modes to be attenuated using the optimal linear quadratic index. The second stage of optimisation is based on the following assumptions:

1. The optimal locations of sensor/actuator pairs n_{sa} , n_{sa+1} , , , n_{sa+n} are determined using the placement strategy and objective function proposed in chapter five as the first stage of optimisation.
2. The optimal feedback gain matrix K for n_{sa} , n_{sa+1} , , , n_{sa+n} is determined using optimal linear quadratic control as explained in chapter three.
3. A disturbance unit amplitude sinusoidal voltage is applied at the first optimal actuator or a specified actuator throughout the optimisation as a reference for comparison.
4. The variation of average closed loop gain reduction for the first number of piezoelectric pairs in the optimal location (fitness value) equals 100% compared with the open loop gain reduction (or no sensor/actuator).

Consider the following state space equations for a plate bonded with specified numbers of sensor/actuator pairs n_{sa} in optimal locations:

$$\dot{X} = AX + B\phi_a \quad , \quad \phi_s = CX \tag{9.1}$$

Take the Laplace transform of equation 9.1:

$$sX(s) = AX(s) + B\phi_a(s) \quad , \quad \phi_a(s) = B^{-1}(sI - A)X(s)$$
$$\phi_s(s) = CX(s) \tag{9.2}$$

The open loop transfer function of a system in the frequency domain is:

$$GO(\omega) = \frac{\phi_s(s)}{\phi_a(s)} = C(j\omega I - A)^{-1}B \tag{9.3}$$

$$GO(\omega) = C(j\omega I - A)^{-1}B \tag{9.4}$$

The open loop dB gain for the first sensor j as a result of the unit voltage applied to the first actuator at the specified natural mode i is:

$$GO_{j,i} = 20\log_{10}(|C_i(j\omega_i I - A_i)^{-1}B_i|) \tag{9.5}$$

The average open loop dB gain for all sensors and modes due to applying the sinusoidal unit voltage at a specified single actuator is:

$$MGO = \frac{1}{n_m n_{sa}} \sum_{i=1}^{n_m} \sum_{j=1}^{n_{sa}} GO_{j,i} \tag{9.6}$$

where MGO refers to the average open loop dB gain for all sensors n_{sa} as a result of the applied sinusoidal unit voltage at the first actuator at all natural frequencies n_m to be suppressed. The closed loop state matrix is:

$$Ac_i = A_i - B_i K_i \tag{9.7}$$

The closed loop dB gain for a single sensor j as a result of applying the unit sinusoidal voltage disturbance at a specified single actuator and for a single mode i is:

$$GC_{j,i} = 20 \log_{10}(|C_i(j\omega_i I - Ac_i)^{-1} B_i|) \tag{9.8}$$

The mean average closed loop dB gain for all sensor/actuator pairs and modes as a result of applying the unit voltage disturbance at a specified single actuator for different values of linear quadratic weighted matrices is:

$$MGC = \frac{1}{3 n_m n_{sa}} \sum_{k=1}^{3} \sum_{i=1}^{n_m} \sum_{j=1}^{n_{sa}} GC_{j,i} \Bigg|_{at\ R=1, Q_k = 10^6, 10^7, 10^8} \tag{9.9}$$

where MGC refers to the average closed loop dB gain for all sensor/actuator pairs n_{sa} as a result of applying the unit voltage at a specified actuator at all natural frequencies n_m for three values of linear quadratic weighted matrix settings. The average closed loop dB gain reduction for an arbitrary number of piezoelectric pairs located at optimal locations MGR is equal to the absolute difference in value between the open and closed loop dB gain:

$$MGR = |MGC - MGO| \tag{9.10}$$

$$J(n_{sa} + 1) = MGV = \frac{MGR_{n_{sa}+1} - MGR_{n_{sa}}}{MGR_{n_{sa}+1}} \times 100\% \tag{9.11}$$

$$J_{opt}(n_{sa}) = MGV|_{n_{sa}+1} \leq 20 \tag{9.12}$$

The developed fitness function MGV is a percentage of the variation of the closed loop dB gain of a number of sensor/actuator pairs n_{sa} and $n_{sa} + 1$ bonded at optimal locations on a flexible structure. The fitness function MGV is represented by the ratio

of the difference in average closed loop dB gain reduction for a structure bonded with numbers of optimal piezoelectric pairs equal to n_{sa} and $n_{sa}+1$ divided by the average closed loop dB gain reduction for an optimal piezoelectric pair equal to ($n_{sa}+1$). According to the objective function equation 9.12, the optimal number of piezoelectric actuators n_{sa} is selected at a fitness value $J(n_{sa}+1)$ of less than or equal to 20%, where the designer can choose a specific value depending on the requirements of the system.

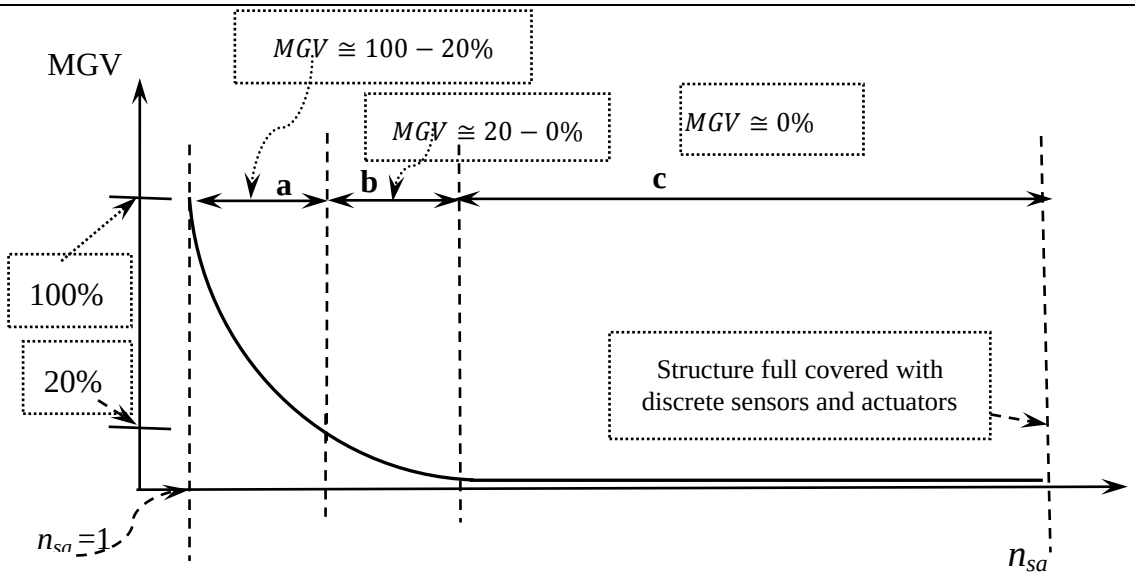

Figure 9.1 Relationship between fitness function and number of sensor/actuator pairs (n_{sa}).

The expected relationship between the average closed loop dB gain reduction *MGV* and the number of sensor/actuator pairs n_{sa} is represented in Figure 9.1. It can be seen that the curve is divided into three zones ***a***, ***b*** and ***c.*** The first zone **a** is considered to be the active zone limited to between 100% and 20% of *MGV*. The active zone is considered as a highly progressive zone which gives a sensibly increasing closed loop vibration reduction with increasing numbers of optimally placed sensor/actuator pairs. The second zone ***b*** is an important transition zone between the active zone ***a*** and the passive zone ***c***, limited to between 20% and 0% *MGV*. In this zone, the variation in closed loop vibration reduction is low and is considered as an objective function zone for the optimal number of sensor/actuator pairs according to the objective function equation 9.12. The final and biggest zone ***c*** is a passive zone with no variation in closed

loop vibration reduction irrespective of the number of sensor/actuator pairs. This is zone of saturation where the slope of the tangent to the *MGR* curve is almost equal to zero at any point along the x-axis. The passive zone $\boldsymbol{c}$ involves merely drawback effects, by increasing the weight of the structure, the cost of materials, system complexity, theoretical and experimental computational effort.

9.4. Genetic algorithm

The working mechanism of the genetic algorithm and the main features of its placement strategy in locating discrete actuators and sensors are explained in chapters five and six respectively. In this chapter, the optimisation technique used is composed of two stages. The first stage is explained in chapters five and six, and this is now improved to include a second stage which optimises the number of piezoelectric actuators based on the objective function explained in section 9.3. The genetic algorithm MATLAB computer program is improved to include the second stage with the following additional features:

1. The location of one piezoelectric actuators ($n_{sa} = 1$) is optimised according to the method in section 5.5.
2. The linear quadratic control scheme is used with three settings of values of the weighting matrices values for $R = 1$ and $Q = 10^6, 10^7$ and 10^8. The average closed loop dB gain reduction is calculated for all optimal piezoelectric pairs, all vibration modes and all three weighted matrix values according to equation 9.10. The results are inserted into the optimal chromosome string for recalculation.
3. The area of the first optimal sensor/actuator pair is divided into five segments as a percentage from 4% to 100% in order to achieve more precise results as shown in Table 9.2 and Table 9.3.
4. The fitness function is calculated according to equation 9.11.
5. If the fitness value is less than or equal to 20%, then the process is halted and the previous chromosome is taken to represent an optimal number and location of piezoelectric pairs according to the objective function in equation 9.12. Otherwise, the first step is repeated with a greater number of actuators $n_{sa} + 1$ until the condition of the objective function is achieved.

9.5. Results and Discussion

9.5.1. Research problem

The cantilever plate and piezoelectric investigated in chapters five, six and eight were used in this chapter with same dimensions and properties for further investigation and comparison with the results obtained in section 5.6.10. In this research problem, the optimal placements and feedback gain of two, four, six, eight and ten actuators is investigated on the cantilever plate based for the linear quadratic index as an objective function. The optimal number of actuators is determined based on the fitness function developed in section 9.3.

The complexity of the genetic algorithm problem for active vibration control becomes greater as the number of candidate solutions increases. This depends on the fitness of the finite element mesh and the number of piezoelectric sensors and actuators to be optimised. The number of candidates for the cantilever plate discretised to 10×10 elements when two actuators are to be optimised is a combination of 2 from 100 which gives 4,950 candidate solutions, four actuators gives 3,921,225 candidates, six actuators 1.1921×10^{9} candidates, eight actuators 1.861×10^{11} candidates and ten actuators 1.731×10^{13} candidates.

It could be said that the optimisation of the number of sensors and actuators requires fewer computational time than an arbitrary selection as a result of conducting the optimisation starting from one pair up till the optimal number. The total number of candidates for 1 to n_{sa-1} is much fewer than n_{sa} candidates. This proves that the developed fitness and objective functions are lower costs in computational effort than arbitrarily selection of limited number of sensors and actuators for location optimisation.

9.5.2. Optimisation of piezoelectric location

The genetic algorithm described in section 9.4 was used to find the optimal locations for different numbers of sensor/actuator pairs on a 0.5m square cantilever plate. The process of optimisation was continued after the determination of optimal placement and number in order to investigate the correctness and effectiveness of this work. Table 9.1 gives the optimal locations found for between one and ten sensor/actuator pairs, and a selection of these is shown graphically in Figure 9.2. The results in the next two sections are based on the information Table 9.1.

Table 9.1 Optimal locations of one to ten sensor/actuator pairs on the cantilever plate

case	Optimal piezoelectric location on the plate									
One pair	01									
Two pairs	01	91								
Three pairs	01	91	02							
Four pairs	01	91	02	92						
Five pairs	01	91	02	92	11					
Six pairs	01	91	02	92	11	81				
Seven pairs	01	91	02	92	11	81	08			
Eight pairs	01	91	02	92	11	81	08	98		
Nine pairs	01	91	02	92	11	81	08	98	30	
Ten pairs	01	91	02	92	11	81	08	98	30	80

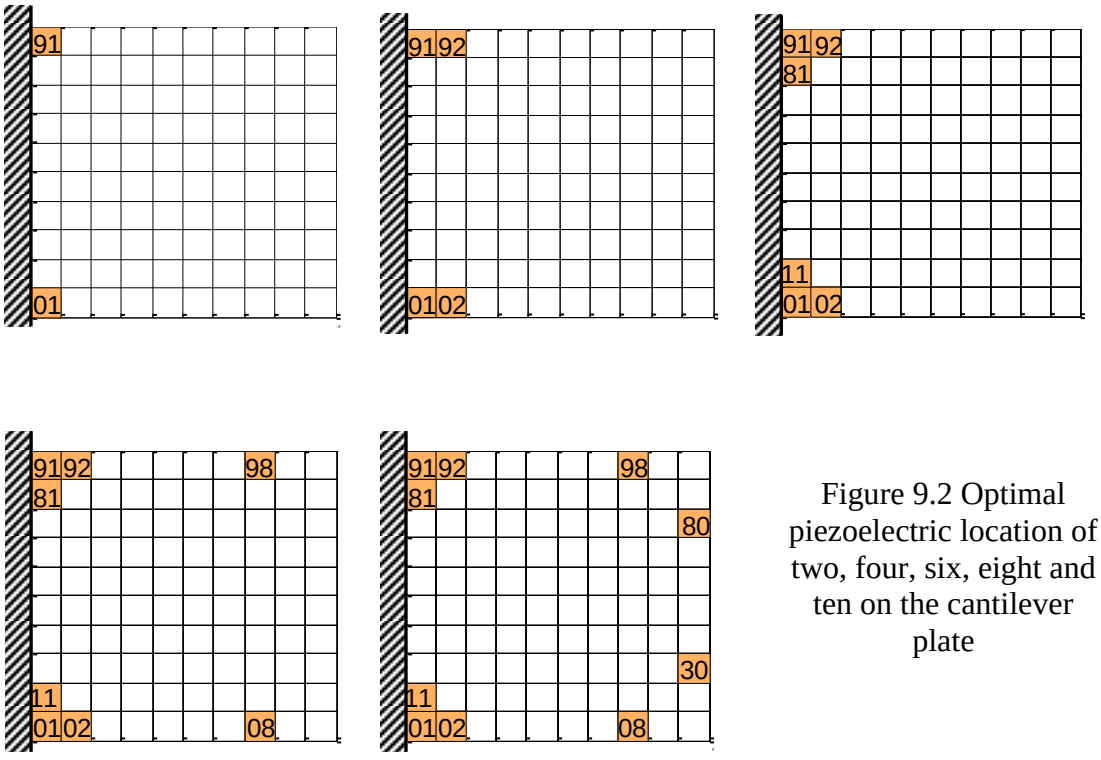

Figure 9.2 Optimal piezoelectric location of two, four, six, eight and ten on the cantilever plate

9.5.3. Optimisation of the number of actuators

The second stage of the genetic algorithm is the determination of the optimal number of actuators based on measuring the variation in the average closed loop gain reduction for all optimal sensor/actuator pairs according to the fitness equation. A measure of the closed loop dB gain reduction over the whole plate is obtained by taking the average

vibration reduction for all pairs at the first six modes of vibration for three settings of Q according to equation 9.10. These results are shown in Table 9.2, in which the optimal location of the first sensor/actuator pair 01 on the plate is discretised to five areas according to the step three in section 0.

It can be observed from Table 9.2 that the addition of more than two optimally placed patches has a small effect on vibration reduction at low and high values of quadratic weighted matrix, and that one patch gives only a small decline in dB gain of reduction. However, using only less than one patch (by reducing the area of the sensor/actuator pair) gives a serious loss of reduction over the six modes.

Table 9.2 Closed loop dB gain reduction for the cantilever plate with different numbers of piezoelectric patches in optimal locations

Number of piezoelectric pairs	Linear quadratic weighted matrices R=1 with three Q settings			
	$Q = 10^6$	$Q = 10^7$	$Q = 10^8$	MGR
(1/25),1×1cm	0.26	1.81	6.61	2.90
(4/25),2×2cm	2.22	7.50	15.61	8.44
(9/25),3×3 cm	5.04	12.26	21.52	12.94
(16/25),4×4cm	7.62	15.89	25.58	16.36
(25/25),1=5×5cm	9.80	18.74	28.59	19.05
2	12.20	21.08	30.00	21.09
3	12.75	21.78	30.60	21.71
4	13.21	22.35	31.31	22.29
5	13.89	22.88	31.85	22.87
6	14.40	23.26	31.78	23.15
7	14.57	23.47	32.00	23.34
8	14.70	23.57	32.09	23.45
9	15.42	23.88	32.13	23.81
10	15.73	24.16	32.51	24.13

Table 9.3 shows the percentage variation of closed dB-gain reduction for each addition of sensor/actuators according to the fitness function equation 9.11. It can be observed that three sensor/actuator pairs gives close to zero variation and further increases in sensor/actuator numbers have negligible effects.

Table 9.3 Percentage variation of closed loop gain reduction ($100\% * \Delta dB/dB$) for the cantilever plate with different numbers of piezoelectric patches in optimal locations

Number of piezoelectric pairs	Linear quadratic weighted matrices R=1 with three Q settings			
	$Q = 10^6$	$Q = 10^7$	$Q = 10^8$	Fitness
(1/25),1×1cm	100	100	100	100
(4/25),2×2cm	88.11	75.77	57.61	73.83
(9/25),3×3 cm	55.86	38.81	27.44	40.71
(16/25),4×4cm	33.79	22.83	15.86	24.16
(25/25),1=5×5cm	22.24	15.20	10.55	16.00
2	19.64	11.07	4.69	11.80
3	4.34	3.21	1.94	3.17
4	3.44	2.55	2.27	2.75
5	4.91	2.33	1.69	2.98
6	3.54	1.62	-0.23	1.64
7	1.16	0.87	0.69	0.90
8	0.87	0.41	0.27	0.52
9	4.70	1.31	0.13	2.04
10	1.95	1.14	1.15	1.41

The results are represented in Figure 9.3 (a) and (b) for average vibration reduction and its percentage variation for different values of weighted matrices respectively. It can be seen that the Figure 9.3 (b) is divided into three zones: an active progressive zone, an objective less progressive zone and a passive drawback effect zone. According to the objective function, the optimal number of piezoelectric sensor/actuator pairs found between one and three pairs as maximum as shown in Figure 9.3 (b) “objective zone”.

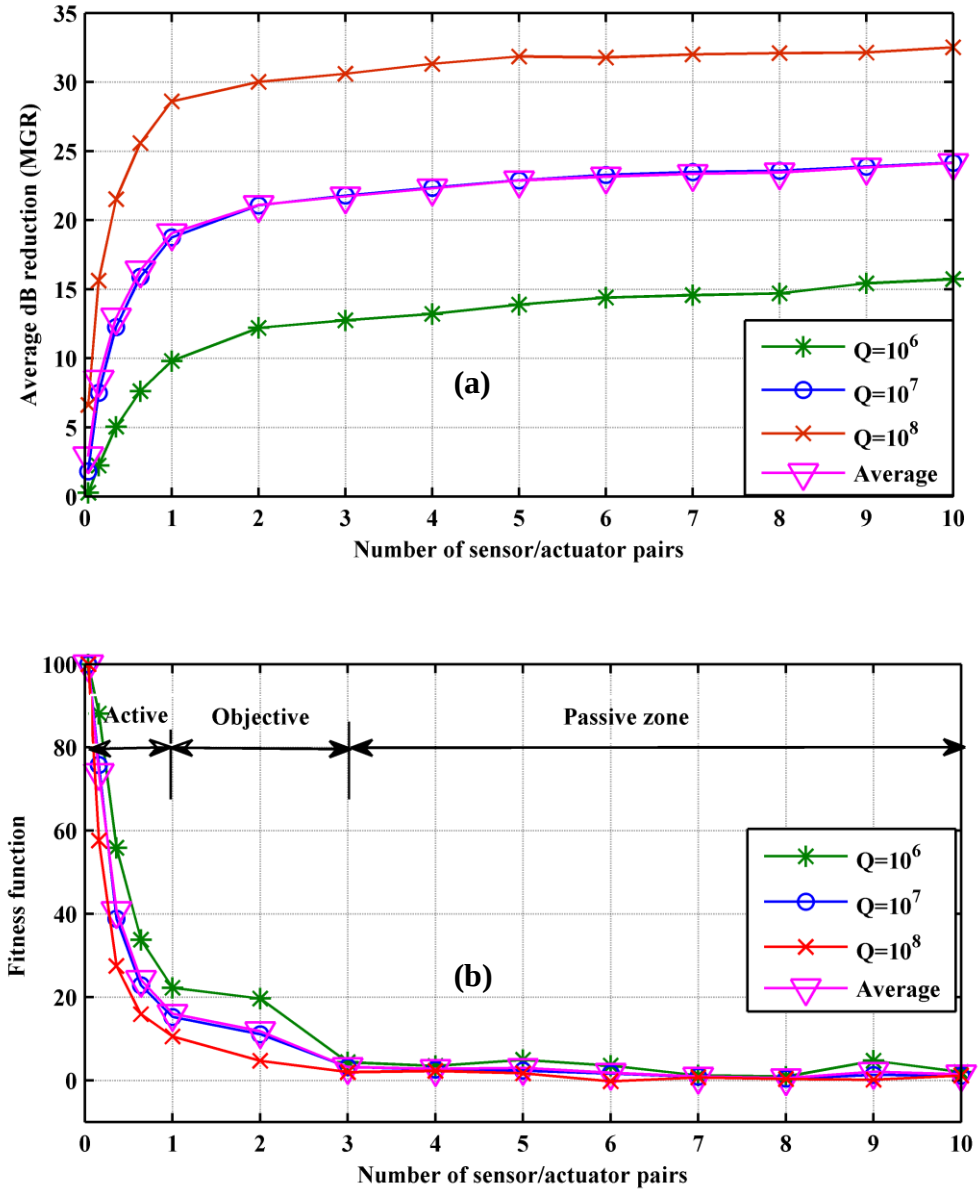

Figure 9.3 (**a**), Average closed loop dB gain reduction, and (**b**) its variation for different values of weighted matrices against number of piezoelectric pairs.

9.5.4. Validation of the optimal location and number of sensor/actuator pairs

From the previous section and compared with the previously published studies [38, 66] using ten sensor/actuator pairs for the same cantilever plate and piezoelectric dimensions, it can be considered a significant achievement to suppress the first six modes of vibration using just one, two or three sensor/actuator pairs. Therefore, in this section, the developed fitness and objective functions are tested and validated using the ANSYS finite element package and implementing the proportional differential control scheme to investigate the closed loop time responses against the number of sensor/actuator pairs in optimal locations. The difference between the work reported in this section and section 5.6.10 is that the proportional differential feedback gain is doubled.

Here, the open and closed loop acceleration time responses are investigated for one corner of the free end of the cantilever plate, which is a representative node that has large displacement in all modes, against the increased number of sensor/actuator pairs. The investigation includes the closed loop time response of actuator feedback voltage against the increasing in the number of pairs. The cantilever plate is driven by a sinusoidal voltage at the appropriate natural frequency with 20V amplitude at actuator location 91, which was used just for driving the plate, as in chapter five. In this section, the open and closed loop time responses are tested in the ANSYS package based the procedure described in section 5.6.10 and Figure 5.18.

In each case the ANSYS model was configured with the sensor/actuator pairs in the optimal locations as shown in Figure 9.2. The results are shown in Figure 9.4 to Figure 9.7 and summarised in Table 9.4 and Table 9.5. Figure 9.4 shows the open and closed loop time responses for the first mode. It can be observed that there is a significant vibration reduction in the closed loop using one and two sensor/actuator pairs, while little further improvement occurs using more than two sensor/actuator pairs.

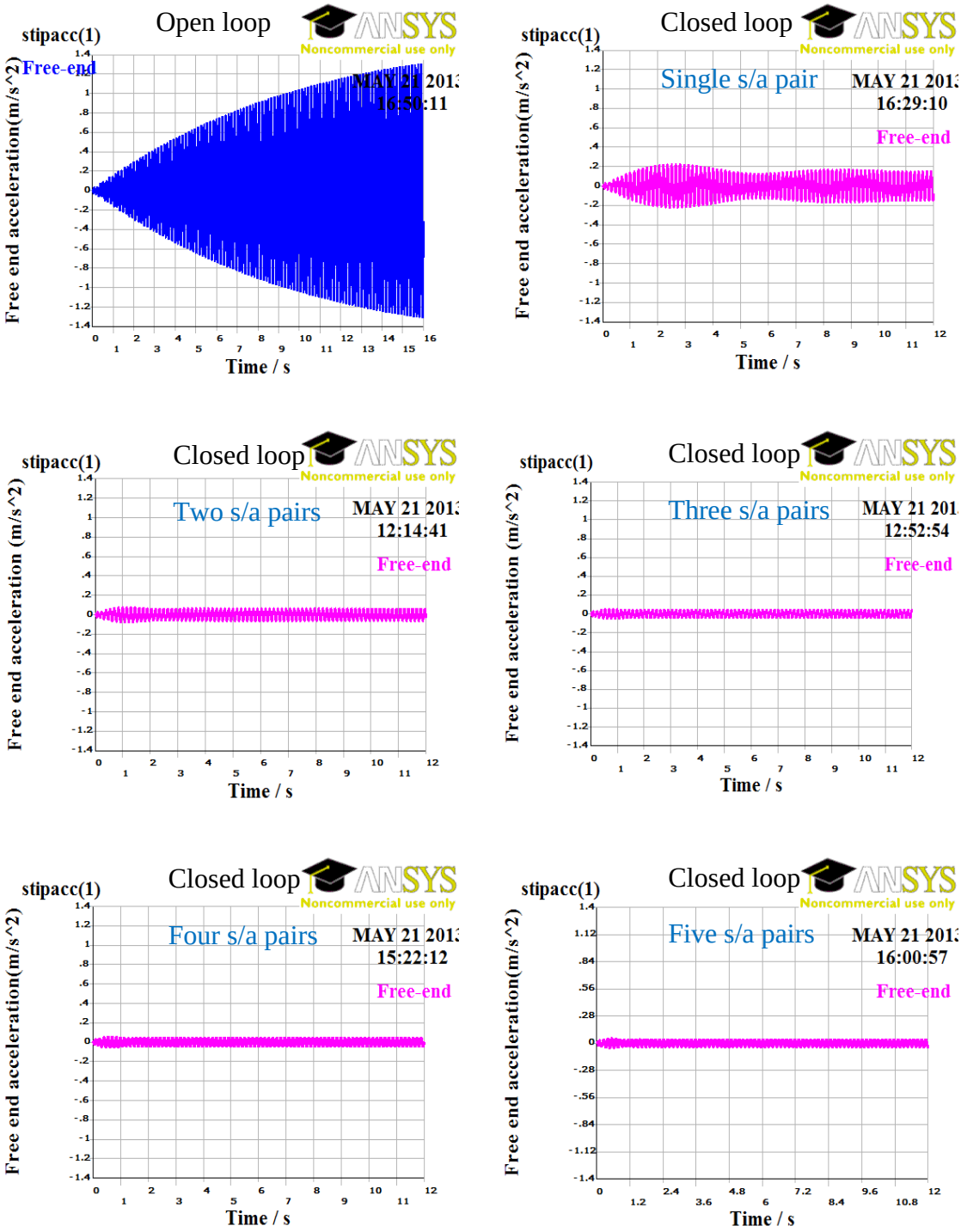

Figure 9.4 Open and closed loop time responses of the free end plate displacement response at the first mode for the cantilever plate bonded to various number of sensor/actuator pairs in the optimal locations, $K_p = 24, K_d = 12$

Figure 9.5 shows the steady state closed loop actuator feedback voltage for increasing numbers of sensor/actuator pairs at the first mode. It can be seen that the increase in the number of sensor/actuator pairs gives a small reduction in the feedback voltage to actuator 01, but increases in the summation of the overall actuator feedback voltage and hence power in each case.

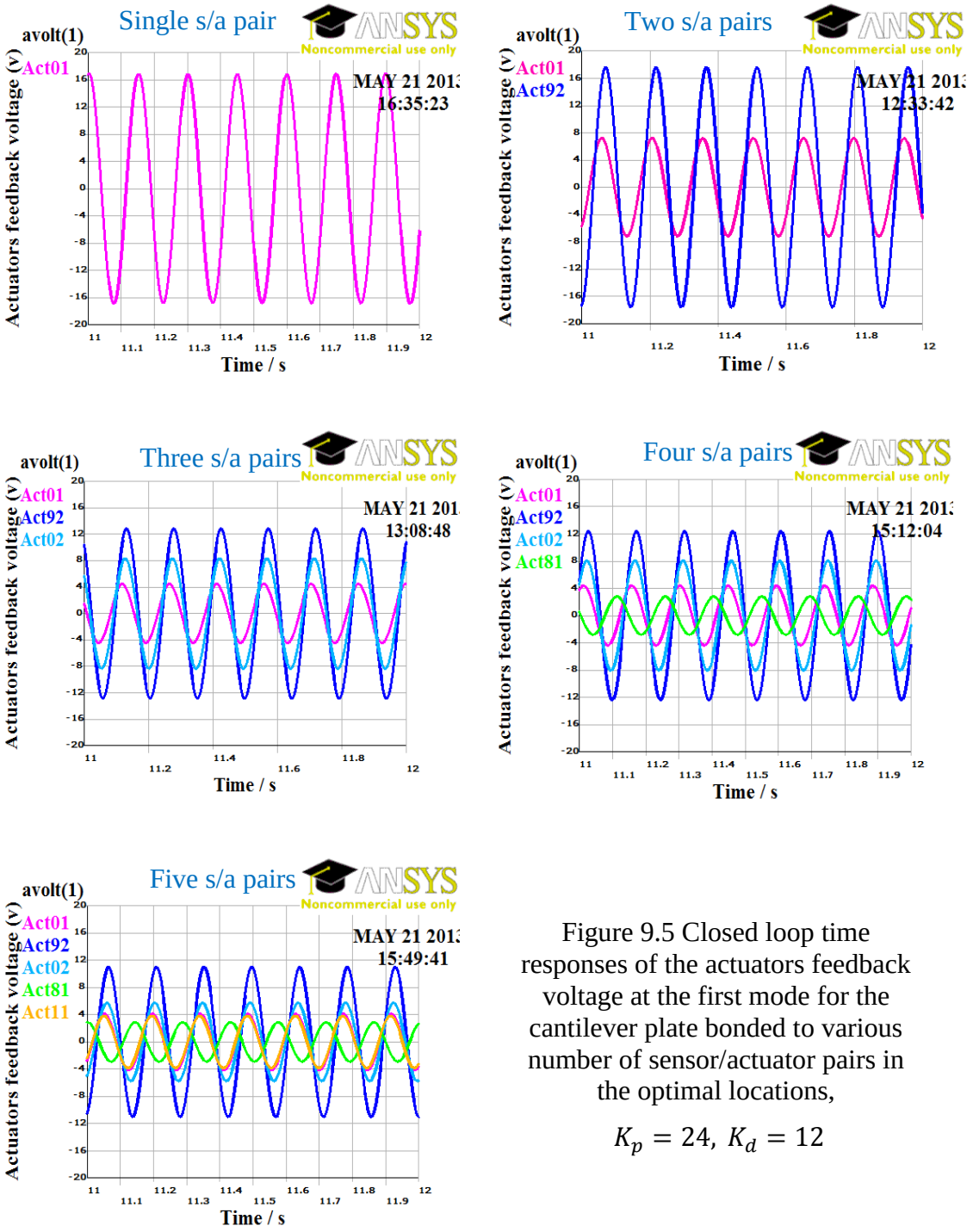

Figure 9.5 Closed loop time responses of the actuators feedback voltage at the first mode for the cantilever plate bonded to various number of sensor/actuator pairs in the optimal locations,

$K_p = 24,\ K_d = 12$

Figure 9.6 shows the open and closed loop acceleration time responses at the same point on the cantilever plate for various numbers of sensor/actuator pairs at the second mode. It can be seen from the figure that there is again a large improvement in closed loop vibration attenuation using one sensor/actuator pair, and little further improvement using two pairs, while negligible improvements occur using higher numbers compared to the reduction obtained with one or two sensor/actuator pairs.

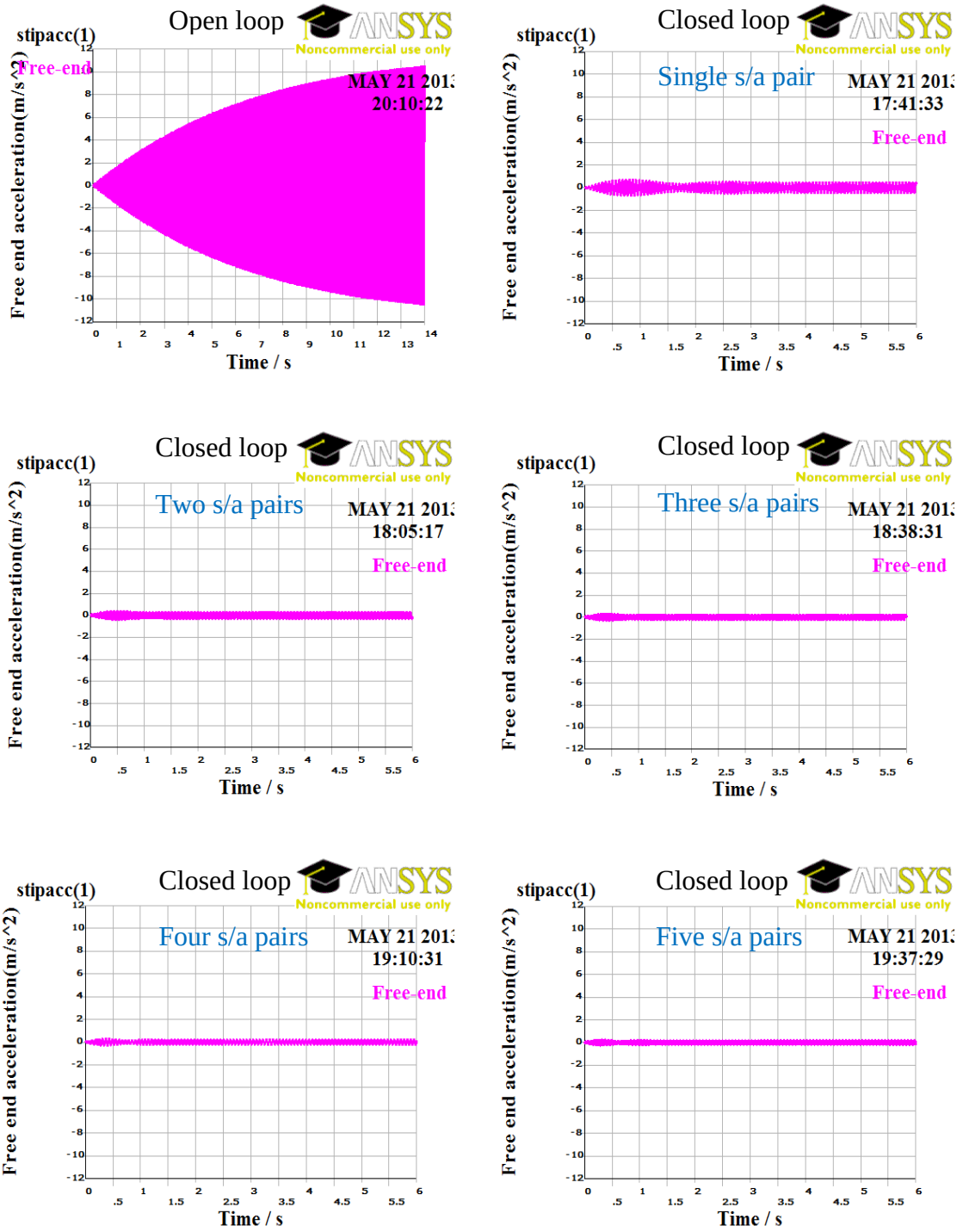

Figure 9.6 Open and closed loop time responses for the free end plate displacement at the second mode for the cantilever plate bonded to various number of sensor/actuator pairs in the optimal locations , $K_p = 24$, $K_d = 12$

Figure 9.7 shows the steady state closed loop actuator feedback voltage time response at the second mode against the increase in the number of sensor/actuator pairs. It can be seen that the increasing in the number of sensor/actuator pairs gives little reduction in the feedback voltage to actuator 01, and required considerable voltage, and hence power, for the added actuators.

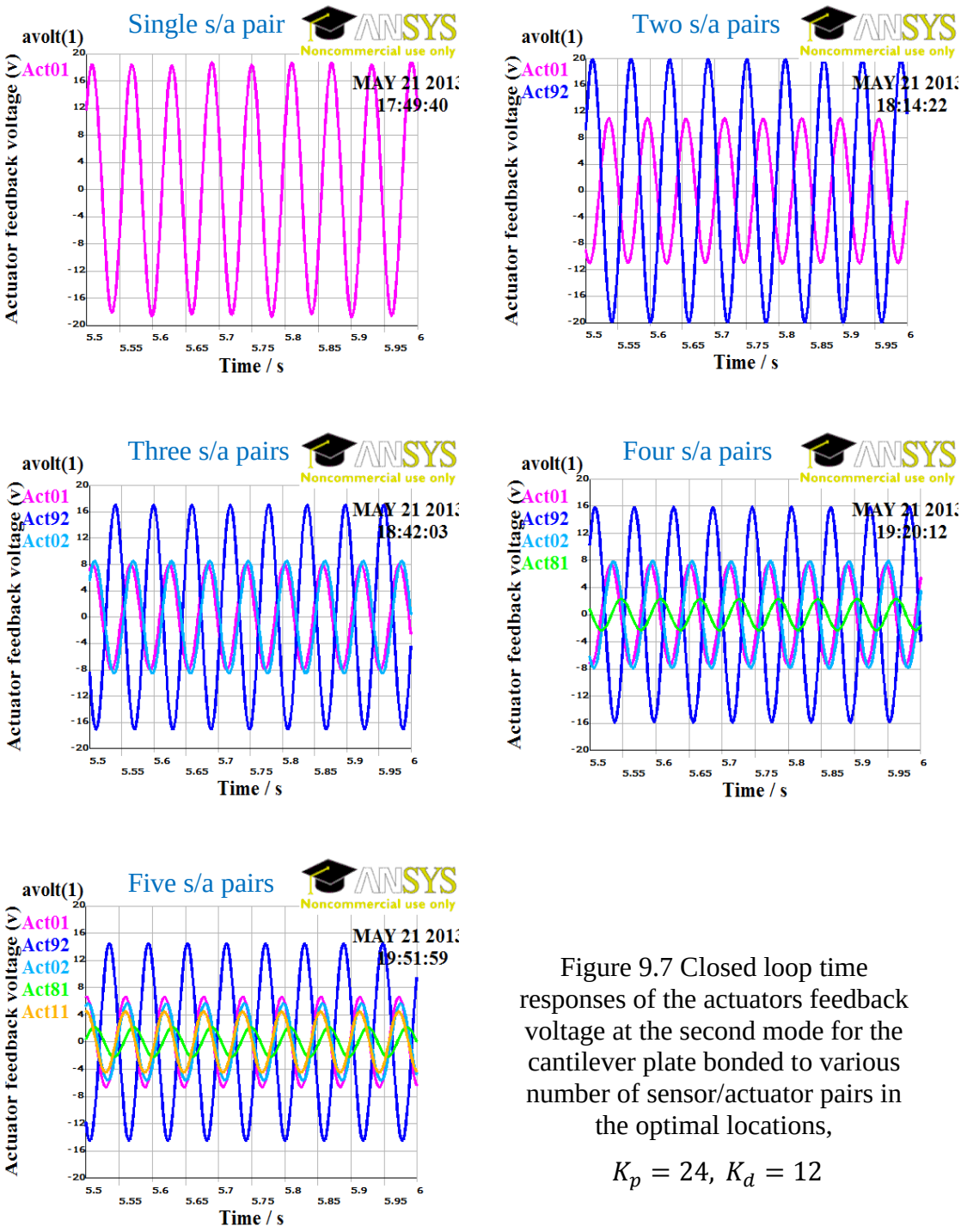

Figure 9.7 Closed loop time responses of the actuators feedback voltage at the second mode for the cantilever plate bonded to various number of sensor/actuator pairs in the optimal locations,

$K_p = 24,\ K_d = 12$

These ANSYS results shown in the Figure 9.4 to Figure 9.7 are summarised in Table 9.4 and Table 9.5 and compared with the results obtained in section 5.6.10 (Table 5.5 and

Table 5.6) for the first and second mode respectively. It can be seen from Table 9.4 (at feedback gain K_p=24 ,K_d=12) that there is a very large vibration reduction of 88.46% at the first mode using a single sensor/actuator pair, while a further improvement to 95.38% occurs using two pairs. However, negligible further reduction is achieved with more than two pairs. On the other hand, the overall actuator feedback voltage is increased by 64.7% at the first mode using five actuators compared with that using a single optimally placed sensor/actuator pair.

Table 9.4 also shows a comparison study between this chapter and the results obtained in section 5.6.10 using ten sensor/actuator pairs. In this chapter, the vibration reduction using a single optimally placed sensor/actuator pair found to be greater than that using ten sensor/actuator pairs. This indicates and shows that the effectiveness of optimising the number and location of sensor/actuator pairs and the effectiveness of increasing the feedback gain are much more than increasing in the number of sensor/actuator pairs.

Table 9.4 Percentage vibration reduction against number of sensor/actuator pairs in the optimal locations for the first mode using ANSYS finite element package

Case	Number of sensor/actuator pairs in optimal locations					
	Feedback gain K_p=24 ,K_d=12					K_p=12,K_d=6
	1 pair	2 pairs	3 pairs	4 pairs	5 pairs	10 pairs
Closed loop maximum amplitude($m.s^{-2}$)	0.15	0.06	0.043	0.045	0.038	0.1
Percentage reduction%	88.46	95.38	96.69	96.53	97.53	87.62
Total voltage consumption (V)	17	24.5	24.5	27	28	21.24
Percentage increased in feedback voltage %	-	44.1	44.1	58.8	64.7	24.9

Table 9.5 shows similar effects when controlling the second mode of vibration.

Table 9.5 Percentage vibration reduction against number of sensor/actuator pairs in the optimal locations for the second mode using ANSYS finite element package

Case	Number of sensor/actuator pairs in optimal locations					
	Feedback gain K_p=24 ,K_d=12					K_p=12,K_d=6
	1 pair	2 pairs	3 pairs	4 pairs	5 pairs	10 pairs
Closed loop maximum amplitude($m.s^{-2}$)	0.48	0.28	0.228	0.208	0.17	0.46
Percentage reduction%	95.42	97.33	97.86	98.01	98.38	92.9
Total voltage consumption (V)	18	31	33	34.1	33.2	30.85
Percentage increased in feedback voltage %	-	72.2	83.3	89.4	84.4	71.3

It can be concluded from this section that increasing the number of sensor/actuator pairs gives little advantage provided if they are correctly located. On the other hand, it has many drawback effects, such as increasing material costs, weight, overall feedback voltage, computational effort and adding more complexity to the control system. The results in this section validate the correctness of the developed fitness and objective functions in finding the optimal location and number of sensor/actuator pairs and feedback gain.

9.6. Conclusions

The optimisation of placement, feedback gain and numbers of piezoelectric actuators using the genetic algorithm has been investigated for the attenuation of the first six modes of vibration of an isotropic cantilever plate. The sensor/actuator placement and feedback gain are optimised based on the minimisation of the linear quadratic index as an objective function in the first stage of the genetic algorithm. In this work, fitness and objective functions are developed to determine the optimal number of piezoelectric actuators based on variations in closed loop dB gain reduction with respect to the number of optimally located piezoelectric pairs using the optimal linear quadratic control scheme and taking the average effects of all optimal piezoelectric pairs and all modes to be attenuated. It has been shown that a few sensor/actuator pairs give effective vibration reduction over the first six modes, where just two pairs in optimal locations give almost the same level of attenuation up to five pairs.

The results are validated by investigating the open and closed loop responses using the ANSYS finite element package and implementing the proportional differential control scheme. Negligible improvements were shown in vibration reduction as the number of sensor/actuator pairs was increased to more than two. Furthermore, the actuator feedback voltage increased by 64.7% at the first mode and 84.4% at the second mode using five sensor/actuator pairs compared with using just one.

This study is compared with the results obtained in chapter five. It was found that the vibration reduction using one sensor/actuator pair is higher and uses lower feedback voltage than using ten pairs. This indicates that the increase in feedback gain has much effect on vibration reduction at lower feedback voltage if the number of sensors and actuators are optimised and located properly.

Chapter 10. Experimental Apparatus, Methods and Results

An experimental rig was constructed to validate the optimal number and location of sensor/actuator pairs bonded to a cantilever flat plate based on the findings in chapter nine. A single sensor/actuator pair in the optimal location 01 was bonded on the same cantilever flat plate as used in the previous chapters to attenuate vibration, while the plate was driven by an actuator at location 91. An electronic board was built for converting an electric charge induced on the top surface of the sensor electrode to voltage and to manipulate this voltage and send it to the input port of the microcontroller. An Arduino MEGA3 2560 microcontroller board was selected for its low cost and high functionality. Another electronic board was built to convert the controller's digital output to analogue voltage in a form suitable to send to the piezoelectric high voltage driver and then to the actuator in order to suppress vibration. The plate was driven in the resonance plate modes and after the vibration reached the steady state maximum amplitude then the controller was activated.

10.1. Experimental Apparatus

The rig was constructed and the flat plate mounted vertically as a cantilever on a heavy cast iron bed, as shown in Figure 10.1. A single piezoelectric sensor/actuator pair was bonded to the plate at the optimal location 01 on the cantilever plate for sensing and attenuating external mechanical vibration. Another single actuator was located at position 91 on the plate in order to generate an external mechanical vibration by applying a sinusoidal voltage to drive the plate at natural frequencies. The rig is composed of the following elements listed in Figure 10.1:

1. A cast iron block was fixed on a heavy cast iron bed.
2. The flat steel plate mounted upward as a cantilever.
3. Single actuator bonded at the optimal location on the plate for driving the plate in normal modes of vibration.
4. Single piezoelectric sensor/actuator pair bonded at the optimal location on the plate for sensing and attenuating mechanical vibration.

5. A charge amplifier with voltage manipulator was built to convert the electric charge from the sensor into voltage to be manipulated in the specified range 0-3.3V, according to the microcontroller input signal requirements.
6. Microcontroller board type ARDUINO MEGA3 2560
7. A digital to analogue converter and voltage manipulation board was built to generate analogue voltage and to send it to the controller driving unit type E-500.

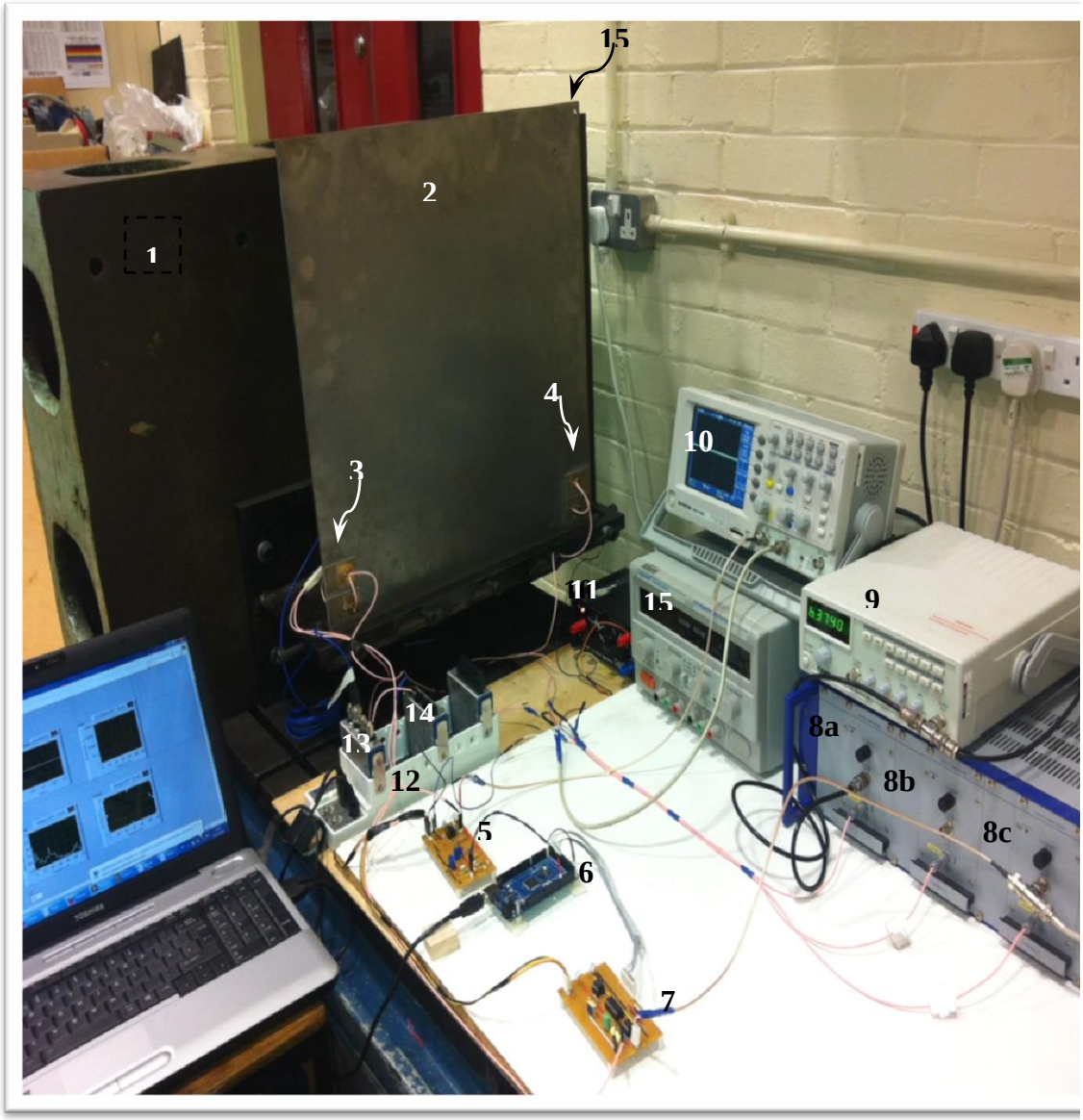

Figure 10.1 Vibration attenuation testing rig

8. Controller voltage driver unit type E-500 series PZT servo controller with three individual units; each of which can be driven a single actuator. The driver unit has a range of gain settings using a selectable jumper.
9. A function generator type TENMA serial No. 72-7710 was used to generate a sinusoidal voltage at natural frequencies to drive the plate at normal modes

using a driving unit E-500. The accuracy of this function generator is $1^{\pm 0.5}$ Hz. whereas the experimental work requires a function generator with high accuracy and at least three digits resolution to drive the plate in natural frequencies.

10. An oscilloscope used for observing and monitoring any point in the system.
11. DC power supply.
12. National Instruments Compact DAQ type cDAQ-9178 was used to insert NI-9234 module to acquire accelerometer signal, and NI-9239 to acquire the sensor output and controller feedback voltage signal.
13. National Instrument module NI-9234 used to acquire the accelerometer signal.
14. Accelerometer type PCB model 352C68 fixed on the free end plate corner.
15. DC power supply.

A schematic diagram of the experimental rig is shown in Figure 10.2 and the experiment works as follows;

1. The experiment starts by setting the function generator to produce a sinusoidal voltage with a particular frequency and amplitude; this signal passes through a high voltage driving unit E-500, and is then applied to the actuator location 91 on the plate in order to drive the plate in its resonance frequencies, as shown in Figure 10.2.
2. The sensor at location 01 on the plate starts to detect vibration and electric charge is generated on its surface. This electric charge passes through a charge to voltage converter board. This board also includes a voltage manipulator to set the voltage according to the microcontroller's maximum input voltage. This sensor voltage is sent to three locations: to be displayed on the oscilloscope; to NI-9239 module to display it on the laptop; and to the microcontroller.
3. The microcontroller modifies the sensor voltage signal according to the built-in control software and produces digital 8-bits signals as shown in Figure 10.2. These are sent to a digital to analogue converter board. The output voltage of this is sent to three locations: to display it on the oscilloscope and to the NI-9239 module to display on the laptop; and to the high voltage driving single E-500 and then to the actuator at location 01 on the plate to apply the opposite strain in order to suppress the vibration.

4. The vibration signal is displayed on the laptop by acquiring the accelerometer signal located on the plate at the free end after it has passed through the NI-9234 module, as shown in Figure 10.2.

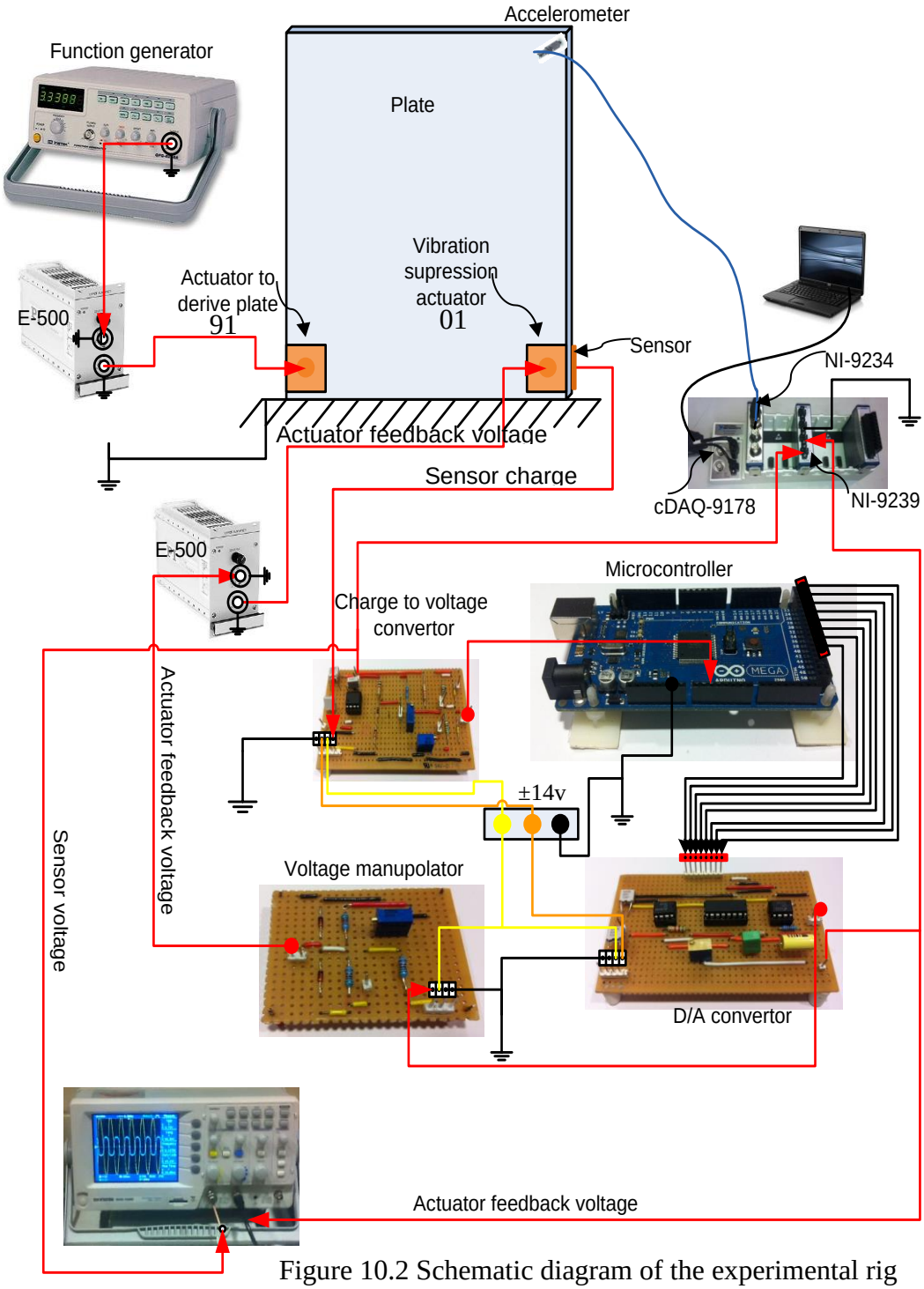

Figure 10.2 Schematic diagram of the experimental rig

10.2. Piezoelectric Sensor and Actuator

Piezoelectric material generates electrical charge when subjected to external load and vice versa. This property makes this material suitable for use in sensors and actuators. Piezoelectric ceramic material type PIC255 of 0.5mm thickness was supplied by the PI Ceramic Company and used in the experimental work. PIC255 is a modified soft piezoelectric ceramic material optimised for actuator application under dynamic conditions and high ambient temperature. The tensile stress should not exceed 10Mpa during gluing/assembly or operation or both and the voltage applied to the piezoelectric material should not lie outside the range between -200 and +1000 V. The plate's piezoelectric element contains an electrode and ground terminals. The piezoelectric plate is covered with metal alloy of a CuNi composite with noble metals such as gold as an electrode at a range of thickness between 1-10μm using either screen printing to generate a thick film electrode of 10μm or spluttering techniques to produce thin film electrode of 1μm. The adhesion strength of the electrode to the piezoelectric plate is around 5MPa. Depolarisation losses or degradation could occur when the piezoelectric sensor and actuator is subjected to excessive electric fields, or mechanical strain or temperature [109].

10.3. Piezoelectric Electrode Soldering and Ground Bonding to the Plate

An important step in building the experimental rig was the soldering of the positive electrode of the piezoelectric elements to a wire terminal and bonding the piezoelectric ground to the plate. The electrode of the piezoelectric transducer was connected to wire terminals using tin wire soldering, and the piezoelectric ground was bonded to the plate using two types of epoxy. The electrode of the piezoelectric transducer can be attached to the wire terminal using either conductive epoxy or direct tin soldering. The first method using conductive epoxy is safer and easier to apply onto the top of the electrode than the second method using direct soldering. The heating temperature of direct soldering has an effect on piezoelectric performance, which is limited to 350^0 C and held for a short time interval of 1-2 seconds. The direct soldering method can also be applied for the piezoelectric ground.

10.3.1. Direct soldering method

The piezoelectric transducers elements were supplied by the PI Ceramic Company manufacturer. The supplier gives the following specifications that can be used in the soldering process[109].

Solder: made of the system L-Sn95-97, Ag3-4, Cu0.5-1

Flux: defined as 1.1.1 or 1.1.3 according to DIN EN 29454 Part1;

or defined as ROLO or ROMO according to ANSI J-STD-004.

The following steps were taken in the soldering process according to the PI Ceramic Co. instruction:

1. The end of the wire was stripped end, twisted and tinned and then trimmed to 1-2 mm as shown in Figure 10.3.
2. The flux was applied to the tinned end and the pre-tinned point on the electrode surface. The wire was held and kept flat with its end at that point on the electrode surface.
3. The wire soldering tip was coated with a small amount of solder; where the soldering temperature must not exceed 350^0C. The soldering tip was held against the wire tinned end for 1 to 2 seconds, until the solders flowed. The solder joint must be flat or hemispherical.
4. The residual flux was removed by a cleaning process using ethanol.

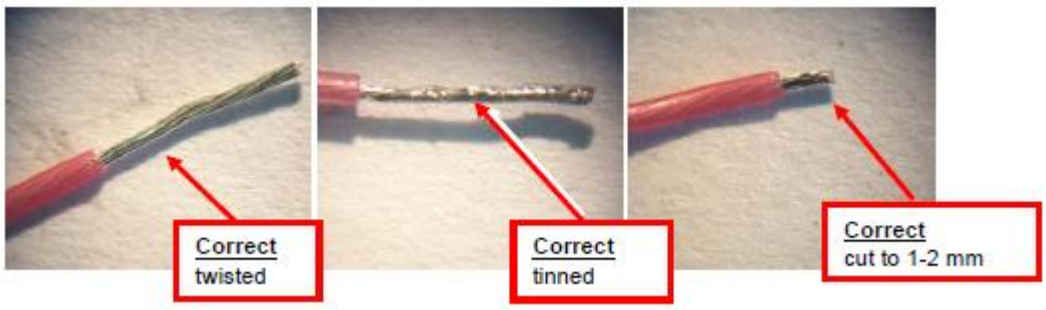

Figure 10.3 Wire stripped, twisted, tinned and trimmed [109]

10.3.2. Conductive epoxy method

This method used the following two steps:

1. A thin copper flat plate 1-4cm^2 in area was used for soldering a wire terminal directly on top of it.
2. Silver loaded epoxy was used for bonding the copper plate to the top of the piezoelectric electrode surface by putting a small amount on the bottom surface of the copper plate and then bonding the two together as shown in Figure 10.4.

Figure 10.4 Piezoelectric electrode before and after bonding to a copper flat plate

The ground of the piezoelectric electrode was bonded to the plate using two types of epoxy; conductive silver loaded and Araldite epoxy. This process was performed as follows:

1. The top surface of the plate was cleaned using isopropanol to remove oil contamination, and then the surface topography was roughened using abrasive paper. This improves the surface adhesion of the silver epoxy to the steel plate surface.
2. A small amount of silver epoxy was mixed and put on the centre of the top surface of the electrode ground as shown in Figure 10.5, while the remaining area was coated with conventional Araldite two-pack epoxy. Then the piezoelectric ground surface was bonded to the plate.

Figure 10.5 Piezoelectric ground before and after being coated with silver epoxy on the centre of the area

These two types of electrode connection to the wire terminal were used in this experiment. The second method was found to be both simpler than the first, requiring less skill, and safer than direct soldering.

10.4. Electronic Circuit for the Charge Amplifier and Voltage Manipulator

The electronic circuit of the charge amplifier and voltage manipulator are shown in Figure 10.6. The electronic circuit is composed of three parts. The first part of the electronic circuit converts the electric charge induced on the top of the piezoelectric sensor electrode area into voltage V1 [110]. The second part of the electronic circuit trims the output voltage of the charge amplifier V1 to the maximum voltage amplitude V2 in order to protect the controller board. The last part of this circuit gives a positive DC shifting to the sinusoidal voltage V2 and trims it to between 0 and 3.3 volt, according to the requirements of the controller analogue input board. The equations of the electronic circuit are:

$$V1 = -\frac{1}{C_f}\int Idt = -\frac{Charge}{C_f} \quad 10.1$$

$$V1 = V2 \quad 10.2$$

$$V3 = V2 * R1/R2 \quad 10.3$$

$$V5 = (V3 + V4)/2 \quad 10.4$$

The electronic circuit was built on the board as shown in Figure 10.7. This board was connected between the piezoelectric sensor electrode terminal and the controller board input port.

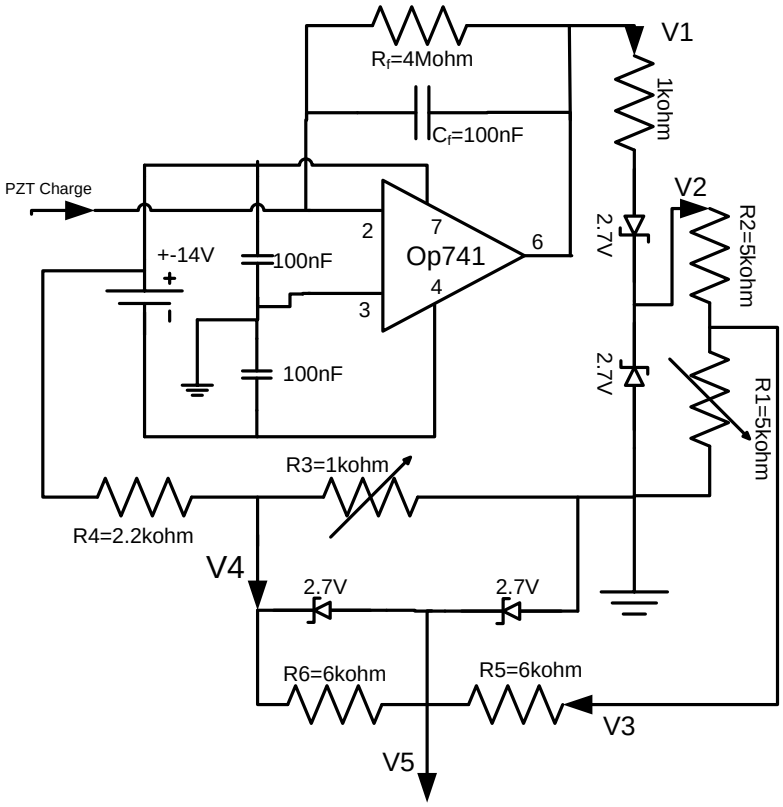

Figure 10.6 Electronic circuit of charge voltage converter and manipulator, the output of this circuit is a positive sinusoidal wave limited between 0-3.3V

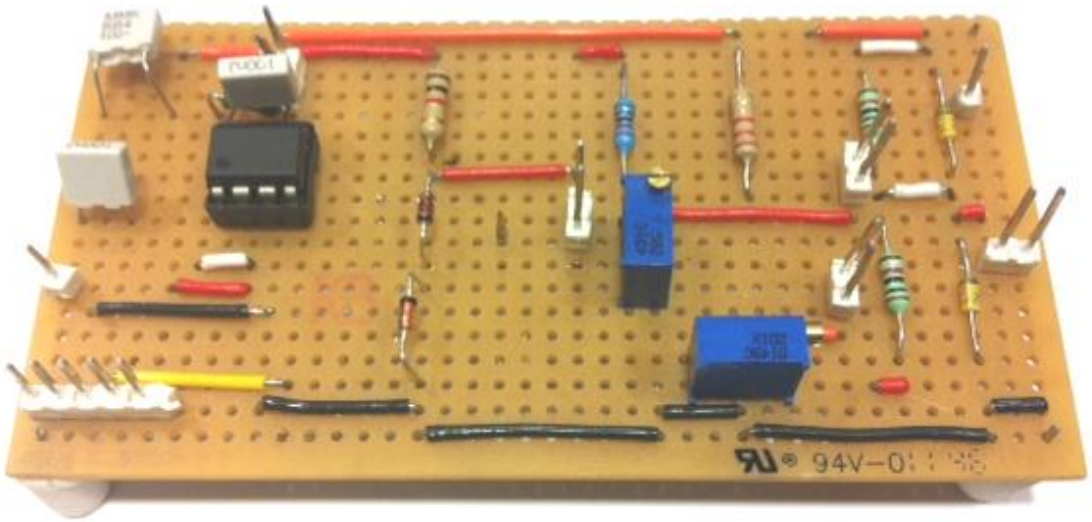

Figure 10.7 Charge voltage converter and voltage manipulator electronic board, the output of this circuit is positive sinusoidal wave limited between 0-3.3V

10.5. Microcontroller Electronic Boards

The Arduino microcontroller board which is based on the ATmega 2560 was used in the experimental test. The controller board has 16 pins analogue inputs, 40 digital input/output pins, 14 pins PWM outputs and 4 pins for the hardware serial port. The board has a 16 MHz crystal oscillator, a USB connection, a power jack, an ICSP header and a reset button. The Arduino ATmega 2560 processor can be programmed with Arduino software and comes preburned with a bootloader that allows a new code to be uploaded to it without the use of an external hardware programmer. Moreover, the Atmega2560 can be connected with MATLAB and downloads simulink directly to the controller. The Arduino board is cheap at £20, functional and simple to use. The main hardware features are:

1. Microcontroller : ATMEGA2560
2. Operating voltage 5V
3. Input voltage : 7-12V
4. Digital I/O 54 (14 provide PWM outputs)
5. Analogue input pins: 16
6. DC current per I/O pin :40mA
7. DC current for 3.3v Pin: 50mA
8. Memory : flash 256 kB, sram 8 kB, efprom 4 kB
9. Clock speed: 16 MHz

Figure 10.8 Microcontroller board type ARDUINO MEGA 2650

The controller board has an internal built-in A/D converter while the output voltage signal of the board is digital. Therefore, a digital to analogue converter (DAC) interface is required between the controller board and the E-500 high voltage piezoelectric driver unit.

10.6. Electronic Circuit of D/A Converter and Voltage Manipulator

The electronic circuit diagram of the digital to analogue voltage converter in the data sheet of the DAC08 integrated circuit chip was used and some modifications added to it

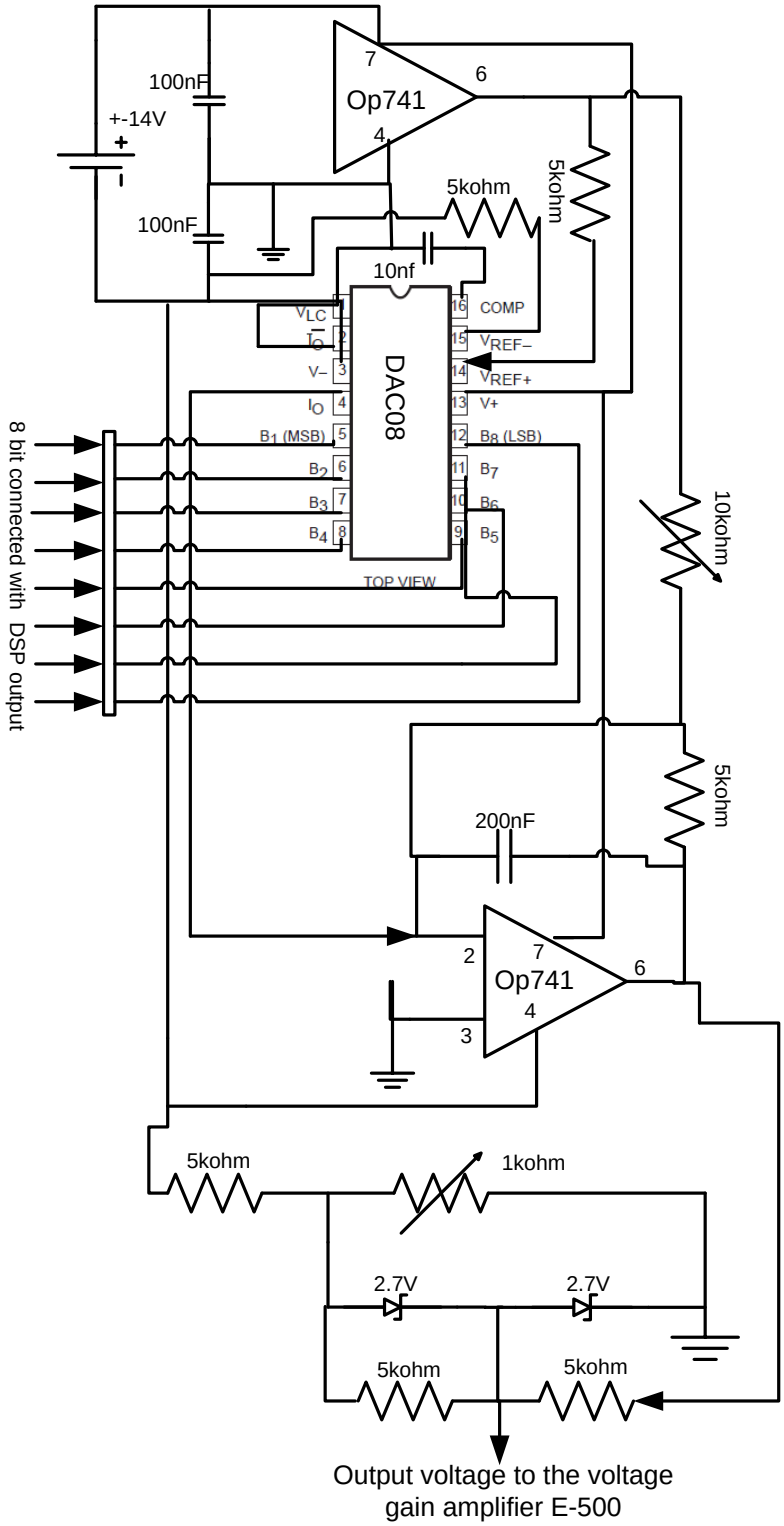

Figure 10.9 Electronic circuit diagram of digital to analogue voltage convertor and manipulator

according to the requirements of the experimental work as shown in Figure 10.9. The first part of the electronic circuit converts eight bits 0-1 to analogue, and was taken from the data sheet of the DAC08. The second part of the electronic circuit gives a negative DC shifting to the output voltage of the first part. The electronic circuit was built on the board as shown in Figure 10.10.

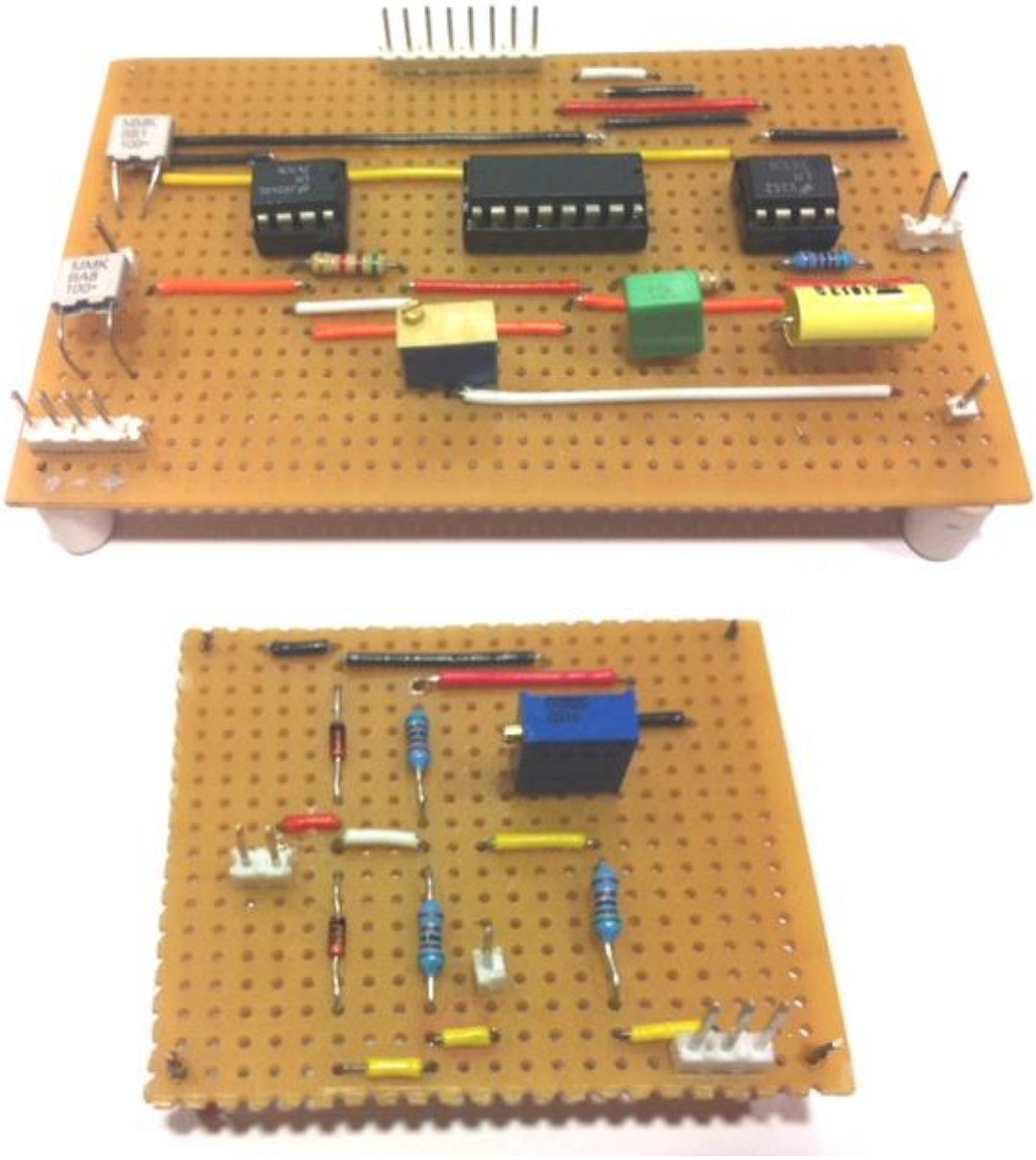

Figure 10.10 Electronic board of digital to analogue convertor and voltage manipulator

10.7. Experimental Results

10.7.1. Problem descriptions

Vibration attenuation was investigated for the same cantilever flat plate used in chapter nine with a single piezoelectric sensor/actuator pair bonded to the optimal location 01 on the plate. The piezoelectric sensor and actuator dimensions were $6 \times 5cm$ and their properties are listed in Table 4.1. The plate was driven by sinusoidal voltage $20sin\omega t$ at natural frequencies on the actuator at location 91 on the plate. The testing rig is shown in Figure 10.1.

10.7.2. The key challenge of the experimental work

The key challenges of the experimental work were the quality of the piezoelectric material, the strength of the bonding epoxy and the method of bonding the piezoelectric patches to the plate. The material properties and effectiveness of the piezoelectric sensor and actuator were reduced after bonding. Some of them did not fully work after bonding, while the effectiveness of others was reduced and this worsened after a number of experimental tests so that they also eventually stopped working. Removing non-functioning piezoelectric patches was difficult due to the high bonding strength of the silver load epoxy, and could only be done by grinding. Problems which occurred during and after the bonding of sensors and actuators were as follows:

1. Two sensor/actuator pairs of dimensions $3 \times 5cm$ were bonded to the plate, but one of them was found to be not working and it was then replaced with a new one. The process of removing of the idle piece was difficult and might have had effect on its pair.
2. An additional two sensor/actuator pairs were added and bonded to increase the dimensions of the individual piezoelectric from $3 \times 5cm$ to $6 \times 5cm$ and in order to make the dimensions close to the piezoelectric dimensions used in the previous theoretical investigation. However, one piezoelectric of dimension $6 \times 5cm$ was found to be not working directly after bonding. The total number of working sensors and actuators bonded to the plate was three: a single piezoelectric pair was used for sensing and actuating for active vibration control and a single actuator was used for driving the plate at natural modes of vibration.

3. The capacitance value of the piezoelectric of dimensions $5 \times 6cm$ was 95.4nF before bonding to the plate, and this was close to the theoretical value of 104.5nF. However the capacitance was reduced by 23% directly after bonding, indicating that the ferroelectric properties had been degraded.
4. During the experimental test, the vibration in the first mode was attenuated and was completely stopped using a single piezoelectric sensor/actuator pair, and this test was recorded as a video. However, the effectiveness of the piezoelectric actuator was reduced after a number of tests and the actuator used for vibration attenuation became completely non-functional, and in addition all values of piezoelectric capacitance were decreased as shown in Table 10.1.

Table 10.1 Piezoelectric capacitance value effects before and after bonding and after a number of experiments

Piezoelectric capacitance value/ nF	Sensor/actuator pair		Driving plate actuator
	sensor	actuator	
Experimentally, Before bonding	95.4	95.4	95.4
Theoretically	104.5	104.5	104.5
After bonding	74	71	73.5
After doing number of experimental tests	63.3	47.6 (s. w.)	64.5

10.7.3. Non -functional piezoelectric solution

The piezoelectric manufacturer PI Ceramic Company was informed about these problems, and suggested the following solutions.

1. Any elevation in temperature in order to increase the speed of epoxy curing time should be prevented.
2. The piezoelectric patches might have cracked and this might be prevented by using thicker patches.
3. The thin copper shim used to make contact as (shown in Figure 10.4) should be enlarged to cover the whole surface area of the positive electrode to ensure that a

full electrical connection exists in case any cracks occur during bonding or in the experimental tests.

4. The surface area of conductive epoxy used to make contact with the piezoelectric ground (as shown in Figure 10.5) should be increased to cover the whole area of the piezoelectric ground which is bonded to the plate, in order to ensure that the electrical connection exists at all points of the piezoelectric ground again in case any cracks occur.
5. In this work, the most significant cause of actuator degradation and failure was the activation of the controller after the amplitude of vibration reached the maximum at steady state. This led the controller to produce high peak voltage at activation for a short time (a transient state) which progressively increased actuator degradation and failure. This problem can be eliminated by setting the controller always to the active (ON) condition before drive the plate at natural frequencies in order to eliminate the effect of high peak voltage.

10.7.4. First experiment

The experimental open and closed loop time responses were investigated for the cantilever plate with a single sensor/actuator pair bonded at the optimal location 01. The plate was driven at actuator location 91 at the first mode natural frequency by a sinusoidal voltage ($40sin\omega_1 \times t$). After the amplitude of vibration reached a steady state, the controller using a proportional differential control scheme was activated, stopping the vibration rapidly. In this test, high sinusoidal voltage amplitude of 40V was used to drive the plate at the first mode in order to see clearly the amplitude of vibration by the naked eye. This test was repeated more than ten times for purposes of inspection and was recorded as a video which is attached to the thesis.

Oscilloscope pictures for the open and closed loop time responses of sensor and actuator voltage were taken from the recoded video, as shown in Figure 10.11. Figure 10.11 (a) shows the open loop sensor voltage time response at steady state. The controller was then activated as shown in Figure 10.11 (b). In this experiment, the actuator feedback voltage was limited to a maximum value of ±150V to protect the microcontroller and piezoelectric material.

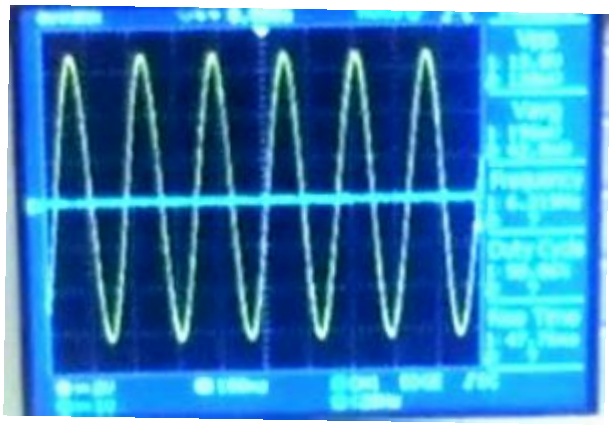

Sensor voltage

Actuator voltage

(a) Steady state time response sensor voltage

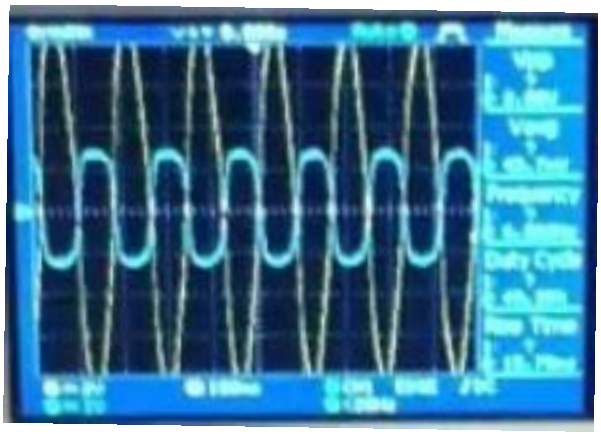

Sensor voltage

Actuator voltage

(b) Controller is activated

Subsequently, the closed loop sensor and actuator feedback voltage amplitude were dropped as shown in Figure 10.11 (c), and finally reached the steady state shown in Figure 10.11 (d). The plate vibration was reduced and eliminated completely and the sensor voltage was reduced by 89% where the actuator feedback voltage was about 40V at the steady state, as can be seen in the complete events of this test in the attached video.

Sensor voltage

Actuator voltage

(c) Transient closed loop time responses of sensor voltage and actuator feedback voltage

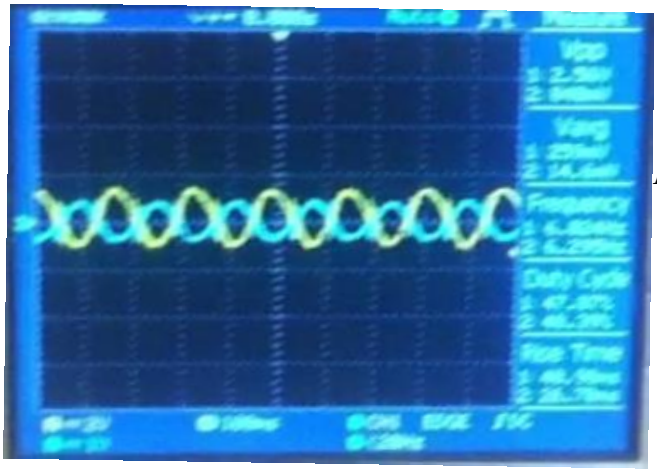

Sensor voltage

Actuator voltage

(d) Steady state closed loop time responses of sensor and actuator feedback voltage

Figure 10.11 Experimental vibration suppression of the cantilever plate at the first mode

.

10.7.5. Second experiment

In the second experiment, the plate was driven by a sinusoidal voltage ($20sin\omega \times t$) at the first, second and third modes. The vibration reduction for the first three modes was tested and the results for the sensor/actuator voltage and free end plate acceleration were acquired in LabView software using the same control scheme as in the first experiment. Figure 10.12 shows the open and closed loop time responses at the first, second and third modes, for a point located on the free end plate corner. The closed loop free end plate acceleration was attenuated by 50%, 44.44% and 73.6% at the first, second and third mode respectively.

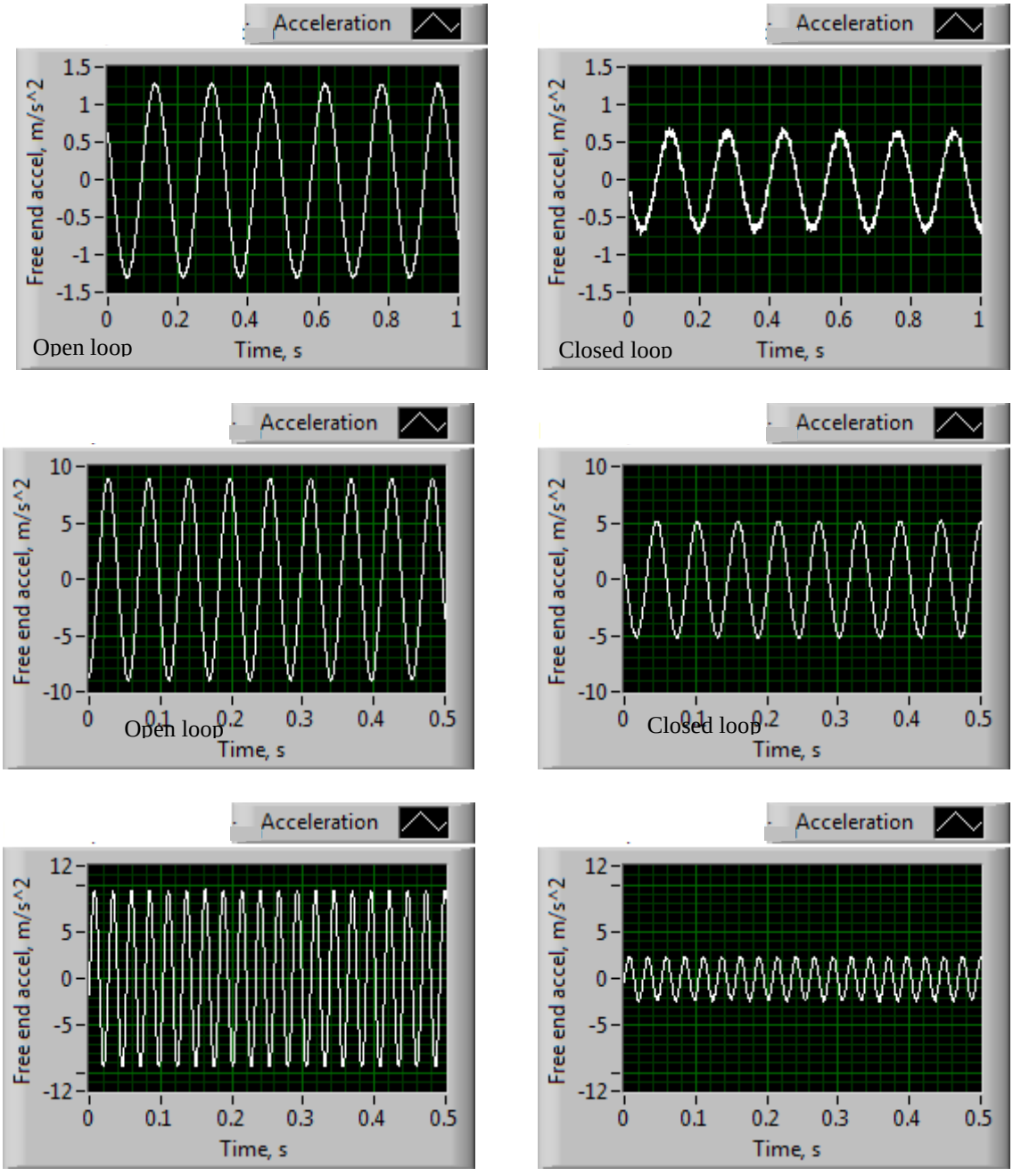

Figure 10.12 Experimental open and closed loop free end plate acceleration responses in the first, second and third mode

The effectiveness of the actuator during the second experiment was significantly reduced to the first experiment, as shown by 50% vibration reduction (compared with 100%) in the first mode. It is believed that this is caused by the large feedback voltage applied by the controller in the first experiment.

Many studies have investigated piezoelectric degradation over time as a result of various cycling load, and electric field. The National Physical Laboratory has reported that soft piezoelectric material is more sensitive than hard material when subjected to repeated electric stress, and even under static mechanical load suffers more rapid change in properties [111]. Chen et al reported that the properties of piezoelectric material clearly degrade over their lifetime as a result of working under high strain and electric field, and sometimes fail suddenly during service. Application of high electric voltages to an actuator can cause microcracks as a result of sizable mechanical vibrations, and the progression of cracks causes damage to the actuator [112].

In this experiment, vibration was reduced and completely eliminated at the first mode using a single sensor actuator pair, and by 44.44% and 73.6% at the second and the third modes using a single sensor/actuator pair with degraded properties.

10.8. Conclusions

In this chapter, a cantilever flat plate with a single sensor/actuator pair bonded at the optimal location 01 was driven experimentally in its various resonant modes by a sinusoidal voltage applied to the actuator at location 91. A piezoelectric sensor charge to voltage converter and voltage manipulator were built and connected to a microcontroller board, Arduino ATMEGA3 5060. An electronic interface board between the controller and voltage driver was built to convert the digital signal to analogue and for voltage manipulation. The key challenge of the experimental rig was bonding the piezoelectric elements to the plate.

In the experimental test, the plate was driven in the first mode and after the amplitude of vibration reached the steady state, the controller was activated. The amplitude of vibration was completely eliminated using this single sensor/actuator pair at the optimal location. This test was repeated more than ten times and recorded as a video. However, during these experimental tests, the effectiveness of the feedback actuator was reduced apparently due large voltage applied to it in early experiments.

The experimental test was continued, testing vibration in the other modes. The vibration was reduced by 44.44% and 73.6% at the second and the third modes using the single sensor/actuator pair with degraded properties.

Chapter 11. Conclusions and Future Work

In this study, active vibration reduction by optimally placed sensors and actuators was investigated for stiffened and unstiffened plates by beams with various geometries and fixations. The main achievements of this work are as follows:

1. A finite element model was developed for a stiffened plate incorporating piezoelectric elements bonded to its surface. The model uses isoparametric quadrilateral four node elements for the plate and piezoelectric transducers and isoparametric two node beam elements for the stiffeners fixed on the plate element edges. The modelling is based on first order shear deformation theory and Hamilton's principle. The importance of this model is that it can be used to investigate the dynamic behaviour of flat plates with any number of discrete sensors and actuators and with any arrangement of stiffeners passing through plate element nodes.
2. A genetic algorithm placement strategy was proposed to optimise actuator location and feedback gain for active vibration reduction based on the minimisation of the linear quadratic index as an objective function. A MATLAB m-file computer program was written to optimise positions of various numbers of sensor/actuator pairs and feedback gain for a cantilever plate. The optimal sensor/actuator configuration was found to be symmetrically distributed about the axis of symmetry of the plate and this agreed with the results for the modal electric charge distribution over the piezoelectric surface achieved using the ANSYS package. The optimal symmetrical piezoelectric configuration gave higher vibration suppression than previously published asymmetrical sensor/actuator distribution which was claimed to be optimal. The results were validated using open and closed loop time responses by implementing optimal linear quadratic control and proportional differential control schemes in the ANSYS package.
3. New fitness and objective functions were developed based on modified H_∞ to optimise sensor location. The same cantilever plate used in the rest of this study was tested to optimise ten sensor/actuator pairs using the new objective function. The optimal piezoelectric configuration was also found to be symmetrically distributed about the plate's dynamic axis of symmetry in spite of using this new

objective function. The objective function reduced the search space greatly and gave good vibration reduction compared to the previous studies.

4. A new topic including the effect of dynamic axes of symmetry of a structure on the global optimal distribution of sensors and actuators was investigated for unstiffened and stiffened plates arranged with various symmetries in geometries and fixations. The global optimal configuration was found to follow the structural dynamic axes of symmetry.
5. A new half- and quarter-chromosome technique was developed based on the finding that the global optimal configuration of sensors and actuators followed the structural dynamic axes of symmetry. The use of this technique greatly reduced the search space of the optimisation problem and holds great potential for finding global optimal solution to large-scale mechanical structures after a small number of generations.
6. New fitness and objective functions were developed using optimal linear quadratic control to optimise the feedback gain and the number and location of sensor/actuator pairs based on the closed loop frequency response. It was found that two sensor/actuator pairs in the optimal locations gave almost the same level of vibration reduction over the first six modes as up to five pairs.

11.1. Future Work

Future investigation in the area of active vibration control involves number of topics dealing with the optimisation of sensor and actuators, the type of structure considered and the theoretical and experimental application of different control schemes to suppress vibration. The following topics would be fruitful areas for future research.

1. The modelling can be extended to cover stiffened and unstiffened shell structures, so as to implement the placement strategies and objective functions used in this study.
2. In this study, the objective function based on open loop modified H_∞ was used to optimise the location of sensor/actuator pairs when the disturbance occurs at fixed location. This could be extended to cover moving disturbance and closed loop control.
3. Half and quarter chromosomes technique can be extended to cover another optimisation algorithms and applications.

4. New objective function could be developed to optimise piezoelectric area, location and feedback gain. These are based on chapter nine by extend the calculations based on the piezoelectric area in the first part of Table 9.2 and Table 9.3 .
5. Further improvements to the effectiveness of active vibration control by optimally located sensors and actuators might be investigated using optimal proportional differential, LQR and fuzzy neural control schemes.

11.2. Publications

1. Daraji, A.H. and J.M. Hale. *Optimisation of number and placement of piezoelectric sensor /actuator pairs for active vibration reduction of a flexible plate using the genetic algorithm*. 19th International Congress on Sound and Vibration 2012 2, ICSV 2012, pp. 1251-1266.
2. Daraji, A.H. and J.M. Hale. *A conditional filter for reduction of the search space in genetic algorithm optimisation of sensor and actuator location in active vibration control*. 19th International Congress on Sound and Vibration 2012, ICSV 2012 2, pp. 1199-1211.
3. Daraji, A.H. and J.M. Hale, *Active vibration reduction of a flexible structure bonded with optimised piezoelectric pairs using half and quarter chromosomes in genetic algorithms*. Journal of Physics: Conference Series, 2012. 382(1).
4. Hale, J.M. and A.H. Daraji, *Optimal placement of sensors and actuators for active vibration reduction of a flexible structure using a genetic algorithm based on modified Hinfinity*. Journal of Physics: Conference Series, 2012. 382(1).
5. Daraji, A.H. and J.M. Hale, *Determination of state space matrices for active vibration control using ANSYS finite element package* in Proceedings of the ASME 2012 International 24th Conference on Mechanical Vibration and Noise: Chicago, IL, USA.
6. Daraji, A.H. and J.M. Hale, *The effects of symmetry on optimal transducer location for active vibration control* in Proceedings of the ASME2012 International 24th Conference on Mechanical Vibration and Noise: Chicago, IL, USA.
7. Hale, J.M. and A.H. Daraji, *Active vibration reduction of stiffened plates with optimally placed sensors and actuators*. 2012. International Conference on Noise and Vibration Engineering (ISMA): Leuven Belgium.

References

[1] Mead, D.J., *Passive Vibration Control*. 2000, England: Wiley

[2] Rao, S.S., *Mechanical Vibration*. 3th ed. 1995, USA: Addison-Wesley.

[3] Cartmell, M., *Introduction to Linear, Parametric and Nonlinear Vibrations* 1st ed. 1990, Great Britain: Padstow Ltd.

[4] Preumont, A. and K. Seto, *Active Control of Structures* 2008, United Kingdom: Wiley

[5] Manjunath, T.C. and B. Bandyopadhyay, *Vibration control of Timoshenko smart structures using multirate output feedback based discrete sliding mode control for SISO systems.* Journal of Sound and Vibration, 2009. **326**(1-2): p. 50-74.

[6] Preumont, A., *Vibration Control of Active Structures* 3td ed. 2011, Chennai, India: Springer.

[7] Warminski, J. and K. Kecik, eds. *Nonlinear Dynamic Phenomena in Mechanics-Solid Mechanics and its Applications*. 2012, Springer Berlin Heidelberg. pp. 1-61.

[8] Zak, A.J., M.P. Cartmell, and W. Ostachowicz, *Dynamics of multilayered composite plates with shape memory alloy wires.* Journal of Applied Mechanics, Transactions ASME, 2003. **70**(3): p. 313-327.

[9] Cartmell, M.P., A.J. Zak, and O.A. Ganilova, eds. *Nonlinear Dynamic Phenomena in Mechanics-Solid Mechanics and its Applications*. 2012, Springer: Berlin Heidelberg. pp.115-158.

[10] Ganilova, O.A. and M.P. Cartmell, *An analytical model for the vibration of a composite plate containing an embedded periodic shape memory alloy structure.* Composite Structures, 2010. **92**(1): p. 39-47.

[11] Zak, A.J., M.P. Cartmell, and W.M. Ostachowicz, *A sensitivity analysis of the dynamic performance of a composite plate with shape memory alloy wires.* Composite Structures, 2003. **60**(2): p. 145-157.

[12] Zak, A.J., M.P. Cartmell, and W.M. Ostachowicz, *Static and Dynamic Behaviour of Composite Structures with Shape Memory Alloy Components*, M.P. Cartmell, Editor. 2003: Glasgow, Scotland. p. 345-352.

[13] Zak, A.J., et al., *One-dimensional shape memory alloy models for use with reinforced composite structures.* Smart Materials and Structures, 2003. **12**(3): p. 338-346.

[14] Su, X. and M.P. Cartmell, *Modifications to the response of a parametrically excited cantilever beam by means of smart active elements.* Proceedings of the Institution of Mechanical Engineers, Part C: Journal of Mechanical Engineering Science, 2010. **224**(8): p. 1579-1591.

[15] Banks, H.T., R.C. Smith, and Y. Wang, *Smart Material Structures: Modeling, Estimation, and Control* 1996, Paris: Wiley.

[16] Roh, J.H. and J.H. Kim, *Adaptability of hybrid smart composite plate under low velocity impact.* Composites Part B: Engineering, 2003. **34**(2): p. 117-125.

[17] Rediniotis, O.K., et al. *Active skin for turbulent drag reduction*. 2002.

[18] Jalili, N., *Piezoelectric-Based Vibration Control* 2010, Boston, USA: Springer

[19] Choi, S.-B. and Y.-M. Han, *Piezoelectric Actuators Control Applications of Smart Materials*. 1st ed. 2010, USA: CRC Press.

[20] *http://www.piezo.com/tech2intropiezotrans.html*.

[21] Rao, S.S., *Engineering Optimizaton Theory and Practice* 4th ed. 2009, New Jersy: Wiley

[22] Rao, S.S., T.-S. Pan, and V.B. Venkayya, *Optimal placement of actuators in actively controlled structures using genetic algorithms.* AIAA journal, 1991. **29**(6): p. 942-943.

[23] Yao, L., W.A. Sethares, and D.C. Kammer, *Sensor placement for on-orbit modal identification via a genetic algorithm.* AIAA journal, 1993. **31**(10): p. 1922-1928.

[24] Lee, I. and J.-H. Han. *Optimal placement of piezoelectric actuators in intelligent structures using genetic algorithms*. 1996.

[25] Sadri, A.M., J.R. Wright, and R.J. Wynne, *Modelling and optimal placement of piezoelectric actuators in isotropic plates using genetic algorithms.* Smart Materials and Structures, 1999. **8**(4): p. 490-498.

[26] Han, J.H. and I. Lee, *Optimal placement of piezoelectric sensors and actuators for vibration control of a composite plate using genetic algorithms.* Smart Materials and Structures, 1999. **8**(2): p. 257-267.

[27] Zhang, H., et al., *Float-encoded genetic algorithm technique for integrated optimization of piezoelectric actuator and sensor placement and feedback gains.* Smart Materials and Structures, 2000. **9**(4): p. 552-557.

[28] Yan, Y.J. and L.H. Yam, *Optimal design of number and locations of actuators in active vibration control of a space truss.* Smart Materials and Structures, 2002. **11**(4): p. 496-503.

[29] Sheng, L. and R.K. Kapania, *Genetic algorithms for optimization of piezoelectric actuator locations.* AIAA journal, 2001. **39**(9): p. 1818-1822.

[30] Sadri, A.M., J.R. Wright, and R.J. Wynne, *LQG control design for panel flutter suppression using piezoelectric actuators.* Smart Materials and Structures, 2002. **11**(6): p. 834-839.

[31] Jha, A.K. and D.J. Inman, *Optimal sizes and placements of piezoelectric actuators and sensors for an inflated torus.* Journal of Intelligent Material Systems and Structures, 2003. **14**(9): p. 563-576.

[32] Ning, H.H., *Optimal number and placements of piezoelectric patch actuators in structural active vibration control.* Engineering Computations (Swansea, Wales), 2004. **21**(6): p. 651-665.

[33] Li, Q.S., et al., *Combinatorial optimal design of number and positions of actuators in actively controlled structures using genetic algorithms.* Journal of Sound and Vibration, 2004. **270**(4-5): p. 611-624.

[34] Yang, Y., Z. Jin, and C.K. Soh, *Integrated optimal design of vibration control system for smart beams using genetic algorithms.* Journal of Sound and Vibration, 2005. **282**(3-5): p. 1293-1307.

[35] Peng, F., A. Ng, and Y.R. Hu, *Actuator placement optimization and adaptive vibration control of plate smart structures.* Journal of Intelligent Material Systems and Structures, 2005. **16**(3): p. 263-271.

[36] Jin, Z., Y. Yang, and C.K. Soh, *Application of fuzzy GA for optimal vibration control of smart cylindrical shells.* Smart Materials and Structures, 2005. **14**(6): p. 1250-1264.

[37] Rader, A.A., et al., *Optimization of Piezoelectric Actuator Configuration on a Flexible Fin for Vibration Control using Genetic Algorithms.* Journal of Intelligent Material Systems and Structures, 2007. **18**(10): p. 1015-1033.

[38] Kumar, K.R. and S. Narayanan, *The optimal location of piezoelectric actuators and sensors for vibration control of plates.* Smart Materials and Structures, 2007. **16**(6): p. 2680-2691.

[39] Ramesh Kumar, K. and S. Narayanan, *Active vibration control of beams with optimal placement of piezoelectric sensor/actuator pairs.* Smart Materials and Structures, 2008. **17**(5).

[40] Roy, T. and D. Chakraborty, *Optimal vibration control of smart fiber reinforced composite shell structures using improved genetic algorithm.* Journal of Sound and Vibration, 2009. **319**(1-2): p. 15-40.

[41] Tavakolpour, A.R., et al., *Genetic algorithm-based identification of transfer function parameters for a rectangular flexible plate system.* Engineering Applications of Artificial Intelligence.

[42] Spier, C., et al., *Placement of Multiple Piezo Patch Sensors and Actuators for a Cantilever Beam to Maximize Frequencies and Frequency Gaps.* Journal of Vibration and Control, 2009. **15**(5): p. 643-670.

[43] Bruant, I., L. Gallimard, and S. Nikoukar, *Optimal piezoelectric actuator and sensor location for active vibration control, using genetic algorithm.* Journal of Sound and Vibration.

[44] Liu, H.B., C.L. Wu, and J. Wang, *Sensor optimal placement for bridge structure based on Single Parents Genetic Algorithm with different fitness functions*. 2011. p. 115-124.

[45] Qin, B.Y., et al., *Optimal sensor placement based on integer-coded genetic algorithm.* Zhendong yu Chongji/Journal of Vibration and Shock, 2011. **30**(2): p. 252-257.

[46] Cha, Y.J., et al., *Optimal placement of active control devices and sensors in frame structures using multi-objective genetic algorithms.* Structural Control and Health Monitoring, 2013. **20**(1): p. 16-44.

[47] Mao, K., et al., *The optimal placement about actuators of active structural control based on genetic algorithm.* Zhongshan Daxue Xuebao/Acta Scientiarum Natralium Universitatis Sunyatseni, 2013. **52**(2): p. 129-132.

[48] Sivanandam, S.N. and S.N. Deepa, *Introduction to Genetic Algorithms* 2008, Berlin Heidelberg New York: Springer

[49] Liu, W., Z. Hou, and M.A. Demetriou, *A computational scheme for the optimal sensor/actuator placement of flexible structures using spatial H2 measures.* Mechanical Systems and Signal Processing, 2006. **20**(4): p. 881-895.

[50] Kumar, R., B.K. Mishra, and S.C. Jain, *Static and dynamic analysis of smart cylindrical shell.* Finite Elements in Analysis and Design, 2008. **45**(1): p. 13-24.

[51] Roy, R., ed. *Network models and optimization multiobjective genetic agoritm approach* 2008, Springer Verlag London Limited

[52] Gawronski, W.K., *Advanced Structural Dynamics and Active Control of Structures*. 2004, Verlage, New York: Springer.

[53] Devasia, S., et al., *Piezoelectric actuator design for vibration suppression: placement and sizing.* Journal of Guidance, Control, and Dynamics, 1993. **16**(5): p. 859-864.

[54] Quek, S.T., S.Y. Wang, and K.K. Ang, *Vibration control of composite plates via optimal placement of piezoelectric patches.* Journal of Intelligent Material Systems and Structures, 2003. **14**(4-5): p. 229-245.

[55] Sadri, A.M., R.J. Wynne, and J.R. Wright. *Robust strategies for active vibration control of strain actuated plate like structures*. in *IEE Conference Publication*. 1998.

[56] Viswanathan, C.N., R.W. Longman, and P.W. Likins, *Degree of controllability definition: fundamental concepts and applications to modal systems.* Journal of Guidance, Control, and Dynamics, 1984. **7**(2): p. 222-230.

[57] Kondoh, S., C. Yatomi, and K. Inoue, *Positioning of sensors and actuators in the vibration control of flexible systems.* JSME international journal, 1990. **33**(2): p. 145-152.

[58] Demetriou, M.A. *Numerical algorithm for the optimal placement of actuators and sensors for flexible structures*. in *Proceedings of the American Control Conference*. 2000.

[59] Fahroo, F. and M.A. Demetriou, *Optimal actuator/sensor location for active noise regulator and tracking control problems.* Journal of Computational and Applied Mathematics, 2000. **114**(1): p. 137-158.

[60] Chen, D., S. Zheng, and H. Wang, *Genetic algorithm based LQR vibration wireless control of laminated plate using photostrictive actuators.* Earthquake Engineering and Engineering Vibration, 2012. **11**(1): p. 83-90.

[61] Li, W.P. and H. Huang, *Integrated optimization of actuator placement and vibration control for piezoelectric adaptive trusses.* Journal of Sound and Vibration, 2013. **332**(1): p. 17-32.

[62] Hiramoto, K., H. Doki, and G. Obinata, *Optimal sensor/actuator placement for active vibration control using explicit solution of algebraic Riccati equation.* Journal of Sound and Vibration, 2000. **229**(5): p. 1057-1075.

[63] Arabyan, A. and S. Chemishkian, *H∞-optimal mapping of actuators and sensors in flexible structures.* Proceedings of the IEEE Conference on Decision and Control, 1998. **1**: p. 821-826.

[64] Chemishkian, S. and A. Arabyan. *Intelligent algorithms for H∞-optimal placement of actuators and sensors in structural control*. 1999.

[65] Gawronski, W.K., *Advanced Structural Dynamics and Active Control of Structures*. 2004, Verlage, New York: Springer.

[66] Darivandi, N., K. Morris, and A. Khajepour, *An algorithm for LQ optimal actuator location.* Smart Materials and Structures, 2013. **22**(3).

[67] Roy, T. and D. Chakraborty, *Genetic algorithm based optimal control of smart composite shell structures under mechanical loading and thermal gradient.* Smart Materials and Structures, 2009. **18**(11).

[68] Sadek, E.A. and S.A. Tawfik, *Finite element model for the analysis of stiffened laminated plates.* Computers and Structures, 2000. **75**(4): p. 369-383.

[69] Ojeda, R., et al., *A new approach for the large deflection finite element analysis of isotropic and composite plates with arbitrary orientated stiffeners.* Finite Elements in Analysis and Design, 2007. **43**(13): p. 989-1002.

[70] Birman, V. and S. Adali, *Vibration damping using piezoelectric stiffener-actuators with application to orthotropic plates.* Composite Structures, 1996. **35**(3): p. 251-261.

[71] Young, A.J. and C.H. Hansen, *Control of flexural vibration in stiffened structures using multiple piezoceramic actuators.* Applied Acoustics, 1996. **49**(1): p. 17-48.

[72] Mukherjee, A., S.P. Joshi, and A. Ganguli, *Active vibration control of piezolaminated stiffened plates.* Composite Structures, 2002. **55**(4): p. 435-443.

[73] Balamurugan, V. and S. Narayanan, *Finite element modeling of stiffened piezolaminated plates and shells with piezoelectric layers for active vibration control.* Smart Materials and Structures. **19**(10).

[74] Meirovitch, L., *Dynamics and Control of Structures*. 1990, Canda: Wiley

[75] Tzou, H.S. and H.Q. Fu, *A Study of segmentation of distributed piezoelectric sensors and actuators, part II: parametric study and active vibration controls.* Journal of Sound and Vibration, 1994. **172**(2): p. 261-275.

[76] Junkins, J.L. and Y. Kim, *Introduction to Dynamics and Control of Flexible Structures*. 1993, Washington USA: AIAA Education series.

[77] Lim, Y.H., *Finite-element simulation of closed loop vibration control of a smart plate under transient loading.* Smart Materials and Structures, 2003. **12**(2): p. 272-286.

[78] Shen, Y. and A. Homaifar, *Vibration control of flexible structures with PZT sensors and actuators.* JVC/Journal of Vibration and Control, 2001. **7**(3): p. 417-451.

[79] Shen, Y., A. Homaifar, and D. Chen. *Vibration control of flexible structures using fuzzy logic and genetic algorithms*. in *Proceedings of the American Control Conference*. 2000.

[80] Balamurugan, V. and S. Narayanan, *Multilayer higher order piezolaminated smart composite shell finite element and its application to active vibration control.* Journal of Intelligent Material Systems and Structures, 2009. **20**(4): p. 425-441.

[81] Moheimani, S.O.R. and T. Ryall. *Considerations on placement of piezoceramic actuators that are used in structural vibration control*. 1999.

[82] Kapuria, S. and M. Yaqoob Yasin, *Active vibration control of piezoelectric laminated beams with electroded actuators and sensors using an efficient finite element involving an electric node.* Smart Materials and Structures, 2010. **19**(4).

[83] Kapuria, S. and M.Y. Yasin, *Active vibration suppression of multilayered plates integrated with piezoelectric fiber reinforced composites using an efficient finite element model.* Journal of Sound and Vibration. **329**(16): p. 3247-3265.

[84] Balamurugan, V. and S. Narayanan, *Active vibration control of piezolaminated smart beams.* Defence Science Journal, 2001. **51**(2): p. 103-114.

[85] Narayanan, S. and V. Balamurugan, *Finite element modelling of piezolaminated smart structures for active vibration control with distributed sensors and actuators.* Journal of Sound and Vibration, 2003. **262**(3): p. 529-562.

[86] Zabihollah, A., R. Sedagahti, and R. Ganesan, *Active vibration suppression of smart laminated beams using layerwise theory and an optimal control strategy.* Smart Materials and Structures, 2007. **16**(6): p. 2190-2201.

[87] Uyanik, H. *Active vibration control of a fully clamped laminated composite plate subjected to impulsive pressure loadings*. in *Recent Advances in Space Technologies, 2009. RAST '09. 4th International Conference on*. 2009.

[88] Allik, H. and T.J.R. Hughes, *Finite element method for piezoelectric vibration.* International Journal for Numerical Methods in Engineering, 1970. **2**(2): p. 151-157.

[89] Lee, C.K., *Theory of laminated piezoelectric plates for the design of distributed sensors/actuators. Part I: Governing equations and reciprocal relationships.* Journal of the Acoustical Society of America, 1990. **87**(3): p. 1144-1158.

[90] Tzou, H.S. and C.I. Tseng, *Distributed piezoelectric sensor/actuator design for dynamic measurement/control of distributed parameter systems: A piezoelectric finite element approach.* Journal of Sound and Vibration, 1990. **138**(1): p. 17-34.

[91] Ha, S.K., C. Keilers, and F.-K. Chang, *Finite element analysis of composite structures containing distributed piezoceramic sensors and actuators.* AIAA journal, 1992. **30**(3): p. 772-780.

[92] Detwiler, D.T., M.H.H. Shen, and V.B. Venkayya, *Finite element analysis of laminated composite structures containing distributed piezoelectric actuators and sensors.* Finite Elements in Analysis and Design, 1995. **20**(2): p. 87-100.

[93] Reddy, J.N., *On laminated composite plates with integrated sensors and actuators.* Engineering Structures, 1999. **21**(7): p. 568-593.

[94] He, X.Q., et al., *Active control of FGM plates with integrated piezoelectric sensors and actuators.* International Journal of Solids and Structures, 2001. **38**(9): p. 1641-1655.

[95] Simões Moita, J.M., et al., *Active control of adaptive laminated structures with bonded piezoelectric sensors and actuators.* Computers & Structures, 2004. **82**(17-19): p. 1349-1358.

[96] Liu, G.R. and S.S. Quek, *The Finite Element Method* 1st ed. 2003, Oxford Butterworth-Heinenmann.

[97] Tiersten, H.F., *Linear Piezoelectric Plate Vibrations* 1969, New York: Plenum press

[98] Kogl, M. and M.L. Bucalem, *A family of piezoelectric MITC plate elements.* Computers and Structures, 2005. **83**(15-16): p. 1277-1297.

[99] Marinkovic, D., *A New Finite Composite Shell Element for Piezoelectric Active Structures* 2007, Germany: VDI Verlog Gmbh-Dusseldort.

[100] De Abreu, G.L.C.M., J.F. Ribeiro, and V. Steffen Jr, *Finite element modeling of a plate with localized piezoelectric sensors and actuators.* Journal of the Brazilian Society of Mechanical Sciences and Engineering, 2004. **26**(2): p. 117-128.

[101] Hatch, M.R., *Vibration Simulation Using MATLAB and ANSYS*. 2001, USA: Chapman and Hall/crc.

[102] Ogata, K., *Modern Control Engineering*. 3td ed. 1997, London: Prentice-Hall.

[103] Levine, W.S. and M. Athans, *On the determination of the optimal constant output feedback gains for linear multivariable systems* IEEE Transactions on Automatic Control, 1970. **AC-15**(1): p. 44-48.

[104] Ferreira, A.J.M., *MATLAB Codes for Finite Element Analysis Solids and Structures*. 2008, Dordrecht Springer.

[105] Lee, A.-C. and S.-T. Chen, *Collocated sensor/actuator positioning and feedback design in the control of flexible structure system.* Journal of Vibration and Acoustics, Transactions of the ASME, 1994. **116**(2): p. 146-154.

[106] Gawronski, W., *Actuator and sensor placement for structural testing and control.* Journal of Sound and Vibration, 1997. **208**(1): p. 101-109.

[107] Wang, Q. and C.M. Wang, *Optimal placement and size of piezoelectric patches on beams from the controllability perspective.* Smart Materials and Structures, 2000. **9**(4): p. 558-567.

[108] Zimmerman, D.C., *A Darwinian approach to the actuator number and placement problem with non-negligible actuator mass.* Mechanical Systems and Signal Processing, 1993. **7**(4): p. 363-374.

[109] *http://www.piceramic.com*.

[110] Blackbum, J.A., *Modern Instrumetation for Scientists and Engineers* Vol. II. 2001, New York: Springer

[111] *Degradation of Piezoelectric Materials* 1999, National Phsysical Laboratory Teddington Middlesex UK.

[112] Chen, W.P., et al., *Water-induced degradation in lead zirconate titanate piezoelectric ceramics.* Applied Physics Letters, 2002. **80**(19): p. 3587-3589.

Appendix (A)

State, actuators, sensors, controller gain and estimator gain discrete time matrices for the cantilever plate bonded with ten piezoelectric sensor/actuator pairs in the optimal location (chapter five).

$A_d =$

0.99991	0.00000	0.00000	0.00000	0.00000	0.00000
0.00000	0.99948	0.00000	0.00000	0.00000	0.00000
0.00000	0.00000	0.99667	0.00000	0.00000	0.00000
0.00000	0.00000	0.00000	0.99494	0.00000	0.00000
0.00000	0.00000	0.00000	0.00000	0.99286	0.00000
0.00000	0.00000	0.00000	0.00000	0.00000	0.97815
-0.01325	0.00000	0.00000	0.00000	0.00000	0.00000
0.00000	-0.03235	0.00000	0.00000	0.00000	0.00000
0.00000	0.00000	-0.08150	0.00000	0.00000	0.00000
0.00000	0.00000	0.00000	-0.10042	0.00000	0.00000
0.00000	0.00000	0.00000	0.00000	-0.11925	0.00000
0.00000	0.00000	0.00000	0.00000	0.00000	-0.20785

0.01325	0.00000	0.00000	0.00000	0.00000	0.00000
0.00000	0.03235	0.00000	0.00000	0.00000	0.00000
0.00000	0.00000	0.08150	0.00000	0.00000	0.00000
0.00000	0.00000	0.00000	0.10042	0.00000	0.00000
0.00000	0.00000	0.00000	0.00000	0.11925	0.00000
0.00000	0.00000	0.00000	0.00000	0.00000	0.20785
0.99958	0.00000	0.00000	0.00000	0.00000	0.00000
0.00000	0.99918	0.00000	0.00000	0.00000	0.00000
0.00000	0.00000	0.99626	0.00000	0.00000	0.00000
0.00000	0.00000	0.00000	0.99448	0.00000	0.00000
0.00000	0.00000	0.00000	0.00000	0.99234	0.00000
0.00000	0.00000	0.00000	0.00000	0.00000	0.97753

$$B_d^T = \begin{vmatrix} -1.35E-09 & -9.53E-09 & 5.41E-08 & -1.77E-08 & -1.19E-07 & -2.72E-07 \\ -1.47E-09 & -6.43E-09 & 2.47E-08 & -9.39E-09 & -3.84E-08 & -3.76E-08 \\ -1.42E-09 & -7.00E-09 & 4.58E-08 & 5.12E-09 & -9.04E-08 & -1.26E-07 \\ -2.31E-10 & 2.01E-09 & -3.50E-08 & 8.72E-09 & 3.97E-08 & -4.52E-08 \\ -9.11E-11 & -1.50E-09 & -1.62E-08 & 5.60E-08 & 3.35E-08 & -7.31E-08 \\ -9.11E-11 & 1.50E-09 & -1.62E-08 & 5.60E-08 & -3.35E-08 & -7.31E-08 \\ -2.31E-10 & -2.01E-09 & -3.50E-08 & 8.72E-09 & -3.97E-08 & -4.52E-08 \\ -1.42E-09 & 7.00E-09 & 4.58E-08 & 5.12E-09 & 9.04E-08 & -1.26E-07 \\ -1.35E-09 & 9.53E-09 & 5.41E-08 & -1.77E-08 & 1.19E-07 & -2.72E-07 \\ -1.47E-09 & 6.43E-09 & 2.47E-08 & -9.39E-09 & 3.84E-08 & -3.76E-08 \end{vmatrix}$$

$$\begin{vmatrix} -2.04E-07 & -5.89E-07 & 1.33E-06 & -3.51E-07 & -1.99E-06 & -2.59E-06 \\ -2.22E-07 & -3.97E-07 & 6.05E-07 & -1.87E-07 & -6.42E-07 & -3.58E-07 \\ -2.14E-07 & -4.33E-07 & 1.12E-06 & 1.02E-07 & -1.51E-06 & -1.20E-06 \\ -3.49E-08 & 1.25E-07 & -8.57E-07 & 1.73E-07 & 6.62E-07 & -4.30E-07 \\ -1.38E-08 & -9.24E-08 & -3.97E-07 & 1.11E-06 & 5.60E-07 & -6.95E-07 \\ -1.38E-08 & 9.24E-08 & -3.97E-07 & 1.11E-06 & -5.60E-07 & -6.96E-07 \\ -3.49E-08 & -1.25E-07 & -8.57E-07 & 1.73E-07 & -6.62E-07 & -4.30E-07 \\ -2.14E-07 & 4.33E-07 & 1.12E-06 & 1.02E-07 & 1.51E-06 & -1.20E-06 \\ -2.04E-07 & 5.89E-07 & 1.33E-06 & -3.51E-07 & 1.99E-06 & -2.59E-06 \\ -2.22E-07 & 3.97E-07 & 6.05E-07 & -1.87E-07 & 6.42E-07 & -3.58E-07 \end{vmatrix}$$

$$C_d = \begin{vmatrix} -205.5580 & -242.6823 & 216.9086 & -46.5910 & -222.1247 & -166.1553 \\ -223.4782 & -163.8120 & 99.0470 & -24.7656 & -71.7327 & -22.9362 \\ -215.6530 & -178.3843 & 183.5663 & 13.4906 & -168.8358 & -77.0526 \\ -35.0743 & 51.3299 & -140.2439 & 22.9944 & 74.0628 & -27.5920 \\ -13.8404 & -38.0974 & -64.9551 & 147.7404 & 62.6036 & -44.6160 \\ -13.8404 & 38.0972 & -64.9518 & 147.7380 & -62.6029 & -44.6179 \\ -35.0743 & -51.3313 & -140.2447 & 22.9945 & -74.0646 & -27.5918 \\ -205.5580 & -242.6823 & 216.9086 & -46.5910 & -222.1247 & -166.1553 \\ -223.4782 & -163.8120 & 99.0470 & -24.7656 & -71.7327 & -22.9362 \\ -215.6530 & -178.3843 & 183.5663 & 13.4906 & -168.8358 & -77.0526 \end{vmatrix}$$

0.0000	0.0000	0.0000	0.0000	0.0000	0.0000
0.0000	0.0000	0.0000	0.0000	0.0000	0.0000
0.0000	0.0000	0.0000	0.0000	0.0000	0.0000
0.0000	0.0000	0.0000	0.0000	0.0000	0.0000
0.0000	0.0000	0.0000	0.0000	0.0000	0.0000
0.0000	0.0000	0.0000	0.0000	0.0000	0.0000
0.0000	0.0000	0.0000	0.0000	0.0000	0.0000
0.0000	0.0000	0.0000	0.0000	0.0000	0.0000
0.0000	0.0000	0.0000	0.0000	0.0000	0.0000
0.0000	0.0000	0.0000	0.0000	0.0000	0.0000

$K_d =$

-18.347847	23.8817104	-90.650272	-217.57466	-36.410645	105.51899
-54.020557	-12.338458	0.38299539	-99.23784	-43.050635	-28.732399
-34.318294	19.5785399	15.0692078	-216.03879	-25.44967	2.17110226
-33.534564	-14.906295	18.1661397	141.60785	1.3052719	96.7406787
-15.08402	-31.722449	139.169826	-15.970418	-28.738544	81.4318456
-15.083291	31.7223136	139.165841	-15.971403	28.7430921	81.4320543
-33.534595	14.9066915	18.1654269	141.610433	-1.3028638	96.7397667
-34.318837	-19.578497	15.0721729	-216.04215	25.4488875	2.17320002
-18.348201	-23.881154	-90.648001	-217.5803	36.4095428	105.522455
-54.02083	12.3377147	0.38356895	-99.239219	43.048798	-28.731295

-1466.4802	-2053.7952	1913.8028	-773.41056	-2217.5125	-2611.1923
-1637.0728	-1401.5656	883.045609	-414.08465	-713.61456	-357.32659
-1568.3618	-1508.5632	1674.08534	349.94787	-1685.6985	-1206.4935
-267.11435	429.121659	-1275.0125	360.94372	740.250918	-439.34374
-118.73178	-341.41204	-494.80242	2756.8632	628.107324	-702.32076
-118.73089	341.410642	-494.7746	2756.8219	-628.10184	-702.3506
-267.11432	-429.13328	-1275.0205	360.94489	-740.26946	-439.34008
-1568.3624	1508.56014	1674.07906	349.95928	1685.68569	-1206.4872
-1466.4805	2053.78877	1913.80865	-773.41503	2217.48236	-2611.2012
-1637.0728	1401.56612	883.044269	-414.09129	713.626474	-357.32722

$$K_{ed}^{T} = \begin{vmatrix} -8.27E\text{-}05 & 0.00024535 & 4.41E\text{-}05 & 0.00015372 & -0.0001216 & -0.0003501 \\ 0.0006886 & 3.63E\text{-}05 & -0.0001612 & 2.15E\text{-}05 & 9.07E\text{-}05 & 9.76E\text{-}05 \\ 5.39E\text{-}04 & -0.0001196 & -4.36E\text{-}05 & -6.99E\text{-}05 & -1.16E\text{-}06 & 0.00018268 \\ 0.00027732 & 2.43E\text{-}04 & 8.18E\text{-}05 & 0.00025525 & -8.15E\text{-}05 & -3.52E\text{-}04 \\ 0.00074662 & 5.60E\text{-}04 & -2.91E\text{-}04 & 9.45E\text{-}05 & -5.91E\text{-}05 & -0.0001348 \\ 0.00061083 & -1.91E\text{-}04 & 0.00018439 & -2.97E\text{-}05 & -0.0001508 & 0.00014408 \\ 3.25E\text{-}04 & 4.61E\text{-}05 & 0.00022902 & 0.0002212 & -0.0001159 & -0.0002673 \\ 0.00029785 & -0.0001104 & -1.15E\text{-}04 & -6.42E\text{-}05 & 3.02E\text{-}05 & 0.00014551 \\ -4.17E\text{-}04 & 0.00020008 & -1.56E\text{-}05 & 0.00015188 & -8.65E\text{-}05 & -0.0003787 \\ 0.00039592 & -0.0005915 & 0.00018719 & -7.91E\text{-}05 & 3.63E\text{-}05 & 0.00030568 \end{vmatrix}$$

$$\begin{vmatrix} 3.21E\text{-}05 & -0.0001775 & -9.69E\text{-}05 & -0.0003064 & 8.85E\text{-}05 & -0.0003681 \\ -2.44E\text{-}04 & -0.0001034 & 0.00019317 & -0.0002083 & 0.00023013 & 0.000684 \\ -0.0001374 & 9.26E\text{-}05 & 9.87E\text{-}05 & 0.0002469 & -0.0001803 & -8.48E\text{-}05 \\ -0.0001224 & -2.23E\text{-}04 & -0.0002524 & -5.40E\text{-}04 & 0.00047548 & 0.00019948 \\ -0.0002157 & -4.15E\text{-}04 & 2.27E\text{-}04 & 6.37E\text{-}05 & 0.00049405 & 0.00014196 \\ -0.0001115 & 0.00022335 & -0.0002573 & 0.00057 & -0.0003079 & -0.0007874 \\ -0.0001122 & -5.60E\text{-}05 & -0.0004005 & -0.0003865 & 0.0001977 & -9.47E\text{-}05 \\ -8.85E\text{-}05 & 8.61E\text{-}05 & 0.0001661 & 0.000181 & 2.58E\text{-}05 & 7.33E\text{-}05 \\ 0.00010576 & -0.0001372 & -4.35E\text{-}05 & -0.0003561 & 0.00030392 & -0.0002269 \\ -0.0001199 & 0.00043112 & -0.0001659 & 0.0001706 & -0.000295 & 1.59E\text{-}05 \end{vmatrix}$$

Appendix (B)

This is a sample of APDL program for the cantilever flat plate to determine the first six natural frequencies and mode shapes.

```
/CLEAR                    !CLEAR THE DATABASE
/GRAPHICS, POWER    !DEFINE THE TYPE OF GRAPHICS DISPLAY
/VIEW,1,1,1,1            !DEFINE THE VIEWING DIRECTION FOR THE DISPLAY
/FILENAME, ACONT
/OUTPUT, ADISP, OUT,,APPEND  !DIRECT OUTPUT TO A FILE
/PREP7                                ! ENTER PREPROCESSOR
ANTYPE,MODAL                    ! MODE FREQUENCY ANALYSIS
MODOPT,SUBSP,6                   ! CHOOSE SUBSPACE MODE EXTRACTION METHOD
MXPAND,6
ET,1,SHELL63                     !SPECIFY ELEMENT TYPE
R,1,0.0019                        !SPECIFY PLATE THICKNESS
MP,EX,1,21e10                   !SPECIFY ELEASTIC MODULUS
MP,NUXY,1,0.3                   !SPECIFY POISSONS RATIO
MP,DENS,1,7810                  !DENSITY FOR MATERIAL 1
K,1,0,0,0                          !CREAT  PLATE KEYPOINTS
K,2,0.5,0,0
K,3,0.5,0.5,0
K,4,0,0.5,0
A,1,2,3,4                          !CREAT AREA THROGH KEYPOINTS
ESIZE, 0.01                      !SPECIFY NO. OF DIVISIONS ON LINES
AMESH,ALL                       !ENFORCE MAPPED MESHING
NSEL,S,LOC,X,0                 ! SELECT SUBSET NODEES AT X=0
D,ALL,ALL                        !FIXED THE SUBSET NODES IN ALL DIRECTIONS
SAVE
FINISH                             !EXIT PREPROCESSOR

/SOLU                              !ENTERS THE SOLUTION PROSSOR
ANTYPE, MODAL                 ! SPECIFY THE ANALYSIS TYPE
MODOPT,SUBSP,6,,,,OFF      ! SPECIFY MODAL ANALYSIS OPTIONS
OUTPR, ALL, ALL,                !CONTROLS THE SOLUTION PRINTOUT
OUTRES, STAT                  !CONTROLS THE SOLUTION DATA WRITTEN TO THE DATABASE
SOLVE                          !STARTS SOLUTION
SAVE                           !SAVE GRAPHICS SETTINGS TO A FILE FOR LATER USE
FINISH                         !EXITE THE SOLUTION PROSSOR
```

Appendix (C)

This is a sample of APDL program to investigate active vibration control of the cantilever plate using optimal linear quadratic control with weighted matrices R=1 and Q=10^8. The results of this program can be shown in chapter five Figure 5.20 and Figure 5.21

```
!!!!!!!!ACTIVE VIBRATION CONTROL OF A FLEXIBLE CANTILEVER PLATE !!!!!!!!!
!!!!!!!!!!BY OPTIMALY PLACED TEN SENSOR/ACTUATOR PAIRS USING!!!!!!!!!!!!
!!!!!!!!!!!!!!!!!!!!OPTIMAL LINEAR QUADRATIC CONTROL SCHEME !!!!!!!!!!!!!!!!!!!!!!
!!!!!!!!!!!!!!!!!!!!AND THREE DIMENTIONAL SOLID45/5 ELEMENTS!!!!!!!!!!!!!!!!!!!!!
!!!!!!!!!!!!!!!!!!!!!!!!!!!!!!!!!!WIEGHTED MATRICES R=1, Q=10^8!!!!!!!!!!!!!!!!!!!!!!!!!!!!!!!!
/COM                          !PLACE A COMMENT IN THE OUTPUT
/GRAPHICS,FULL                !DEFINES THE TYPE OF GRAPHICS DISPLAY
/VIEW,1,1,1,1                 !DEFINE THE VIEWING DIRECTION FOR THE DISPLAY
/PNUM,TYPE,1                  !CONTROLS ENTITY NUMBERING/COLORIN ON PLOTS
/PNUM,MAT,1                   !CONTROLS ENTITY NUMBERING/COLORIN ON PLOTS
/NUM,1
/ESHAPE,1                     !DISPLAYS ELEMENTS WITH SHAPES DETERMINED
FOROM REAL CONSTANTS
/CONFIG,NRES,30000            !ASSIGNS VALUES TO ANSYS CONFIGURATION
PARAMETRS
*SET,NSA,10                   !ASSIGNS VALUES TO USER-NAMED PARAMETRS
*SET,SNTOP                    !ASSIGNS VALUES TO USER-NAMED PARAMETRS
*SET,ANTOP
*DIM,SNTOP,ARRAY,NSA  !DEFINES AN ARRAY PARAMETER AND ITS
DIMENSIONS
*DIM,ANTOP,ARRAY,NSA
/PREP7                        !ENTER PREPROSSOR
ET,1,SOLID45                  !SPECIFY ELEMENT TYPE
MP,EX,1,21E10                 !DEFINE A LINEAR METERIAL PROPERTIES
MP,NUXY,1,.3
BETAD,0.0001                  !DEFINE STIFFNESS MATRIX MUTIPLIER FOR DAMPING
MP,DENS,1,7810
MAT,1                         !SETS ELEMENT MATERIAL ATTRIBUTE POINTER
TYPE,1                        !SETS ELEMENT TYPE  ATTRIBUTE POINTER
BLOCK, 0,0.5,0,0.5,0,0.0019   !CREATE A BLOCK VOLUME

ET,2,SOLID5,3                  !SPECIFY ELEMENT TYPE
MP,DENS,2,7800                !DEFINE A LINEAR METERIAL PROPERTIES
!EMUNIT,EPZRO,8.85E-12   !FREE SPACE PERMITTIVITY
MP,PERX,2,1.45e-8             ! PIEZOELECTRIC PERMITTIVITY
MP,PERY,2,1.45e-8
MP,PERZ,2,1.55e-8              ! PERMITTIVITY (Z DIRECTION)...F/m
TB,PIEZ,2                      ! DEFINE PIEZELECTRIC COUPLING  TABLE
```

```
TBDATA,3,-7.15              ! e31 PIEZOELECTRIC CONSTANT
TBDATA,6,-7.15              ! e32 PIEZOELECTRIC CONSTANT
TBDATA,9,13.7               ! e33 PIEZOELECTRIC CONSTANT
TBDATA,14,11.9              ! e15 PIEZOELECTRIC CONSTANT
TBDATA,16,11.9              ! e16 PIEZOELECTRIC CONSTANT

TB,ANEL,2                   ! DEFINE STRUCTURAL TABLE/ UPPER MATRIX
TRIANGLE
TBDATA,1,1.23e11,7.67e10,7.025e10   !C11, C12, C13   FIRST ROW
TBDATA,7,1.23e11,7.025e10           !C11=C22, C13,  SECOND ROW
TBDATA,12,9.711e10                  !C33            THIRD ROW
TBDATA,16,2.26e10                   !C44            FOURTH ROW
TBDATA,19,2.226e10                  !C55            FIFTH ROW
TBDATA,21,2.315e10                  !C66            SIXTH ROW

TYPE,2                      !SETS ELEMENT TYPE  ATTRIBUTE POINTER
MAT,2                       !SETS ELEMENT MATERIAL ATTRIBUTE POINTER
BLOCK, 0,0.05,0,0.05,0.0019,0.0024      ! SENSOR 01
BLOCK, 0.06,0.11,0,0.05,0.0019,0.0024   ! SENSOR 02
BLOCK, 0,0.05,0.06,0.11,0.0019,0.0024   ! SENSOR 03
BLOCK, 0.35,0.4,0,0.05,0.0019,0.0024    ! SENSOR 04
BLOCK, 0.45,0.5,0.1,0.15,0.0019,0.0024  !SENSOR 05
BLOCK, 0.45,0.5,0.35,0.4,0.0019,0.0024  !SENSOR 06
BLOCK, 0.35,0.4,0.45,0.5,0.0019,0.0024  !SENSOR 07
BLOCK, 0,0.05,0.44,0.39,0.0019,0.0024   !SENSOR 08
BLOCK, 0,0.05,0.45,0.5,0.0019,0.0024    !SENSOR 09
BLOCK, 0.06,0.11,0.45,0.5,0.0019,0.0024 !SENSOR 10


BLOCK, 0,0.05,0,0.05,0,-0.0005          !ACTUATOR 01
BLOCK, 0.06,0.11,0,0.05,0,-0.0005       !ACTUATOR 02
BLOCK, 0,0.05,0.06,0.11,0,-0.0005       !ACTUATOR 03
BLOCK, 0.35,0.4,0,0.05,0,-0.0005        !ACTUATOR 04
BLOCK, 0.45,0.5,0.1,0.15,0,-0.0005      !ACTUATOR 05
BLOCK, 0.45,0.5,0.35,0.4,0,-0.0005      !ACTUATOR 06
BLOCK, 0.35,0.4,0.45,0.5,0,-0.0005      !ACTUATOR 07
BLOCK, 0,0.05,0.44,0.39,0,-0.0005       !ACTUATOR 08
BLOCK, 0,0.05,0.45,0.5,0,-0.0005        !ACTUATOR 09
BLOCK, 0.06,0.11,0.45,0.5,0,-0.0005     !ACTUATOR 10

ESIZE,0.01                  ! SPECIFIES THE DEFAULT NUMBER OF DEVISONS
MAT,1                       !SETS ELEMENT MATERIAL ATTRIBUTE POINTER
TYPE,1                      !SETS ELEMENT TYPE ATTRIBUTE POINTER
NUMSTR,NODE,100             !ESTABLISHES STARTING NUMBERS
VSEL,S,VOLU,,1              !SELECT A SUBSET VOLUMES
VMESH,1                     !GENERATE NODES AND TETRAHEDRAL ELEMENTS

TYPE,2
MAT,2
VSEL,S,VOLU,,2
```

```
VMESH,2
VSEL,S,VOLU,,3
VMESH,3
VSEL,S,VOLU,,4
VMESH,4
VSEL,S,VOLU,,5
VMESH,5
VSEL,S,VOLU,,6
VMESH,6
VSEL,S,VOLU,,7
VMESH,7
VSEL,S,VOLU,,8
VMESH,8
VSEL,S,VOLU,,9
VMESH,9
VSEL,S,VOLU,,10
VMESH,10
VSEL,S,VOLU,,11
VMESH,11
VSEL,S,VOLU,,12
VMESH,12
VSEL,S,VOLU,,13
VMESH,13
VSEL,S,VOLU,,14
VMESH,14
VSEL,S,VOLU,,15
VMESH,15
VSEL,S,VOLU,,16
VMESH,16
VSEL,S,VOLU,,17
VMESH,17
VSEL,S,VOLU,,18
VMESH,18
VSEL,S,VOLU,,19
VMESH,19
VSEL,S,VOLU,,20
VMESH,20
VSEL,S,VOLU,,21
VMESH,21
ALLSEL                  !SELECT ALL ENTITIES
NUMMRG,NODE             !MERGES CONCIDENT OR EQUIVALENTY DEFINED ITEMS
AGLUE,ALL               !GENERATES NEW AREAS BY GLUING AREAS
!BOUNDRY CONDITION APPLICATION
VSEL,S,VOLU,,1,,1       !SELECT A SUBSET VOLUMES
NSEL,R,LOC,X,0          !SELECTS A SUBSET OF NODES
D,ALL,UX                !DEFINE DEGREE OF FREEDOM CONSTRAINTS AT NODES
D,ALL,UY
D,ALL,UZ
NSEL,ALL
```

```
VSEL,S,VOLU,,2,,,1
NSEL,R,LOC,Z,0.0024
CP,1,VOLT,ALL                    ! DEFINE A SET OF COUPLED DEGREES OF
FREEDOM
*GET,SNTOP(1),NODE,0,NUM,MIN     ! GET MASTER NODE ON THE BOTTOM OF
ELECTRODE
VSEL,S,VOLU,,2,,,1
NSEL,R,LOC,Z,0.0019
CP,2,VOLT,ALL
*GET,SNBOT1,NODE,0,NUM,MIN       ! GET MASTER NODE ON THE TOP OF
ELECTRODE
NSEL,ALL
D,SNBOT1,VOLT,0                  ! GROUND BOTTOM ELECTRODE
D,SNTOP(1),VOLT,1                ! APPLY 1V LOAD ON TOP ELECTRODE

VSEL,S,VOLU,,3,,,1
NSEL,R,LOC,Z,0.0024
CP,3,VOLT,ALL
*GET,SNTOP(2),NODE,0,NUM,MIN
VSEL,S,VOLU,,3,,,1
NSEL,R,LOC,Z,0.0019
CP,4,VOLT,ALL
*GET,SNBOT2,NODE,0,NUM,MIN
NSEL,ALL
D,SNBOT2,VOLT,0
D,SNTOP(2),VOLT,1

VSEL,S,VOLU,,4,,,1
NSEL,R,LOC,Z,0.0024
CP,5,VOLT,ALL
*GET,SNTOP(3),NODE,0,NUM,MIN
VSEL,S,VOLU,,4,,,1
NSEL,R,LOC,Z,0.0019
CP,6,VOLT,ALL
*GET,SNBOT3,NODE,0,NUM,MIN
NSEL,ALL
D,SNBOT3,VOLT,0
D,SNTOP(3),VOLT,1

VSEL,S,VOLU,,5,,,1
NSEL,R,LOC,Z,0.0024
CP,7,VOLT,ALL
*GET,SNTOP(4),NODE,0,NUM,MIN
VSEL,S,VOLU,,5,,,1
NSEL,R,LOC,Z,0.0019
CP,8,VOLT,ALL
*GET,SNBOT4,NODE,0,NUM,MIN
NSEL,ALL
D,SNBOT4,VOLT,0
```

```
D,SNTOP(4),VOLT,1

VSEL,S,VOLU,,6,,,1
NSEL,R,LOC,Z,0.0024
CP,9,VOLT,ALL
*GET,SNTOP(5),NODE,0,NUM,MIN
VSEL,S,VOLU,,6,,,1
NSEL,R,LOC,Z,0.0019
CP,10,VOLT,ALL
*GET,SNBOT5,NODE,0,NUM,MIN
NSEL,ALL
D,SNBOT5,VOLT,0
D,SNTOP(5),VOLT,1

VSEL,S,VOLU,,7,,,1
NSEL,R,LOC,Z,0.0024
CP,11,VOLT,ALL
*GET,SNTOP(6),NODE,0,NUM,MIN
VSEL,S,VOLU,,7,,,1
NSEL,R,LOC,Z,0.0019
CP,12,VOLT,ALL
*GET,SNBOT6,NODE,0,NUM,MIN
NSEL,ALL
D,SNBOT6,VOLT,0
D,SNTOP(6),VOLT,1

VSEL,S,VOLU,,8,,,1
NSEL,R,LOC,Z,0.0024
CP,13,VOLT,ALL
*GET,SNTOP(7),NODE,0,NUM,MIN
VSEL,S,VOLU,,8,,,1
NSEL,R,LOC,Z,0.0019
CP,14,VOLT,ALL
*GET,SNBOT7,NODE,0,NUM,MIN
NSEL,ALL
D,SNBOT7,VOLT,0
D,SNTOP(7),VOLT,1

VSEL,S,VOLU,,9,,,1
NSEL,R,LOC,Z,0.0024
CP,15,VOLT,ALL
*GET,SNTOP(8),NODE,0,NUM,MIN
VSEL,S,VOLU,,9,,,1
NSEL,R,LOC,Z,0.0019
CP,16,VOLT,ALL
*GET,SNBOT8,NODE,0,NUM,MIN
NSEL, ALL
D, SNBOT8,VOLT,0
D,SNTOP(8),VOLT,1
```

```
VSEL,S,VOLU,,10,,,1
NSEL,R,LOC,Z,0.0024
CP,17,VOLT,ALL
*GET,SNTOP(9),NODE,0,NUM,MIN
VSEL,S,VOLU,,10,,,1
NSEL,R,LOC,Z,0.0019
CP,18,VOLT,ALL
*GET,SNBOT9,NODE,0,NUM,MIN
NSEL,ALL
D,SNBOT9,VOLT,0
D,SNTOP(9),VOLT,1

VSEL,S,VOLU,,11,,,1
NSEL,R,LOC,Z,0.0024
CP,19,VOLT,ALL
*GET,SNTOP(10),NODE,0,NUM,MIN
VSEL,S,VOLU,,11,,,1
NSEL,R,LOC,Z,0.0019
CP,20,VOLT,ALL
*GET,SNBOT10,NODE,0,NUM,MIN
NSEL,ALL
D,SNBOT10,VOLT,0
D,SNTOP(10),VOLT,1

!ACTUATOR TERMINAL CONNECTION NUMBER
VSEL,S,VOLU,,12,,,1
NSEL,R,LOC,Z,-0.0005
CP,21,VOLT,ALL
*GET,ANTOP(1),NODE,0,NUM,MIN
VSEL,S,VOLU,,12,,,1
NSEL,R,LOC,Z,0
CP,22,VOLT,ALL
*GET,ANBOT1,NODE,0,NUM,MIN
NSEL,ALL
D,ANBOT1,VOLT,0
D,ANTOP(1),VOLT,1

VSEL,S,VOLU,,13,,,1
NSEL,R,LOC,Z,-0.0005
CP,23,VOLT,ALL
*GET,ANTOP(2),NODE,0,NUM,MIN
VSEL,S,VOLU,,13,,,1
NSEL,R,LOC,Z,0
CP,24,VOLT,ALL
*GET,ANBOT2,NODE,0,NUM,MIN
NSEL,ALL
D,ANBOT2,VOLT,0
D,ANTOP(2),VOLT,1
```

```
VSEL,S,VOLU,,14,,,1
NSEL,R,LOC,Z,-0.0005
CP,25,VOLT,ALL
*GET,ANTOP(3),NODE,0,NUM,MIN
VSEL,S,VOLU,,14,,,1
NSEL,R,LOC,Z,0
CP,26,VOLT,ALL
*GET,ANBOT3,NODE,0,NUM,MIN
NSEL,ALL
D,ANBOT3,VOLT,0
D,ANTOP(3),VOLT,1

VSEL,S,VOLU,,15,,,1
NSEL,R,LOC,Z,-0.0005
CP,27,VOLT,ALL
*GET,ANTOP(4),NODE,0,NUM,MIN
VSEL,S,VOLU,,15,,,1
NSEL,R,LOC,Z,0
CP,28,VOLT,ALL
*GET,ANBOT4,NODE,0,NUM,MIN
NSEL,ALL
D,ANBOT4,VOLT,0
D,ANTOP(4),VOLT,1

VSEL,S,VOLU,,16,,,1
NSEL,R,LOC,Z,-0.0005
CP,29,VOLT,ALL
*GET,ANTOP(5),NODE,0,NUM,MIN
VSEL,S,VOLU,,16,,,1
NSEL,R,LOC,Z,0
CP,30,VOLT,ALL
*GET,ANBOT5,NODE,0,NUM,MIN
NSEL,ALL
D,ANBOT5,VOLT,0
D,ANTOP(5),VOLT,1

VSEL,S,VOLU,,17,,,1
NSEL,R,LOC,Z,-0.0005
CP,31,VOLT,ALL
*GET,ANTOP(6),NODE,0,NUM,MIN
VSEL,S,VOLU,,17,,,1
NSEL,R,LOC,Z,0
CP,32,VOLT,ALL
*GET,ANBOT6,NODE,0,NUM,MIN
NSEL,ALL
D,ANBOT6,VOLT,0
D,ANTOP(6),VOLT,1
```

```
VSEL,S,VOLU,,18,,,1
NSEL,R,LOC,Z,-0.0005
CP,33,VOLT,ALL
*GET,ANTOP(7),NODE,0,NUM,MIN
VSEL,S,VOLU,,18,,,1
NSEL,R,LOC,Z,0
CP,34,VOLT,ALL
*GET,ANBOT7,NODE,0,NUM,MIN
NSEL,ALL
D,ANBOT7,VOLT,0
D,ANTOP(7),VOLT,1

VSEL,S,VOLU,,19,,,1
NSEL,R,LOC,Z,-0.0005
CP,35,VOLT,ALL
*GET,ANTOP(8),NODE,0,NUM,MIN
VSEL,S,VOLU,,19,,,1
NSEL,R,LOC,Z,0
CP,36,VOLT,ALL
*GET,ANBOT8,NODE,0,NUM,MIN
NSEL,ALL
D,ANBOT8,VOLT,0
D,ANTOP(8),VOLT,1

VSEL,S,VOLU,,20,,,1
NSEL,R,LOC,Z,-0.0005
CP,37,VOLT,ALL
*GET,ANTOP(9),NODE,0,NUM,MIN
VSEL,S,VOLU,,20,,,1
NSEL,R,LOC,Z,0
CP,38,VOLT,ALL
*GET,ANBOT9,NODE,0,NUM,MIN
NSEL,ALL
D,ANBOT9,VOLT,0
D,ANTOP(9),VOLT,1

VSEL,S,VOLU,,21,,,1
NSEL,R,LOC,Z,-0.0005
CP,39,VOLT,ALL
*GET,ANTOP(10),NODE,0,NUM,MIN
VSEL,S,VOLU,,21,,,1
NSEL,R,LOC,Z,0
CP,40,VOLT,ALL
*GET,ANBOT10,NODE,0,NUM,MIN
NSEL,ALL
D,ANBOT10,VOLT,0
D,ANTOP(10),VOLT,1

ALLSEL,ALL
```

```
VGLUE,ALL       !GENERATE NEW VOLUMESE BY GLUING VOLUMES
ALLSEL,ALL
SAVE
FINISH              !EXITS FROM PREPROSSOR

/POST1              !ENTERS THE DATABASE RESULTS POSTPROCESSOR
*SET,NSA,10
*SET,NMODE,1
*SET,STIPNODE
*DIM,STIPNODE,ARRAY,NSA

*SET,STIPNODE(1),2702
*SET,STIPNODE(2),5436
*SET,STIPNODE(3),5508
*SET,STIPNODE(4),5583
*SET,STIPNODE(5),5651
*SET,STIPNODE(6),5724
*SET,STIPNODE(7),5795
*SET,STIPNODE(8),5868
*SET,STIPNODE(9),5940
*SET,STIPNODE(10),6012

* SET,FREQ,6.7607
*SET,STIME,0.0
*SET,FTIME,1
*SET,TSTEP,1/(60*FREQ)
*SET,PI,22/7
*SET,FREQR,2*PI*FREQ
*SET,NSTEP,NINT(FTIME/TSTEP)
*SET,HNSTEP,NINT(0.5*NSTEP)
*SET,TIMEF
*DIM,TIMEF,TABLE,NSTEP
*SET,SINEWAVE
*DIM,SINEWAVE,ARRY,NSTEP
*DO,ICOUNT,1,NSTEP,1
SINEWAVE(ICOUNT)=20*(SIN(FREQR*(ICOUNT-1)*TSTEP))    ! GENERATE SINE
WAVE VOLTAGE
*ENDDO
!!!!!!!!!!!!!!!!!!!!!!!!!!!!!!!!
!! OPTIMAL LINEAR QUADRATCI CONTROL PARAMETERS DEFINITIONS
*SET,AMAT          ! STATE MATRIX
*SET,BMAT          !ACTUATORS MATRIX
*SET,CMAT          !SENSORS MATRIX
*SET,KGAIN         !FEEDBACK GAIN MATRIX
*SET,GGAIN         !ESTIMATOR ERROR GAIN MATRIX

*DIM,AMAT,ARRAY,2*NMODE,2*NMODE
*DIM,BMAT,ARRAY,2*NMODE,NSA
*DIM,CMAT,ARRAY,NSA,2*NMODE
*DIM,KGAIN,ARRAY,NSA,2*NMODE
```

*DIM,GGAIN,ARRAY,2*NMODE,NSA

!!!!!!!!!FREQUENCY 6.7607Hz, SAMPLING TIME=1/(60*6.7607), R=1, Q=10^8!!!!!!

*SET,AMAT(1,1),0.994526649003166,-0.104392410806455
*SET,AMAT(1,2),0.104392410806455,0.991929365822302
*SET, BMAT(1,1),-8.43818216515863e-08,-1.60940195422243e-06
*SET, BMAT(1,2),-9.17380895249700e-08,-1.74970695901472e-06
*SET, BMAT(1,3),-8.85258271510991e-08,-1.68843995575744e-06
*SET, BMAT(1,4),-1.43980308881857e-08,-2.74611505118714e-07
*SET, BMAT(1,5),-5.68149669417171e-09,-1.08362342783534e-07
*SET, BMAT(1,6),-5.68150293691606e-09,-1.08362461850470e-07
*SET, BMAT(1,7),-1.43980308881857e-08,-2.74611505118715e-07
*SET, BMAT(1,8),-8.85258250482800e-08,-1.68843991565068e-06
*SET, BMAT(1,9),-8.43818206001767e-08,-1.60940193416906e-06
*SET, BMAT(1,10),-9.17380832165126e-08,-1.74970683869445e-06
*SET,CMAT(1,1),0,0,0,0,0,0,0,0,0,0
*SET,CMAT(1,2),-205.557976458178,-223.4781814115,-215.652963367,-35.074261688,-13.84038577,-13.8404009785,-35.074261688,-215.65295824,-205.557973896896,-223.478166043880
*SET,KGAIN(1,1),453.7295909641,493.2849874687,476.0123277366,77.4196685698378,30.549982456582,30.55001602445,77.419668569838,476.01231642953,453.72958531056,493.284953547531
*SET,KGAIN(1,2),5084.46670366787,5527.72211500418,5334.16572141471,867.560183182957,342.341279236558,342.341655396081,867.560183182958,5334.16559470835,5084.46664031469,5527.72173488509
*SET, GGAIN(1,1),5.07524618828147e-05,-0.000108923967518975
*SET, GGAIN(1,2),5.51769777031207e-05,-0.000118419779143069
*SET, GGAIN(1,3),5.32449238496186e-05,-0.000114273241943165
*SET, GGAIN(1,4),8.65986890941335e-06,-1.85856457955771e-05
*SET, GGAIN(1,5),3.41720454434947e-06,-7.33393933980674e-06
*SET, GGAIN(1,6),3.41720829912318e-06,-7.33394739823058e-06
*SET, GGAIN(1,7),8.65986890941336e-06,-1.85856457955772e-05
*SET, GGAIN(1,8),5.32449225848527e-05,-0.000114273239228749
*SET, GGAIN(1,9),5.07524612504318e-05,-0.000108923966161767
*SET, GGAIN(1,10),5.51769739088231e-05,-0.000118419770999820
!!

*SET,VPS
*SET,VES
*SET,SDIS
*SET,FBVOLT
*SET,SFBVOLT
*SET,XDOT
*SET,ERRG
*SET,XSTAT
*SET,XSTATO
*SET,AET
*SET,ERROR
*SET,ERRGO

```
*SET,XDOTO
*SET,DISF
*SET,EDISF
*SET,FDBCK
*DIM,FDBCK,ARRAY,NSA
*DIM,VPS,ARRAY,NSA
*DIM,VES,ARRAY,NSA
*DIM,FBVOLT,ARRAY,NSA
*DIM,SFBVOLT,ARRAY,NSA
*DIM,SDIS,ARRAY,NSA
*DIM,EDISF,ARRAY,2*NMODE
*DIM,DISF,ARRAY,NSA
*DIM,XDOT,ARRAY,NMODE*2
*DIM,ERRG,ARRAY,NMODE*2
*DIM,XSTAT,ARRAY,NMODE*2
*DIM,XSTATO,ARRAY,NMODE*2
*DIM,AET,ARRAY,NMODE*2
*DIM,ERROR,ARRAY,NSA
*SET,MXSTA
*DIM,MXSTAT,ARRAY,2*NMODE
*SET,SEVOLT
*DIM,SEVOLT,TABLE,NSTEP,NSA
*SET,SVOLT
*SET,AVOLT
*DIM,SVOLT,TABLE,NSTEP,NSA
*DIM,AVOLT,TABLE,NSTEP,NSA
*SET,STIPDIS
*DIM,STIPDIS,TABLE,NSTEP,NSA
*SET,STIPVELO
*DIM,STIPVELO,TABLE,NSTEP,NSA
*SET,STIPACC
*DIM,STIPACC,TABLE,NSTEP,NSA
*SET,MSTRAIN
*DIM,MSTRAIN,TABLE,NSTEP,NSA
FINISH

/PREP7
*DO,IIC,1,NSA,1
DDELE,ANTOP(IIC),VOLT     ! DELETE VOLTAGE ON ACTUATORS ELECTRODE
DDELE,SNTOP(IIC),VOLT     !DELETE  VOLTAGW ON SENSORS ELECTRODE
*ENDDO
FINISH

!!!!!!SOLUTION!!!!!!
*DO,ICOUNT,1,NSTEP,1
*SET,CURRTIME,STIME+ICOUNT*TSTEP
/SOLU                     !ENTERS THE SOLUTION PROCESSOR
*IF,ICOUNT,EQ,1,THEN
ANTYPE,TRANS,NEW          !SPECIFIES THE ANALYSIS TYPE
```

```
*ELSE
ANTYPE,TRANS,REST
*ENDIF
TIME,CURRTIME
DELTIM,TSTEP                !SPECIFIES THE TIME STEP SIZES TO BE USED THIS
STEP
TINTP,,0.25,0.5,0.5         !DEFINES TRANSIENT INTEGRATION PARAMETRS
BETAD,0.0001

*SET,DISF(1,1), 0,0,0,0,0,0,0,0,SINEWAVE(ICOUNT),0
*VOPER,FDBCK,FBVOLT,ADD,DISF     !OPERATES ON TWO ARRAY PARAMETERS
*SET,FDBCK(9,1),DISF(9,1)
!!!!!!!!!!FEEDBACK VOLTAGE APPLIED ON ACTUATORS!!!!!!!!
*DO,IIC,1,NSA,1
D,ANTOP(IIC),VOLT,FDBCK(IIC,1)    ! APPLY FEEDBACK VOLTAGE ON
ACTUATORS
*ENDDO
!!!!!!!!END FEEDBACK VOLTAGE APPLICATION!!!!!!!!!
ALLSEL,ALL
SOLVE
FINISH      !EXITES THE SOLUTION PROCESSOR

/POS1
*DO,IIC,1,NSA,1
*GET,SDIS(IIC),NODE,STIPNODE(IIC),UZ          !GET DISPLACEMENTS
*GET,VPS(IIC),NODE,SNTOP(IIC),VOLT            ! GET SENSOR VOLTAGE
*GET,MSTRAIN(ICOUNT,IIC),NODE,STIPNODE(IIC),EPEL,INT  !GET STRAIN
INTENSITY
*ENDDO
!!!!!!ESTIMATOR!!!!
 *DO,IIC,1,NSA,1
*SET,SVOLT(ICOUNT,IIC),VPS(IIC,1)
*SET,SEVOLT(ICOUNT,IIC),VES(IIC,1)
*ENDDO

*VOPER,ERROR,VPS,SUB,VES
*MOPER,ERRG,GGAIN,MULT,ERROR       !PERFORMS MATRIX OPERATIONS ON
ARRAY PARAMETERS MATRICES
*MOPER,EDISF,BMAT,MULT,FBVOLT
*MOPER,XDOT,AMAT,MULT,XSTATO
*VOPER,MXSTAT,ERRG,ADD,EDISF
*VOPER,XSTAT,XDOT,ADD,MXSTAT
*MOPER,FBVOLT,KGAIN,MULT,XSTAT
*MOPER,VES,CMAT,MULT,XSTAT
*SET,XSTATO(1,1),XSTAT(1,1)
*SET,XSTATO(2,1),XSTAT(2,1)

*DO,IIC,1,NSA,1
*SET,SVOLT(ICOUNT,IIC),VPS(IIC)
*SET,SEVOLT(ICOUNT,IIC),VES(IIC)
```

```
*SET,AVOLT(ICOUNT,IIC),FBVOLT(IIC)
*SET,STIPDIS(ICOUNT,IIC),SDIS(IIC)
*SET,STIPVELO(ICOUNT,IIC),FREQR*SDIS(IIC)
*SET,STIPACC(ICOUNT,IIC),-FREQR*FREQR*SDIS(IIC)
*ENDDO
*SET,TIMEF(ICOUNT),CURRTIME
*ENDDO
```